Micelles, Reverse Micelles and Microemulsions as Media for Kinetic Studies and Electrodeposition of Co, Cu, Zn, Ni and Sn

A Dissertation Submitted to Dhaka University for the Partial Fulfillment of the Requirements of the Degree of Doctor of Philosophy in Chemistry

Submitted by

Ferdousi Begum

Registration No. 116

Session: 2010-2011

DEPARTMENT OF CHEMISTRY

PHYSICAL CHEMISTRY RESEARCH LABORATORY

University of Dhaka

Dhaka-1000, Bangladesh

November 2015

To

My Parents

and

Supervisors

Acknowledgements

I would like to express my sincere gratitude and appreciation to my supervisor **Professor Md. Abu Bin Hasan Susan**, Department of Chemistry, University of Dhaka, for his scholastic supervision, keen interest, constructive suggestions and continual guidance throughout the research work and his emendation of the manuscript without which the present research work might not have been completed. I sincerely owe to him for giving me an opportunity to work in close association with him.

I am also grateful to my respected supervisor **M. Yousuf Ali Mollah**, University Grants Commission of Bangladesh, Dhaka for his valuable comments, advices and kind assistance for various problems in any situation during experiments. His patience and guidance were true inspiration for me.

I am indebted to **Professor Dr. M. Muhibur Rahman,** University Grants Commission of Bangladesh and **Dr. M. Mominul Islam**, Associate Professor, Department of Chemistry, University of Dhaka, for their valuable comments, friendly collaboration, invaluable suggestions which helped me to resolve critical points related to this research work. I sincerely express my gratitude to **Dr. Muhammed Shah Miran**, Associate Professor, and **Dr. Saika Ahmed**, Lecturer, Department of Chemistry, University of Dhaka, for their encouragement during this work.

I sincerely acknowledge friendly and invaluable helps of the members of Material Chemistry Research Laboratory. My efforts would have been fruitless without their relentless help towards me whenever I required them. I wish to express my heartfelt thanks to all the teachers and students of Physical Chemistry section of the Department for their cooperation.

I gratefully acknowledge support from the sub project (CP-231) of the Higher Education Quality Enhancement Project of the University Grants Commission of Bangladesh financed by World Bank and the Government of Bangladesh.

I gratefully express my sincere thank to the Ministry of Science and Technology, Bangladesh for Bangabandhu Ph.D. Fellowship.

I am thankful to my husband Anwar Hossain and son Ahanaf Hossain for their continuous moral support. I am grateful to my parents and all other family members and well-wishers for their encouragement.

(Ferdousi Begum)

Declaration

Experiments described in this thesis were carried out by the author of this thesis in the Department of Chemistry, University of Dhaka, Dhaka-1000, Bangladesh. This work has not been presented and will not be presented, for any other degree.

Dr. Md. Abu Bin Hasan Susan
Professor
Department of Chemistry
University of Dhaka
Dhaka-1000
Bangladesh
Ph.D. Supervisor

Dr. M. Yousuf Ali Mollah
Professor
Department of Chemistry
University of Dhaka
Dhaka-1000
Bangladesh
Ph.D. Supervisor

Ferdousi Begum
Department of Chemistry
University of Dhaka
Dhaka-1000
Bangladesh
Author (Ph.D. Student)

Title of the thesis:

Micelles, Reverse Micelles and Microemulsions as Media for Kinetic Studies and Electrodeposition of Co, Cu, Zn, Ni and Sn

Submitted by:

Ferdousi Begum, Ph.D. Student, Department of Chemistry, University of Dhaka

The General description and outline of this thesis are given below:

Chapter 1: General Introduction

Chapter 1 describes the necessity and objective of the present research.

Chapter 2: Micelles, Reverse Micelles and Microemulsions of CTAB, SDS and TX-100: Study of Physicochemical Properties

Chapter 2 presents physicochemical properties of micelles, reverse micelles and microemulsions of CTAB, SDS/SDBS and TX-100 investigated by measurements of turbidity, conductivity, density, viscosity, refractive index and surface tension/interfacial tension. The CMC of CTAB and SDBS/SDS were determined by conductivity method; while the CMC of TX-100 was determined by fluorescence method. The turbidity, conductivity, viscosity, refractive index and density increase, while surface tension decreases to attain a limiting value with increasing concentration of CTAB or SDS or TX-100. In reverse micelles and microemulsions of CTAB and SDS, the conductivity, viscosity and density increase and the refractive index decreases. The interfacial tension at first decreases and then increases with ϕ_W or w_o. Three different microstructure regions (such as *w*/*o*, *BC* and *o*/*w* phases) in reverse micelles and microemulsions with increasing ϕ_W or w_o could be established from viscosity results. The reverse micelles and microemulsions were stable at room temperature for about one year as monitored by visual inspection. The transparency and homogeneity of these reverse micelles and microemulsions were observed by measuring % transmittance at 650 nm and centrifugation, respectively. The nanometer droplet sizes of reverse micelles and microemulsions were measured by dynamic light scattering method.

Chapter 3: Microstructures of Reverse Micelles and Microemulsions of CTAB and SDS: Analyzed by Percolation Theory

Chapter 3 discuss about different microstructures of reverse micelles and microemulsions of CTAB and SDS determined by applying percolation theory on dynamic properties, i.e. conductivity, turbidity, viscosity and interfacial tension. The conductivity, viscosity and interfacial tension measurements have provided evidence for percolation behavior with variation in the ϕ_W. The conductivity results of these reverse micelles and microemulsions are discussed in terms of a percolation theory. The phase transitions in conductivity results correspond to the structural change from *w*/*o* to *o*/*w* via

BC microemulsions. The percolation thresholds (ϕ_C) obtained from conductivity measurements are in accordance with those obtained from viscosity and interfacial tension measurements. The volumetric and refraction properties of reverse micelles and microemulsions were studied by measuring density and refractive index, respectively. Excess volume - ϕ_W, excess refraction - ϕ_W and excess molar refraction - ϕ_W profiles for these reverse micelles and microemulsions also indicate the structural phase transitions from *w*/*o*-*BC*-*o*/*w* microemulsions.

Chapter 4: Hydrolysis of CV Catalyzed by Micelles, Reverse Micelles and Microemulsions of CTAB, SDS and TX-100

In Chapter 4, kinetic results of hydrolysis of CV in micelles, reverse micelles and microemulsions of CTAB, SDS and TX-100 under pseudo first order condition are reported. The pseudo first order rate constant (k') of alkaline hydrolysis of CV in absence of surfactants obeyed the rate equation $k' = k_w [OH^-]$ yielding a value of 0.234 $M^{-1}s^{-1}$ for the bimolecular rate constant, k_w in aqueous solution. The reaction rates were found to be catalyzed by micellar solutions of CTAB and TX-100 but inhibited by SDBS. The k'-[CTAB] profiles show a maximum at [CTAB] = ca. 10 mM after which k' gradually decreases with increasing [CTAB]. On the other hand, with increasing [SDBS], the k' decreases and passes through a minimum at 1.84 mM (close to the CMC), above which the rate constant increases slightly. In presence of TX-100 in aqueous solution, the rate of the reaction was also accelerated up to [TX-100] = ca. 0.76 mM and then the rate constant becomes almost constant. The catalysis of the reaction by micelles of CTAB, SDBS and TX-100 was treated using Piszkiewicz and PPIE model to fit the experimental data for obtaining the binding constant of CV with CTAB, SDBS and TX-100 and other kinetic parameters. In reverse micelles and microemulsions of CTAB, SDS and TX-100, the k' - ϕ_W profiles for hydrolysis of CV show special patterns for structural variation of microemulsions, such as *w*/*o* to *o*/*w* microemulsions via *BC* microemulsions. Thus, the rate of reactions can be controlled by using micelles, reverse micelles and microemulsions of different surfactants.

Chapter 5: Hydrolysis of Bz Catalyzed by Micelles, Reverse Micelles and Microemulsions of CTAB, SDS/SDBS and TX-100

Chapter 5 presents kinetic results of hydrolysis of Bz in aqueous and micellar solutions of SDBS/SDS, CTAB and TX-100 and reverse micelles and microemulsions of CTAB studied by using spectrophotometric method under pseudo first order condition. In aqueous solution, the k' for acid hydrolysis of Bz increases non linearly with increasing $[H^+]$. The presence of SDBS/SDS and TX-100 produced an inhibitory effect while addition of CTAB has been found to enhance the rate of hydrolysis of Bz at concentrations below the CMC. Above the CMC, the k' increases slightly for some concentration of SDBS/SDS whereas for TX-100, the k' was almost constant. As [CTAB] increases at low $[H^+]$, the rate constant attains a limiting value; while at high $[H^+]$, the rate constant passes through a maximum and then decreases. This enhancement and inhibition of the rate of hydrolysis of Bz by CTAB, SDBS/SDS and TX-100 micelles

were treated by Piszkiewicz and PPIE model to obtain the binding constant of Bz with CTAB, SDBS/SDS and TX-100 and other kinetic parameters. In CTAB/cyclohexane/1-butanol/water microemulsions, at $[H^+]$ = 0.001 M, the k' of acid hydrolysis of Bz decreases sharply followed by a slight increase while at $[H^+]$ = 0.01 M, k' increases first followed by a sharp decrease with increasing ϕ_W increases.

Chapter 6: Comparative Study of Hydrolysis of CV and Bz in Micelles, Reverse Micelles and Microemulsions of CTAB, SDS and TX-100

In Chapter 6, kinetic results of hydrolysis of CV and Bz in aqueous media were compared with those in micelles, reverse micelles and microemulsions of CTAB, SDS and TX-100. The hydrolysis of CV was carried out under alkaline conditions; while that of Bz was followed under acidic conditions. The k'-[CTAB] profiles for hydrolysis of CV show a maximum at ca. 10 mM of CTAB concentration, after which k' gradually decreases with increasing [CTAB]; while for the hydrolysis of Bz, the addition of CTAB has been found to enhance the rate of the hydrolysis of Bz at concentrations below the CMC. Above the CMC of CTAB, at a low $[H^+]$, as [CTAB] increases the rate constant to attain a limiting value; while at a high $[H^+]$, the rate constant passes through a maximum and then decreases. SDBS produced an inhibitory effect on the reaction rate for both reactions. Micellar solution of TX-100 accelerates and inhibits hydrolysis of CV and Bz, respectively. The rate constants of the reactions are also greatly affected by reverse micelles and microemulsions of CTAB, SDS and TX-100 under identical experimental conditions. The rates are higher in *w*/*o* microemulsions and decrease with ϕ_W while rates are almost constant in BC microemulsions and decrease in *o*/*w* microemulsions.

Chapter 7: Electrodeposition of Co, Cu, Zn, Ni and Sn from Reverse Microemulsions of CTAB and SDS

Chapter 7 discusses about electrodeposition of Co, Cu, Zn, Ni and Sn from aqueous solution and reverse microemulsions of CTAB and SDS with different w_o. Electrochemical behavior of different metal ions: Co^{2+}, Cu^{2+}, Zn^{2+}, Ni^{2+} and Sn^{2+} has been studied in aqueous solution and reverse microemulsions of CTAB and SDS with different w_o on CuE by cyclic voltammetry. The electrochemical reduction of different metal ions to metals has been found to occur easily on CuE in aqueous solution. Electrodeposition of different metals was therefore performed from aqueous solution at a fixed potential below the reduction potential using constant potential electrolysis method on CuE. In reverse microemulsions with different w_o, electrodeposition of different metals on CuE has been performed at different reduction potentials. Morphology and microstructures of the electrodeposited metals were examined by scanning electron microscopy; while elemental characterization was carried out by energy dispersive x-ray spectroscopic method. From aqueous medium, electrodeposition of metals occurs very fast and a gross deposition of bulk metal results without any definite morphology. In CTAB/1-butanol/water and SDS/1-butanol/water reverse microemulsions with fixed w_o, deposition rate varies with change in applied potentials and thickness of deposited metals

only changed with change in deposition potential. The variation of w_o of reverse microemulsions brings about changes in size distribution of reverse microemulsions as revealed by dynamic light scattering measurements and consequently influences morphology of electrodeposited metals. SEM images show that deposition of metals occurs with definite size and shape; even the shape changes with w_o of reverse microemulsions. Electrodeposits from reverse microemulsions of CTAB and SDS with different w_o were compared to judge the suitability of the reverse microemulsions for electrodeposition of metal with tunable morphology.

Chapter 8: Correlation of Different Physicochemical Properties of Reverse Micelles and Microemulsions and with Kinetic Results and Morphology of Electrodeposited Metals

Chapter 8 correlates different physicochemical properties of micelles, reverse micelles and microemulsions of CTAB and SDS with each other and with kinetic results of hydrolysis of CV and Bz and morphology of electrodeposited metals in those media. With increasing ϕ_W, conductivity and density increase while refractive index decreases. Viscosity, turbidity and interfacial tension-ϕ_W profiles show specific patterns due to existence of three different microstructure regions in *w*/*o*, *BC* and *o*/*w* microemulsions with increasing ϕ_W. The structural change from *w*/*o* to *BC* and *BC* to *o*/*w* microemulsions was also confirmed by percolation thresholds obtained by applying percolation theory and percolation scaling law on conductivity results. The CTAB/1-butanol/cyclohexane/water and SDS/1-butanol/cyclohexane/water microemulsions have been used as media for kinetic studies of hydrolysis of CV and Bz. The k' - ϕ_W profiles for hydrolysis of CV and Bz show that the hydrolysis rates are greatly affected by structures and structural transitions of CTAB/1-butanol/cyclohexane/water and SDS/1-butanol/cyclohexane/water microemulsions. The rates are higher in *w*/*o* microemulsions having lower conductivity and viscosity and decrease with ϕ_W. The rates are almost constant in *BC* microemulsions and decrease in *o*/*w* microemulsions having higher conductivity and viscosity. The transition of the hydrolysis rates could be observed at the structural transitions from *w*/*o* to *BC* and from *BC* to *o*/*w* obtained. Electrochemical behaviors of Co and morphology of the electrodeposited Co were also correlated with conductivity of reverse microemulsions. Cathodic peak potential and peak current as well as morphology of electrodeposits change with increasing conductivity of reverse microemulsions.

Chapter 9: General Conclusions

Chapter 9 summarizes the results for a general conclusion and discussed the future prospect of these systems for development of suitable media to control the rate of reactions and morphology and structure of electrodeposited metals.

Abstract

Series of micelles, reverse micelles and microemulsions of cationic, anionic and surfactants were prepared with varying water to surfactant molar ratios in a wide range of compositions and their physicochemical properties have been studied in detail. These have been evaluated as media and catalysts for model reactions through systematic kinetic studies and theoretical treatments. Their suitability as media for electrodeposition of different metals with controllable size, shape and morphology has also been studied in detail. Efforts have been made to correlate physicochemical properties of the micelles, reverse micelles and microemulsions with kinetic behavior and electrodeposition.

Kinetics of the hydrolysis of crystal violet (CV) and bromazepam (Bz) has been studied in micelles, reverse micelles and microemulsions of cetyltrimethylammonium bromide (CTAB), sodium dodecyl sulfate (SDS)/sodium dodecyl benzene sulfate (SDBS) and tritonX-100 (TX-100) by using spectrophotometric method under pseudo first order condition. The physicochemical properties of micelles, reverse micelles and microemulsions have been investigated by measuring turbidity, conductivity, density, viscosity, refractive index and surface tension/interfacial tension. The Critical micelle concentrations (CMC) of CTAB and SDBS/SDS were determined by conductivity method; while the CMC of TX-100 was determined by fluorescence method. Turbidity, conductivity, viscosity, refractive index and density increase while surface tension decreases to attain an almost constant value with increasing [CTAB] or [SDS] or [TX-100]. Hydrolysis of CV was carried out under alkaline conditions; while that of Bz was followed under acidic conditions. The pseudo first order rate constants, k'-[CTAB] profiles for hydrolysis of CV show a maximum at ca. [CTAB] = 10 mM, after which k' gradually decreases with increasing [CTAB]; while for hydrolysis of Bz, addition of CTAB has been found to enhance the rate of hydrolysis of Bz at concentrations below the CMC. Above the CMC of CTAB, at low $[H^+]$, as [CTAB] increases the k' attains a limiting value; while at high $[H^+]$, the k' passes through a maximum and then decreases. SDBS produced an inhibitory effect on the reaction rates for both reactions. The micellar solution of TX-100 accelerates and inhibits hydrolysis of CV and Bz, respectively. The catalysis of these reactions by micelles of CTAB, SDS/SDBS and TX-100 were treated in terms of Piszkiewicz and Pseudophase Ion-Exchange (PPIE) model to fit the experimental data for obtaining the binding constant of CV or Bz with CTAB, SDBS and TX-100 and other kinetic parameters. The k's of the reactions were also greatly affected by reverse micelles and microemulsions of CTAB, SDS and TX-100 under identical experimental conditions. The k' - volume fraction of water (ϕ_W) profiles for hydrolysis of CV and Bz shows special pattern in reverse micelles and microemulsions, such as water in oil (*w*/*o*) to oil in water (*o*/*w*) via bicontinuous (*BC*) microemulsions with different microstructures, which have been determined by measuring physicochemical properties of reverse micelles and microemulsions. Conductivity, viscosity and density increase as well as refractive index decreases and the interfacial tension at first decreases and then

increases with increasing ϕ_W. Three different microstructure regions with increasing ϕ_W were also established by applying percolation theory and percolation scaling law on conductivity results and the percolation thresholds (ϕ_C) obtained from conductivity results were in accordance with viscosity results. The phase transitions at these two percolation thresholds correspond to structural change from *w*/*o* to *BC* (ϕ_{C_1}) and *BC* to *o*/*w* (ϕ_{C_2}) microemulsions. Excess volume - ϕ_W, excess refraction - ϕ_W and excess molar refraction - ϕ_W profiles for these microemulsions also indicates structural transitions. The k' - ϕ_W profiles for hydrolysis of CV and Bz shows that the transition of hydrolysis rates could be observed at structural transitions from *w*/*o* to *BC* and from *BC* to *o*/*w* obtained from percolation theory and the rates of both reaction are higher in *w*/*o* microemulsions and decrease with ϕ_W while almost constant in *BC* microemulsions and decrease in *o*/*w* microemulsions.

Electrochemical behavior of different metal ions: cobalt (II) (Co^{2+}), copper (II) (Cu^{2+}), zinc (II) (Zn^{2+}), nickel (II) (Ni^{2+}) and tin (II) (Sn^{2+}) also have been studied in aqueous solution and reverse microemulsions of CTAB and SDS with different water to surfactant ratios (w_o) on copper electrodes (CuE) by cyclic voltammetry. The reduction of different metal ions to metals has been found to occur with ease at CuE in aqueous solution. Electrodeposition of different metals was therefore performed from aqueous solution at a fixed potential below reduction potential using constant potential electrolysis method on CuE. In reverse microemulsions with different w_o, electrodeposition of different metals on CuE has been performed at different reduction potentials. Morphology and structures of the electrodeposited metals were examined by scanning electron microscopy; while elemental characterization was carried out by energy dispersive x-ray spectroscopic method. From aqueous solution, electrodeposition of metals occur very fast and a gross deposition of bulk metal results without any definite morphology. In CTAB/1-butanol/water and SDS/1-butanol/water reverse microemulsions with fixed w_o, the deposition rate varies with change in applied potentials and thickness of deposited metals only changed with change in deposition potential. The variation in w_o brings about changes in size and size distribution of reverse microemulsion as revealed by dynamic light scattering measurements and consequently influences morphology of electrodeposited metals. SEM images show that deposition of metals occurs with definite size and shape even the shape changes with increasing w_o of reverse microemulsions. The electrodeposits from reverse microemulsions of CTAB and SDS with different w_o were compared to judge the suitability of the reverse microemulsions for electrodeposition of metals with tunable morphology.

Kinetic results of those hydrolysis reactions and morphology of electrodeposited metals have been correlated with physicochemical properties such as viscosity and conductivity of reverse micelles and microemulsions. The k' of the reactions decreases with increasing

conductivity and viscosity of reverse micelles and microemulsions. The reduction potentials for reduction of metal ions to metal shifted to more negative values with increasing conductivity of reverse microemulsions. An increase in conductivity of the system brings about changes in the structures of electrodeposited metals depending on the diffusion as well as deposition rate. Thus, micelles, reverse micelles and microemulsions can serve as suitable media to control the reaction rates of different reactions and the morphology and structure of different metals by electrodepostion.

CONTENTS

LIST OF FIGURES

LIST OF SCEMES

LIST OF TABLES

1.1. General Introduction

Micelles, reverse micelles and microemulsions are self-assembled systems of surfactants, surface active agents which in small quantity markedly affect the surface characteristics of a system. Micelles are colloidal aggregates of a unique number of surfactant. In polar media, the hydrophobic part of the surfactant forming the micelle tends to locate away from the polar phase while the polar parts of the surfactant (head groups) tend to locate at the polar micelle-solvent interface [1]. In highly non-polar solvents, the polar groups of the surfactant become solvophobic and in such media, aggregation occurs in which the polar groups form the core. Such species are referred to as inverse, reverse, or reverted micelles [2] where the hydrophilic groups are sequestered in the micelle core and the hydrophobic groups remain solvent-exposed on the surface of the micelle. Thus, micellar systems have the unique property of being able to solubilize both hydrophobic and hydrophilic compounds.

Microemulsions, on the other hand, are thermodynamically stable homogeneous mixtures composed of two mutually immiscible liquid phases, one spontaneously dispersed in the other with the assistance of one or more surfactants and co-surfactants [3]. The surfactants are mostly located at the interface between the domains of the polar and nonpolar fluids. They can be water-continuous (oil-in-water), oil-continuous (water-in-oil) or bicontinuous (middle phase) and usually behave like Newtonian fluids; their viscosity is low comparable to that of water, even at high droplet concentrations. Microemulsion is formed on addition of an aliphatic alcohol (co-surfactant) to an ordinary emulsion [4]. It is well established that large amounts of two immiscible liquids (e.g. water and oil) can be brought into a single phase (macroscopically homogeneous but microscopically heterogeneous) by addition of an appropriate surfactant or a surfactant mixture. This unique class of optically clear thermodynamically stable and usually low viscous solutions, called ‘microemulsions’ [5] have been the subject of extensive research over the last two decades primarily because of their scientific and technological importance. Micromulsions find application in enhanced oil recovery, as well as in the pharmaceuticals and cosmetic industries. Water-in-oil microemulsions have been extensively used as microreactors to prepare monodisperse nanosized particles, such as metal, metal borides and metal oxides [6].

The catalysis of reactions by micelles, reverse micelles and microemulsions has proved to be of great importance in chemical, industrial as well as biological fields. The ability of a micellar system to solubilize a reactant may affect its action as a catalyst or inhibitor in a reaction. When a surfactant system serves as a reservoir for increasing the availability of one reactant, any change that increases the solubilizing capacity of the micelle should also increase its effectiveness as catalysis. If, on the other hand, the reaction must occur in the bulk phase, increased solubilizing power may remove reactant from the reaction medium and therefore lower catalytic or increase inhibitor efficiency. Reverse micelles

and microemulsions can also solubilize a wide variety of compounds simultaneously and offer the possibility of reagent compartmentalization and other effects. Thus, catalysis by reverse micelles and microemulsions represents an alternative to phase-transfer catalysis [7] and other techniques [8] for reaction of water insoluble organic substrates with water-soluble reagents. Electrolysis in micelles, reverse micelles and microemulsions is a promising approach for environmentally friendly chemical synthetic methods of the future. Employing microemulsion instead of organic solvents for electrosynthesis has the advantages of lower toxicity and cost, high dissolving power for reactants and mediators of unlike solubility, enhancement of reaction rates by controlling the reduction potentials of mediators, possible reaction pathway control, and recycling of microemulsion components [9].

Surfactants-based self-assembled systems thereby, offer the potential to change the kinetics of a wide variety of reactions. A change in the reaction medium by controlling the organization of the surfactant can not only significantly influence the rate of a chemical reaction, but may also bring about change in the reactivity and reaction mechanism.

Micelles and reverse micelles are thermodynamically stable aggregates of colloidal dimensions, while microoemulsions, both *w*/*o* or *o*/*w* is mixtures of micelles and reverse micelles in two immiscible solvents. Such surfactants based organized media have different cores in the aggregated states in solution. When electro-active substances are solubilized in such a medium, the diffusibity of the electro-active species significantly lowers due to larger size of the aggregates. The difference in the hydrophobic/hydrophilic behavior of the cores and the bulk solutions also brings about significant changes in the redox behavior of electroactive materials and the electrode kinetics. These offer micelles, reverse micelles and microemulsions the potential to electrochemically reduce metals from their salts with controlled rate and the electrochemical depositions [10] become feasible at tunable morphologies. A surge of interest has therefore been focused on the deposition of certain metals with controllable morphologies under controlled potential electrtrolysis. Aeiyach et al [11] carried out the electrodeposition of poly-(3,4-ethylenedioxythiophene) films on iron, mild steel and aluminium in aqueous anionic micellar media. Kaplin and Qutubuddin [12] reported on the electrodeposition of pyrrole into a porus film by microemulsions. Aragon et al [13] studied the effect of a polyethoxylate surfactant on the electrodeposition of tin. Zhou et al [14] carried out the electrodeposition of nanoscaled nickel in reverse microemulsions. Copper nanorods were synthesized using microemulsions by controlled current electrochemical methods by Yang et al [15]. Electrodeposition of metals has, in fact, been technologically important for manifold applications, which include, inter alia, corrosion-resistants, electronics, optics and sensors, automobile and aerospace systems. The first electrodeposition was based solely on aqueous solutions due to high solubility of electrolytes and metal salts

resulting in high conducting solutions. Research to date included numerous attempts to electrochemically deposit wide range of metals from aqueous solutions. However, the deposition of large number of metals of large negative reduction potentials such as Zn, Cr, Ti, W, Tl, Sb, In, Ta, Ge is hindered due to a relatively narrow potential window (about 1.2 V) [16] in aqueous medium.

With a view to a clearer understanding of the mechanism of catalysis and electrodeposition of metals in different organized media, it is necessary to study the kinetics of different model reactions based on different substrates and carry out electrochemical deposition of different metals from different surfactant based organized media. It is also interesting to investigate how a change in environment causes change in the mechanism of the reaction pathway and change in the morphology of electrodeposited metals.

1.1.1. Outline of the Research

In this work, we study the kinetics of two model reactions: alkaline hydrolysis of crystal violet, CV (a carobocationic dye) and acid hydrolysis of bromazepam, Bz (a benzodiazipidine drug) and electrodeposition different metals (Co, Cu, Zn, Ni and Sn) in micelles, reverse micelles and microemulsions of cationic, anionic and non-ionic surfactant. The effect of water to surfactant ratio or volume fraction of water in micremulsions of different surfactants on the rate of the title reactions and electrode kinetics for reduction of metal salts and morphology of the electrodeposited metals were investigated. The physicochemical behavior of the reverse micelles and the microemulsions were studied and correlated with the kinetic results of hydrolysis reactions and morphology of the electrodeposited metals.

1.2. Supramolecular Chemistry

Supramulecular chemistry concerns chemistry beyond the molecules and focuses on the chemical systems made up of a discrete number of assembled molecular subunits or components [17, 18]. While molecular chemistry focuses on the covalent bond, supramolecular chemistry examines the weaker and reversible non-covalent interactions between molecules. These forces include hydrogen bonding, metal coordination, hydrophobic forces, van der Waals forces, π-π interactions and electrostatic effects. Supramolecular chemistry include molecular self-assembly, folding, molecular recognition, host-guest chemistry, mechanically-interlocked molecular architectures, and dynamic covalent chemistry [19].

Supramolecular chemistry may be divided into two broad areas concerning: (1) *supermolecules* that result from the intermolecular association of a few components (a receptor and its substrate(s)) following a built-in scheme based on the principles of molecular recognition; (2) *supramolecular assemblies*, that result from the spontaneous association of a large undefined number of components into a specific phase having more

or less well-defined microscopic organization and macroscopic characteristics depending on its nature (such as micelles, microemulsions, vesicles, films, layers, membranes, mesomorphic phase and so on) [18].

Research in supramolecular chemistry has already a long and productive history. Above and beyond the chemistry of covalent bonds, a chemistry of supramolecular systems is now emerging. The last two decades have in reality, witnessed fast progress in supramolecular chemistry and many research groups have already involved themselves in this field of chemistry in the pursuit of the construction of supramolecular systems of both chemical and biological importance.

The rate of a chemical reaction significantly changes in supramolecular systems, specifically in surfactant-based organized media involving hydrophobic interactions, such as, micelles, reverse micelles and microemulsions. This has resulted in a surge of interest in the kinetics of reactions involving different substrates solubilized in such organized media with a view to the fundamental understanding of the mechanism of reactions in different environments for their potential applications. In the following sections, a brief introduction on organized media based on surfactants has been made.

Surfactant (figure 1.1.) is a substance which in solution, particularly aqueous solution, tends to congregate at the bounding surface, i.e. the air-solution interface, the walls of the containing vessel and the liquid-liquid interface (if a second liquid phase is present) [20]. As a result, the various interfacial tensions are reduced. The reason for this behavior is that the surfactant contains two structurally distinct parts, one of which is hydrophilic while the other is hydrophobic.

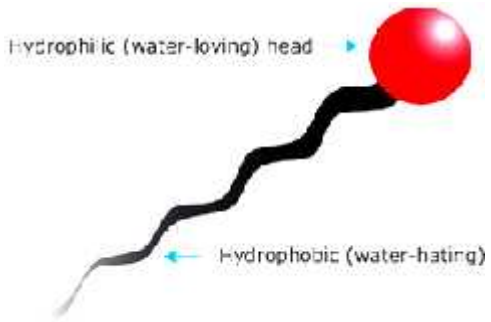

Figure 1.1. Schematic representation of a surfactant.

Surfactant in aqueous solution seeks the interface, because its hydrocarbon tail is repelled by water and it tends to remain there, with the hydrophobic part above the surface and the hydrophilic part below, i.e. in the water phase. Further surfactants seek the surface or the walls of the vessel until both are full, at which point further additions result in the formation of micelles, which are clusters of surfactant arranged with the hydrophobic parts towards the centre and the hydrophilic parts on the outside.

Figure 1.2 shows schematically the three environments in which surfactant reside in a typical aqueous solution. Surfactants disperse as monomers in the aqueous phase, form aggregates (micelles), or adsorb as a film at the air/water interface [20]. The surfactant is in dynamic equilibrium between these states. Thus, at a given temperature, pressure and concentration, the number of monomers, micelles and monomers adsorbed at the air/water interface is fixed under equilibrium conditions.

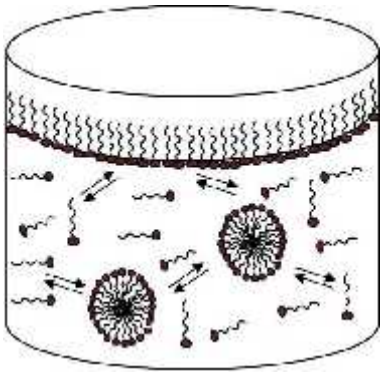

Figure 1.2. Surfactants in aqueous phase

Surfactants can be classified by the presence of formally charged groups in its head. Nonionic surfactants have no charge groups in its head. The head of ionic surfactants carries a net charge. If the charge is negative, the surfactant is more specifically called anionic; if the charge is positive, it is called cationic. If a surfactant contains a head with two oppositely charged groups, it is termed zwitterionic (Figure 1.3) [21].

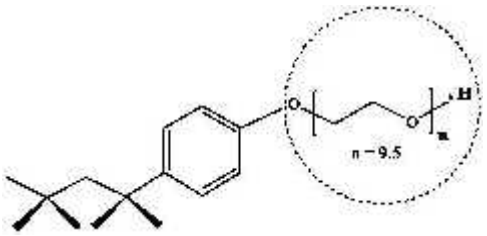

(a) Polyoxyethylene octyl phenyl ether (TX-100), non-ionic surfactant

(b) Sodium dodecyl benzene sulfonate (SDBS), anionic surfactant

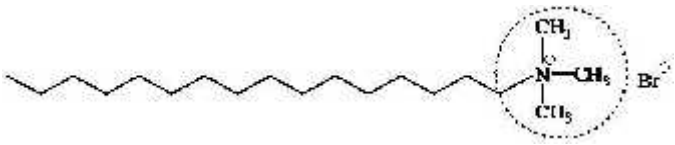

(c) Cetyltrimethylammonium bromide (CTAB), cationic surfactant

(d) Dodecyl betaine, zwitterionic surfactant

Figure 1.3. Different types of surfactants.

Supramolecular self-assembly is the tendency for surfactant to organize themselves into extended structures in water. Surfactant at low concentration in aqueous solution exists as monomers (free or unassociated surfactant). These monomers pack together at the interface, form monolayer and contribute to surface and interfacial tension lowering. Although this phenomenon is highly dynamic (surfactant arrive and leave the interface on a very rapid timescale), surfactant at the interface interact with the neighboring surfactant very strongly, which enables measurement of the rheological properties of the monolayer.

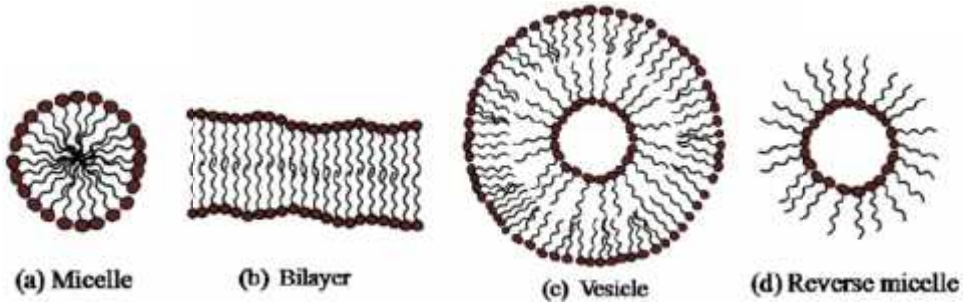

Figure 1.4. Self- assembly of surfactants.

As the surfactant concentration increases, the available area at the surface for surfactant adsorption diminishes and surfactant monomers start accumulating in the solution. However, the hydrophobic tail of the surfactant has extremely small solubility in water and the hydrophilic head has extremely small solubility in non-polar solvents. Hence, the hydrophobic effect will drive surfactant monomers to form self-assembled aggregates above certain aggregate concentration. These aggregates are micelles, bilayers, vesicles, and reverse micelles etc (Figure 1.4) and exist in equilibrium with the surfactant monomers [20].

Above a certain concentration, surfactant monomers assemble to form a closed aggregate (micelle) in which the hydrophobic tails shielded from water while the hydrophilic heads face water. The narrow concentration range above which any added surfactants appear with high probability as micellar aggregates is defined as the critical micelle concentration (CMC). Beyond this concentration the addition of more surfactant will result in an increase in the number of micelles, while the concentration of monomeric surfactant remains almost constant. Thus, the CMC represents a phase separation between monomers of surfactant and surfactant aggregates in dynamic equilibrium. It indicates the point at which monolayer absorption completes and the surface active properties are at an optimum. As the concentration of surfactants increases in a solution, the physical properties of the solution will change sharply at the CMC (Figure 1.5). Above the CMC, the surfactants come together to form spherical aggregates (micelles) in which polar groups populate the core with hydrophobic chains and the corona.

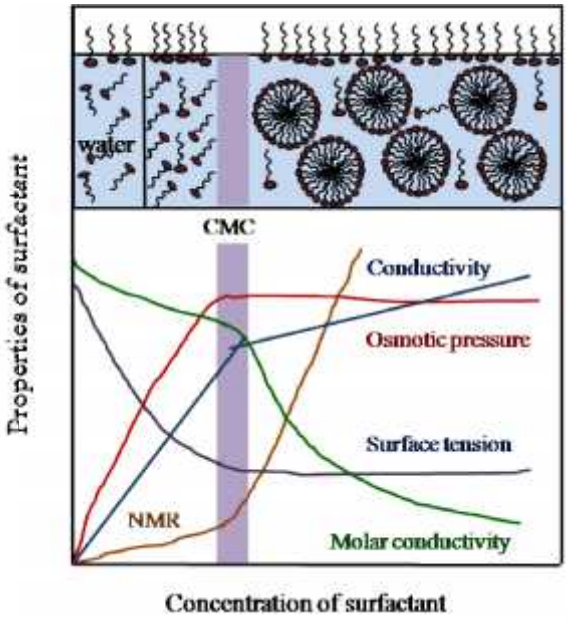

Figure 1.5. Schematic representation of the concentration dependence of the physical properties for solutions of micelle-forming surfactant.

Experimentally, the CMC is determined from the discontinuity or inflection point in the plot of a physical property of the solution as a function of surfactant concentration. This is demonstrated in [22] Figure 1.5. Clear breaks of almost every measurable physical property that depends on size and number of particles in solution are shown by all types of surfactants, i.e. nonionic, anionic, cationic and zwitterionic in aqueous media. A wide variety of method including tensiometry, conductometry, viscometry, light scattering, fluorimetry, calorimetry, spectrophotometry, and nuclear magnetic resonance (NMR) spectroscopy [23] involving the measurement of physical properties have been used to determine the CMC values. Plotting the derivatives of the values of physical properties may also be a convenient way of precisely locating the CMC [24].

The CMC can be affected by many variables [3], temperature and pressure being of relatively minor importance. It decreases with increasing hydrocarbon chain-length of the apolar groups, and for ionic surfactants it also depends on the nature and concentration of counter-ions in solution. Added electrolytes decrease the CMC, and the effect increases with decreasing charge density of the counter-ion.

Micelles (Figure 1.4(a)) are organized assemblies of surfactants. They have no surface activity and any increase in the surfactant concentration does not affect the number of monomers in the solution but affects the structure of micelles. They are usually spherical in shape, and can be cationic, anionic, ampholitic (zwitterionic), or nonionic depending on the chemical structure of the surfactant. Micelles are formed in non-polar media such as benzene, where the amphiphiles cluster around small water droplets in the system, forming an assembly known as a reverse micelle (Figure 1.4 (d)). Micellar systems have the unique property of being able to solubilize both hydrophobic and hydrophilic compounds. They are used extensively in industry for detergency and as solubilizing agents.

The micellar solutions above the CMC are homogeneous and transparent, thus it is difficult to observe size and structure of micelles. In general, it is known that the size of micelles formed in aqueous surfactant solution ranges from 10 to 100 Å, and that the shape of micelles varies with increasing concentration in order of spherical, cylindrical, hexagonal, and lamellar in aqueous surfactant solutions [25]. The shape of micelles depends on the relative values of tail length (l), head group area (a) and the molecular volume (v) of the molecule. Israelachvili et al [27] have argued that depending on the value of packing parameter p (= v/al), the surfactant aggregates could acquire different shapes (Figure 1.4). They showed that, in general, micelles are spherical for $p < 1/3$ and ellipsoidal and cylindrical for $1/3 < p < 1/2$. The surfactant aggregates tend to be bilayers for $p > 1/2$ and in suitable cases this results in formation of vesicles.

In non-polar solvent or water mixed with non-polar solvent, the rapid self-organization of surfactant and water occur in a specific manner that minimizes repulsive and maximizes attractive interactions between surfactant-surfactant, water-water, surfactant-nonpolar solvent, and surfactant-water. Such energetic requirement, above the CMC, forces the surfactant and water to attain an aggregate structure, which is called *reverse micelle* (Figure 1.6) [28]. In such cases, hydrocarbon tails are exposed to the solvent, while the polar heads point toward the interior of the aggregate to escape the contacts with the solvent. They are able to hold relatively large amounts of water in their interior. In that way, a "pocket" is formed which is particularly suited for the dissolution and transportation of polar solutes through a non polar solvent.

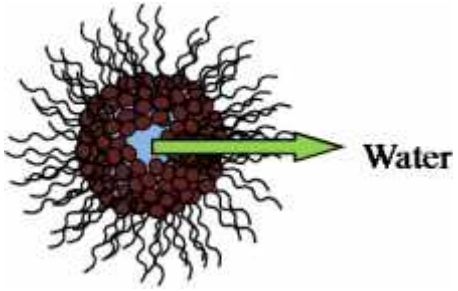

Figure 1.6. Reverse micelle

Such reverse association of surfactants is also in rapid equilibrium with monomeric surfactants. At a very low concentration of surfactant (above the CMC) in non-polar solvent, the reverse micelles are very close to spherical in which water molecules occupy the central part of the sphere, thus forming a so called microwater-pool and these water is in contact with head groups of reversed micelle forming surfactant. The shape of reverse micelle also changed from sphere-rod-hexagonal like structure depends on the concentration and composition of surfactants. The size of reverse micelle can be changed by increasing or decreasing the amount of solubilized water in the inner core of the micellar aggregate of surfactant [29].

1.3 Micellar (Microheterogeneous) Catalysis

Micellar solutions are in general, transparent to UV-visible electromagnetic radiation but the existence of invisible micelles and even much larger aggregates in aqueous solution containing micelle or vesicle-forming surfactant has been ascertained experimentally. Thus, the effect of such aggregates form of surfactant on reaction rates is referred to as *micellar catalysis*. Effect of both hydrophobic and electrostatic interaction between micelles and reactants appear to be the source for micellar catalysis [29].

1.3.1. Micellar Effects on the Rate of Chemical Reactions

The rate of micelle-mediated reaction may be described by considering one or more than one of the following factors [2]: (1) micellar medium effect (2) micellar effect on keeping reactants apart from each other (3) electrostatic effect (4) hydrophobic effect (5) ionic strength effect of ionic micellar surface (6) ion-exchange between two counter-ions of ionic micelles, and (7) the effect of ion-pair formation between counter-ions or ionic head groups of ionic micelles and ionic reactants. According to the physicochemical nature of micelle, the micellar effects on chemical reactions may be divided in two types:

i) The change in the reactivity of the substances transferred from water or in general bulk phase: The micellar medium produces a strong effect on the rate of chemical reactions. The influence of the microenvironment, which includes electrostatic interactions, enhances chemical reactivity. The following interactions could be considered.

- ❖ Deactivation of one of the reactants as a consequence of its interactions with the ionic surfactant heads.
- ❖ Activation of the other reactant as a consequence of the repulsion with the surfactant heads.

❖ The approaching process between reactive species.

The mutual orientation of the reagents absorbed on the micelle can also change the reactivity.

ii) Enhancement of the concentration of the reagents in the micellar phase:

The binding of the reagents with micelles and hence enhancement of their concentration in the micellar phase is mostly due to ionic (electrostatic) and hydrophobic interactions. With binding constants of the order of $10 - 10^3$ $Lmol^{-1}$, the contribution of the concentration factor to the second order rate constant should give $10 - 10^3$ fold acceleration [3].

1.3.2 Theoretical Aspects for the Mechanism of Micellar Catalysis on Reaction Rates

To establish a reaction mechanism, kinetic study has been one the best mechanistic tools. For this, kinetic experimental data on the reaction rate are obtained under a set of reaction conditions that could be explained by a kinetic equation derived on the basis of a proposed reaction mechanism. Similar approach has been used to provide quantitative explanations for the micellar effects on the reaction rates. The different micellar kinetic models developed for apparent quantitative explanations of the effects of micelles on reaction rates are as follows:

Menger and Portnoy [30] developed a quantitative treatment on the micellar-madiated reactions analogous to Michaelis-Menten equation of enzyme kinetics which is known as *pre-equilibrium kinetic (PEK)* model. Here, only substrate (S) distribution has to be considered, which is the situation for micelle-inhibited bimolecular or spontaneous unimolecular reactions. Scheme 1.1 shows the substrate distribution and reaction in each pseudophase [31].

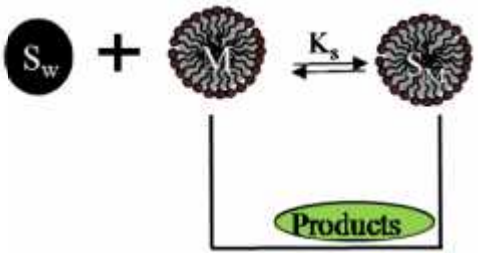

Scheme 1.1. The substrate distribution and reaction in each pseudophase.

In scheme 1.1, M denotes micellized surfactant; S is substrate, subscripts W and M denote aqueous and micellar pseudophases respectively, K_S is the binding constant for distribution of S with M. $k_M^{'}$ and $k_W^{'}$ are first order rate constants. The concentration of micellized surfactant, [M] is that of total surfactant less that of monomer, which is assumed to be given by the CMC.

The overall first-order rate constant k_{obs} is then given by equation (1.1).

$$k_{obs} = \frac{k_W^{'} + k_M^{'} K_S[M]}{1 + K_S[M]} \text{ - - - - - - - - (1.1)}$$

This equation is formally similar to the Michaelis-Menten equation of enzyme kinetics, although the analogy is limited because most enzymatic reactions are studied with substrate in large excess over enzyme. Variations of equation (1.1) have been developed to fit rate-[surfactant] profiles for spontaneous reactions that occur after a rapid pre-equilibrium.

PEK model generally fails for bimolecular, micelle-assisted reaction because the first-order rate constants should reach a constant, limiting value at high [surfactant] when the substrate is fully micelle bound, but rate maxima are observed for the corresponding bimolecular reactions when surfactant counter-ions are inert.

The rate - [surfactant] profiles can be treated quantitatively by taking into account the distribution of both reactants between water and micelles. This can be done by extending equation (1.1) and a simple formalism involves writing the first-order rate constants in terms of second-order rate constants in water and micelles and reactant concentrations in each pseudophase [32] which is known as *pseudophase model.* This model based on the assumption that transfer of materials between water and micelle is so fast that reaction does not perturb the equilibrium distribution of reactants between the pseudophases. Provided that equilibrium is maintained between the aqueous and the micellar pseudophases, the overall reaction rate will be the sum of rates in water and in the micelles and will therefore depend on the distribution of reactants between each pseudophase and the appropriate rate constants in the two pseudophases.

The first-order rate constants are written in equations (1.3) and (1.4) as second-order rate constants, k_W and k_M, for reaction of a reactive anion, Y^- where the mole ratio is

$$m_Y^S = \frac{[Y_M^-]}{[M]} \text{ - - - - - - - - - (1.2)}$$

$$k_W^{'} = k_W[Y_W^-] \text{ - - - - - - - - (1.3)}$$

$$k_M^{'} = k_M^{'} m_Y^S = k_M \frac{[Y_M^{'}]}{[M]} \text{ - - - - - - (1.4)}$$

By combining equations (1.1), (1.3) and (1.4), equation (1.5) is obtained for the observed pseudo-first-order kinetic constant,

$$k_{obs} = \frac{k_W[Y_W^-] + k_M K_S[Y_M^-]}{1 + K_S[M]} \text{ - - - - - - - (1.5)}$$

This equation readily explains why first order rate constants of micelle-assisted bimolecular reactions typically go through maxima with increasing surfactant

concentration if the overall reactant concentration is kept constant and if surfactant counter-ion is inert. Addition of surfactant leads to binding of both reactants to micelles, and this increased concentration increases the reaction rate. Eventually, however, increase in surfactant concentration dilutes the reactants in the micellar pseudophase and the rate falls. This behavior supports the original assumption that substrate in one micelle does not react with reactant in another and that equilibrium is maintained between aqueous and micellar pseudophases.

Thus, for a bimolecular reaction, the reaction between a reactant, R_M in the micellar pseudophase and other reactant, S_W in the aqueous pseudophase does not occur, i.e. the cross-interface reaction such as that between R_M and S_W or R_W and S_M does not take place (Scheme 1.2).

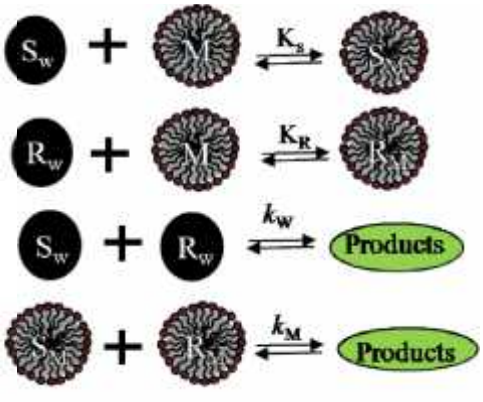

Scheme 1.2. The individual reaction between two reactants in aqueous phase and micellar phases.

Equation (1.4) is written in different ways can be applied to bimolecular micelle-assisted reactions provided that the distribution of both reactants can be determined. Estimation of the extent of micellar binding (β) can be estimated by conductivity if the organic ion is very hydrophobic, because then it is completely micelle bound under essentially all conditions [32]. For bimolecular reactions of hydrophilic ions, the conductivity method is not useful for estimating β for CTAOH, because it seems that β increases with increasing surfactant concentration [33] and then β has to be calculated.

The *pseudophase ion-exchange (PPIE)* model of bimolecular ionic reactions was developed by Romsted [32] to explain the rate maxima with increasing surfactant concentration, and inhibition by inert counter-ion competition between ions, e.g., Y^- and X^-, is written in terms of equation (1.6), which is similar to that used with ion-exchange resins (scheme 1.3).

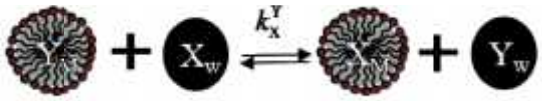

Scheme 1.3. Ion exchange mechanism between counterions and reactants.

$$K_X^Y = \frac{[Y_W^-][X_M^-]}{[Y_M^-][X_W^-]} \text{ - - - - - - - - - - (1.6)}$$

According to this model the observed pseudo-first order rate constant can be derived as,

$$k_{obs}^{'} = \frac{k_W[Y^-] + (k_M K_S - k_W) m_Y^S [M]}{1 + K_S[M]} \text{ - - - - - - - - - (1.7)}$$

PIE model considers the β (=1-α) is constant, where α is the degree of counter-ion dissociation for the micelle. By combining equations (1.2) and (1.6), the expression for m_Y^S is given by

$$m_Y^{S\,2} + m_Y^S \{\frac{[Y] + K_X^Y[X]}{(K_X^Y - 1)[M]} - \beta\} - \frac{\beta[Y]}{(K_X^Y - 1)[M]} = 0 \text{ - - - - - - - - - - - - (1.8)}$$

The PIE model is based on constant β which is only possible for lower concentration of surfactant because the value of β is no longer remains constant [34]. So, it is necessary to consider an additional route in which the reactive ion in the aqueous phase reacts with the micelle-bound substrate.

Analogous to the Hill model [35] for enzymatic reaction, Piszkiewicz [36] developed a new kinetic model. Piszkiewicz model explains the dependence of rate constants on the surfactant concentration especially below the CMC. In this model a substrate (S) and a small number (n) of detergent (D) aggregate to form pre-micelle (D_nS). This pre-micelle will react at a different rate to yield the product while the normal reaction also occurs in the aqueous phase (scheme 1.4).

$$S + nD \xleftrightarrow{K_D} D_n - S$$

$$D_n - S \xrightarrow{k_m} \text{Product}$$

$$S \xrightarrow{k_W} \text{Product}$$

Scheme 1.4. The premicellar catalysis.

K_D is the dissociation constant of the premicelle back to its free components, k_m is second-order rate constant of the reaction for the premicelle or micellar phase and k_w is the second-order rate constant in absence of surfactant. For this reaction scheme, the observed rate constant (k_{obs}) is expressed as a function of [surfactant] by the relation, (1.9).

$$k_{\text{obs}} = \frac{k_m[D]^n + k_w K_D}{K_D + [D]^n} \text{ - - - - - - - - - - - - (1.9)}$$

This equation may be rearranged to give (10)

$$\log \frac{k_{\text{w}} - k_{\text{obs}}}{k_{\text{obs}} - k_m} = n \log[D] - \log K_D \text{ - - - - - - - - (1.10)}$$

According to the above relation, a plot of $\log[(k_{\text{w}} - k_{\text{obs}})/(k_{\text{obs}} - k_{\text{m}})]$ vs. log[D] should be linear with a slope of '*n*', which is known as cooperativity index.

1.4. Microemulsions

Microemulsions are mixtures of two mutually insoluble liquids (such as oil and water) whose stability is essentially due to the presence relatively large amounts of surfactant (s) frequently in combination with co-surfactant(s) whose task is to dispose at the hydrophilic liquid and lipophilic liquid interface to reduce the interfacial tension [37]. Thus, microemulsion becomes a thermodynamically stable and homogeneous system able to form spontaneously without requesting any additional external energy. The concept of microemulsion was first introduced by Hoar and Schulman in 1959. Accordingly, microemulsion can be defined as a system of water, oil, and amphiphile, which is a single optically isotropic and thermodynamically stable liquid solution [38].

Microemulsion can have characteristic properties such as ultralow interfacial tension, low viscosity, large interfacial area, and capacity to solubilize both aqueous and oil-soluble compounds. The droplet diameter of microemulsion is usually within the range of 10-100 nm and therefore these systems are also termed as nanoemulsions [39].

Microemulsions form due to the adsorption of surfactants at the interface plus the entropy of dispersion of droplets in the continuous phase overcome the positive product of the small interfacial tension and the large interfacial area. In this case, the free energy of the system becomes zero or negative [40] which explains the thermodynamic stability of the microemulsion. Thus the main driving force for microemulsion formation is the ultra low interfacial tension, which is usually achieved by the use of two or more emulsifier, one predominantly water soluble and other predominantly oil soluble called co-surfactant, which reduce the interfacial tension to the of $< 10^{-2}$ mNm^{-1} generally required for the microemulsion formation.

Microemulsion shows different organization due to the use of wide range of surfactant concentration, water-oil ratios, temperature etc [41]. Three types of microemulsion are most likely to be formed depending on the composition (Figure 1.7):

1. Oil-in-water (*o*/*w*) microemulsion where oil droplets are dispersed in the continuous aqueous phase.

2. Water-in-oil (*w*/*o*) microemulsion where water droplets are dispersed in the continuous oil phase;
3. Bicontinuous microemulsion where microdomains of oil and water are inter-dispersed within the system.

In all the three types of microemulsions, the interface is stabilized by an appropriate combination of surfactants and/or co-surfactants [42]. The three different microemulsions are shown in figure 1.7.

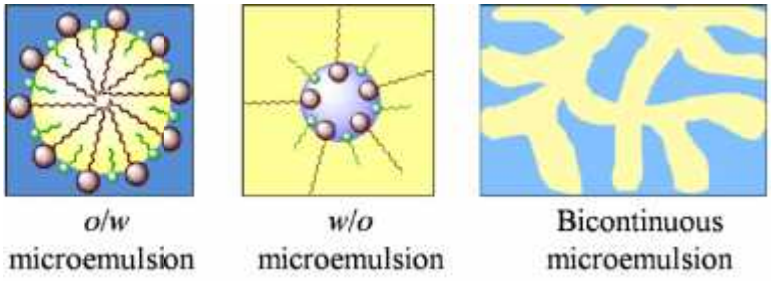

Figure 1.7. Different types of microemulsions.

The shapes of the droplets of microemulsions depend on the surfactant properties that can be conveniently represented by the hydrophillic-liphopillic balance (HLB) [43] and critical packing parameter (CPP) [25]. In general [41], low HLB (3–6) favors the formation of *w*/*o* microemulsions whereas high HLB (8–18) is better suited for the realization of *o*/*w* microemulsions. When CPP < 1/3, *o*/*w* globular structures are more probable, for CPP ≈ 1/2, *o*/*w* cylindrical structures form, for CPP ≈ 1, planar structures are favored, for CPP ≈ 2, *w*/*o* cylindrical structures are more probable and for CPP > 3, *o*/*w* droplets occur. [41].

Although there are no strict rules for choosing the appropriate components for microemulsion formation, still choosing surfactant is a crucial step. The surfactants such as cationic, anionic and nonionic that chosen must have [44]:

- Lower interfacial tension to a very small value to facilitates dispersion process.
- Provide a flexible film that can readily deform round small droplets.
- Be of appropriate HLB character to provide the correct curvature at the interfacial region for the desired micromulsion type.

Surfactant having HLB (>20) often require the presence of co-surfactants (short or medium chain alcohols) to reduce their effective HLB to value within the range required for microemulsion formation. The presence of co-surfactant in microemulsions helps by:

- Further reducing the interfacial tension by the dilution effect
- Increasing the mobility of the hydrocarbon tail and allowing greater penetration of the oil into this region.
- Influences the solubility properties of the aqueous and oily phases.
- Delaying the occurrence of liquid crystalline phases.

The most typical oil phase for microemulsion formation is hydrocarbons, which would be characterized by its length or alkane carbon number [6]. The oil phase influences curvature by its ability to penetrate and hence swell the tail group region of the surfactant monolayer [45] usually, water is used as polar phases for the preparation of microemulsion. An aqueous solution containing electrolytes and other additives are also used as polar phases provided that they behave reasonably as a pseudophase [6].

The characterization of microemulsion systems is highly challenging due to their small droplet size with fluctuating boundaries and complex structure. Alkaline components in a physicochemical characterization of microemulsions systems are observed by following techniques:

- Phase stability and phase behavior by measuring conductivity, viscosity, refractive index, differential scanning calorimetry [46], polarizing light microscopy, etc.
- Microstructures by using dielectric constant measurement, dimension (size and size distribution by dynamic light scattering method), shape and surface features (specific area, charge, and distribution),
- Local molecular arrangements, interactions and dynamics by electron microscopy (EM) techniques, such as freeze fracture transmission EM (FF-TEM) and cryo-field emission scanning and transmission EM (cryo-FESEM and cryo-TEM) [47,48].

1.4.1. Percolation in Miroemulsions

The physicochemical properties of microemulsions are influenced by the events occurring upon collision between microemulsion droplets. These properties of microemulsions changes when the volume fraction of the dispersed phase, ϕ is increased. The electrical conductivity is especially sensitive to the aggregation of droplets. This is indeed observed in several reported studies [49-53] in aqueous microemulsions. The paper of 1978 by Lagues is the first to interpret the dramatic increase of the conductivity with droplet volume fraction for a *w*/*o* microemulsion in terms of a percolation model and termed this physical situation as stirred percolation, referring to the Brownian motion of the medium.

The conductivity of the microemulsions is very sensitive to their structure [54-57]. The occurrence of percolation conductance reveals the increase in droplet size, attractive interactions and the exchange of materials between the droplets. The percolation threshold corresponds to the formation of first infinite cluster of droplets [55]. Even before the occurrence of percolation transition the change in conductivity indicates the variation of reverse micellar microstructure. The conductivity is closely related to the radius of the droplet but other factors like the composition of the microemulsions system, presence of external entity, temperatures etc. Under normal conditions, water in oil microemulsions represents very low specific conductivity. After a certain volume of the disperse phase, the conductivity abruptly increases to give values of up to four orders of

magnitude, which is greater than typical conductivity of water in oil microemulsions. This increase remains invariable after reaching the maximum value, which is much higher than that for the microemulsion present before the transition occurs. Similar behavior is observed with variation in water content, temperature or volume fraction for the fixed composition of the microemulsion. This phenomenon is known as *electric percolation*, [58-62] the moment at which an abrupt transition occurs from poor electric conductor, system to the system with fluid electric circulation. As a consequence of ion transfer it yields a sigmoidal $\sigma - \theta$ and $\sigma - \phi$ profile. The point of maximum gradient of the $d\log\sigma/d\theta$ or $d\log\sigma/d\phi$ profile corresponds to the transition of the percolation process and is designated as the threshold volume fraction (ϕ_C) or the threshold temperature (θ_C), characteristic feature of a percolating system.

According to percolation model, which is based on the dynamic nature of the microemulsions [63-65], there are two pseudophases: one in which the charge is transported by the diffusion of the microemulsion droplets and the other phase in which the change is conducted by diffusion of the charge carrier itself inside the reversed micelle clusters. According to this theory, two approaches (static and dynamic) have been proposed for the mechanism leading to percolation [51].

$$\sigma = A(\phi_c - \phi)^{-s} \text{ where, } \phi < \phi_C \text{ (below percolation) - - - - - - (1.11)}$$

$$\sigma = B(\phi - \phi_c)^{t} \text{ where, } \phi > \phi_C \text{ (above percolation) - - - - - - (1.12)}$$

where σ is the electrical conductivity, ϕ is the volume fraction and ϕ_C is the critical volume fraction of the conducting phase (percolation threshold), and A and B are free parameters. These laws are only valid near percolation threshold (ϕ_C). It is impossible to use these laws at extremely small dilutions ($\phi \rightarrow 0$) or at limit concentration ($\phi \rightarrow 1$) and in the immediate vicinity of ϕ_C. The critical exponent t generally ranges between 1.5 and 2, whereas the exponent s allows the assignment of the time dependent percolation regime. Thus, $s > 1$ (generally around 1.3) identifies a dynamic percolation [62, 66-67].

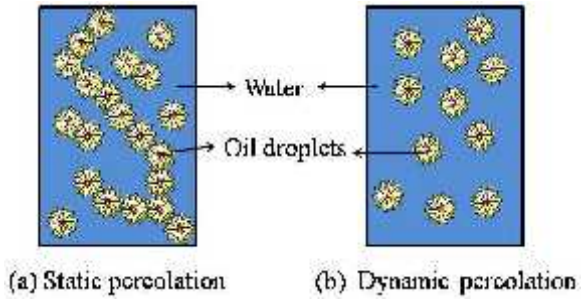

Figure 1.8. Dynamics of droplet fission.

The *static percolation* is related to the appearance of bicontinuous microemulsions, where a sharp increase in conductivity, due to both counter-ions and to lesser extent,

surfactant ions, can be justified by a connected water path in the system. The dynamic percolation is related to rapid process of fusion- fission among the droplets. Transient water channels form when the surfactant interface breaks down during collisions or through the merging of droplets (Figure 1.8). In this case, conductivity is mainly due to the motion of counter ions along the water channels. For dynamic percolation model, the overall process involves the diffusional approach of two droplets, leading to an encounter pair [68].

In a small fraction of the encounters, the interpenetration proceeds to a degree where the aqueous pools become directly exposed to each other through a large open channel between the two compartments, created by the rearrangement of surfactants at the area of mutual impact of the droplets. The channel is probably a wide constriction of the monolayer shell between the two interconnected compartments. Due to the geometry of the constriction, the monolayer at that site has an energetically unfavorable positive curvature, which contributes to the instability of the droplet dimmer. The short lived droplet dimmer than decalescence with a concomitant randomization of the occupancy of all the constituents and the droplets re-separate. Thus, during the transient exchange of channels, solubilizate can exchange between the two compartments. This offers an elegant approach to study the dynamic percolation phenomenon. However, another approach depicts a static percolation picture which attributes percolation to the appearance of a "bicontinuous structure" i.e. formation of open water channels [69].

1.4.2. Catalysis by Microemulsions

The use of microemulsions as media for organic reactions is a way to overcome the reagent incompatibility problems that are frequently encountered in organic synthesis. In this sense, microemulsions can be regarded as an alternative to phase transfer catalysis. The microemulsion approach and the phase transfer approaches can also be combined, i.e. the reaction can be carried out in a microemulsion in the presence of a small amount of phase transfer agent. A very high reaction rate may then be obtained. The reaction rate in a microemulsion is often influenced by the charge at the interface and this charge depends on the type of surfactant used. For instance, reactions involving anionic reactants may be accelerated by cationic surfactants. The surfactant counter-ion also plays a major role for the reaction rate. The highest reactivity is obtained with small counter-ions, such as acetate, that are only weakly polarizable. Large polarizable anions, such as iodide, bind strongly to the interface and may prevent other anionic species to reach the reaction zone [70].

In addition to reactions with ionic reactants, synthesis of macrocyclic lactones, the Diel–Alder reaction, oxidation with H_2O_2, nitration of aromatics, nitrosation reductions of carbonyl compounds, catalytic reductions and oxidations and deacylation as well as acylation have been carried out [71].

The nitration of phenol in an AOT-based microemulsion system has been performed, 80% ortho product in microemulsion in comparison to 35% in aqueous system has been observed. Regioselectivity of product has been established in microemulsion media. The kinetics of various reactions, for example, inversion of cane sugar, fading of crystal violet, hydrolysis of phenyl acetate and reaction between hexacyanoferrate (III)-iodide, etc. has been studied [71]. Comprehensive information on chemical reactions (organic and inorganic) in microemulsions can be found in recent reviews by Sjoblom et al [72] and Bunton and Romsted [6].

The use of waterless microemulsions (formamide or other non-aqueous solvents instead of water) for investigations of Wacker process and Diel–Alder reactions has been shown to be prospective; the reactions are faster in these media than in water.

1.5. Electrodeposition of Metals

Electrodeposition, a short version of "electrolytic deposition" is the process of coating a thin layer of one metal on top of a different metal to modify its surface properties. It is the application of a metal coating to a metallic or other conducting surface by an electrochemical process. The deposition of a metallic coating onto an object is achieved by putting a negative charge on the object to be coated and immersing it into a solution which contains a salt of the metal to be deposited (in other words, the object to be plated is made the cathode of an electrolytic cell). The metallic ions of the salt carry a positive charge and are thus attracted to the object. When they reach the negatively charged object (that is to be electroplated), it provides electrons to reduce the positively charged ions to metallic form:

$$\text{at cathode: } M^{z+} + ze^{-} \rightarrow M_{(s)}$$

$$\text{at anode: } M_{(s)} \rightarrow M^{z+}{}_{(aq)} + ze^{-}$$

Electrodeposition of metals is one of the most fascinating domains of current research because of its technological importance for manifold applications, which inter alia, includes: corrosion-resistant, electronic, optic and sensor materials, automobile aerospace systems etc. Research to date experienced numerous attempts to deposit wide range of metals by using electrochemical techniques from aqueous solutions. The physical, chemical and magnetic properties of such electrodeposited films of metal have been found to depend on the morphology, that is, shape, size, and structure [73].

Electrodeposition is based on Faraday's two physical laws. These laws are–

1. The weight of a substance formed at an electrode is proportional to the amount of current passed through the cell; and
2. The weights of different substances produced at an electrode by the same amount of current are proportional to their equivalent weights.

These two laws can be summarized by the equation

$$V = Cit \text{- - - - -} \quad (1.13)$$

V is the volume of metal plated (mm^3), C is a plating constant based on electrochemical equivalent and density (mm^3/amp-s), i is current in amps and t is time in which the current is applied. No cathode is 100% efficient though due to other chemical reactions occurring and this has to be taken into account. The equation actually reads as

$$V = ECIt \text{- - - - - - - -} (1.14)$$

E is the cathode efficiency which is the actual amount of metal deposited by the cathode divided by the theoretical amount given by the first equation.

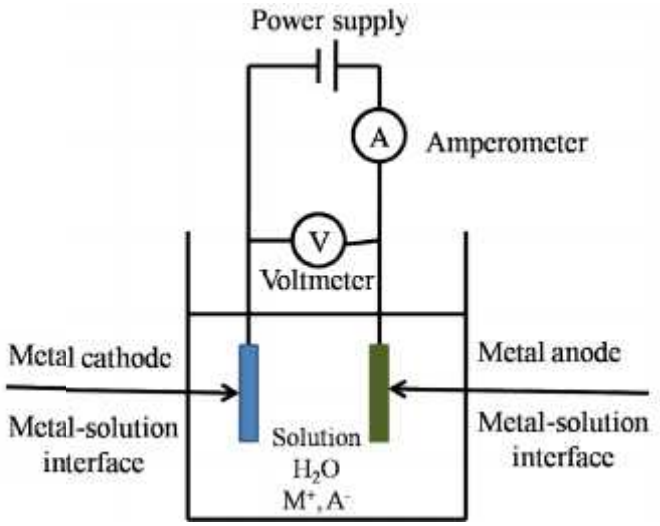

Figure 1.9. An electrolytic cell for electrodeposition of a metal "M" from an aqueous (water) solution of metal salt "MA".

Figure 1.9 schematically represents the principle of electrodeposition of a metal. If an object is made of one of the common metals, like copper, in order to plate it with nickel, a wire will have to be attached to the object while the other end of the wire should be attached to the negative pole of a battery (or a power supply). The positive pole of the battery (or power supply) should be connected to another wire with its other end connected to a rod made of nickel. Next the cell should be filled with a solution of the metal salt to be plated. It is possible to use a molten salt and in some not so common cases, such as the deposition of tungsten. In most, more common, cases the salt is simply dissolved in water.

In practical electrodeposition processes, the chemical reaction around the electrode area occurs in a complicated way. Under the influence of an applied potential, rearrangement of ions near the electrode surface results in an electrical double layer called the Helmholtz double layer, followed by the formation of a diffusion layer as shown in Figure 1.10. These two layers are referred as the Gouy-Chapman layer. The process may be described using the followings:

- *Migration:* The hydrated metal ions in the solution migrate towards the cathode under the influence of impressed current as well as by diffusion and convection.
- *Electron transfer*: At the cathode surface, a hydrated metal ion enters the diffused double layer where the water molecules of the hydrated ion are aligned. Then the metal ion enters the Helmholtz double layer where it is deprived of its hydrate envelope. The dehydrated ion is neutralized and adsorbed on the cathode surface. The adsorbed atom then migrates or diffuses to the growth point on the cathode surface.

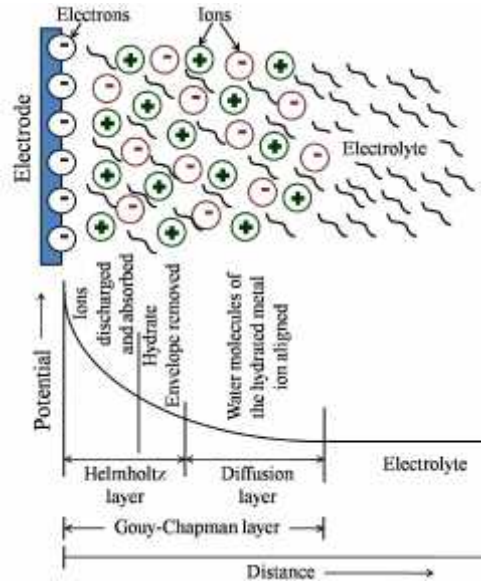

Figure 1.10. Electric double layers.

In a wider sense, all electron-transfer reactions are considered oxidation-reduction. The substance gaining electrons (oxidizing agent, or oxidant) oxidizes the substance that is losing electrons (reducing agent, or reductant). In the process, the oxidizing agent is itself reduced by the reducing agent. Consequently, the reduction process is sometimes called electronation, and the oxidation process is called ‘‘de-electronation.’’ Because a cathode is attached to the negative pole of the electric source, it supplies electrons to the electrolyte. On the contrary, an anode is connected to the positive pole of the electric source; therefore, it accepts electrons from the electrolyte. Various reactions take place at the electrodes during electrolysis. In general, reduction takes place at the cathode, and oxidation takes place at the anode

Thickness of the electroplated layer on the substrate is determined by the time duration of the plating. In other words, the longer the time the object remains in the operating plating bath, the thicker the resulting electroplated layer will be. Typically, layer thicknesses may vary from 0.1 to 30 microns. An electroplated layer is usually composed of a single

metallic element. Co-deposition of two or more metals is possible under suitable conditions of potential and polarization, such as a Cu-Zn alloy or Au-Sn alloy.

Electrodeposition has three main attributes that make it so well suited for nano-, bio- and microtechnologies.

- It can be used to grow functional material through complex 3D masks
- It can be performed near room temperature from water-based electrolytes
- It can be scaled down to the deposition of a few atoms or up to large dimensions

Electrodeposition has become an extensively used industry coating technology. Its applications are mainly in the following four groups:

1. *Decoration*: Coating a more expensive metal onto a base metal surface in order to improve the appearance. Applications are jewellery, furniture fittings, hardware and tableware of builders.
2. *Protection*: Corrosion-resistant coatings such as chromium plating of automobile parts and domestic appliances, zinc and cadmium plating of nuts, screws and electrical components. Wear-resistant coatings such as nickel or chromium plating of bearing surfaces and worn shafts.
3. *Electroforming*: Manufacture of sieves, screens, dry shaver heads, record stampers, moulds, and dies.
4. *Enhancement*: Coatings with improved electrical and thermal conductivity, solderability, reflectivity etc.

At the earlier stage of electrodeposition, two electrode systems were used. In such a system, the working electrode, which makes contact with the analyte, must apply the desired potential in a controlled way and facilitate the transfer of charge to and from the analyte. A second electrode acts as the other half of the cell. This second electrode must have a known potential to gauge the potential of the working electrode, furthermore it must balance the charge added or removed by the working electrode (Figure 1.11(a)).

While this is a viable setup, it has a number of shortcomings. Most significantly, it is extremely difficult for an electrode to maintain a constant potential while passing current to counter redox events at the working electrode. To solve this problem, the role of supplying electrons and referencing potential has been divided between two separate electrodes (Figure 1.11(b)). The reference electrode is a half cell with a known reduction potential. Its only role is to act as reference in measuring and controlling the working electrodes potential and at no point does it pass any current. The auxiliary electrode passes all the current needed to balance the current observed at the working electrode. To achieve this current, the auxiliary often swings to extreme potentials at the edges of the solvent window, where it oxidizes or reduces the solvent or supporting electrolyte. These electrodes: working, reference, and auxiliary make up the modern three electrode system.

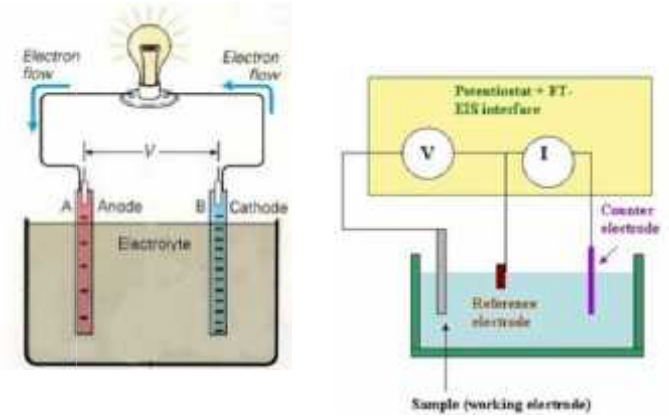

Figure 1.11. (a) Two electrode system and (b) Three electrode system

The morphology and composition of electrodeposits depend on:

- Current density
- Nature of the anions or cations in the solution
- Bath composition and temperature
- Solution concentration
- Power supply current waveform
- Presence of impurities
- Physical and chemical nature of substrate surface

To achieve desired electrodeposited materials of technological importance from electrodeposition, it is necessary to examine the details of the mechanism and all the required different parameters that would affect the process. For this purpose cyclic voltammetry technique is used. The study of cyclic voltammogram provides all the information necessary to select the appropriate potential for the reduction of a desired metal, individually, without the necessity of rigorously analyzing all the interactions involved.

Cyclic voltammetry falls into a class of potentiodynamic experimental methods. It is used for studying the redox properties of chemicals and interfacial structures. For the majority of experiments the electroactive species is in the form of a solution. This method uses a reference electrode, working electrode, and counter electrode. The three-electrode method is most widely used because the electrical potential of reference electrode does not change easily during the measurement. A supporting electrolyte is usually added to the test solution to ensure sufficient conductivity. The combination of the solvent, electrolyte and specific working electrode material determines the range of the potential.

From the earlier age aqueous medium has been frequently used for electroplating or electrodeposition which has certain draw backs. The notables are:

- Limited potential window restricts electrodeposition of certain metals

- Gas evolution processes can be technically difficult to handle and result in hydrogen embrittlement
- Passivation of metals can cause difficulties with both anodic and cathodic materials
- Complexing agents such as cyanide sometimes become necessary
- All water must eventually be returned to the water course.

These prevent aqueous solutions being applied to the deposition of several technically important materials [10]. This necessitates the use of alternate systems, such as nonaqueous electrolytes, ionic liquids and surfactant-based organized media such as, micelles, reverse micelles and microemulsions. In this study, surfactant- based organized media are introduced to deposit Co, Ni, Zn Cu and Sn. In the above sections, a brief introduction of such systems has been made.

1.6. Reactions for Kinetic Study

The alkaline hydrolysis of CV and acid hydrolysis of Bz may be chosen as model reactions for kinetic investigations. In fact, both of CV and Bz have proved themselves as potential substrates for kinetic studies.

CV is a carbocationic dye. The alkaline hydrolysis of CV (Figure 1.12) gives carbinol (CVOH) as a product which is a colorless form of CV. The reaction is reversible and its equilibrium constant in water is 4×10^4 [74]. In neutral media more than 99% of the compound exists as the colored carbocationic form, but at pH < 10 more than 99% exists as the colorless carbinol form.

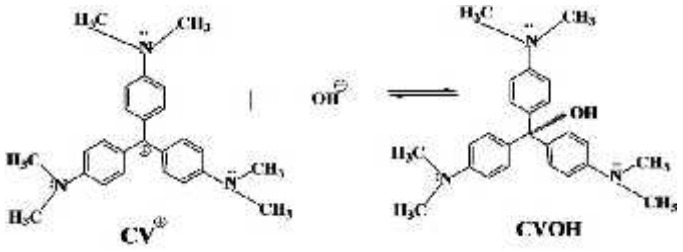

Figure 1.12. Alkaline hydrolysis of CV.

Bz, used as a psychotropic drug, undergoes acid-base hydrolysis in aqueous solution and study of this reaction, within the physiological pH range, is of great importance because the absorption of these drugs in the gastrointestinal tract is affected by the nature of the chemical species involved. The mechanism of acid hydrolysis of Bz changes with change in pH (Figure 1.13). At high pH (low $[H^+]$), the breakage of the ring is produced at the 1,2-amidic bonds, which is considered to be reversible. At low pH (high $[H^+]$), the rupture of remaining 1,2-amidic or 4,5-azomethine group and the formation of the final hydrolysis products, the 2-amino-5 substituted benzophenones and glycine derivatives.

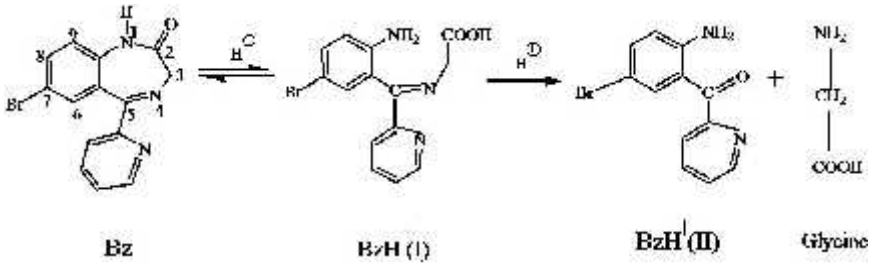

Figure 1.13. Acid hydrolysis of Bz.

It is worth noting that both of CV and Bz have good solubility in micelles, reverse micelles, and microemulsions of CTAB, SDBS/SDS and TX-100. The mechanism of alkaline hydrolysis of CV in aqueous solution is well established and the kinetics of the reaction can be conveniently measured using spectrophotometry. The change in reaction environment in different organized media thereby is likely to influence the reaction kinetics by changing the solubilization of the CV in different region of the media. The mechanism of acid hydrolysis of Bz is, on the other hand, a complicated one and changes with change in the pH of the reaction medium. The difference in the type and extent of products changes with change in acid concentration, and as a whole in the reaction environment. It is of great interest to see whether the change in reaction mechanism is evidenced in different organized media. The acid hydrolysis of Bz as well as alkaline hydrolysis CV may provide extensive and useful information to understand catalysis by micelles, reverse micelles and microemulsions.

1.7. Objectives of the Work

- To study the kinetics of the hydrolysis of CV and Bz in aqueous and micelles, reverse micelles and microemulsions of CTAB, SDS/SDBS and TX-100
- To study the different morphology of the electrodeposited Co, Cu, Ni, Zn and Sn in reverse microemulsions of CTAB and SDS
- To correlate the physicochemical properties of these media with the kinetic results of the hydrolysis reactions and the morphology of the electrodeposited metals

1.8. Present Work

Surface activity, associated with the interesting aggregation behavior in aqueous solutions and non-aqueous solutions has made surfactants important for diversified applications. It is of great importance to study the micellization behavior and the mechanistic details of the catalysis of reactions by micelles, reverse micelles and microemulsions. This prompted us to study the micellization behavior of surfactants, SDBS/SDS, CTAB and TX-100, the behavior in reverse micelles and microemulsions of CTAB and SDS in aqueous solution and non-aqueous solution and to determine the factors influencing these behaviors. The main focus is however, centered on the investigation of the kinetics of two model reaction, alkaline hydrolysis of CV and acid

hydrolysis of Bz in the present case and electrodeposition of metals in reverse microemulsions.

The work was initiated to have reliable data sets on the kinetics of the two-title reactions with changing the reaction environment by changing gradually the concentration of the mentioned surfactants. The interaction of two surfactants with the substrates, CV and Bz has been thoroughly checked. Finally, a complete comparison of the two surfactants in terms of the micellization behavior and catalytic/inhibitory action by micelles have been made to understand and to correlate the effect of the change in the nature of the surfactants with micellar catalysis.

In this present work, an attempt has also been made to make a comprehensive investigation of the kinetics of alkaline hydrolysis of CV and acid hydrolysis of Bz in reverse micelles and microemuslions of CTAB and SDS. The kinetic results in microemulsions have been compared and contrasted with the kinetic results of the reactions in aqueous solution, reverse micelles and micelles of CTAB and SDS. The aim was correlating micellization behavior of the different surfactants with the rate of the reactions in aqueous media and several compositions of reverse micelles and microemulsions. The fundamental physical properties of the micelles, reverse micelles and microemulsions have been studied and correlated with the kinetic behavior of the hydrolysis of Bz and CV in these organized media. The ultimate goal is to understand the mechanism of catalysis by *w*/*o* or *o*/*w* or *BC* microemulsions and reverse micelles of CTAB under different reaction environment.

The electrochemical behaviors of Co, Ni, Zn, Cu and Sn have been carried out in aqueous solution and reverse microemulsions of CTAB and SDS on CuE. The electrodeposition of these metals have been performed in reverse micelles of CTAB and SDS on CuE with different potentials and water to surfactant ratios to observed the change in morphology and microstructure of these metals. The elemental characterization of deposited metals was carried out by energy dispersive x-ray spectroscopic method and morphology and structures of the electrodeposited metals were examined by scanning electron microscopy

References

[1] M. J. Rosen, *Surfactants and interfacial phenomena*, John Wiley and Sons, 2004.

[2] K. L. Mittal, *Micellization, solubilization and microemulsion* Ed., Plenum Press, New York, V 1, 1979.

[3] D. Meyers, *Surfaces, interfaces and colloids*, VCH Publishers, Inc., New York, 1991.

[4] L .E. Scriven, in *Micellization, solubilisation and microemulsions*, K. L. Mittal (Ed.), Plenum, New York, 1977, 2, 877.

[5] T. P. Hoar, J. H. Schulman, *Transparent water-in-oil dispersions: the oleopathic hydro-micelle*, Nature, 1943, 152,102-103.

[6] P. Kumar, K. L. Mittal, *Handbook of microemulsion science and technology* Eds., M. Dekker, New York, 1999, 849.
[7] C. M. Starks, C. Liotta, *Phase transfer catalysis*, Academic Press: New York, 1978.
[8] S. L. Regen, *Triphase catalysis*, Angewandte Chemie International Edition, 1979, 18, 421-429.
[9] J. F Rusling, *Green synthesis via electrolysis in microemulsions*, Pure Applied Chemistry, 2001, 73, 1895-1905.
[10] F. Endres, M. Farlane, D. Abbott, *Electrodeposition from Ionic Liquids*, Wiley, 2008.
[11] N. Sakmeche, J-J Aaron, S. Aeiyach, P-C. Lacaze, *Usefulness of aqueous anionic micellar media for electrodeposition of poly-(3,4-ethylenedioxythiophene) films on iron, mild steel and aluminium*, Electrochimica Acta, 2000, 45, 1921-1931.
[12] D. A. Kaplin, S. Qutubuddin, *Electrodeposition of pyrrole into a porous film prepared by microemulsion polymerisation*, Synthetic metals, 1994, 63,187-194.
[13] A. Aragon, M. G. Figueroa, R. E. Gana, J. H. Zagal , *Effect of a polyethoxylate surfactant on the electrodeposition of tin*, Journal of Applied Electrochemistry, 1992, 22, 558-562.
[14] H. Zhou, C. Peng, S. Jiao, W. Zeng, J. Chen, Y. Kuang, *Electrodeposition of nanoscaled nickel in a reverse microemulsion*, Electrochemical Communication, 2006, 8, 1142-1146.
[15] X. Yang, S. Chen, S. Zhao, D. Li and Houyima, *Synthesis of copper nanorods using electrochemical methods*, Journal of the Serbian Chemical Society, 2003, 68, 843-847.
[16] F. Endres, S. Z. E. Abedin, *Air and water stable ionic liquids in physical chemistry*, Physical Chemistry Chemical Physics, 2006, 8, 2101-2116.
[17] J. M. Lehn, *Supramolecular chemistry*, Science, 1993, 260, 1762-1763.
[18] J. M. Lehn, *Supramolecular chemistry*, Wiley-VCH 1995.
[19] V. O. Gennady, D. N. Reinhoudt, I. W. Verboom, *Supramolecular chemistry in water*, Angewandte Chemie International Edition, 2007, 46, 2366-2393.
[20] D. C. Cullum, *Introduction to surfactant analysis*, Springer Science and Business Media, 1994.
[21] L. L. Schramm, E. N. Stasiuk ,D. G. Marangoni, *Surfactants and their applications*, Annual Reports Section "C" (Physical Chemistry), 2003, 99, 3-48.
[22] B. Lindman, *Surfactants,* T. F. Tadros (ed.): Academic Press, London, 2003, 1984.
[23] S. P. Moulik, *Micelles: self-organized surfactant assemblies*, Current Science, 1996, 71, 368-375.
[24] V. Mosquera, *A comparative study of the determination of the critical micelle concentration by conductivity and dielectric measurements*, Langmuir, 1998, 14, 4422-4426.
[25] G. S. Hartley, *Aqueous solutions of paraffin chain salts*, Hermann, Paris, 1936.
[26] Y. Chevalier, C. Chachaty, *NMR investigation of the micellar properties of monoalkylphoshpates*, Colloid and Polymer Science, 1984, 262, 489-496.

[27] J. N. Israelachvili, D. J. Mitchell, B. W. Ninham, *Theory of self-assembly of hydrocarbon amphiphiles into micelles and bilayers*, Journal of Chemical Society, Faraday Transactions 1, 1976, 72, 1525-1567.

[28] M. N. Khan, *Micellar catalysis*, Surfactant science series, Boca Raton, New York, London: CRC Press, Taylor and Francis Group, LLC, 2006, 133, 1-482.

[29] H. F. Eicke, P. Kvita, *In reverse micelles*, P. L. Luisi, B. E. Straub, Eds., Plenum Press, New York, 1984.

[30] F. M. Menger, C. E. Portnoy, *Chemistry of reactions proceeding inside molecular aggregates*, Journal of the American Chemical Society, 1967, 89, 4698-4703.

[31] C. A. Bunton , L. Robinson, *Micellar effects upon nucleophilic aromatic and aliphatic substitution*, Journal of the American Chemical Society, 1968, 90, 5972-5979.

[32] L. S. Romsted, in *Micellization, solubilization and microemulsion*, K. L. Mittal, ed., Plenum, New York, 1977, 2, 489-530.

[33] M. F. Neves, D. Zanette, F. Quina, M. T. Moretti, F. Nome, *Origin of apparent breakdown of the pseudophase ion-exchange model for micellar catalysis with reactive counter-ion surfactants*, Journal of Physical Chemistry, 1989, 93, 1502-1505.

[34] L. C. M. Ferreira, C. Zucco, D. Zanette, F. Nome, *Pseudophase ion-exchange model applied to kinetics in aqueous micelles under extreme conditions: a simple modification*, Journal of Physical Chemistry, 1992, 96, 9058-9061.

[35] A.V. Hill, *A new mathematical treatment of changes of ionic concentration in muscle and nerve under the action of electric currents*, *with a theory as to their mode of excitation*, The Journal of Physiology (Lond.), 1910, 40, 190-224.

[36] D. Piszkiewicz, *Positive cooperativity in micelle-catalyzed reactions*, Journal of the American Chemical Society, 1977, 99, 1550-1557.

[38] T. P. Hoar, J. H. Schulman, *Transparent water-in-oil dispersions: the oleopathic hydro-micelle*, Nature, 1943, 152, 102-103.

[39] G. M. Eccleston, *Emulsions and microemulsions: Encyclopedia of pharmaceutical Technology,* Marcel Dekker, NewYork, 1994, 9, 375-421.

[40] M. Shevachman, N. Garti, A. Shani, *Enhanced percutaneous permeability of diclofenac using a new U-type dilutable microemulsion*, Drug development and industrial pharmacy, 2008, 34, 403-412.

[41] M. J. Lawrence, G. D. Rees, *Microemulsions-based media as novel drug delivery systems*, Advanced Drug Delivery Reviews, 2000, 45, 89-121.

[42] J. H. Schulman, D. Stoekenius, L. M. Prince, *Mechanism of formation and structure of microemulsions by electron microscopy*, Journal of Physical Chemistry, 63, 1959, 1677-1680.

[43] J. Carlfors, I. Blute, V. Schmidt, *Lidocaine in microemulsions-a dermal delivery system*, Journal of Dispersion Science and Technology, 1991, 12, 467-482.

[44] S. Talegaonkar, A. Azeem, F. J. Ahmad, R. K. Khar, S. A. Pathan, Z. I. Khan, *Microemulsions: A novel approach to enhanced drug delivery*, Recent Patents on Drug Delivery and Formulation, 2008, 2, 238-257.

[45] P. K. Ghosh, R. S. Murthy, *Microemulsions: a potential drug delivery system,* Current Drug Delivery, 2006, 3, 167-180.

[46] D. Senatra, *Procedures for DSC analysis of percolative microemulsions*, Thermochimica Acta, 2000, 345, 39-46.

[47] W. Jahn, R. Strey, *Microstructure of microemulsions by freeze fracture electron microscopy*, The Journal of Physical Chemistry, 1988, 92, 2294 - 2301.

[48] W. Jahn, R. Strey, *Images of bicontinuous microemulsions by freeze fracture electron microscopy*, Physics of Amphiphilic Layers, 1987, 21, 353-356.

[49] M. Lagues, *Study of structure and electrical conductivity in microemulsions: Evidence for percolation mechanism and phase inversion*, Journal of Physics (France) Letters, 1978, 39, 487-491.

[50] M. Lagues, C. Sauterey, *Percolation transition in water in oil microemulsions. Electrical conductivity measurements*, The Journal of Physical Chemistry, 1980, 84, 3503-3508.

[51] B. Lagourette, J. Peyrelasse, C. Boned, *Bicontinuous structure zones in microemulsions*, Nature, 1979, 5726, 60-62.

[52] B. Moha-Ouchane, J. Peyrelasse, C. Boned, *Percolation transition in microemulsions: Effect of water-surfactant ratio, temperature, and salinity*, Physical Review A, 1987, 35, 3027-3032.

[53] B. Antalek, J. Williams, J. Texter, Y. Feldman, N. Garti, *Microstructure analysis at the percolation threshold in reverse microemulsions*, Colloids and Surfaces: A Physicochemical and Engineering Aspects A, 1997, 128, 1-11.

[54] H. F. Eicke, M. Borkovec, B. D. Gupta, *Conductivity of water-in-oil microemulsions: a quantitative charge fluctuation model*, The Journal of Physical Chemistry, 1989, 93, 314-317.

[55] N. Kallay, A. Chittofrati, *Conductivity of microemulsions: refinement of charge fluctuation model*, The Journal of Physical Chemistry, 1990, 94, 4755-4756.

[56] M. Giustini, G. Palazzo, G. Colafemmina, Monica, M. D. Marcello Giomini, C. Ceglie, *Microstructure and dynamics of the water-in-oil CTAB/n-pentanol/n-hexane/water microemulsion: A spectroscopic and conductivity study*, The Journal of Physical Chemistry, 1996, 100, 3190-3198.

[57] Y. Feldman, N. Kozlovich, I. Nir, N. Garti, V. Archipov, Z. Idiyatullin, Y. Zuev, V. Fedotov, *Mechanism of transport of charge carriers in the sodium bis(2-ethylhexyl) sulfosuccinate-water-decane microemulsion near the percolation temperature threshold*, The Journal of Physical Chemistry, 1996, 100, 3745-3748.

[58] R. T. Hamilton, J. F. Billman, E. W. Kaler, *Measurements of interdroplet attractions and the onset of percolation in water- in –oil microemulsions*, Langmuir, 1990, 6, 1696-1700.

[59] L. Garcia- Rio, P. Herves, J. R. Leis, J. C. Mujeto, *Influence of crown ethers and macrocyclic kryptands upon the percolation phenomenon in AOT/isooctane/H_2O microemulsions*. Langmuir, 1997, 13, 6083-6088.

[60] M. Borkovec, H. F. Eicke, H. Hammerich, B. D. Gupta, *Two percolation processes in microemulsions*, The Journal of Physical Chemistry, 1988, 92, 206-211.

[61] V. Papadimitriou, A. Xenakis, P. Lianos, *Electric percolation in enzyme-containing microemulsions*, Langmuir, 1993, 9, 912-915.

[62] S. K. Mehta, K. Bala, *Volumetric and transport properties in microemulsions and the point of view of percolation theory*, Physical Review E, 1995, 51, 5732-5737.

[63] G. S. Grest, I. Webman, S. A. Safran, A. L. R. Bug, *Dynamic percolation in microemulsions*, Physical Review A, 1986, 33, 2842-2845.

[64] A. L. R. Bug, S.A. Safran, G. S. Grest, I. Webman, *Do interactions raise or lower a percolation threshold*, Physical Review Letters, 1985, 55, 1896-1899.

[65] S.A. Safran, I. Webman, G. S. Grest, *Percolation in interacting colloids*, Physical Review A, 1986, 32, 506-511.

[66] C. Cametti, P. Codastefno, P. Tartaglia, S. Chen, J. Rouch, *Electrical conductivity and percolation phenomena in water-in-oil microemulsions*, Physical Review A. 1992, 45, 5358-5361.

[67] P. Pitzalis, A. Angelico, O. Soderman, M. Monduzzi, *A structural investigation of Ca AOT/water/oil microemulsions*, Langmuir, 2000, 16, 442-450.

[68] P. D. I. Fletcher, A. M. Howe, B. R. Robinson, *The kinetics of solubilizate exchange between water droplets in water in oil microemulsions*, Faraday Transactions I, 1987, 83, 985-1006.

[69] S. Bhattacharya, J. P. Stokes, M. W. Kim, J. S. Huang, *Percolation in an oil-continuous microemulsion*, Physical Review Letters, 1985, 55, 1884-1857.

[70] K. Holmberg, *Organic reactions in microemulsions*, Current Opinion in Colloid and Interface Science, 2003, 8, 187-196.

[71] L. Mukherjee, N. Mitra, P. Bhattacharya, S. P. Moulik, *Kinetics in microemulsion medium. 4. Alkaline fading of crystal violet in aqueous (H_2O/aerosol OT /isooctane and H_2O/aerosol OT/decane) and nonaqueous (ethylene glycol/ aerosol OT/isooctane) microemulsions*, Langmuir, 1995, 11, 2866-2871.

[72] J. Sjoblom, R. Lindberg, S. E. Friberg, *Microemulsion-phase equilibria characterizatin, structure, applications and chemical reactions*, Advances in Colloid and Interface Science, 1996, 95,125-287.

[73] U. Landau, in *Electrochemistry in industry: New directions*, U. Landau, E. Yeager, D. Kortan (Eds.), Plenum Press, New York, 1982.

[74] C. D. Ritchi, *Cation-anion combination reactions. XIII. Correlation of the reactions of nucleophiles with esters*, Journal of American Chemical Society, 1975, 97, 1170-1179.

Abstract

Physicochemical properties of micelles, reverse micelles and microemulsions of CTAB, SDS/SDBS and TX-100 have been investigated by measurements of turbidity, conductivity, density, viscosity, refractive index and surface tension/interfacial tension. The CMC of CTAB and SDBS/SDS were determined by conductivity method; while the CMC of TX-100 was determined by fluorescence method. The turbidity, conductivity, viscosity, refractive index and density increase, while surface tension decreases to attain a limiting value with increasing concentration of CTAB or SDS or TX-100. In reverse micelles and microemulsions of CTAB and SDS, the conductivity, viscosity and density increase and the refractive index decreases. The interfacial tension at first decreases and then increases with ϕ_W or w_o. Three different microstructure regions (such as *w*/*o*, *BC* and *o*/*w* phases) in reverse micelles and microemulsions with increasing ϕ_W or w_o could be established from viscosity results. The reverse micelles and microemulsions were stable at room temperature for about one year as monitored by visual inspection. The transparency and homogeneity of these reverse micelles and microemulsions were observed by measuring % transmittance at 650 nm and centrifugation, respectively. The nanometer droplet sizes of reverse micelles and microemulsions were measured by dynamic light scattering method.

2.1. Introduction

Micelles, reverse micelles and microemulsions are self organized media of a surfactant which have special properties such as low viscosity, ultralow interfacial tension, optical transparency and thermodynamic stability etc [1].

Micelles and reverse micelles are colloidal aggregates of a surfactant in polar and nonpolar media, respectively whereas microemulsions are mixtures of oil, water and surfactant with or without the assistance of cosurfactants. They are thermodynamically stable, in other words, the stability of microemulsions formed under a given condition of temperature and pressure is time independent. The stability of microemulsions is due to the presence of surfactant or a mixture of surfactant and co-surfactant that brings down the water/oil interfacial tension to a very low value. Originally, it was thought that there exists a negative interfacial tension which imparts stability to microemulsions [2]. The droplet sizes of microemulsions are <100 nm which is much below the wavelength of visible light to pass through the dispersed system making it optically transparent or translucent [3].

The physicochemical properties of micelles, reverse micelles and microemulsions are of great importance as they are used in various applications such as chemical reactions, nanoparticle synthesis, drug delivery etc. Furthermore, the microstructures of microemulsions can be determined by transport properties. The transport properties of microemulsions are measured by conductivity and viscosity. Investigations on transport

of ions in microemulsions can provide information on their internal dynamics as well as the microstructures. For *o*/*w* system, the continuum is aqueous and the conductance is fairly large and very nominally depends on oil concentration. This is quite opposite for *w*/*o* systems, where conductance is appreciably dependent on overall composition or w_o. Two mechanisms are under active consideration for such ion transport in *w*/*o* microemulsion systems with respect to ϕ_W or w_o medium in microemulsions:

- The droplets associate and surfactant ions hop from droplet to droplet manifesting large increase in conductance (Scheme 2.1).
- The droplets coalesce or fuse and transfer of ions takes place followed by fission of associated droplets (Scheme 2.2) [4].

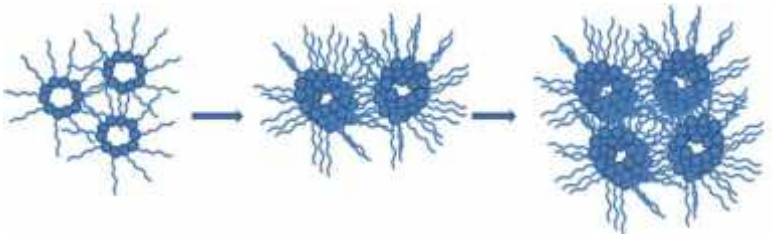

Scheme 2.1. Droplet association mechanism.

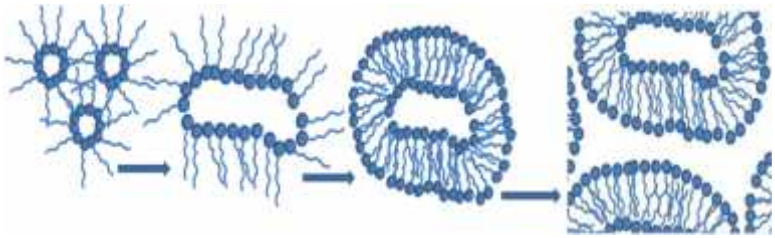

Scheme 2.2. Fusion-fission droplets mechanism.

Microemulsions are usually Newtonian fluids with low viscosity. Typically, the viscosity of microemulsion increases with the volume fraction of water that can be properly described by theoretical models based on the assumption of a rigid spherical dispersed phase. Nevertheless, for high concentrations and temperatures, attractive interactions among droplets favor a reversible droplets clustering that causes a viscosity increase. Consequently, though for low temperatures, microemulsion viscosity can be properly described by models based on the rigid sphere hypothesis, when temperature approaches a critical value, these models fail and viscosity increase with dispersed phase volume fraction is much more pronounced [5, 6]. The optical properties and transparency of microemulsions are measured by refractive index. The refractive index of microemulsions does not show any structural changes [7].

Research to date includes numerous attempts to explore the physicochemical properties of micelles, reverse micelles and microemulsions by using different experimental

methods. The reverse micelles and microemulsions are characterized by measuring conductivity [8-24], viscosity [9-22], refractive index [7], dynamic light scattering [10], cyclic voltammetry [10, 11], interfacial tension [13], turbidity [14-17], ultrasonic velocity and density [18, 19] to establish different microstructures in various regions. In order to use microemulsions as drug delivery systems, the pH [20-22] and zeta- potential [23, 24] were also measured in addition to the above properties. The direct images of microemulsions were observed by freeze fracture electron microscopy [25, 26] to characterize the size and shape of aggregates in microemulsions. Among these small-angle x-ray scattering, small angle neutron scattering, NMR-self diffusion and conductivity proved to be most useful, drawing conclusions on the characteristic sizes and connectivity of the water and oil rich domains [27]. The differential scanning calorimetry measurement of microemulsions identifies the free and bound water in different types of microemulsions [28, 29].

Despite numerous studies, there is still the need for a considerable amount of fundamental work for characterizing the physicochemical behaviors of microemulsions for their potential use in manifold applications. In this work, the micelles, reverse micelles and microemulsions of CTAB and SDS were characterized by measuring physicochemical properties, which include: turbidity, conductivity, density, viscosity, refractive index and interfacial tension. The droplet size of these reverse micelles and microemulsions was also measured by dynamic light scattering (DLS) method. Furthermore, the microstructures and different phase transitions with ϕ_W or w_o were established by using these physicochemical properties of reverse micelles and microemulsions which can help to create a medium for specific applications in multidisciplinary areas.

2.2. Experimental

2.2.1. Materials and Methods

CTAB (E. Merck), SDS/SDBS (Sigma) and TX-100) (Sigma), 1-butanol (Merck), cyclohexane (Merck) were used as received without further purification. Solutions were prepared with double distilled de-ionized water (conductivity: 0.055 μScm^{-1} at 25.0 °C) from HPLC grade water purification systems (BOECO, Germany).

The aqueous solutions with CTAB, SDBS/SDS and TX-100 were prepared by dissolving varying amount of surfactants in de-ionized water. The CTAB/1-butanol/cyclohexane/water microemulsions were prepared at fixed CTAB (20 %wt.) and cyclohexane (0 and 3.4 %wt.) with different water and 1-butanol contents that ranged from high water to high alcohol content. The SDS/1-butanol/cyclohexane/water microemulsions were prepared at fixed SDS (15 %wt.) and cyclohexane (0 and 20 %wt.) with different water and 1-butanol contents that ranged from high water to high 1-butanol

content. De-ionized double distilled water with specific conductivity < 0.5×10^{-6} Scm^{-1} at 25 ^{o}C was used for this purpose. The ϕ_W is calculated from the following equation,

$$\phi_W = \frac{V_{Water} w_o}{V_{Surfactant} + V_{Water} w_o} \phi_{Water+Surfactant}$$

w_o = water to surfactant ratio = [water]/[surfactant], V = molar volume, $\phi_{Water+surfactant}$ = volume fractions of dispersed phase [30].

Fluorescence experiments were carried out by employing a fluorescence spectrophotometer (Hitachi, Model F-7000). Rectangular quartz cells were used throughout the experiments. Pyrene was used as a probe at a fixed concentration of 1.0 M and was excited at 337 nm. The excitation and emission slit widths were maintained at 5.0 nm. The emission spectrum was scanned over the range 360–500 nm. Due to low solubility of pyrene in water a sonicator (LU-2, Labnics, USA) was used to prepare the stock solution.

The homogeneity of the microemulsions was checked using centrifugation. The effective gravitational force on a test tube can be increased so as to more rapidly and completely cause the precipitate to gather on the bottom of the tube if the system is not stable. Centrifugation was carried out in this study at 3000 rpm for 15 minutes using a centrifuge CENCOM II (230VAC Spain).

The isotropic nature of micelles, reverse micelles and microemulsions and their optical clarity was studied by measuring percentage transmittance through a double beam Shimadzu UV visible spectrophotometer (UVD - 3500), equipped with a thermo-regulated cell compartment (temperature control over ± 0.1 ^{o}C). Rectangular quartz cells of path length 1 cm were used throughout the investigation. Percentage transmittance of samples was measured at 650 nm using pure water taken as reference.

Turbidity, the measure of relative clarity of a liquid, was measured for micelles, reverse micelles and microemulsions with Shimadzu UV visible spectrophotometer (UVD-3500) which reads absorbance (defined as log (I_0/I) where I_0 and I are the incident and transmitted light intensities, respectively). The turbidity (defined by $I = I_0 \exp(-\tau l)$ where l is the path length) is related to the sample absorbance measured at a wavelength at which there is no molecular absorption according to τl = 2.303 × absorbance [18, 31].

Specific conductivity of micelles, reverse micelles and microemulsions was measured with a digital conductivity meter (JENWAY, Model 4510, UK) equipped with a dip-type pre-calibrated cell at 25.0 °C.

Viscosity of micelles, reverse micelles and microemulsions was measured with AntonPaar (Lovis 2000M/ME) microviscometer which measures viscosity by rolling ball principle with an accuracy of ± 10^{-6} mPa s. Capillary with diameter 1.5 mm and a steel ball with maximum measurement deviation 0.2% were used for measurement. The capillary was calibrated with supplied S3 oil. The measuring angle was 60^{o}. The temperature of the apparatus was controlled automatically within ± 0.01 K by a built-in Peltier device.

Density of micelles, reverse micelles and microemulsions was measured with AntonPaar vibrating-tube density meter (DMA 4500 ME), based on oscillating U-tube method. The densities were measured directly from density meter reading. The temperature of the apparatus was controlled automatically within ± 0.01 K by a built-in Peltier device.

Surface tension/interfacial tension of micelles, reverse micelles and microemulsions was measured by a sigma force tensiometer (Model: Attension Sigma-701, KSB Instruments, Finland) with a platinum Wilhelmy plate. The accuracy of the measurements, checked by replicate experiments and by frequent measurement of the interfacial tension of pure water, was ± 0.1 mN m^{-1}.

Refractive index of micelles, reverse micelles and microemulsions was directly measured with Abbemat 300 refractometer having high resolution optical sensor. Measurements were made with a resolution and limit error ± 10^{-5}. The temperature of the apparatus was controlled automatically within ± 0.01 K by a built-in Peltier device.

Z-average diameter of different reverse micelles and microemulsions droplets was measured using a Zetasizer Nano ZS90 (ZEN3690, Malvern Instruments Ltd, UK) by DLS. The particle size detection limit was about 0.3 nm - 5μm (diameter) and accuracy of the Z-average diameter determined has been ± 2%. A He-Ne laser of 632.8 nm wavelength was used and the measurements were made at a fixed scattering angle of 90°. The refractive index of each solution was recorded with an Abbemat 300 refractometer having high resolution optical sensor. Viscosity data, as obtained from viscosity measurements, were also used for interpretation of DLS data. Samples were filtered using VALUPREP 0.45 μm poly(terta fluoro ethylene) (PTFE) filter and the Z-average diameters were determined from cumulants mean of the intensity average of 50 runs and the reproducibility was checked from at least 3 measurements. The temperature of the apparatus was controlled automatically within ± 0.01 K by a built-in Peltier device.

2.3. Results and Discussion

2.3.1 The CMC of CTAB, SDBS/SDS and TX-100 in Aqueous Solution

The CMC of SDBS/SDS and CTAB were determined by specific conductivity method whereas the CMC of TX-100 was determined by fluorescence method using pyrene

probe. The variation in specific conductivity with change in concentrations of aqueous solutions of CTAB and SDBS/SDS were measured to determine the CMC. The experimental specific conductivity values of CTAB or SDBS/SDS lie on two straight lines and their point of intersections gave the CMC value for CTAB or SDBS/SDS in aqueous solution. The CMC value at 25 ^{o}C has been found to have value of 0.87 mM [32], 2.07 mM [33] and 8.2 mM [33] for CTAB, SDBS and SDS in aqueous solution, respectively which are in good agreement with literature data [34, 35].

The variation in fluorescence intensity ratio with change in [TX-100] was measured to determine the CMC. The emission spectra show three different peaks and the ratio of the intensity of the 1st peak (I_1) and the 3rd peak (I_3) was used for the determination of the CMC. Figure 2.3.1 shows the fluorescence spectra of 1.0×10^{-6} M pyrene in different [TX-100] and a typical plot of the I_1/I_3 ratio for pyrene vs. [TX-100], respectively. From the curve the CMC of TX-100 is measured at a value of 0.22 mM at 25 ^{o}C.

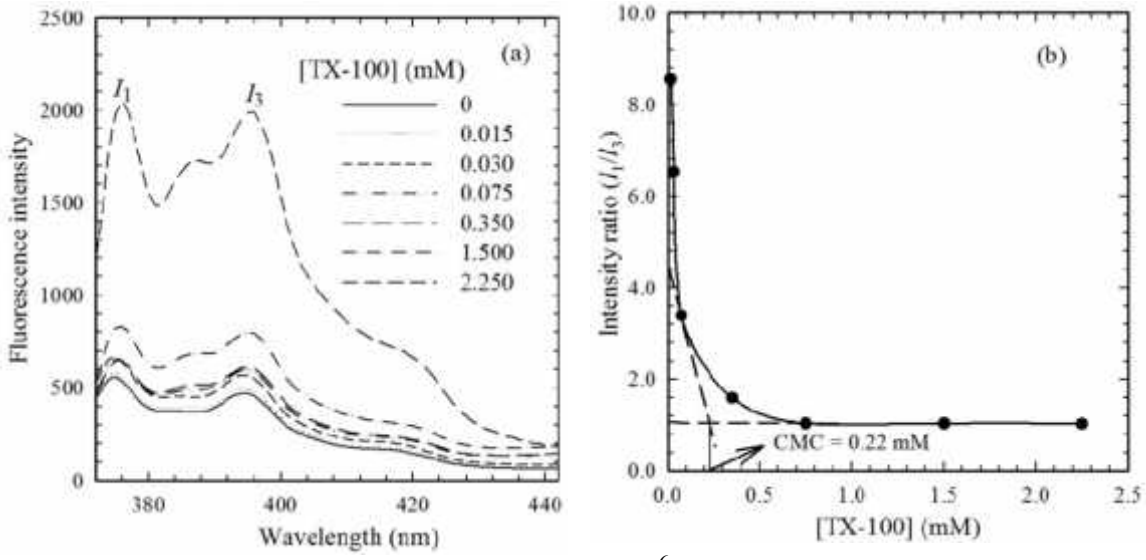

Figure 2.3.1. (a) The fluorescence spectra of 1.0×10^{-6} M pyrene in different [TX-100] and (b) changes in the I_1/I_3 ratio of 1.0×10^{-6} M pyrene with increasing [TX-100].

2.3.2. Physicochemical Properties of Micelles, Reverse Micelles and Microemulsions of CTAB

2.3.2.1. Stability and Homogeneity

The CTAB/1-butanol/cyclohexane/water microemulsions and CTAB/1-butanol/water reverse micelles were stored at different temperature for one year and observed that they were stable after one year. The shelf lives of the stored microemulsions were evaluated by visual inspection (phase separation) and % transmittance [36]. They were centrifuged at rpm 3,000 for 30 minutes at room temperature and observed for any change in homogeneity of microemulsions and reverse micelles.

2.3.2.2. Optical Transparency

The percentage of transmittance of the micelles, reverse micelles and microemulsion of CTAB were checked at 650 nm and the % transmittance of aqueous solution containing CTAB at different concentrations are shown in Figure 2.3.2. The % transmittance increases up to the CMC of CTAB and then gradually decreases. This corresponds to the formation of CTAB micelles. The % transmittance of CTAB/1-butanol/cyclohexane/water microemulsions and CTAB/1-butanol/water reverse micelles were close to 98.8-99.6% which indicates the optical clarity of these reverse micelles and microemulsions of CTAB.

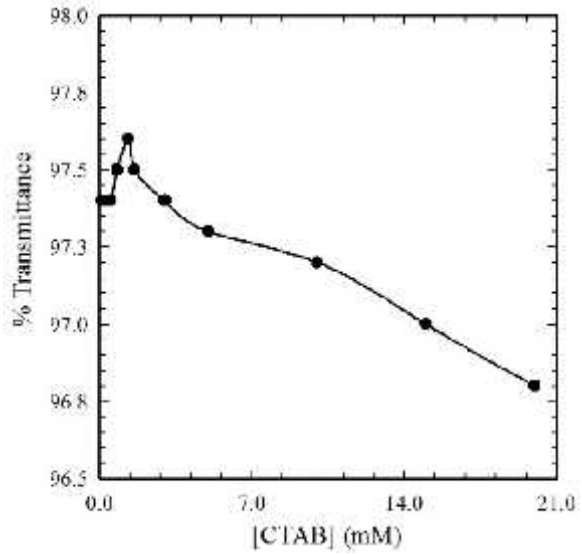

Figure 2.3.2. Transmittance as a function of CTAB concentration.

2.3.2.3. Turbidity

Figure 2.3.3 represents the change in turbidity with increasing [CTAB]. Turbidity decreases up to a certain concentration of CTAB and then increases with increasing [CTAB]. CTAB concentration at which turbidity begins to increase sharply clearly represents the concentration at which aggregation of individual CTAB into micelles is commences to a significant extent. The concentrations, as obtained from turbidity results, also have been chosen as the CMC [37]. Figure 2.3.4 shows the turbidity of CTAB/1-butanol/cyclohexane/water microemulsions and CTAB/1-butanol/water reverse micelles with increasing the ϕ_W or w_o.

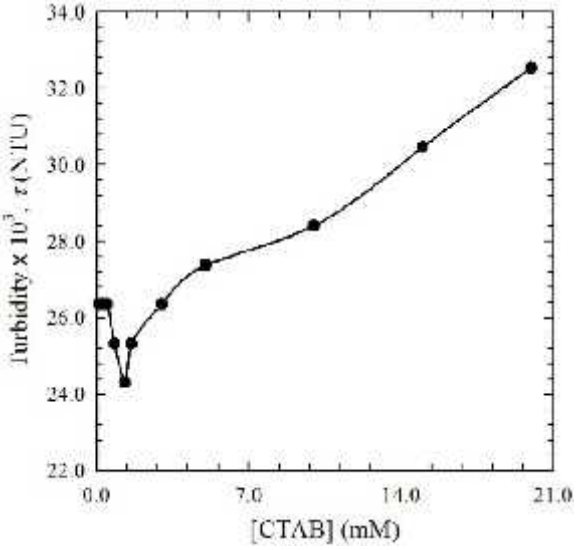

Figure 2.3.3. The turbidity as a function of CTAB concentration.

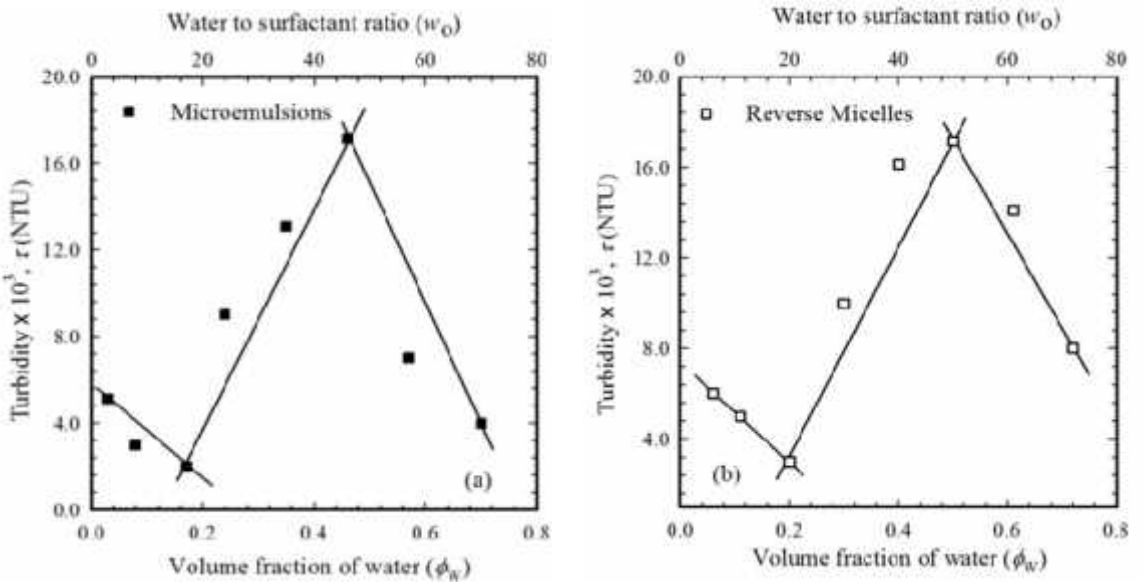

Figure 2.3.4. Turbidity of (a) CTAB/1-butanol/cyclohexane/water microemulsions and (b) CTAB/1-butanol/water reverse micelles as a function of w_o or ϕ_W.

The turbidity decreases up to $\phi_W = 0.17$ ($w_o = 19.7$) and $\phi_W = 0.20$ ($w_o = 23.2$) then increases for $\phi_W = 0.17 \sim 0.46$ ($w_o = 19.7 \sim 50.1$) and $\phi_W = 0.20 \sim 0.50$ ($w_o = 23.2 \sim 53.5$) and finally increases again after $\phi_W = 0.46$ ($w_o = 50.1$) and $\phi_W = 0.50$ ($w_o = 53.5$) for microemulsions and reverse micelles, respectively. Decreased turbidity values up to $\phi_W = 0.17$ and $\phi_W = 0.20$ are due to electrostatic repulsions between the water droplets in *w*/*o* microemulsions and the turbidity increase for $\phi_W = 0.17 \sim 0.46$ and $\phi_W = 0.20 \sim 0.50$ are caused by either droplet growth by coalescence, increased attractive interactions, or a

combination of the two effects. Above ϕ_W = 0.46 and ϕ_W = 0.50, the electrostatic repulsions in *o*/*w* microemulsions of CTAB causes decrease in turbidity [31].

2.3.2.4. Specific Conductivity

The specific conductivity increases with the increasing [CTAB]. The specific conductivity - [CTAB] profile lie on two straight lines and their point of intersection gave the CMC value for CTAB in aqueous solutions. The CMC value at 25 ^oC has been found to have a value of 0.87 mM for CTAB aqueous solutions, which is in good agreement with literature [32, 38]. Figure 2.3.5 shows change in specific conductivity of CTAB/1-butanol/cyclohexane/water microemulsions and CTAB/1-butanol/water reverse micelles with increasing ϕ_W or w_o.

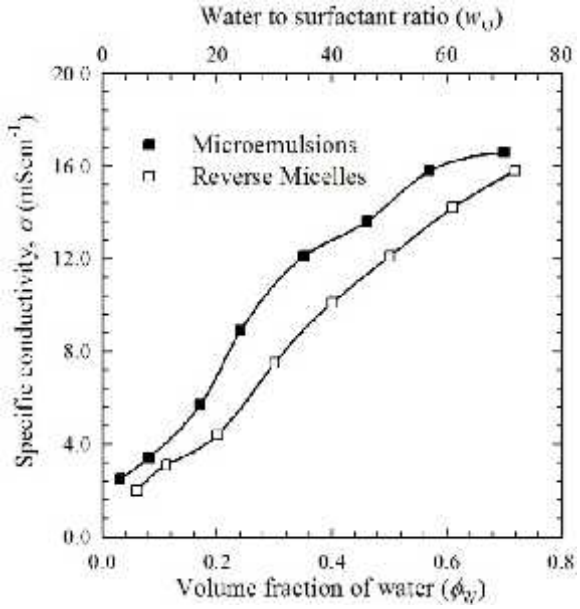

Figure 2.3.5. Specific conductivity of CTAB/1-butanol/cyclohexane/water microemulsions and CTAB/1-butanol/water reverse micelles as a function of w_o or ϕ_W.

Conductivity of the reverse micelles and microemulsions increases with ϕ_W or w_o that indicates an increase in the number of conducting species in the systems [39]. At lower value of ϕ_W or w_o, the value of conductivity is low to indicate that the hydrophilic head groups and counterions of CTAB in contact with the water droplets of CTAB/1-butanol reverse micelles (*w*/*o* microemulsions) are not easily dissociated. At higher value of ϕ_W or w_o, CTAB micelles (*o*/*w* microemulsions) are formed in water and orientation of CTAB changes where the hydrophilic head groups and counterions are freely dissociated into water and increases the specific conductivity. In middle portion, conductivity increase corresponds to the network of the conductive channel (*BC* microemulsions) formed by the aggregation of water and 1-butanol droplets [39].

2.3.2.5. Viscosity

In aqueous solution of CTAB, viscosity increases sharply with increasing [CTAB] [40] and at a concentartion close to the CMC, a sudden change is noticeable after which the viscosity further shows linear increase. This is ascribable to the fact that with increasing [CTAB], the number of micelle increases resulting in an increase in viscosity. Figure 2.3.6 shows the change in viscosity with ϕ_W or w_o for CTAB/1-butanol/cyclohexane/water microemulsions and CTAB/1-butanol/water reverse micelles.

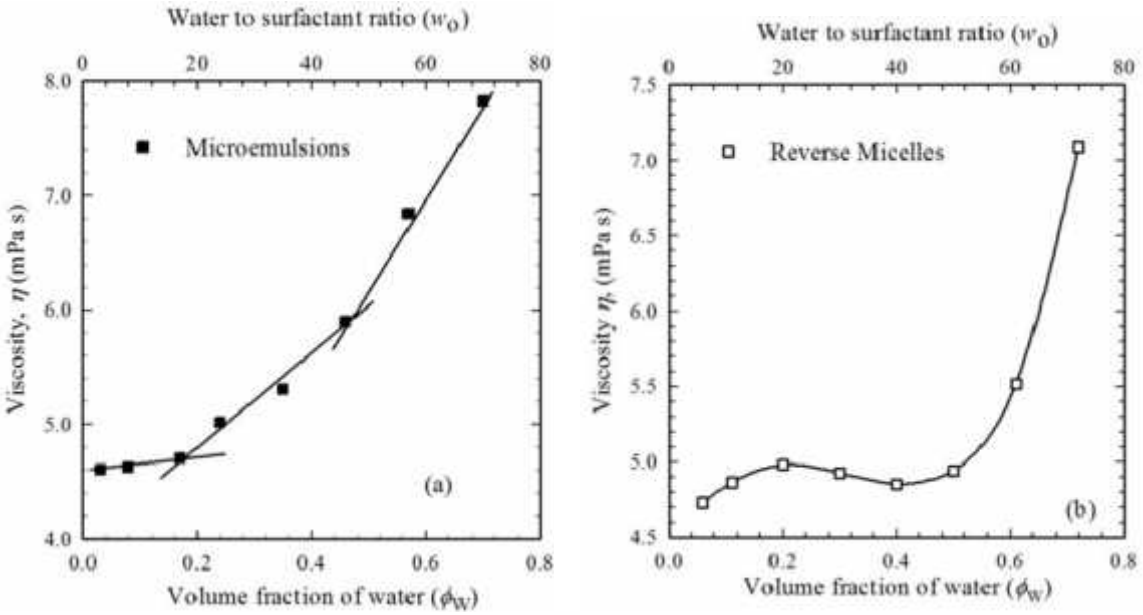

Figure 2.3.6. Viscosity of (a) CTAB/1-butanol/cyclohexane/water microemulsions and (b) CTAB/1-butanol/water reverse micelles as a function of w_o or ϕ_W.

Viscosity of the reverse micelles and microemulsions was very low, less than 120 mPa s which is in agreement with the literature [41]. In CTAB/1-butanol/cyclohexane/water microemulsions (Figure 2.3.6 (a)) at $\phi_W < 0.17$ ($w_o < 19.7$), viscosity increases slightly while for $\phi_W = 0.17 \sim 0.46$ ($w_o = 19.7 \sim 50.1$), it increases gradually whereas at $\phi_W > 0.46$ ($w_o > 50.1$), a sharp increase is apparent and in CTAB/1-butanol/water reverse micelles (Figure 2.3.6(b)), at $\phi_W < 0.20$ ($w_o < 23.2$), the viscosity shows only a very slight increase, while for $\phi_W = 0.20 \sim 0.50$ ($w_o = 23.2 \sim 53.5$), the value decreases slightly and at $\phi_W > 0.50$ ($w_o > 53.5$), a sharp increase is noticeable. The increase in viscosity with addition of water has been ascribed to the increasing diameter of water filled conduits in the *BC* and *o*/*w* microemulsions [41]. The initial increase in viscosity - ϕ_W profile corresponds to the aggregation and attractive interaction of water droplets in CTAB/1-butanol reverse micelles (*w*/*o* microemulsions). With further increase in ϕ_W upto 0.46 (w_o = 50.1), the water and 1-butanol droplets of CTAB micelles and reverse micelles coagulate to form clusters (i.e. *BC* region) where the gradual increase and decrease in viscosity for microemulsions and reverse micelles, respectively is apparent [39]. After ϕ_W

= 0.46, the viscosity increases sharply due to the presence of 1-butanol droplets in CTAB/water micelles (*o*/*w* microemulsions) as the viscosity of water is higher than the1-butanol.

2.3.2.6. Density

The density of 1-butanol (0.8089 gcm^{-3}) is less than that of water (0.9940 gcm^{-3}) at 25 ^{o}C. The addition of CTAB in water raises the corresponding density values. For example, when 20 %wt. of CTAB was added to water, the density was found to be 0.9969 gcm^{-3} at 25 ^{o}C. Figure 2.3.7 shows the change in density of CTAB/1-butanol/cyclohexane/water microemulsions and CTAB/1-butanol/water reverse micelles with respect to ϕ_W or w_o.

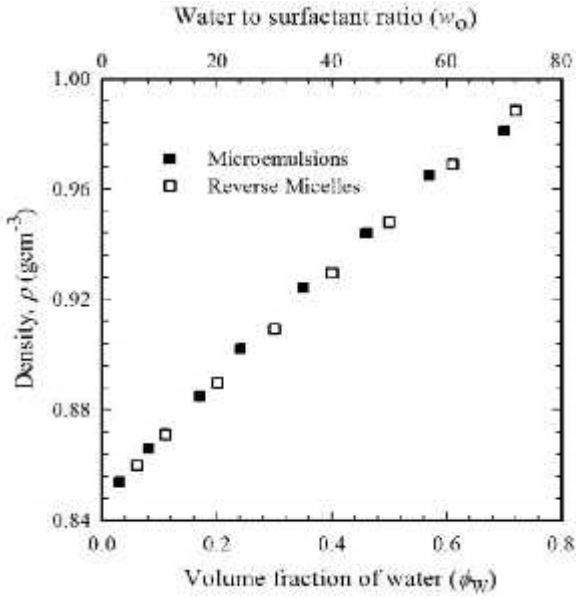

Figure 2.3.7. Density of CTAB/1-butanol/cyclohexane/water microemulsions and CTAB/1-butanol/water reverse micelles as a function of w_o or ϕ_W.

Density of aqueous solutions of CTAB increases with increase in [CTAB] [40] and the density of the reverse micelles and microemulsions also increases with ϕ_W or w_o. In microemulsions and reverse micelles of CTAB, a transition from reverse micellar phase (*w*/*o*) to micellar phase (*o*/*w*) is apparent (*vide supra*). Since at low value of ϕ_W or w_o, the proportion of reverse micelles is much higher than that of micelles which increases the volume of the solution and the density value is low while at high value of ϕ_W or w_o, the number of micelles is higher and the density increases.

2.3.2.7. Surface Tension/Interfacial Tension

With the addition of CTAB, a linear decrease in surface tension is apparent in aqueous solution. The surface tension - log [CTAB] shows a linear decrease up to the CMC, after which no considerable change in surface tension could be marked. The line of intersection gave the CMC value for CTAB in aqueous solutions. The CMC value at 25

°C was 0.85 mM which is in accordance with the conductivity results and in good agreement with literature data [38, 40]. Figure 2.3.8 shows the change of interfacial tension in CTAB/1-butanol/cyclohexane/water microemulsions and CTAB/1-butanol/water reverse micelles with ϕ_W or w_o.

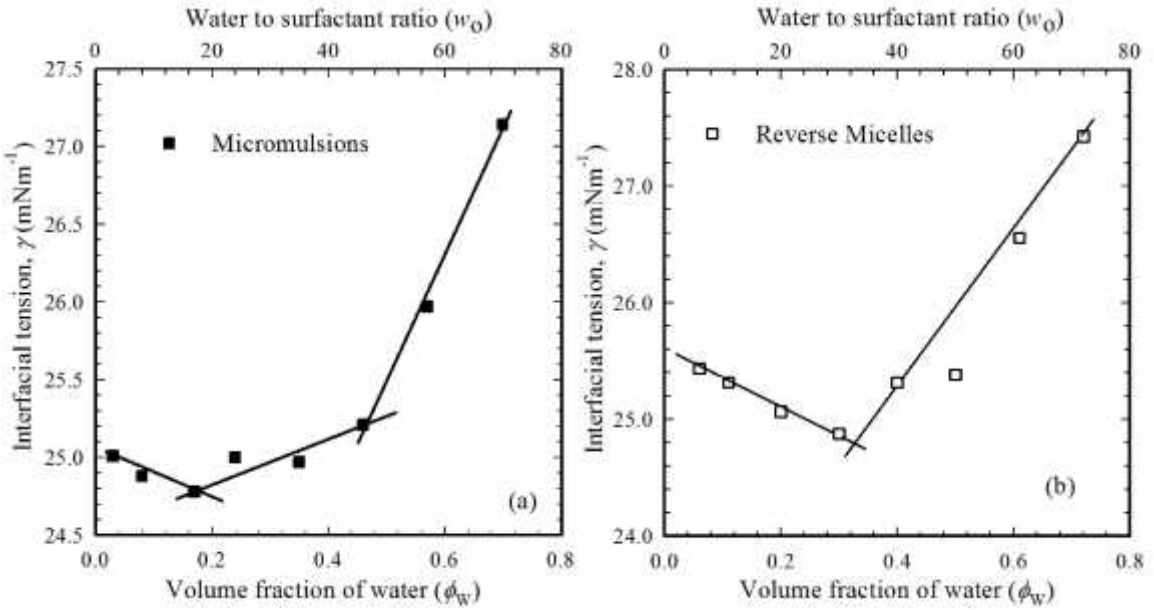

Figure 2.3.8. Interfacial tension of (a) CTAB/1-butanol/cyclohexane/water microemulsions and (b) CTAB/1-butanol/water reverse micelles as a function of w_o or ϕ_W.

In CTAB/1-butanol/cyclohexane/water microemulsions (Figure 2.3.8 (a)), the interfacial tension decreases up to $\phi_W = 0.17$(w_o= 19.7), increases after $\phi_W = 0.46$ (w_o = 50.1) while for ϕ_W = 0.17 ~ 0.46 (w_o = 19.7 ~ 50.1), the interfacial tension slightly increases with increasing ϕ_W. The sharp decrease in interfacial tension up to $\phi_W = 0.17$ with increasing ϕ_W might be due to a weakening of hydrophobic-hydrophobic interactions existing in cyclohexane-1-butanol and development of weaker hydrophobic-hydrophilic interactions between cyclohexane, 1-butanol and water. With increasing ϕ_W, development of hydrophilic-hydrophilic interaction between CTAB, 1-butanol and water caused a constant increase in interfacial tension for ϕ_W = 0.17 ~ 0.46. After ϕ_W = 0.46, the interfacial tensions increase sharply due to diminishing stronger hydrophobic-hydrophobic interaction of cyclohexane-1-butanol and developing stronger hydrophilic-hydrophilic interaction of CTAB, water and 1-butanol [42].

In CTAB/1-butanol/water reverse micelles (Figure 2.3.8 (b)), the interfacial tension decreases up to $\phi_W = 0.32$ (w_o= 33.3) and then increases. The sharp decrease in interfacial tension is due to the weaker hydrophobic-hydrophobic interactions between CTAB and 1-butanol with increasing water and the interfacial tensions increase sharply due to stronger hydrophilic-hydrophilic interaction of CTAB, water and 1-butanol [42].

2.3.2.8. Refractive Index

The refractive index of de-ionized water is 1.33256 at 25 °C. The refractive index of aqueous solution with the addition of 20 %wt. CTAB is 1.36878. This is indicative of the formation of larger number of micelles and with further addition of CTAB more micelles can refract more light [40]. Figure 2.3.9 shows the change in refractive index of CTAB/1-butanol/cyclohexane/water microemulsions and CTAB/1-butanol/water reverse micelles with ϕ_W or w_o. The refractive index specifies the transparency of the reverse micelles and microemulsions. With increasing ϕ_W, the refractive index decreases monotonically. As the refractive index is a property sensitive to structural transitions, the results suggests that no structural modifications are involved [7], i.e., the water and 1-butanol remain encapsulated into the CTAB/1-butanol reverse micelles (low ϕ_W) and CTAB/water micelles (high ϕ_W), respectively.

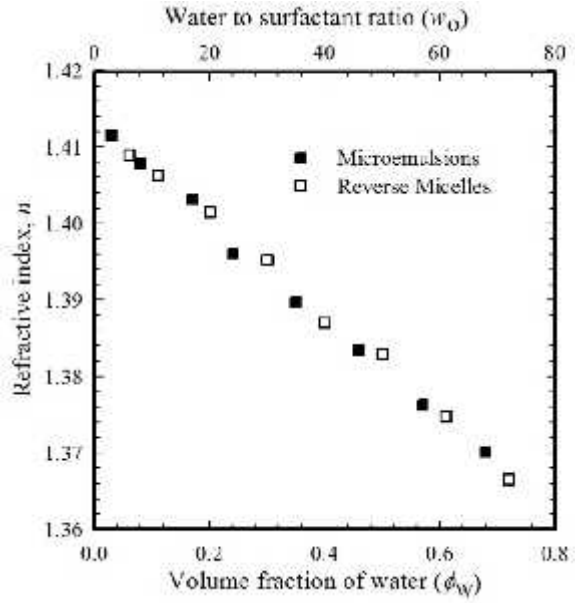

Figure 2.3.9. Refractive index of CTAB/1-butanol/cyclohexane/water microemulsions and CTAB/1-butanol/water reverse micelles as a function of w_o or ϕ_W.

2.3.2.9. Molar Refractivity and Polarizability

Molar refractivity (R) for the reverse micelles and microemulsions were calculated by using Lorentz-Lorentz equation,

$$R = [(n^2 - 1)/(n^2 + 2)]/V_m \quad \text{..... (2.1)}$$

where, V_m (= M/ρ) is the molar volume and n is the refractive index of reverse micelles and microemulsions [43]. The molar refractivity is related to the electronic polarizability,

$$R = 4/3\pi N_A \alpha_e \quad \text{..... (2.2)}$$

N_A = Avogadro's constant (= 6.023 × 10^{23}) [44]. Figure 2.3.10 shows the calculated value of molar refractions (R) and electronic polarizability (α_e) for CTAB/1-butanol/cyclohexane/water microemulsions and CTAB/1-butanol/water reverse micelles. Molar refraction and electronic polarizability reverse micelles and microemulsions also decrease with increasing w_o or ϕ_W in reminiscent to refractive index results.

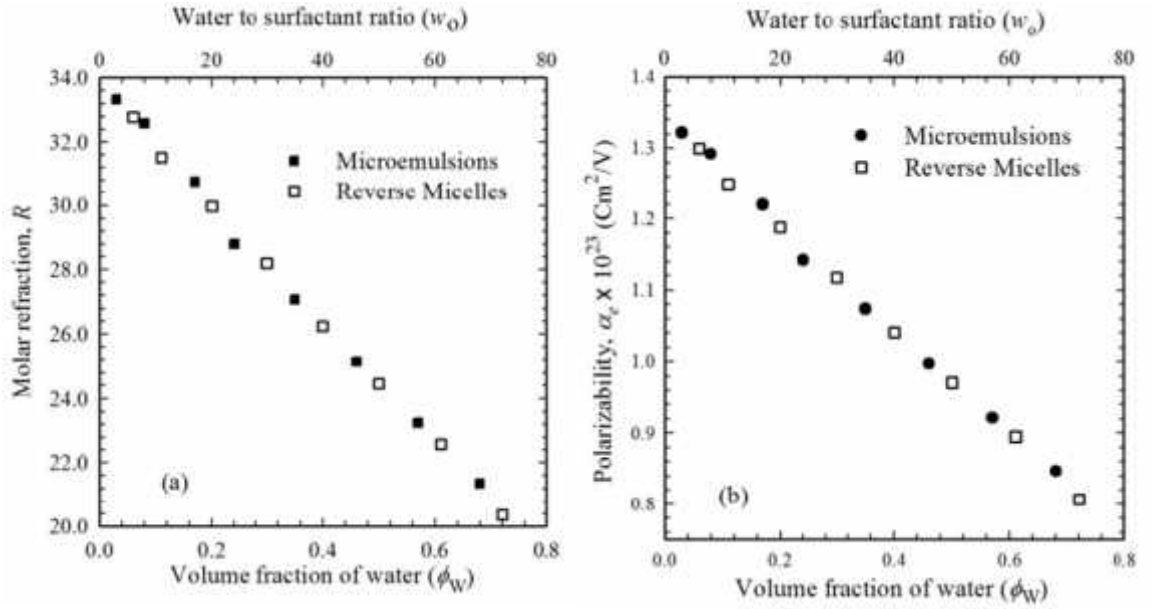

Figure 2.3.10. (a) Molar refraction and (b) electronic polarizability of CTAB/1-butanol/cyclohexane/water microemulsions and CTAB/1-butanol/water reverse micelles as a function of w_o or ϕ_W.

2.3.2.10. Droplet Size

Figure 2.3.11 shows the Z-average diameter vs. w_o or ϕ_W for CTAB/1-butanol/cyclohexane/water microemulsions and CTAB/1-butanol/water reverse micelles. The droplet sizes of all the microemulsions and reverse micelles are less than 100 nm [45]. It can be seen from Figure 2.3.11 that the Z-average diameters of CTAB/1-butanol/water reverse micelles are higher than the corresponding CTAB/1-butanol/cyclohexane/water microemulsions and decrease with increasing w_o. The larger size at ϕ_W = 0.03 (w_o = 3.64) (for microemulsions) and ϕ_W = 0.06 (w_o = 7.00) (for reverse micelles) is due to the formation of CTAB reverse micelles (*w/o* microemulsions) in 1-butanol where the electrostatic repulsion between the polar heads is screened by 1-butanol and facilitates the formation of aggregates as well as larger size of the droplets [46]. As the w_o or ϕ_W increases, the droplet size decreases due possibly to the decrease in the number of reverse micelles. At ϕ_W = 0.70 (w_o = 70.9) (for microemulsions) and ϕ_W = 0.72 (w_o = 73.7) (for reverse micelles), the droplet sizes are so small and correspond to the CTAB micelles in water. Additionally, in the middle region, the droplet sizes are

almost constant that correspond to the transition from reverse micellar phase to micellar phase, via *BC* microemulsions.

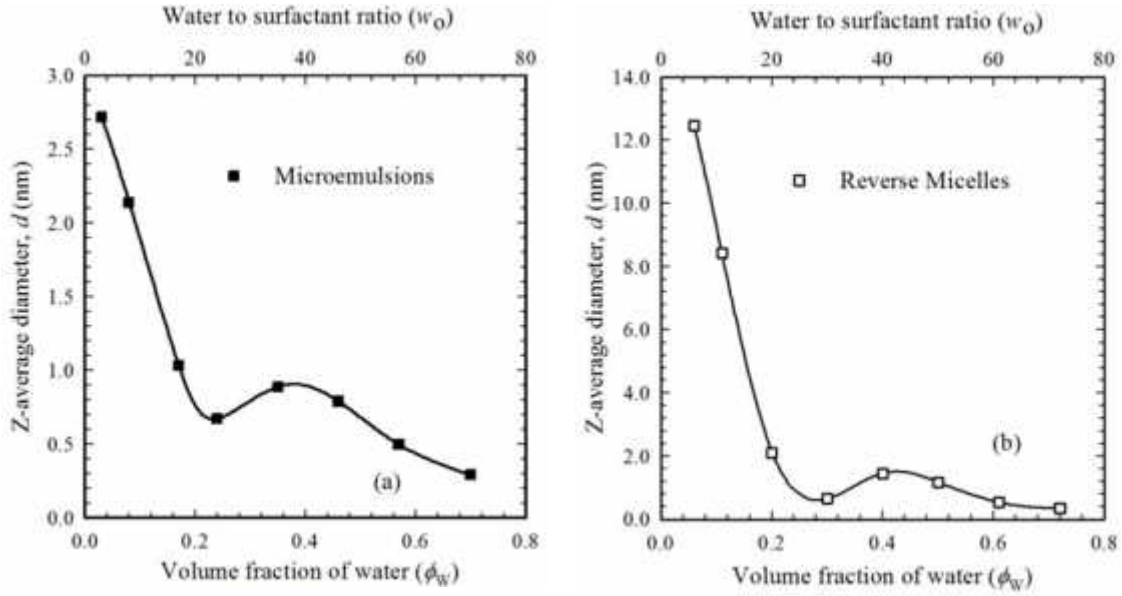

Figure 2.3.11. Z-average diameter of (a) CTAB/1-butanol/cyclohexane/water microemulsions and (b) CTAB/1-butanol/water reverse micelles as a function of w_o or ϕ_W.

The polydispersity index (PDI), a width parameter, has been calculated from a Cumulants analysis of the DLS-measured intensity autocorrelation function. In general, values smaller than 0.1 indicate reasonably narrow distribution and values greater than 0.7 indicates that the sample has a very broad size distribution. The PDI values have been also evaluated for CTAB/cyclohexane/1-butanol/water microemulsions and CTAB/1-butanol/water reverse micelles. It has been found that the PDI values range from 0.107 to 0.354 and 0.226 to 0.499 for reverse micelles and microemulsions of CTAB, respectively. In all cases, the PDI values are within the range of 0.1 - 0.7 which indicates the droplets of reverse micelles and microemulsions are reasonably uniform in their distribution.

The standard deviations in Z-average diameters, *d,* of CTAB/cyclohexane/1-butanol/water microemulsions and CTAB/1-butanol/water reverse micelles have been calculated and these depend on the w_o for all cases, such as: at $\phi_W = 0.03$ ($w_o = 3.64$) (d = 2.72 nm) and $\phi_W = 0.70$ ($w_o = 70.9$) (d = 0.30 nm), the standard deviations in Z-average diameters of microemulsions were ± 0.682 and ± 0.004 nm, respectively while at ϕ_W = 0.06 ($w_o = 7.00$) (d = 12.46 nm) and $\phi_W = 0.72$ ($w_o = 73.7$) (d = 0.35 nm), the standard deviations in Z-average diameters of reverse micelles were ± 0.6140 and ± 0.003 nm, respectively. Thus, for both reverse micelles and microemulsions of CTAB, at high value

of w_o, the results tend to be very close to the expected values that indicates relatively narrow distribution of droplet sizes and at low value of w_o, the results are spread out at a relatively wider range of values.

2.3.3. Physicochemical Properties of Micelles, Reverse Micelles and Microemulsions of SDS

2.3.3.1. Stability and Homogeneity

The SDS/1-butanol/cyclohexane/water microemulsions and SDS/1-butanol/water reverse micelles were stored at different temperature for six months and observed that they were stable after six months. The shelf life of the stored microemulsions was evaluated by visual inspection (phase separation) and % transmittance [39]. They were centrifuged at rpm 3,000 for 30 minutes at room temperature and observed for any change in homogeneity of microemulsions and reverse micelles.

2.3.3.2. Optical transparency

The percentage of transmittance of the micelles, reverse micelles and microemulsion of SDS were checked at 650 nm and the % transmittance of aqueous solution containing SDS at different concentrations is shown in Figure 2.3.12.

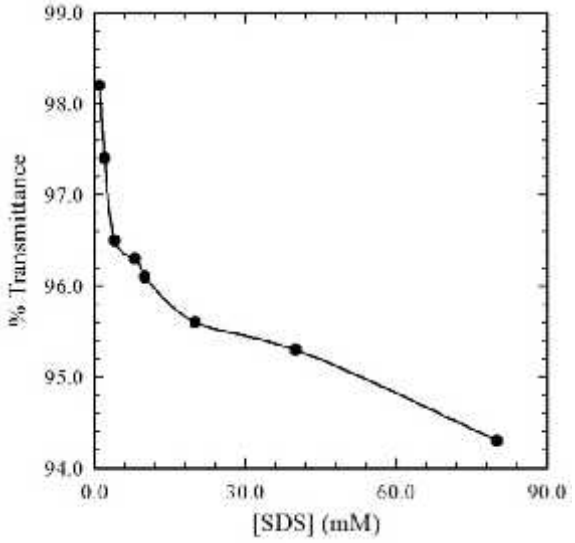

Figure 2.3.12. Transmittance as a function of SDS concentration.

The % transmittance increases upto the CMC of SDS and then gradually decreases which corresponds to the formation of SDS micelles. The % transmittances of SDS/1-butanol/cyclohexane/water microemulsions were ranges from 64.2-89.5 %, might be due to the presence of some impurities in SDS that gives slightly yellowish color of the micromulsions; whereas for SDS/1-butanol/water reverse micelles, the % transmittances were close to 97.8% which indicates the optical transparency of these reverse micelles and microemulsions of SDS.

2.3.3.3. Turbidity

Figure 2.3.13 shows the change in turbidity with increasing [SDS]. The turbidity increases nonlinearly with increasing the [SDS]. Below the CMC, the turbidity increases sharply and after the CMC (8.2 mM) of SDS, a gradual increase is apparent with increasing [SDS]. The sharp increase in turbidity after the CMC indicates the commencement of aggregation of the SDS into micelles [37].

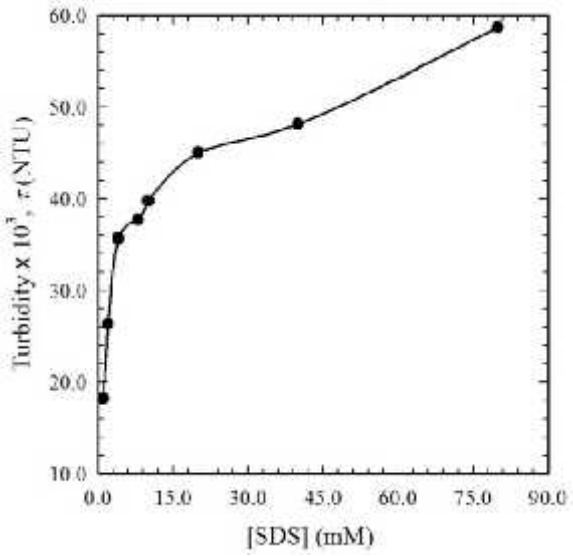

Figure 2.3.13. The turbidity as a function of SDS concentration.

Figure 2.3.14 shows the turbidity of SDS/1-butanol/cyclohexane/water microemulsions and SDS/1-butanol/water reverse micelles with increasing the ϕ_W or w_o. The values of turbidity are higher in microemulsions than in reverse micelles of SDS which is due possibly to the yellowish color of the microemulsions rather than the reverse micelles. The turbidity slightly increases up to $\phi_W = 0.20$ ($w_o = 22.4$) then increases sharply for $\phi_W = 0.20 \sim 0.42$ ($w_o = 22.4 \sim 48.9$); while above $\phi_W = 0.42$ ($w_o = 48.9$) decreases gradually for microemulsions. In the case of reverse micelles, the turbidity decreases slightly up to $\phi_W = 0.32$ ($w_o = 37.4$) then increases sharply for $\phi_W = 0.32 \sim 0.47$ ($w_o = 37.4 \sim 53.4$); while after $\phi_W = 0.47$ ($w_o = 53.4$) decreases abruptly. The unusual pattern in these profiles corresponds to the interactions between the droplets of different types of reverse micelles and micromulsions. The sharp increase in turbidity is due to coalescence of droplets (in the *BC* phases) which increases the attractive interactions. Decreased turbidity is due to electrostatic repulsion between the water droplets in *w*/*o* microemulsions or 1-butanol droplets in *o*/*w* microemulsions of SDS [31].

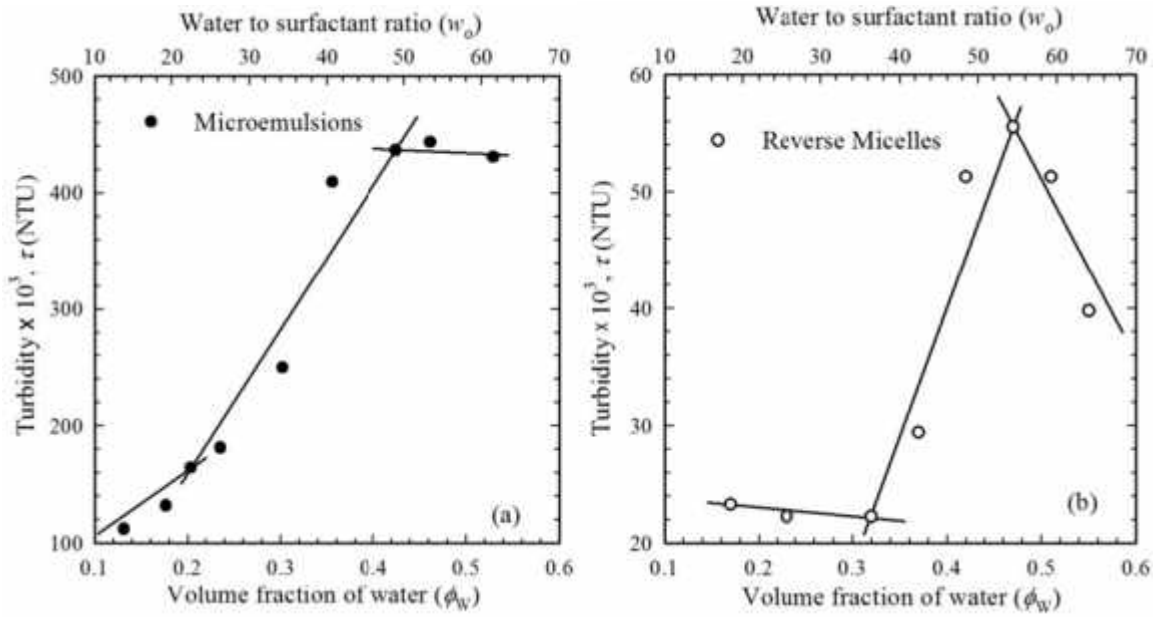

Figure 2.3.14. Turbidity of (a) SDS/1-butanol/cyclohexane/water microemulsions and (b) SDS/1-butanol/water reverse micelles as a function of w_o or ϕ_W.

2.3.3.4. Specific Conductivity

The specific conductivity increases with increasing [SDS]. The specific conductivity - [SDS] profile lie on two straight lines and their point of intersection gave the CMC value for SDS in aqueous solutions. The CMC value at 25 ^oC has been found to have a value of 8.2 mM for SDS aqueous solutions, which is in good agreement with literature [33].

Figure 2.3.15 shows specific conductivity of SDS/1-butanol/cyclohexane/water microemulsions and SDS/1-butanol/water reverse micelles with ϕ_W or w_o in which the specific conductivity increases with increasing ϕ_W or w_o (the concentration of SDS remains constant for both system) indicating an increase in the number of conducting species in the systems. At lower ϕ_W or w_o, reverse micelles were formed where the cores of the reverse micelles comprise the hydrophilic sulfate ion and the counterions, Na^+ are less easily dissociated in cyclohexane. This causes a significant decrease in the degree of ionization and lowers the specific conductivity. With increasing ϕ_W or w_o, the conductivity increases due to the formation of clusters by aggregation of droplets where the charge species are easily moved through this network channel. In contrast, at higher ϕ_W or w_o, micelles are formed and the orientation of surfactant changes in water. The cores of the micelles are composed of the hydrophobic groups and the counterions, Na^+ are easily dissociated in water to bring about an increase in the value of specific conductivity.

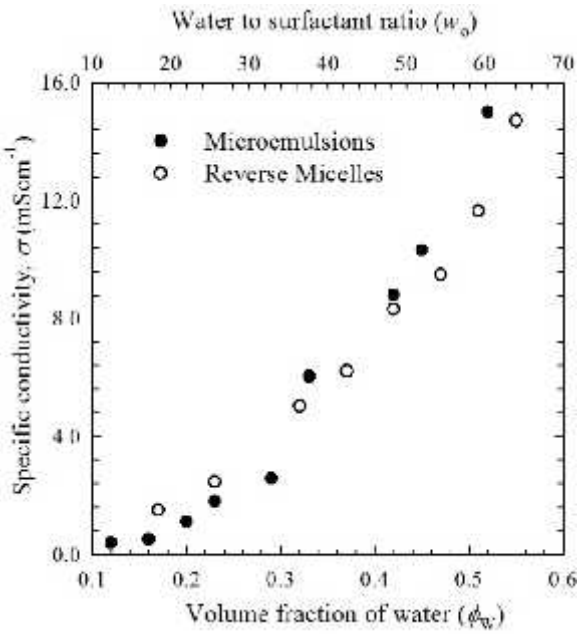

Figure 2.3.15. Specific conductivity of SDS/1-butanol/cyclohexane/water microemulsions and SDS/1-butanol/water reverse micelles as a function of w_o or ϕ_W.

2.3.3.5. Viscosity

Viscosity of de-ionized water is 0.89 mPa s at 25 °C [47]. After the addition of SDS in water the viscosity increases. At 15.0 %wt. of SDS in water the viscosity rises to 2.58 mPa s which is 2.89 times greater than that of water. Figure 2.3.16 shows the change in viscosity with ϕ_W or w_o for SDS/1-butanol/cyclohexane/water microemulsions and SDS/1-butanol/water reverse micelles.

In SDS/1-butanol/cyclohexane/water microemulsions, at $\phi_W < 0.20$ ($w_o < 22.4$), the viscosity increases while $\phi_W = 0.20$~0.42 ($w_o = 22.4$~48.9), it increases gradually; whereas at $\phi_W > 0.42$ ($w_o > 48.9$) a sharp increase is apparent. This increase in viscosity with the addition of water has been ascribed to the increasing diameter of water filled conduits in the *BC* and *w*/*o* [41]. For SDS/1-butanol/water reverse micelles system, the viscosity increases up to $\phi_W = 0.42$ and then decreases sharply. The peak point $\phi_W = 0.42$ ($w_o = 48.1$) in viscosity - ϕ_W or w_o profile indicates the transition point of *w*/*o* to *o*/*w* via *BC* structure.

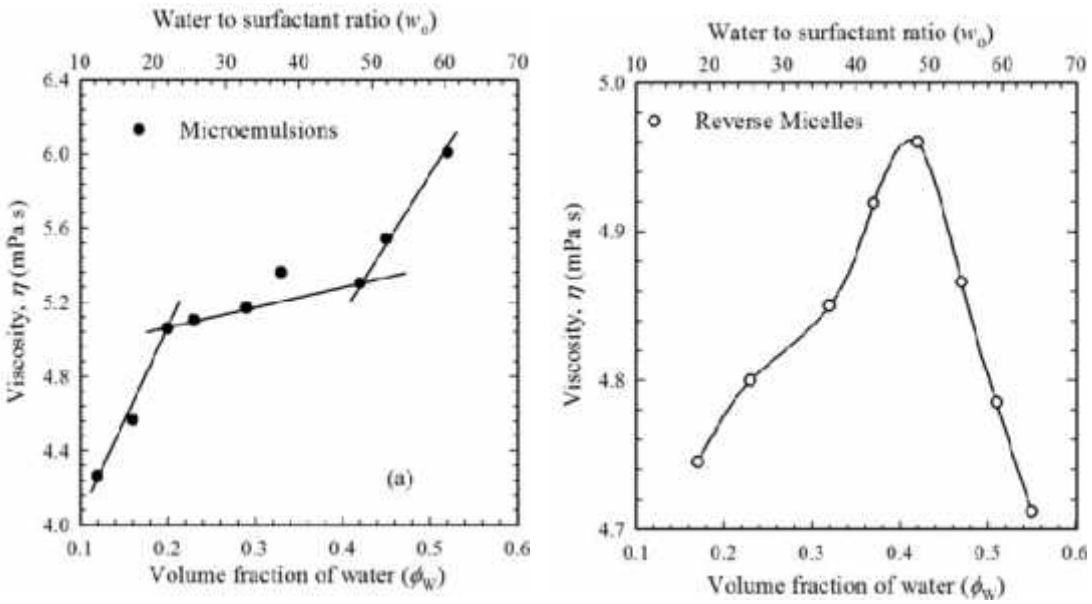

Figure 2.3.16. Viscosity of (a) SDS/1-butanol/cyclohexane/water microemulsions and (b) SDS/1-butanol/water reverse micelles as a function of w_o or ϕ_W.

2.3.3.6. Density

Density of aqueous solution of SDS increases with increasing [SDS]. The addition of SDS (15.0 %wt.) in water raises the density of water to 1.02104 g cm^{-3}. Figure 2.3.17 shows density of SDS/1-butanol/cyclohexane/water microemulsions and SDS/1-butanol/water reverse micelles with ϕ_W or w_o.

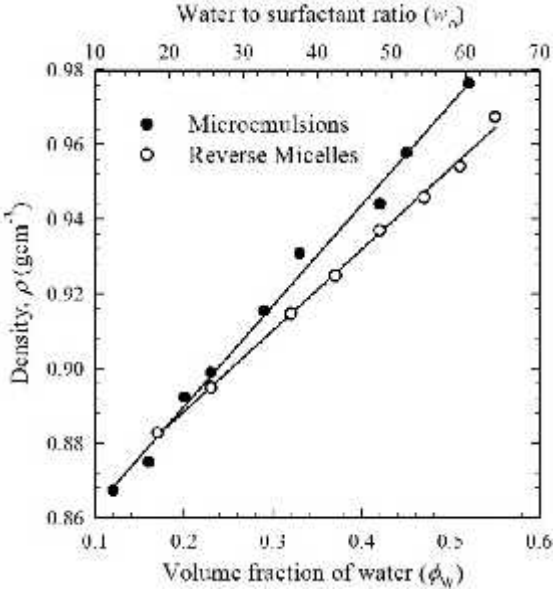

Figure 2.3.17. Density of SDS/1-butanol/cyclohexane/water and SDS/1-butanol/water microemulsion systems as a function of w_o or ϕ_W.

The density of the systems also increases with increase in ϕ_W which is similar to that for CTAB. With increasing ϕ_W in microemulsions, a transition from reverse micellar phase to micellar phase is apparent. In micelle phase (higher value of ϕ_W), surfactant hydrophobic groups are in the core and headgroups, sulfate ions are in the bulk of the solution where the volume of the system decreases and the density increases with increasing ϕ_W.

2.3.3.7. Surface Tension/Interfacial Tension

It is well known that with increasing [surfactant], the surface tension decreases and after the CMC, the surface tensions are almost constant [38, 40]. With addition of 15 %wt. SDS in aqueous solution, the value of surface tension is 32.50 mNm^{-1} at 25 ^oC which is much lower than that of deionized water. This With 15 %wt. of SDS in aqueous solution; the SDS monomers are in aggregated form called micelles which reduced the surface tension of the water. Figure 2.3.18 shows the interfacial tension of SDS/1-butanol/cyclohexane/water microemulsions and SDS/1-butanol/water reverse micelles with ϕ_W or w_o.

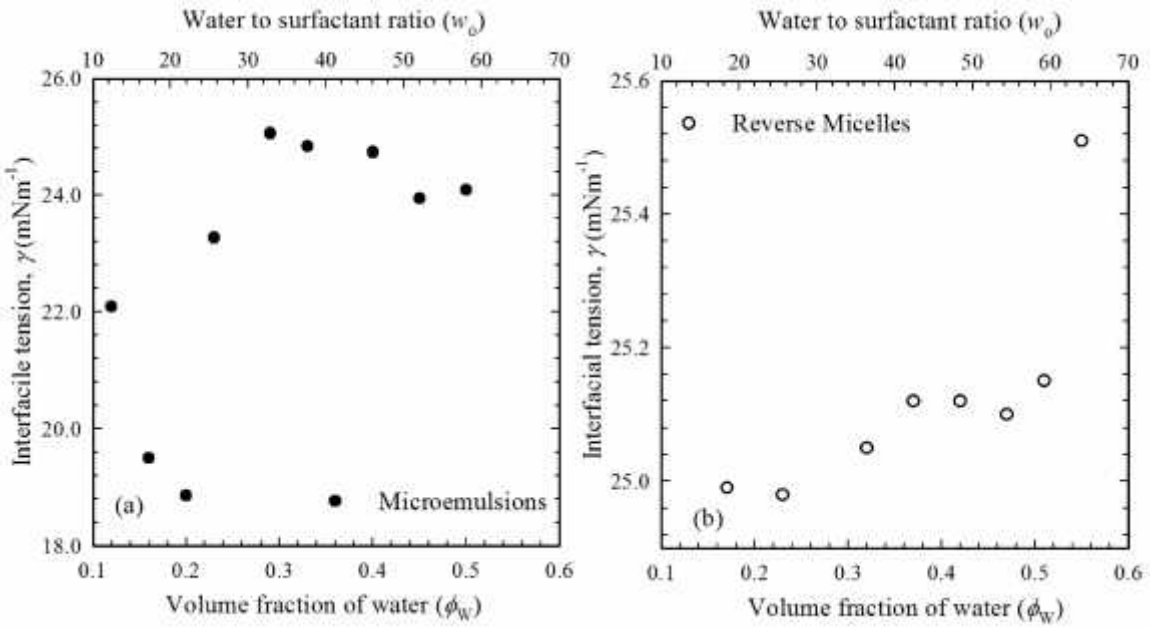

Figure 2.3.18. Interfacial tension of (a) SDS/1-butanol/cyclohexane/water microemulsions and (b) SDS/1-butanol/water reverse micelles as a function of w_o or ϕ_W.

In SDS/1-butanol/cyclohexane/water microemulsions (Figure 2.3.18(a)), the interfacial tension decreases up to $\phi_W = 0.20$ ($w_o = 22.4$) and above $\phi_W = 0.40$ ($w_o = 48.9$); while for $\phi_W = 0.20 \sim 0.40$ ($w_o = 22.4 \sim 48.9$), the interfacial tension sharply increases with increasing ϕ_W. The sharp decrease in interfacial tension up to $\phi_W = 0.20$ with increasing ϕ_W indicates weaker hydrophobic-hydrophilic interactions between cyclohexane, 1-

butanol and water. With increasing ϕ_W, stronger hydrophilic-hydrophilic interaction between CTAB, 1-butanol and water causes a sharp increase in interfacial tension for ϕ_W = 0.20 ~ 0.40. After ϕ_W = 0.46, the interfacial tension decreases slightly due to stronger hydrophilic-hydrophilic interaction of CTAB, water and 1-butanol [42]. In SDS/1-butanol/water reverse micelles (Figure 2.3.18(b)), the interfacial tension increases in different patterns with increasing ϕ_W. This is due to the difference in hydrophilic-hydrophilic interaction of CTAB, water and 1-butanol at different regions of the reverse micelles.

2.3.3.8. Refractive Index

With the addition of 15 %wt. SDS in aqueous solution, the refractive index is 1.35078 which is due to formation of higher number of micelles and more micelles can refract more light [40]. Figure 2.3.19 shows the change in refractive index of SDS/1-butanol/cyclohexane/water microemulsions and SDS/1-butanol/water reverse micelles with ϕ_W or w_o.

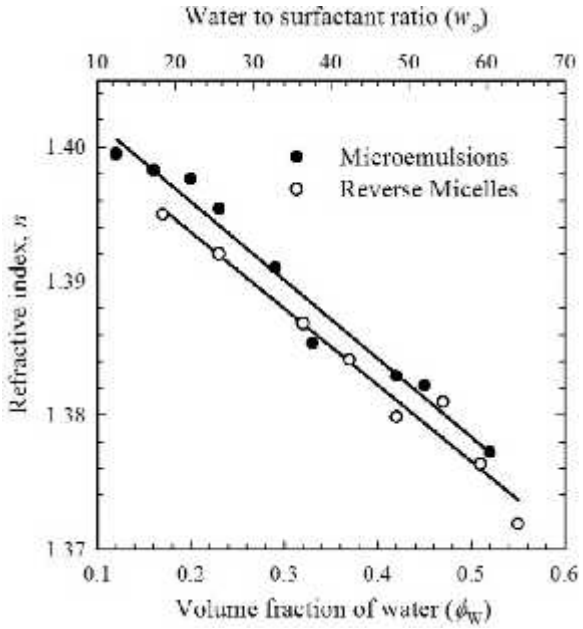

Figure 2.3.19. Refractive index of SDS/1-butanol/cyclohexane/water microemulsions and SDS /1-butanol/water reverse micelles as a function of w_o or ϕ_W.

The refractive index decreases with increasing ϕ_W or w_o. As refractive index specifies the transparency of the microemulsions and it is a property sensitive to structural transitions, no structural modifications can be obtained from the results [7], i.e., the water and 1-butanol remain encapsulated into the SDS/1-butanol reversed micelles (low ϕ_W) and SDS/water micelles (high ϕ_W), respectively.

2.3.3.9. Molar Refraction and Polarizability

Molar refractivity (R) and electric polarizability for the SDS/1-butanol/cyclohexane/water microemulsions and SDS/1-butanol/water reverse micelles were calculated by using equation (2.1) and (2.2), respectively [43, 44]. Figure 2.3.20 shows the calculated value of molar refractions (R) and electronic polarizability (α_e) of SDS/1-butanol/cyclohexane/water microemulsions and SDS /1-butanol/water reverse micelles. Molar refraction and electronic polarizability also decrease with increasing w_o or ϕ_W in close analogy to refractive index results.

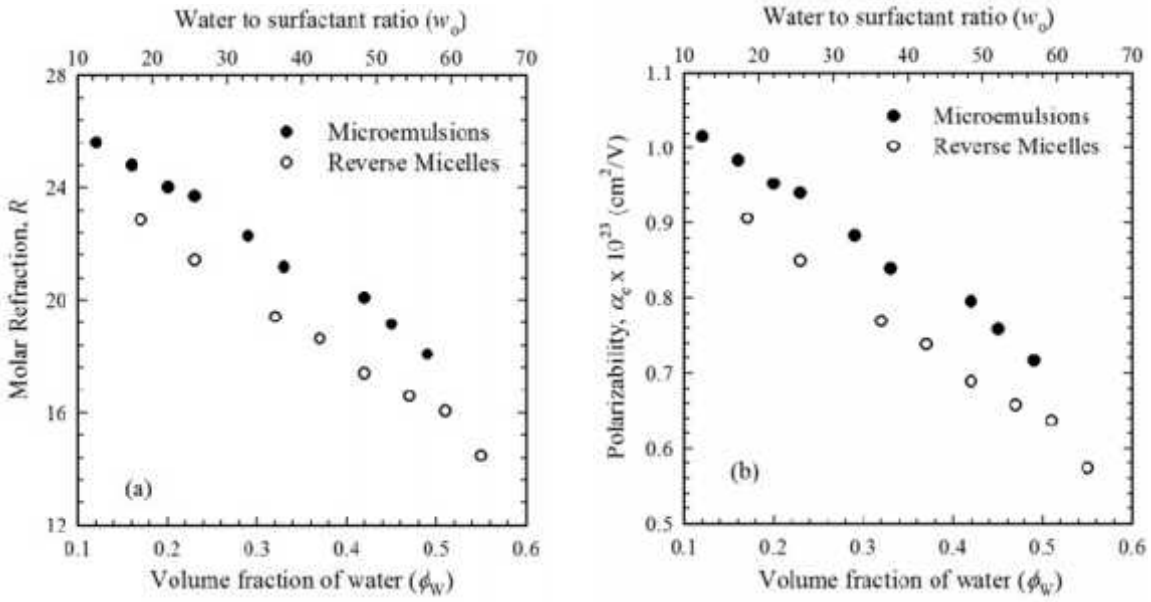

Figure 2.3.20. (a) Molar refraction and (b) electronic polarizability of SDS/1-butanol/cyclohexane/water microemulsions and SDS/1-butanol/water reverse micelles as a function of w_o or ϕ_W.

2.4. Conclusions

Physicochemical properties of micelles, reverse micelles and microemulsions of CTAB and SDS change with compositions for these media. The viscosity, turbidity, conductivity, density and interfacial tension increase; while refractive index decreases with increasing ϕ_W or w_o of reverse micelles and microemulsions. The increase in viscosity, conductivity, turbidity and interfacial tension - ϕ_W or w_o profiles show nonlinear behavior with different patterns indicating different microstructures in reverse micelles and microemulsions such as *w*/*o*, *BC* and *o*/*w* microemulsions.

References

[1] G. M. Eccleston, *Microemulsions, Encyclopedia of pharmaceutical technology.* Marcel Dekker, NewYork, 1992, 9, 375.

[2] M. Fanun, Microemulsions: *Properties and application,* Surfactant science series, 144, CRC press.

[3] M. R. Martin, *Emulsions, In: Theory and practice of industrial pharmacy,* Lea and Febiger*,* Varghese, 1990, 503.

[4] F. Bordi, C. Cametti, *Ion transport and electrical conductivity in heterogeneous systems: the case of Microemulsions in Interfacial Dynamics* ed. N. Kallay, Marcel Dekker, New York, 2000, 541.

[5] M. Grassi, G. Grassi, R. Lapasin, I. Colombo, *Understanding Drug Release and Absorption Mechanisms: A Physical and Mathematical Approach*, Tailor and Francis, CRC press, NewYork 493, 2007.

[6] D. Quemada, D. Langevin, *Rheological modelling of microemulsions,* Journal of Theoretical and Applied Mechanics, (numero special), 201, 1985.

[7] M. Goffredi, V. T. Liveri, G. Vassallo, *Refractive index of water-AOT-n-heptane microemulsions*, Journal of Solution Chemistry, 1993, 22, 941-949.

[8] R. Sripriya, K. M. Raja, G. Santhosh, M. Chandrasekaran, M. Noel, *The effect of structure of oil phase, surfactant and co-surfactant on the physicochemical and electrochemical properties of bicontinuous microemulsion*, Journal of Colloid Interface Science, 2007, 314, 712-717.

[9] C. C. Ruiz, *A photophysical study of the urea effect on micellar properties of sodium dodecylsulfate aqueous solutions*, Colloid Polymer Science, 1995, 273, 1033-1040.

[10] R. Saha, S. Rakshit, R. K. Mitra, S. K. Pal, *Microstructure, morphology, and ultrafast dynamics of a novel edible microemulsion,* Langmuir 2012, 28, 8309-8317.

[11] C. J. Yang, Q. R. Zeng, H. J. Yang, Zou, M. Y. Chin, *Spectrophotometric determination of some polyoxyethylene nonionic surfactants and its application*, Journal of Analytical Chemistry, 2006, 5, 642-646.

[12] Y. Liu, R. Guo, X. J. Guo, *Location of phenothiazine in sodium dodecyl sulfate/n-pentanol/water microemulsions*, The Journal of Physical Chemistry B 2006, 110, 784-790.

[13] A. Bera, A. Mandal, T. Kumar, *Physicochemical characterization of anionic and cationic microemulsions: water solubilization, particle size distribution, interfacial tension, and structural parameters*, Journal of Chemical and Engineering Data, 2014, 59, 2490-2498.

[14] P. D. I. Fletcher, J. S. Morris, *Turbidity of oil-in-water microemulsion droplets stabilised by nonionic surfactants,* Colloids and Surfaces A: Physicochemical and Engineering Aspects, 1995, 98, 147-154.

[15] P. D. I. Fletcher, K. Suhling, *Interactions between weakly charged oil-in-water microemulsion droplets*, Langmuir, 1998, 14, 4065-4069.

[16] Y. Jayalakshmi, D. Beysens, *Critical behavior of a ternary microemulsion studied by turbidity, density, and refractive index*, Physical Review A, The American Physical Society, 1992. 45, 8709-8718.

[17] N. A. Kizilbash, S. Asif, M. F. Nazar, S. S. Shah, D. Alenizi, *Design of a microemulsion-based drug delivery system for diclofenac sodium*, Journal of Chemical Society Pakistan, 2011, 33, 1-6.

[18] S. K. Mehta, Kawaljit, *Isentropic compressibility and transport properties of CTAB-alkanol-hydrocarbon-water microemulsion systems*, Colloids and Surfaces A: Physicochemical and Engineering Aspects, 1998, 136, 35-41.

[19] M. Fanun, Z. Ayad , S. Mudalal , S. Dahoah, D. Meltzer, M. Schwarze, R. Schomacker, J. Blum, *Characterization of water/sucrose laurate/n-propanol/allylbenzene microemulsions*, Journal of Surfactants and Detergents, 2012, 15, 505-512.

[20] B. Kumar, S. K. Jain, S. K. Prajapati, A. Mahor, A. Kumar, *Development and characterization of transdermal microemulsion gel for an antiviral drug*, International Journal of Pharmaceutical Sciences and Research, 2010,1, 57-74.

[21] B. H. Zala, R. B. Pandya, M. D. Prajapat, A. Ramkishan, R. K. Parikh, M. C. Gohel, *Formulation and development of microemulsion drug delivery system of acyclovir for enhancement of permeability*, Journal of Pharmacy Research, 2011, 4, 930-933.

[22] E. Ramadan, T. Borg, G. M. Abdelghani, N. M. Saleh, *Formulation and evaluation of acyclovir microemulsions*, Bulletin of Pharmaceutical Sciences, 2013, 36, 31-47.

[23] H. S. Basheer, M. I. Noordin, M. M Ghareeb, *Characterization of microemulsions prepared using isopropyl palmitate with various surfactants and cosurfactants*, Tropical Journal of Pharmaceutical Research, 2013, 12, 305-310.

[24] V. Patel, H. Kukadiya, R. Mashru, N. Surti, S, Mandal, *Development of microemulsion for solubility enhancement of clopidogrel*, Iranian Journal of Pharmaceutical Research 2010, 9, 327-334.

[25] S. C. Sharma, K. Tsuchiya, K. Sakai, H. Sakai, M. Abe, *Formation and characterization of microemulsions containing polymeric silicone*, Langmuir, 2008, 24, 7658-7662.

[26] W. Jahn, R. Strey, *Microstructure of microemulsions by freeze fracture electron microscopy*, The Journal of Physical Chemistry, 1988, 92, 2294-2301.

[27] W. Jahn, R. Strey, *Images of bicontinuous microemulsions by freeze fracture electron microscopy*, Physics of Amphiphilic Layers, 1987, 21, 353-356.

[28] D. Senatra, *Procedures for DSC analysis of percolative microemulsions*, Thermochimica Acta, 2000, 345, 39-46.

[29] D. Senatra, R. Pratesi, L. Pieraccini, *DSC spectra as thermal fingerprints of percolative microemulsions,* Journal of Thermal Analysis and Calorimetry, 1998, 51, 79-90.

[30] M. A. van Dijk, G. Casteleijn, J. G. H. Joosten, Y. K. Levine, *Percolation in oil-continuous microemulsions. A dielectric study of aerosol OT/water/isooctane*, The Journal of Chemical Physics, 1986, 85, 626-631.

[31] P. D. I. Fletcher, K. Suhling, *Interactions between weakly charged oil-in-water microemulsion droplets*, Langmuir, 1998, 14, 4065-4069.

[32] L. Arzuman, S. N. Karobi, M. J. Islam, G. Ara, M. M. Rahman, M. Y. A. Mollah, M. A. B. H. Susan, *Effect of urea on the kinetics of the alkaline hydrolysis of crystal violet catalyzed by aqueous micellar solutions of cetyltrimethylammonium bromide*, Synthesis and Reactivity in Inorganic, Metal-Organic, and Nano-Metal Chemistry, 2015, 45, 764-769.

[33] A. R. Kabir, M. A. B. H. Susan, *Kinetics of the alkaline hydrolysis of crystal violet in aqueous solution influenced by anionic surfactants*, Journal of Saudi Chemical Society, 2008, 12, 543-554.

[34] Z. Z. Huang, Z. Q. Chen, M. L. Xue, *Effects of temperature on the viscosity of nonionic micellar solution in the presence of salts*, Chemical Journal of Chinese Universities. 1992, 13, 824-827.

[35] A.V. Sineva, D. S. Ermolatev, A. V. Pertsov, *Structural transformations in a water-n-octane + chloroform-sodium dodecyl sulfate-n-pentanol microemulsion*, Colloid Journal, 2007, 69, 89-94.

[36] A. Heinz, C. J. Strachan, F. Atassi, K. C. Gordon, T. Rades, *Characterizing an amorphous system exhibiting trace crystallinity: A case study with saquinavir*, Crystal Growth and Design, 2008, 8, 119 -127.

[37] L. M. Kushner, W. D. Hubbard, R. A. Parker, *Turbidity and viscosity measurements on Some cationic detergents in water and in sodium chloride solutions*, Journal of Research of the National Bureau of Standards,1957, 59, 113-119.

[38] J. Datta, A. Bhattiacharya, K. K. Kundu, *Effect of surfactants on the kinetics of alkaline fading of crystal violet and acid-catalyzed inversion of sucrose*, Indian Journal of Chemistry, 1988, 27, 115-122.

[39] A. Zvonar, B. Rozman, M. B. Rogac, M. Gasperlin, *The influence of microstructure on celecoxib release from a pharmaceutically applicable system*, Acta Chimica Slovenica, 2009, 56, 131-138.

[40] M. M. Rahman, *Electrochemistry of malachite green and crystal violet in aqueous solution and surfactant - based organized media*, Ph. D. thesis, 2013.

[41] B. K. Paul, S. P. Moulik, *The viscosity behaviours of microemulsions: an overview*, Proceedings of the Indian National Science Academy, 2000, 66, 499-519.

[42] V. Patidar, A. Chandra, M. Singh, R. K. Kale, *Physiochemical and phase behaviour study of jatropha curcus oil - ethanol microemulsion fuels using sorbitane fatty esters*, International Journal of Renewable and Sustainable Energy, 2014, 3, 13-19.

[43] D. S. Wankhede, *Refractive indices for binary mixtures of propylene carbonate,* International Journal of Chemistry Research, 2011, 2, 23-26.

[44] R. Talegaonkar, A. S. Burghate, S. A. Wadal, *Study of molar refraction and polarizability constant of substituted thiazolyl schiff's bases from refractive index measurement in different media,* Oriental Journal of Chemistry, 2011, 27, 1285-1288.

[45] Y. S. Rhee, J. G. Choi, E. S. Park, *Transdermal delivery of ketoprofen using microemulsions,* International Journal of Pharmaceutics, 2001, 228, 161-170.

[46] K. Zielinska, K. A. Wilk, A. Jezierski, T. Jesionowski, *Microstructure and structural transition in microemulsions stabilized by aldonamide-type surfactants*, Journal of Colloid and Interface Science, 2008, 321, 408-417.

[47] J. Kestin, M. Sokolov, W. A. Wakeham, *Viscosity of liquid water in the range - 8 ^{o}C to 150 ^{o}C*, Journal of Physical Chemistry Reference Data, 1978, 7, 941-948.

Abstract

Different microstructures of reverse micelles and microemulsions of CTAB and SDS have been determined by applying percolation theory on dynamic properties: conductivity, turbidity, viscosity and interfacial tension. The conductivity, viscosity and interfacial tension measurements have provided evidence for percolation behavior with variation in the ϕ_W. The conductivity results of these reverse micelles and microemulsions are discussed in terms of a percolation theory. The phase transitions in conductivity results correspond to the structural change from *w*/*o* to *o*/*w* via *BC* microemulsions. The percolation thresholds (ϕ_C) obtained from conductivity measurements are in accordance with those obtained from viscosity and interfacial tension measurements. The volumetric and refraction properties of reverse micelles and microemulsions were studied by measuring density and refractive index, respectively. Excess volume - ϕ_W, excess refraction - ϕ_W and excess molar refraction - ϕ_W profiles for these reverse micelles and microemulsions also indicate the structural phase transitions from *w*/*o*-*BC*-*o*/*w* microemulsions.

3.1. Introduction

Microemulsions, as defined in Section 1.4, are thermodynamically stable, isotropic, transparent fluid dispersions of two immiscible liquids (e.g., water and hydrocarbon) and one or more surface active agents (surfactants or surfactant with cosurfactant) [1]. In comparison to micellar systems, they are superior in terms of solubilization potential and thermodynamic stability and offer advantages over unstable dispersions, such as emulsions and suspensions; since they are manufactured with little energy input (heat, mixing) and have a long shelf life [2]. The unique feature associated with microemulsions is the presence of different textures such as oil droplets in water (*o*/*w*), water droplets in oil (*w*/*o*), bicontinuous, (Figure 1.7.) lamellar mixtures etc., which are formed by altering the curvature of interface with the help of different factors such as salinity, temperature, etc. Such a variety in structure of microemulsion is a function of composition of the system. One peculiarity of microemulsions lies in the fact that these structures are interchangeable with change in compositions of the polar or nonpolar phase and with change in temperature [2].

It is well-known that percolation is a phase transition-like phenomenon where an interconnected random structure is formed which spans the entire system and may be governed by universal scaling law. After a threshold concentration of water in the system at a constant temperature or after a threshold temperature at given concentration of water in the system percolation phenomenon occurred. The concentration or temperature at which such dramatic change occurs is called the *percolation threshold.* The phenomenon of percolation is said to be of two types:

(1) *Static percolation*: Percolation in a system which is a mixture of insulators and solid conductors where the conductance is almost zero below the threshold condition (or connectivity).
(2) *Dynamic percolation*: Percolation in a system where the droplets are in motion with chances of collision which is very high at the threshold condition [3].

The conductance of microemulsion system increases with the ϕ or w_o. This dramatic increase in conductivity with droplet volume fraction for microemulsion was first interpreted by Lagues [3] in terms of percolation model referring to Brownian motion of the medium.

According to the most widely used theoretical model, which is based on the dynamic nature of the microemulsions, [4], there are two pseudophases: one in which the charge is transported by the diffusion of the microemulsion droplets (reversed micelles) and the other phase in which the charge is conducted by diffusion of the charge carrier itself inside the reversed micelle clusters. According to this theory, the conductivity can be reproduced in terms of two separate asymptotic power laws having different exponents below and the above the percolation threshold.

$$\sigma = A(\phi_c - \phi)^{-s} \text{ where, } \phi < \phi_C \text{ (below percolation)} \quad \text{.....(3.1)}$$

$$\sigma = B(\phi - \phi_c)^{t} \text{ where, } \phi > \phi_C \text{ (above percolation)} \quad \text{.....(3.2)}$$

where, A and B are free parameters and *s* and *t* are critical exponents.
The slopes of the logσ vs. log (ϕ_C-ϕ) plot for $\phi < \phi_C$ and logσ vs. log(ϕ-ϕ_C) for $\phi > \phi_C$ plot yield *s* and *t* parameter [3]. The difference between the dynamic and static percolation is reflected in terms of deviation in the value of the *s* and *t* from the predicted value. The critical exponent *t* generally ranges between 1.5 and 2 whereas the exponent *s* allows the assignment of the time dependent percolation regime. Thus, $s > 1$(generally around 1.3) identifies a dynamic percolation regime [3].

The *static percolation* is related to the appearance of bicontinuous microemulsions where a sharp increase in conductivity, due to both counterions and to lesser extent surfactant ions can be justified by a connected water path in the system. The conductivity transition is mainly due to the formation of a continuous connected disperse phase in the system. The *dynamic percolation* is connected to rapid process of fusion and fission among the droplets. Transient water channels form when the surfactant interface breaks down during collisions or through the merging of droplets [5]. Thus, conductivity is mainly due to the motion of counter ions along the water channels. The static and dynamic percolations are shown in Section 1.4.1 in Chapter 1 (Figure 1.8).

Based on the ratio of the components, three different microstructures for a microemulsion system may be formed. At high oil content, *w*/*o* microemulsion appears consisting of

water droplets dispersed in a continuous oil phase. At high water content, *o*/*w*microemulsion is formed by oil droplets dispersed in a continuous water phase. At intermediate ratio of oil and water, a bicontinuous phase exists. The microstructure of a microemulsion can be altered from *w*/*o* to *BC* system and from *BC* to *o*/*w* system by increasing the water content at constant temperature or by increasing the temperature at constant water content [6]. The application of electrical conductivity measurements has been very popular since useful information on micellar interaction could be obtained. [7, 8]. Water and oil percolation thresholds are important physical property of a microemulsion, which is frequently, determined using electrical conductivity measurements [9, 10]. Water and oil percolations are the indicators of percolation thresholds of microstructural transition from *w*/*o* to *BC* microemulsions and *BC* to *o*/*w* microemulsions, respectively.

According to percolation model, the conductivity remains low up to a certain ϕ_W due to the nonconducting nature of the continuous phase of the *w*/*o* system. However, as the volume fraction of water reaches and exceeds percolation threshold, i.e., ϕ_C, some of these conductive droplets begin to contact each other and form clusters which are sufficiently close to each other. This causes an efficient transfer of charge carriers between the droplets by charge hopping or transient merging of connected droplets with communication between the water cores, resulting in the sharp increase of conductance from an almost zero value to much higher level. The existence and position of this threshold depend on the interactions between droplets, which control the duration of the collision and the degree of interface overlapping, hence the probability of hopping or merging [11]. It has been reported [6] that without the knowledge of the percolation theoretical models, the percolation threshold can be predicted from numerical optimization of $d(\log\sigma)/d\phi_W$ against ϕ_W, by finding the water content at which $d(\log\sigma)/d\phi_W$ has the maximum or minimum [12-14].

Numerous attempts have been made to recognize different microstructures of reverse micelles and microemulsions by percolation theory using dynamic properties of those media. The structure and dynamics of microemulsions were characterized by using electrical conductivity [15-17] and viscosity results [12, 18]. The percolation transition in AOT/water/isooctane microemulsions has been studied by means of dielectric spectroscopy [19]. The viscosity results of water/AOT/oil microemulsions (undecane, isooctane, cyclohexane) are discussed in connection with a percolation model and the percolation thresholds are compatible with the conductivity and complex permitivity of these microemulsions [18].

In spite of numerous studies, the microstructures of CTAB/1-butanol/cyclohexane/water and SDS/1-butanol/cyclohexane/water reverse micelles and microemulsions are not yet established by percolation theory from dynamic properties. In this work, the phase

transitions or percolation thresholds for these reverse micelles and microemulsions of CTAB and SDS have been determined by percolation model on conductivity results and the different microstructures at above or below percolation thresholds were established by percolation scaling law.

3.2. Experimental

3.2.1. Materials and Methods

Materials used and methods followed have been described in detail in Section 2.2.1.

3.3. Results and Discussion

3.3.1. Percolation Thresholds in Microemulsions and Reverse Micelles of CTAB

3.3.1.1. Percolation Thresholds from Conductivity Results

The percolation thresholds of CTAB/1-butanol/cyclohexane/water microemulsions and CTAB/1-butanol/water reverse micelles were determined from conductivity results using plots of $d(\log\sigma)/d\phi_W$ vs. ϕ_W. Figure 3.3.1 represents the $d(\log\sigma)/d\phi_W$ vs. ϕ_W plots for reverse micelles and microemulsions of CTAB. In CTAB/1-butanol/cyclohexane/water microemulsions, the phase transitions occur at volume fractions of water (ϕ_W) = 0.17 and 0.45 (Figure 3.3.1 (a)), while for CTAB/1-butanol/water reverse micelles, the phase transition occurs at only ϕ_W = 0.30 (Figure 3.3.1(b)).

From Figure 3.3.1, it is apparent that in microemulsions of CTAB, there are two percolation thresholds: water percolation and oil percolation and the system may be called a *double percolation* system. Only water percolation is found in reverse micelles of CTAB and therefore such a system may be called *single percolation* system.

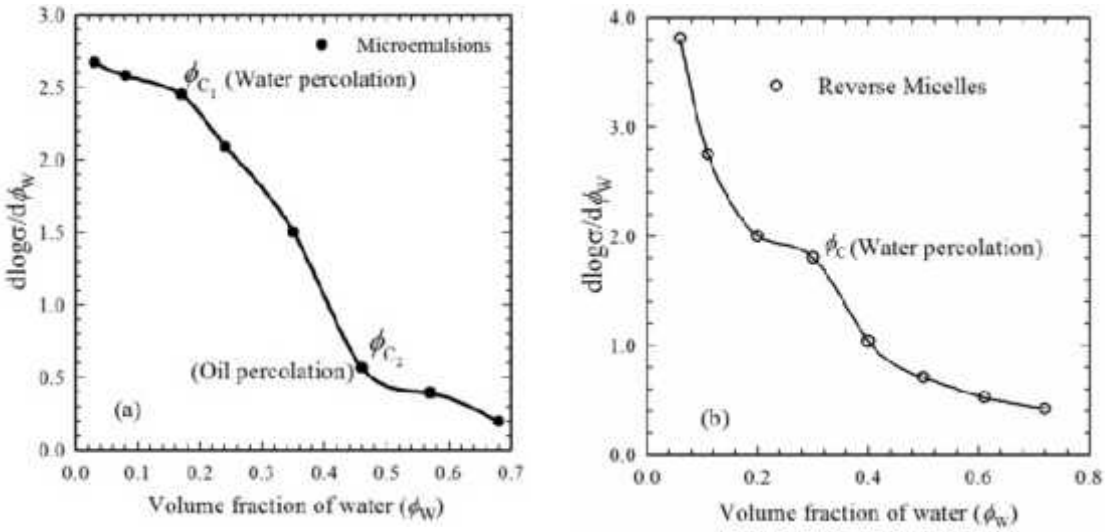

Figure 3.3.1. The $d\log\sigma/d\phi_W$ vs. ϕ_W plots for (a) CTAB/1-butanol/cyclohexane/water microemulsions and (b) CTAB/1-butanol/water reverse micelles.

According to percolation theory, from equation (3.1) and (3.2) for $\phi > \phi_C$ (above percolation threshold), the plot of logσ vs. log($\phi - \phi_C$) should give a slope equal to *t*. For $\phi < \phi_C$, (before the percolation threshold), the plot logσ vs. log($\phi_C - \phi$) should provide the value for *s* [17]. Such plots for the microemulsions and reverse micelles systems of CTAB are shown in Figure 3.3.2. The theoretical model for the percolation in static systems predicts that the exponents *t* and *s* should be < 1 and in dynamic systems *t* and *s* should be >1, respectively [17]. In this study, for microemulsions of CTAB (Figure 3.3.2 (a)), the value of $t = 0.32$ and $s = 0.78$ at above the $\phi_C = 0.17$ which indicates static percolation system to mean the *BC* microemulsions and above $\phi_C = 0.45$, the value of $t = 1.6$ and $s = 1.02$, to signify dynamic percolation system arising from droplet *(w/o* and *o/w*) microemulsions. For reverse micelles of CTAB (Figure 3.3.2 (b)), above $\phi_C = 0.30$, $t = 0.31$ and below $\phi_C = 0.30$, $s = 0.92$ that only shows the static percolation system.

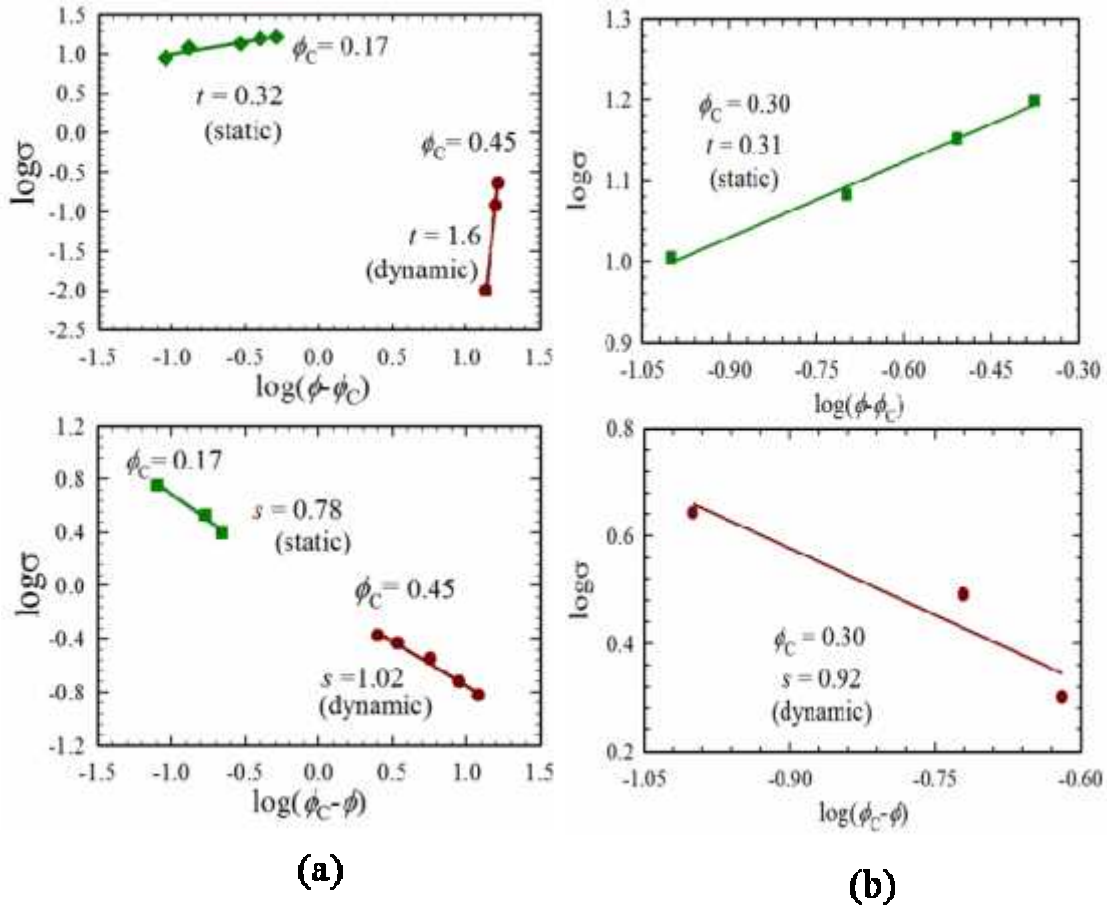

Figure 3.3.2. Plots of logσ vs. log ($\phi - \phi_C$) for $\phi > \phi_C$ and logσ vs. log ($\phi_C - \phi$) for $\phi < \phi_C$ for (a) CTAB/1-butanol/cyclohexane/water microemulsions at $\phi_W = 0.17(\phi_{C_1})$ and $0.45(\phi_{C_2})$ and (b) CTAB/1-butanol/water reverse micelles at $\phi_W = 0.30(\phi_C)$.

3.3.1.2 Excess Volume from Density Results

Density vs. ϕ_W profiles (Figure 2.3.7) for CTAB/1-butanol/cyclohexane/water microemulsions and CTAB/1-butanol/water reverse micelles, show that density increases with increasing ϕ_W. For better understanding of the variation of density with ϕ_W, the excess volume of reverse micelles and microemulsion formation need to be evaluated [20]. The relation (3.3) can evaluate the excess volume (V^E) of reverse micelles and microemulsions formation keeping in view the additively of volumes of the aqueous micellar and oil phase,

$$V^E = V_{Mic} - \sum_i \phi_i V_i \quad \text{.....(3.3)}$$

where, V^E = the excess volume, V_{Mic} = the measured specific volume of the microemulsions or reverse micelles, ϕ_i is the volume fraction of component i in the microemulsion or reverse micelles and V_i is the specific volume of component i.

Figure 3.3.3 represents the variation in V^E of CTAB/1-butanol/cyclohexane/water microemulsions and CTAB/1-butanol/water reverse micelles with ϕ_W.

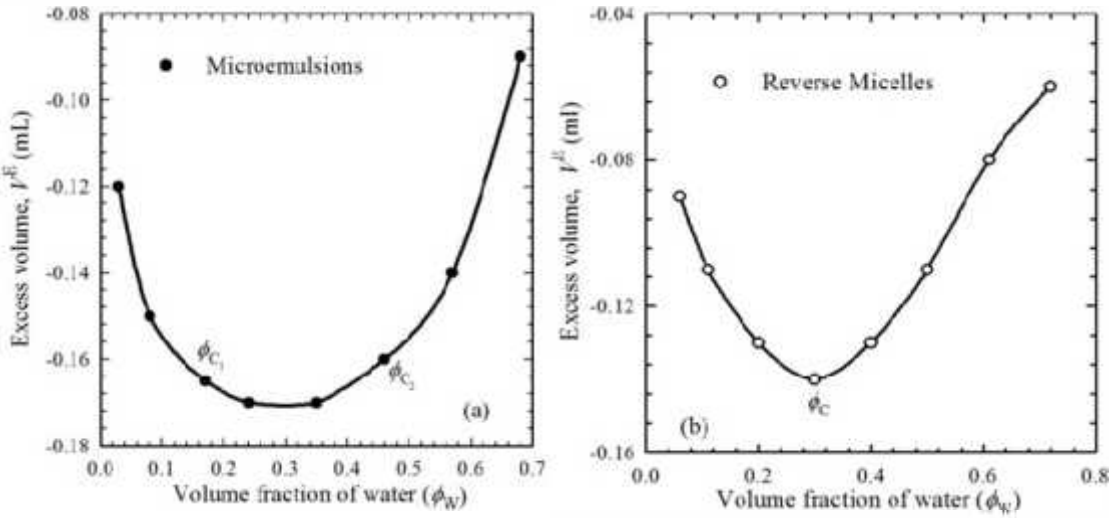

Figure 3.3.3. The V^E of (a) CTAB/1-butanol/cyclohexane/water microemulsions and (b) CTAB/1-butanol/water reverse micelles as a function of ϕ_W.

In microemulsions of CTAB (figure 3.3.3 (a)), V^E decrease for $\phi_W < 0.17$. For $\phi_W = 0.17 \sim 0.45$, V^E is almost constant. For $\phi_W > 0.45$, V^E increases. In reverse micelles of CTAB (figure 3.3.3(b)), V^E decreases up to $\phi_W = 0.30$ then increases. Negative values of V^E in reverse micelles and microemulsions indicate that the system contracts upon mixing. This behavior of V^E indicates that structural transition in microemulsion region occurs at $\phi_W = 0.17$ (ϕ_{C_1}) and 0.45 (ϕ_{C_2}) whereas, in reverse micelles the phase transitions occur at $\phi_W = 0.30(\phi_C)$ [20].

3.3.1.3. Excess Refractive Index from Refractive Index Results

The refractive index of CTAB/1-butanol/cyclohexane/water microemulsions and CTAB/1-butanol/water reverse micelles decreases with increasing ϕ_W (Figure 2.3.9). The excess refractive index (n^E) can be calculated from the following relation (equation 3.4),

$$n^E = n_{\text{Mic}} - \sum_i \phi_i n_i \quad \text{.....(3.4)}$$

where n_{Mic}= measured refractive index of microemulsions or reverse micelles, ϕ_i = volume fraction of component *i* in microemulsions or reverse micelles and n_i = refractive index of component *i*. Figure 3.3.4 represents the change in n^E of CTAB/1-butanol/cyclohexane/water microemulsions and CTAB/1-butanol/water reverse micelles as a function of ϕ_W. In microemulsions of CTAB (Figure 3.3.4 (a)), the value of n^E decreases sharply for $\phi_W < 0.17$. For $\phi_W = 0.17 \sim 0.45$, the n^E decreases slightly. For $\phi_W > 0.45$, the n^E increases. In reverse micelles of CTAB (Figure 3.3.4(b)), the n^E decreases up to $\phi_W = 0.30$ then increases. This behavior of n^E might correspond to the structural transitions in microemulsion region which occurs at $\phi_W = 0.17$ (ϕ_{C_1}) and 0.45 (ϕ_{C_2}) where in the reverse micelles the phase transition occurs at $\phi_W = 0.30(\phi_C)$.

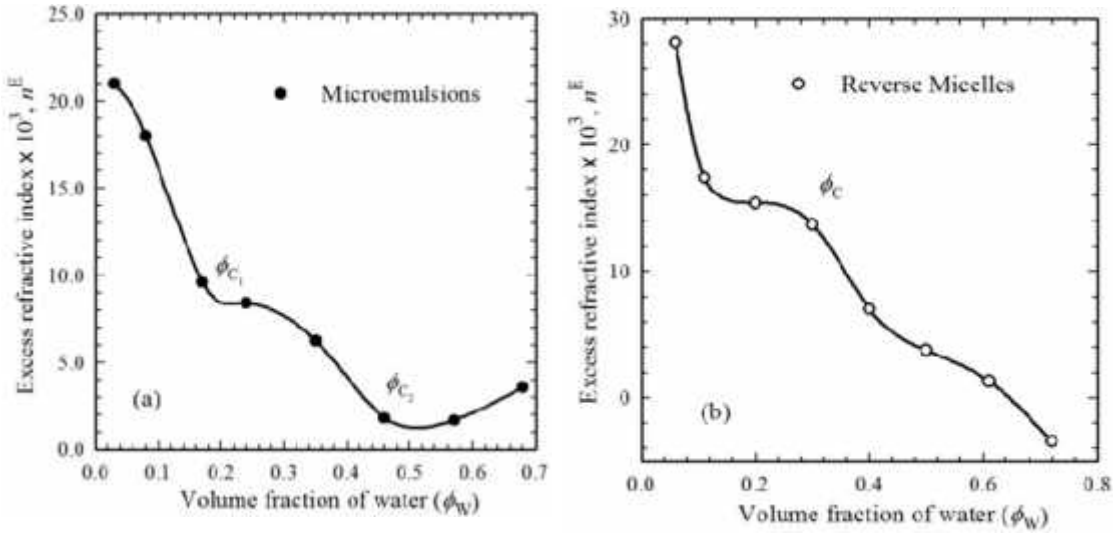

Figure 3.3.4. The n^E of (a) CTAB/1-butanol/cyclohexane/water microemulsions and (b) CTAB/1-butanol/water reverse micelles as a function of ϕ_W.

3.3.1.4. Excess Molar Refraction from Refractive Index Results

Excess molar refraction (R^E) values provide more information than n^E about the mixture phenomenon since molar refraction is directly related to the dispersion forces. The R^E values are calculated for all the mixtures using following equation (3.5)

$$R^E = R_{Mic} - \sum_i \phi_i R_i \quad \text{.....(3.5)}$$

where, R_{Mic} = molar refraction of microemulsions or reverse micelles calculated from refractive index results, ϕ_i = volume fraction of component *i* in microemulsions or reverse micelles and R_i = molar refraction of component *i*. Figure 3.3.5 represents the change in R^E of CTAB/1-butanol/cyclohexane/water microemulsions and CTAB/1-butanol/water reverse micelles as a function of ϕ_W. The phase transitions in microemulsions and reverse micelles of CTAB was further confirmed by the R^E vs. ϕ_W profiles where the R^E decreases with increasing ϕ_W with different patterns in different structures of microemulsions and reverse micelles. These profiles also give two phase transitions in microemulsions and one phase transition in reverse micelles which are consistent with other results.

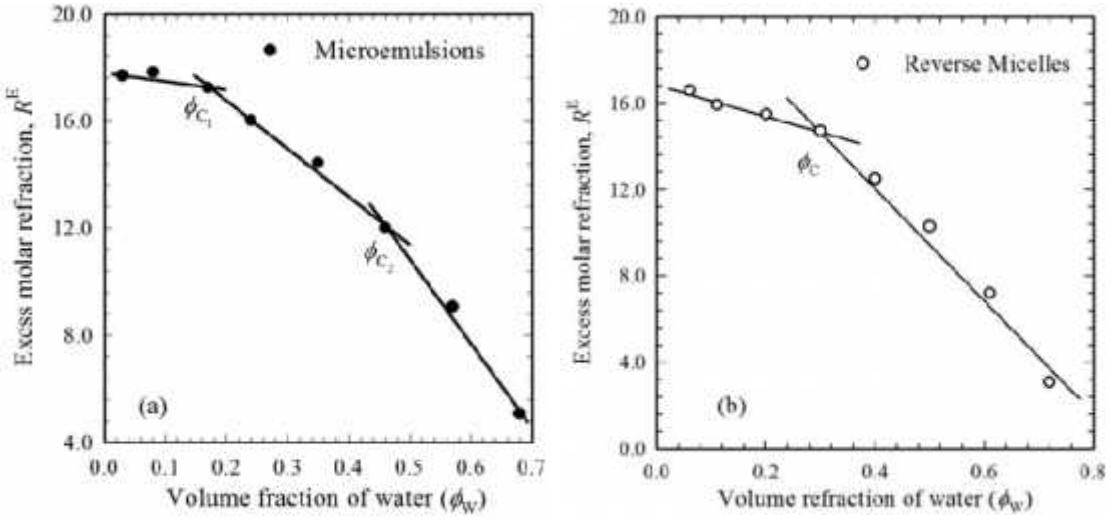

Figure 3.3.5. The R^E of (a) CTAB/1-butanol/cyclohexane/water microemulsions and (b) CTAB/1-butanol/water reverse micelles as a function of ϕ_W.

3.3.2. Percolation Thresholds in Microemulsions and Reverse Micelles of SDS

3.3.2.1. Percolation Thresholds from Conductivity Results

The percolation thresholds in SDS/1-butanol/cyclohexane/water microemulsions and SDS/1-butanol/water reverse micelles were also determined from conductivity results by $d(\log\sigma)/d\phi_W$ vs. ϕ_W plots. Figure 3.3.6 represents the $d(\log\sigma)/d\phi_W$ vs. ϕ_W plots for reverse micelles and microemulsions of SDS. In microemulsions of SDS (Figure 3.3.6(a)), the phase transitions occur at ϕ_W = 0.20 and 0.40, while for reverse micelles (Figure 3.3.6 (b)), the phase transition occurs at only ϕ_W = 0.42. Figure 3.3.6, indicates that microemulsions of SDS are *double percolation* systems and the reverse micelles of that are *single percolation* systems. Figure 3.3.7 represents the plots of $\log\sigma$ vs. $\log(\phi - \phi_C)$ for $\phi > \phi_C$ and $\log\sigma$ vs. $\log(\phi_C - \phi)$ for $\phi < \phi_C$ for SDS/1-butanol/cyclohexane/water microemulsions at ϕ_W = 0.20 (ϕ_{C_1}) and 0.40 (ϕ_{C_2}) and SDS/1-butanol/water reverse micelles at ϕ_W = 0.42 (ϕ_C).

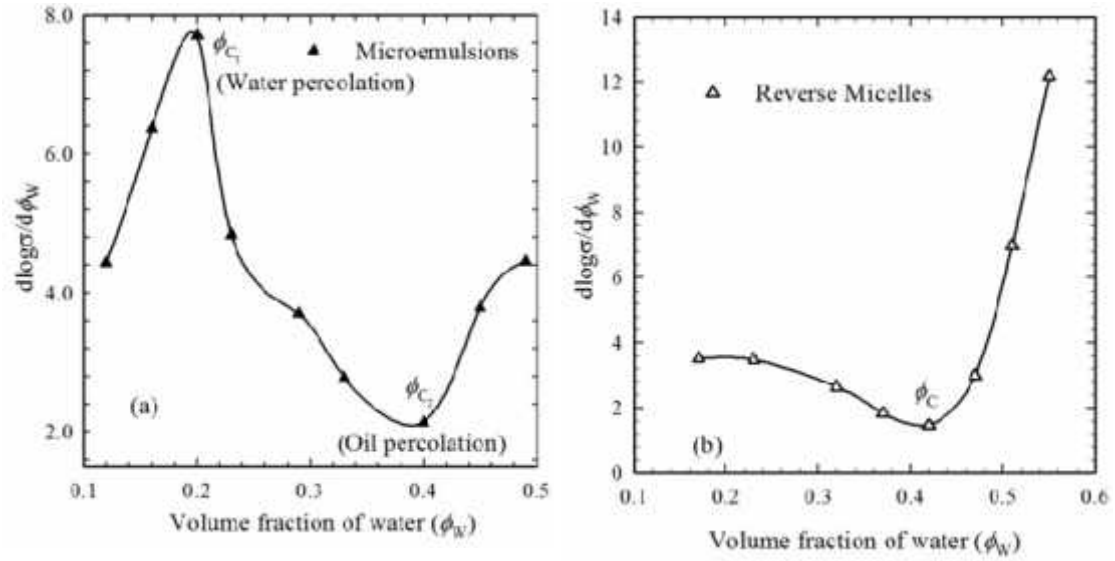

Figure 3.3.6. The $d\log\sigma/d\phi_W$ against ϕ_W for (a) SDS/1-butanol/cyclohexane/water microemulsions and (b) SDS/1-butanol/water reverse micelles.

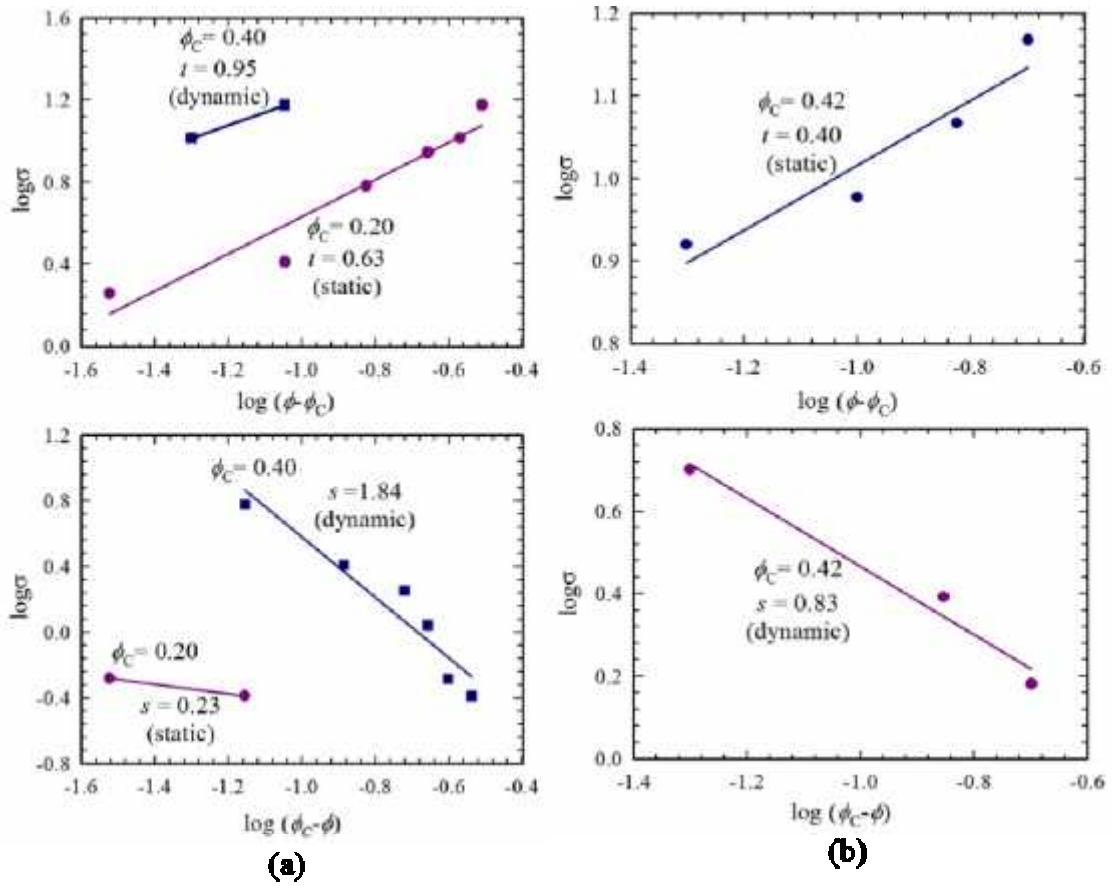

Figure 3.3.7. Plots of logσ vs. log (ϕ - ϕ_C) for $\phi > \phi_C$ and logσ vs. log (ϕ_C - ϕ) for $\phi < \phi_C$ for (a) SDS/1-butanol/cyclohexane/water microemulsions at ϕ_W = 0.20 (ϕ_{C_1}) and 0.40 (ϕ_{C_2}) and (b) SDS/1-butanol/water reverse micelles at ϕ_W = 0.42 (ϕ_C).

For microemulsions of SDS (Figure 3.3.7 (a)), the value of $t = 0.63$ and $s = 0.23$ could be obtained at ϕ_C above 0.20 which indicates static percolation system of the *BC* microemulsions and above $\phi_C = 0.40$, the value of $t = 0.95$ and $s = 1.84$, which signifies dynamic percolation system arising from droplet microemulsions. For reverse micelles of SDS (Figure 3.3.7(b)), above $\phi_C = 0.42$, $t = 0.40$ and below $\phi_C = 0.42$, $s = 0.83$ that only shows the static percolation system.

3.3.1.2. Excess Volume from Density Results

The density increases with increasing ϕ_W for SDS/1-butanol/cyclohexane/water microemulsions and SDS/1-butanol/water reverse micelles (Figure 2.3.17). The V^E of the reverse micelles and microemulsions of SDS formation should be evaluated by using the relation in equation (3.3) [20]. Figure 3.3.8 represents the variation in V^E of SDS/1-butanol/cyclohexane/water microemulsions and SDS/1-butanol/water reverse micelles with ϕ_W.

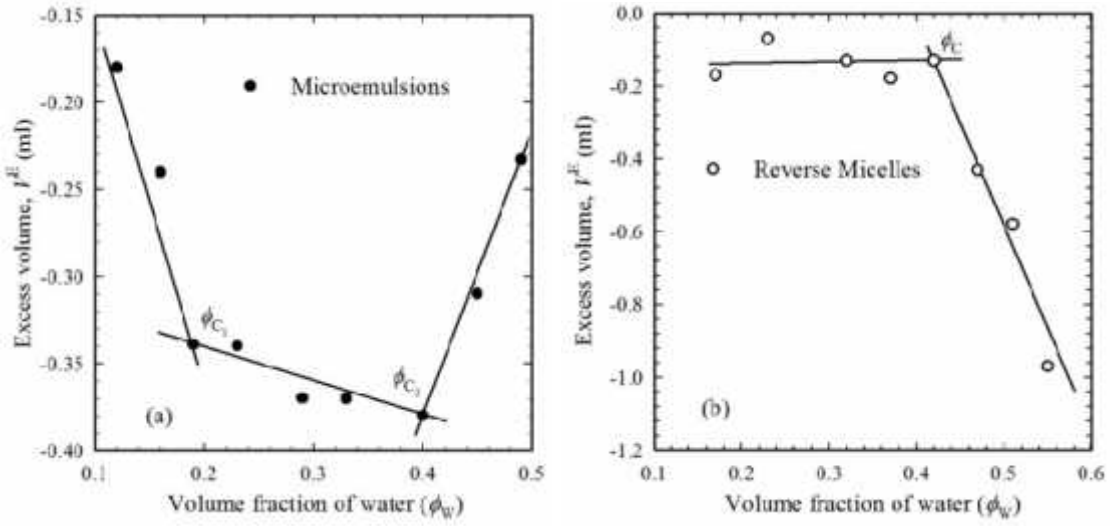

Figure 3.3.8. The V^E of (a) SDS/1-butanol/cyclohexane/water microemulsions and (b) SDS/1-butanol/water reverse micelles as a function of ϕ_W.

In microemulsions of SDS (Figure 3.3.8 (a)), V^E is also negative and decreases for $\phi_W < 0.20$. For $\phi_W = 0.20 \sim 0.40$, V^E decreases slightly. For $\phi_W > 0.40$, V^E increases. In reverse micelles of SDS (Figure 3.3.8 (b)), V^E is almost constant up to $\phi_W = 0.42$ then decreases. This behavior of V^E indicates that structural transition in the microemulsion of SDS occurs at $\phi_W = 0.20$ (ϕ_{C_1}) and 0.45 (ϕ_{C_2}) whereas, in the reverse micelles the transition occurs at $\phi_W = 0.42(\phi_C)$ [20].

3.3.1.3. Excess Refractive Index from Refractive Index Result

The n^E can be calculated using equation (3.4). Figure 3.3.9 represents the change in n^E of SDS/1-butanol/cyclohexane/water microemulsions and SDS/1-butanol/water reverse micelles with ϕ_W.

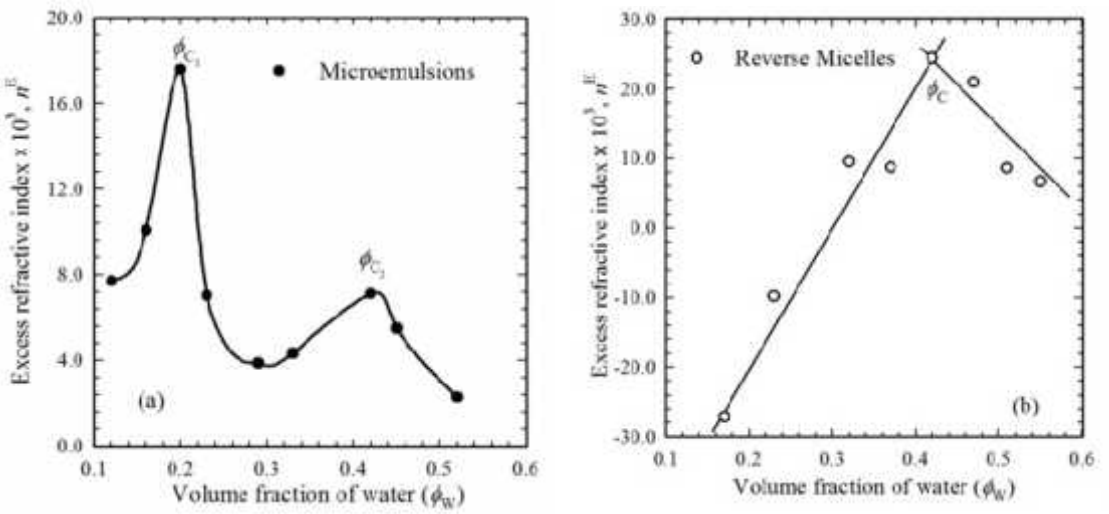

Figure 3.3.9. The n^E of (a) SDS/1-butanol/cyclohexane/water microemulsions and (b) SDS/1-butanol/water reverse micelles as a function of ϕ_W.

The value of n^E in microemulsions of SDS (Figure 3.3.9 (a)), shows special pattern which should be corresponds to three different regions in microemulsions with increasing ϕ_W. In reverse micelles of SDS (Figure 3.3.9 (b), the n^E increases up to $\phi_W = 0.42$ then decreases. This behavior of n^E also indicates that structural transition occurs at $\phi_W = 0.42$ (ϕ_C) such as *w*/*o* to *o*/*w* microemulsions *via BC* microemulsions [21].

3.3.2.4. Excess Molar Refraction - from Refractive Index Results

Figure 3.3.10 represents the change in R^E of SDS/1-butanol/cyclohexane/water microemulsions and SDS/1-butanol/water reverse micelles with ϕ_W.

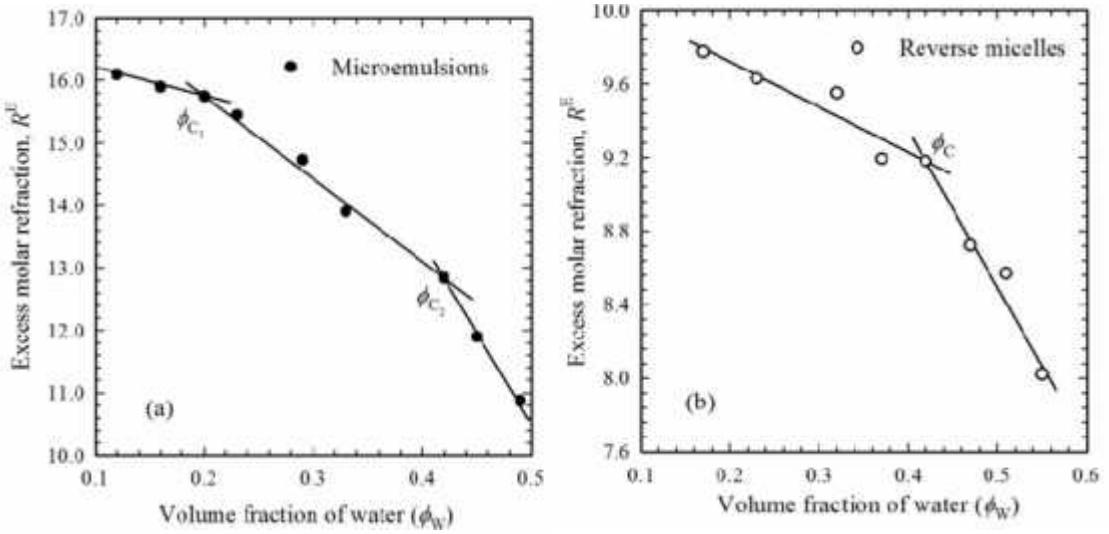

Figure 3.3.10. The R^E of (a) SDS/1-butanol/cyclohexane/water microemulsions and (b) SDS/1-butanol/water reverse micelles as function of ϕ_W.

The phase transitions in microemulsions and reverse micelles of SDS were further confirmed by the R^E vs. ϕ_W profiles where the R^E decreases with increasing ϕ_W with different patterns in different structures of microemulsions and reverse micelles [21, 22]. These profiles also support two phase transitions in microemulsions and one phase transition in reverse micelles which are in agreement with other results.

3.4. Microstructures of Reverse Micelles and Microemulsions

According to percolation theory and percolation scaling law, from conductivity resultsthe phase transitions in CTAB/1-butanol/cyclohexane/water microemulsions occurs in ϕ_W = 0.17 (ϕ_{C_1}) (19.6 %wt. of water) and 0.46 (ϕ_{C_2}) (49.6 %wt. of water). In CTAB/1-butanol/water reverse micelles, the transitions on the other hand, occur at ϕ_W = 0.30 (ϕ_C) (33.0 %wt. of water). For SDS/1-butanol/cyclohexane/water microemulsions, the phase transitions occur in ϕ_W = 0.20 (ϕ_{C_1}) (21.5 %wt. of water) and 0.40 (ϕ_{C_2}) (48.9 %wt. of water). In the case of SDS/1-butanol/water reverse micelles, the transition occurs at ϕ_W = 0.42 (ϕ_C) (45.0 %wt. of water). Thus, we can identify three different structures of reverse micelles and microemulsions such as, *w*/*o*-*BC*-*o*/*w* structures which are in accordance with calculated V^E and n^E results. As a result, in general, the phase transitions from *w*/*o* - *BC* structure and *BC* - *o*/*w* structure in microemulsions occurs at 20 %wt. of water and 50 %wt. of water, respectively. Scheme 3.1 shows three different structures of microemulsions with increasing ϕ_W .

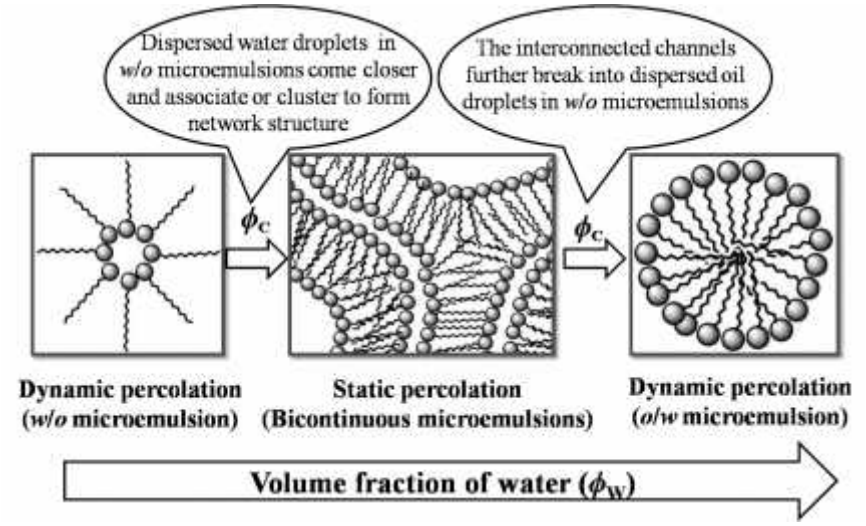

Scheme 3.1. Three different structures of microemulsions with increasing ϕ_W.

3.4. Conclusions

The change in dynamic properties such as conductivity, viscosity and surface tensions with ϕ_W gives definite indication about the microstructures of CTAB/1-butanol/cyclohexane/water and SDS/1-butanol/cyclohexane/water systems. For these systems, by applying percolation scaling law on conductivity results, three different

microstructures could be observed from percolation thresholds such as *w*/*o*, *BC* and *o*/*w* microemulsions. When ϕ_W is below percolation thresholds, the interaction between the isolated water droplets in oil (*w*/*o* microemulsions) is relatively weak. With increasing ϕ_W (above the percolation thresholds), the water droplets appear to retain their identity but probably form either weakly bound clusters or *BC* phase where CTAB/SDS aggregation number changes and they migrate from the continuous phase to the interface. With further increasing ϕ_W, the organization of CTAB/SDS changes reversely and formed *o*/*w* microemulsions. The V^E - ϕ_W, n^E - ϕ_W and R^E- ϕ_W profiles for these systems also indicates the structural phase transitions from *w*/*o* to *o*/*w* microemulsions through *BC* microemulsions.

References

[1] K. L. Mittal, *Micellization, solubilization and microemulsions*, Plenum, New York, 1977.

[2] P. Constantinides, *Lipid microemulsions for improving drug dissolution and oral absorption: physical and biopharmaceutical aspects.* Pharmaceutical Research, 1995, 12, 1561-1572.

[3] M. Lagues, R. Ober et C. Taupin, *Study of structure and electrical conductivity in microemulsions: evidence for percolation mechanism and phase inversion*. Journal De Physique - Letters. 1978, 39, 487-491.

[4] S. A. Safran, G. S. Grest, A. L. R. Bug, *In percolation in interacting microemulsions*, Marcel Dekker: New York, 1987, 235-243.

[5] P. D. I. Fletcher, A. M. Howe, B. R. Robinson, *The Kinetics of solubilizate exchangebetween water droplets in water in oil microemulsions*, Faraday Trans. I, 1987, 83, 985-1006.

[6] Z. Jeirani, B. M. Jan, B. S. Ali, I. M. Noor, S. C. Hwa, W. Saphanuchart, *Prediction of water percolation threshold of a microemulsion using electrical conductivity measurements and design of experiments*, Industrial & Engineering Chemistry Research, 2012, 51, 10147-10155.

[7] L. García-Río, J. R. Leis, J. L. López-Fontán, J. C. Mejuto, V. Mosquera, P. Rodríguez- Dafonte, *Mixed micelles of alkylamines and cetyltrimethylammonium chloride*. Journal of Colloid Interface Science, 2005, 289, 521-529.

[8] M. Fanun, *Conductive flow parameters of mixed nonionic surfactants microemulsions*, Journal of Dispersion Science and Technolology, 2008, 29, 1426-1434.

[9] S. K. Mehta, G. Kaur, R. Mutneja, K. K. Bhasin, *Solubilization, microstructure, and thermodynamics of fully dilutable U-type brij microemulsion*. Journal of Colloid Interface Science, 2009, 338, 542-549.

[10] M. Fanun, *Formulation and characterization of microemulsions based on mixed nonionic surfactants and peppermint oil*, Journal of Colloid Interface Science, 2010, 343, 496-503.

[11] S. K. Mehta, R. K. Dewan, K. Bala, *Percolation phenomenon and the study of conductivity, and ultrasonic velocity in microemulsions*, The American Physical Society, 1994, 50, 4759-4762.

[12] S. K. Mehta, K. Bala, *Tween-based microemulsions: a percolation view*, Fluid Phase Equilibrium. 2000, 172, 197-209.

[13] M. Fanun, *Phase behavior, transport, diffusion and structure parameters of nonionic surfactants microemulsions,* Journal of Molecular Liquids, 2008, 139, 14-22.

[14] M. Fanun, *A study of the properties of mixed nonionic surfactants microemulsions by NMR, SAXS, viscosity and conductivity*, Journal of Moecular Liquid, 2008, 142, 103-110.

[15] W. Meier, H-F Eicke, *Electric, dielectric and Kerr effect investigations in water in oil microemulsions*, Current opinion in colloid and interface science, 1996, 1, 279-286,

[16] B. Antalek, A. J. Williams, J. Texter, *Self-diffusion near the percolation threshold in reverse microemulsions*, The American Physical Society, PHYSICAL REVIEW E, 1996 54, 913-916.

[17] M. Lagues, C. Sauterey, *Percolation transition in water in oil microemulsions: electrical conductivity measurements*, Journal of Physical Chemistry, 1980, 84, 3503-3508.

[18] J. Peyrelasse, M. Moha-Ouchane, C. Boned, *Viscosity and the phenomenon of percolation in microemulsions*, The American Physical Society PHYSICAL REVIEW A, 1988, 38, 4155-4161.

[19] M. A. van Dijk, G. Casteleijn, J. G. H. Joosten, Y. K. Levine, *Percolation in oil continuous microemulsions. A dielectric study of aerosolOT/water/isooctane,* The Journal of Chemical Physics, 1986, 85, 626-631.

[20] M. Fanun, Z. Ayad, S. Mudalal, S. Dahoah, D. Meltzer, M. Schwarze, R. Schomacker, J. Blum, *Characterization of water/sucrose laurate/n-propanol/allylbenzene microemulsions*, Journal of Surfactants and Detergents, 2012, 15, 505-512.

[21] D. S. Wankhede, *Refractive indices for binary mixtures of propylene carbonate,* International Journal of Chemistry Research, 2011, 2, 23-26.

[22] R. Talegaonkar, A. S. Burghate, S. A. Wadal, *Study of molar refraction and polarizability constant of substituted thiazolyl Schiff's bases from refractive index measurement in different media,* Oriental Journal of Chemistry, 2011, 27, 1285-1288.

Abstract

Kinetics of the hydrolysis of CV has been investigated in aqueous solution and micelles, reverse micelles and microemulsions of SDBS/SDS, CTAB and TX-100 using spectrophotometric method under pseudo first order conditions. The k' of alkaline hydrolysis of CV in absence of surfactants obeyed the rate equation $k' = k_w [OH^-]$ yielding a value of 0.234 $M^{-1}s^{-1}$ for the bimolecular rate constant, k_w in aqueous solution. The reaction rates were found to be catalyzed by micellar solutions of CTAB and TX-100 but inhibited by SDBS. The k'-[CTAB] profiles show a maximum at [CTAB] = ca. 10 mM after which k' gradually decreases with increasing [CTAB]. On the other hand, with increasing [SDBS], the k' decreases and passes through a minimum at 1.84 mM (close to the CMC), above which the rate constant increases slightly. In presence of TX-100 in aqueous solution, the rate of the reaction was also accelerated up to [TX-100] = ca. 0.76 mM and then the rate constant becomes almost constant. The catalysis of the reaction by micelles of CTAB, SDBS and TX-100 was treated using Piszkiewicz and PPIE model to fit the experimental data for obtaining the binding constant of CV with CTAB, SDBS and TX-100 and other kinetic parameters. In reverse micelles and microemulsions of CTAB, SDS and TX-100, the k' - ϕ_W profiles for hydrolysis of CV show special patterns for structural variation of microemulsions, such as *w*/*o* to *o*/*w* microemulsions via *BC* microemulsions. Thus, the rate of reactions can be controlled by using micelles, reverse micelles and microemulsions of different surfactants.

4.1. Introduction

The catalysis of reactions by micelles, reverse micelles and microemulsions has a long and productive history because of its importance in chemical, industrial, pharmaceutical, environmental as well as biological fields [1, 2]. With a proper choice of surfactant and a medium, the rate of a reaction can be enhanced 5–10^5-fold compared to the same reaction in the absence of a surfactant. This resulted in an upsurge of interest to unveil the mechanism of catalysis in such surfactant-based organized media through studies on some model reactions.

Numerous attempts have been made to investigate the catalysis of reactions by micelles, reverse micelles, and microemulsions using a wide variety of substrates, which *inter alia,* include: esters [3, 4], drugs [5-8], and some carbocationic dyes [9-16]. The most widely used substrate has been a triphenylmethane dye, crystal violet (CV) due to its high solubility both in aqueous and organic phase and reversibility of the alkaline hydrolysis of the dye to yield colorless carbinol with high value of equilibrium constant. The rate of the alkaline fading of CV has been reported to be greatly accelerated by the addition of cationic surfactants [11, 14, 15] and retarded by anionic surfactants [10, 11, 16, 17]. The addition of some additives in micelles such as, a polymer [18] cyclodextrins [19] and counterions [2, 17] in CTAB or SDS micelles produced inhibitory effect on the rate of the alkaline fading of CV.

Micellization behavior changes with concentration and kind of alcohol and consequently reverse micelles also influence chemical reactivity. For instance, 1-hexanol, 1-octanol incorporation into CTAB micelles inhibits the basic hydrolysis of CV [20]. The reaction has been considerably studied in the medium of anionic, nonionic, and cationic reverse micelles [9-11, 16, 17, 20-25, 27, 28]. Physical properties of such systems can be tuned by changing the composition and nature of surfactants and have the potential to control their behavior as a reaction medium [29].

Microemulsions can solubilize a wide variety of compounds simultaneously and offer the possibility of reagent compartmentalization. These have proved to be very versatile reaction media that induce drastic changes in the reagent concentrations and thus can be specifically used for tuning the reaction rates1. The uses of microemulsions as media for a large number of reactions including: nucleophilic substitution reactions [30-33], enzymatic reactions [34, 35] and hydrolysis reactions [37-41] are well-known. The reaction rate of alkaline hydrolysis of CV was reported in aerosol-T (AOT)/isooctane/water and water/AOT/*n*-decane microemulsions [9]. The alkaline hydrolysis of CV has been also studied in *w*/*o* microemulsions of the CTAB/alkanols/cyclohexane system where the reaction has been considered to occur in the water phase of the droplets [40].

Despite numerous studies, the mechanism of catalysis of the alkaline hydrolysis of CV by micelles, reverse micelles and microemulsions has not yet been well established. In this study, an attempt has been made to make a comprehensive investigation of the kinetics of the alkaline hydrolysis of CV in micelles, reverse micelles and microemulsions of CTAB, SDBS/SDS and TX-100. The binding constant of CV with different surfactants was also measured by applying theoretical treatments based on different micellar kinetic model. The ultimate goal has been to understand the mechanism of catalysis by micelles, reverse micelles and microemulsions of CTAB, SDBS/SDS and TX-100 under different reaction environment.

4.2. Experimental

4.2.1. Materials

CV (BDH), CTAB (BDH), SDBS/SDS (E. Merck) and TX-100 Sigma, NaOH each were reagent grade materials and were used as received without further purification. The CMCs of surfactants in aqueous solution at 25 °C are as follows, CTAB: 0.87 mM [42], SDBS: 2.07 mM [17], TX-100: 0.22 mM (Section 2.3.1) [43].

4.2.1.1. Preparation of Microemulsions and Reverse Micelles

The reverse micelles and microemulsions of CTAB, SDS and TX-100 were prepared at fixed CTAB (20 %wt.) or SDS (15 %wt.) or TX-100 (20 %wt.) and cyclohexane (0 and 3.4 %wt. for CTAB) or (0 and 20 %wt. for SDS) or (0 and 72 %wt. for TX-100) with

different water and 1-butanol contents that ranged from high water to high 1-butanol content. De-ionized double distilled water with specific conductivity $<0.5\times10^{-6}$ Scm^{-1} at 25 ^{o}C was used for this purpose.

4.2.2. Kinetic Measurements

The kinetic measurements were made spectrophotometrically by a double beam Shimadzu UV-visible spectrophotometer model UV1650C with cuvettes having an internal thickness of 1.00 cm, at 25 °C. It was equipped with spectral data processing facilities. The sensitivity of the equipment was 0.001 absorbance unit at a signal to noise ratio of 1. The reaction of alkaline hydrolysis of CV was followed by observing the decrease in absorbance at 590 nm (λ_{max}) as a function of time. In all kinetic runs, the initial CV^+ concentration of 1.00×10^{-5} M was used, whereas that of [NaOH] = 0.01 M. Under the above conditions, $[CV^+] \ll [OH^-]$ and the reaction proceeds as the pseudo-first-order one. The observed pseudo-first-order rate constants, k', were obtained from the slopes of the dependence of lnA versus time using the equation:

$$\ln(A_0 / A) = k' t \text{ ---------- } (4.1)$$

where A and A_0 are the absorbance of the solution at time t and the initial absorbance, respectively. Equation (4.1) describes the experimental dependences of $\ln(A_0)/A)$ on t as a straight line; the good linearity was observed for all experimental data with correlation coefficient more than 0.96. The second-order rate constants of the reaction were calculated as $k = k'/[OH^-]$.

4.3. Results and Discussion

4.3.1. Micellar Catalysis on the Alkaline Hydrolysis of CV in Presence of CTAB, SDBS and TX-100

4.3.1.1. Spectral Behavior of CV in Presence of CTAB, SDBS and TX-100

The visible absorption spectrum of CV in aqueous solution consists [of a band corresponding to the symmetrical helical isomer (A isomer) at 584 nm with a shoulder at 533 nm corresponding to the distorted symmetrical helical isomer (B isomer) 44]. The equilibrium between isomers depends on the dielectric constant of the solvents. The relative intensities of the A and B bands (I_A and I_B) depend on solvent dielectric constant, and the I_A/I_B ratio increases with decrease in dielectric constant [22, 44].

The addition of SDBS in aqueous solution causes shift in the position of absorption maxima of CV towards a shorter wavelength till the CMC and then rises again to have a constant value [16]. The absorbance at 584 nm decreases until the concentration reaches close to the value of the CMC, above which the absorbance increases, On the other hand, absorbance at 533 nm increases with increasing [SDBS] and after a maximum at a concentration close to the CMC, it decreases. In aqueous solution, the absorbance of CV at 584 nm is higher than that of 533 nm; in other word, the A isomer dominates the

system. As SDBS is added till below the CMC, the strong interaction of SDBS with CV^+ distorts the symmetrical helical structure and B isomer dominates. At concentrations far above the CMC, solubilization of CV^+ in the core of micelles reduces the strong influence of the interaction and a situation similar to that in aqueous solution prevails. The A isomer is the major species under such conditions.

In the case of CTAB, the λ_{max} shifts to higher wavelength (592 nm) up to the CMC, then becomes almost constant. It seems that there is no interaction between CV^+ and CTAB. Obviously, at the beginning, a weak electrostatic interaction occurs between $(CH_3)_2N^-$ group of CV and positive head group of CTAB and along with hydrophobic interaction of CV with nonpolar moiety of CTAB results in the red shift in λ_{max} value of CV [42].

In presence of TX-100, increase in TX-100 concentration results in the red shift in λ_{max}(= 590 nm) value of CV^+. This indicates that, a preliminary weak electrostatic interaction occurs between $(CH_3)_2N^-$ group of CV^+ and oxygen atom of ethoxy chains of TX-100 which is similar to interaction of silanol groups of silica gel with TX-100 [16, 45]. This interaction along with further hydrophobic interaction of CV with TX-100 decreases dielectric constant of the CV microenvironment [16].

4.3.1.2. Hydrolysis in Aqueous Solution

The k' for hydrolysis of CV obeyed the equation $k' = k_w [OH^-]$ [11, 42]. The bimolecular rate constant k_w for the title reaction could be easily calculated using the different concentration of OH^-, which has been found to be 0.234 $M^{-1}s^{-1}$. Ritchi et al [46] reported a value of 0.201 $M^{-1}s^{-1}$ without mentioning any error. This value has been frequently quoted in the current literature [11, 17, 27, 42] and is in agreement with the result.

4.3.1.3. Hydrolysis in Presence of CTAB

The k' vs. [CTAB] profile for hydrolysis of CV is shown in Figure 4.3.1 [11, 42]. At [OH^-] = 0.01 M, the rate constant increases with increase in [CTAB] and after the CMC (= 0.87 mM), a pronounced sharp increase in the rate constant is observed and the rate is enhanced up to more than 10-fold in micellar solutions of CTAB. At concentrations below the CMC of CTAB, the reaction rates increase slightly possibly due to reactant-induced micellization or the premicelles may exist that affect the reaction rates, because sometimes hydrophobic nonmicellizing trimethylammonium ions increase reaction rates [47].

The catalytic effect caused by CTAB micelles (above the CMC) can be explained by considering both electrostatic and hydrophobic interactions which operate simultaneously in the reaction system. The CTAB micellar system has non-polar hydrocarbon chains in its core and positively charged head groups at periphery. In the CV, the positive charge is delocalized over the whole molecule and around the three phenyl rings due to resonance stabilization, thereby reducing the charge at specific. Thus, the electrostatic repulsion

between the CV^+ and the positively charged CTAB micellar surface is not strong due to the delocalization of the charge on CV^+ and the hydrophobic interaction can easily overcome the opposing but weak electrostatic interaction, binding CV^+ to the CTAB micelles. The CV^+ would be located in the micellar aggregate due to high hydrophobicity of CV containing benzene ring with alkyl group as substituent [48].

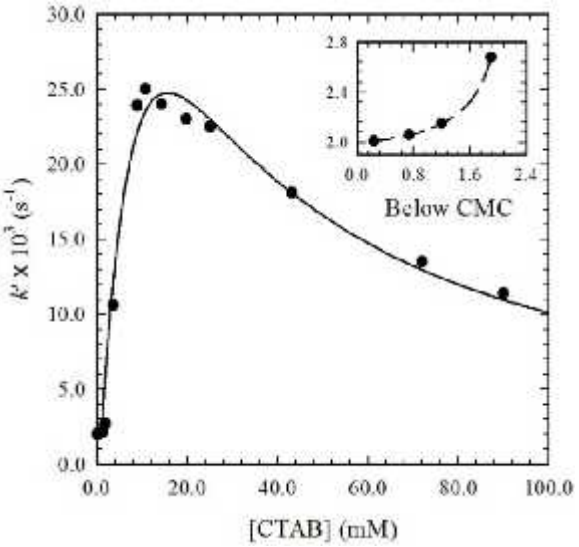

Figure 4.3.1. The *k*' for alkaline hydrolysis of 1.00×10^{-5} M CV as a function of [CTAB] at $[OH^-]$ = 0.01 M. Inset shows the value of *k*' at below the CMC of CTAB. Solid and dash line drawn using calculated values according to PPIE and Piszkiewicz's model, respectively.

The reagent OH^- being negative charged has favorable electrostatic attraction with the positively charged micellar surface of CTAB which facilitates the approach of OH^- to CV^+ incorporated into micellar aggregates. This results in the relative increase of $[OH^-]$ around the micellar surface as compared to the bulk phase where micelles are not present. Thus, the increase of local concentration of reactants (CV^+ and OH^-) around micellar interfaces causes the catalysis of the reaction of CV^+ with OH^- in the presence of CTAB which is illustrated in (SScheme 4.1).

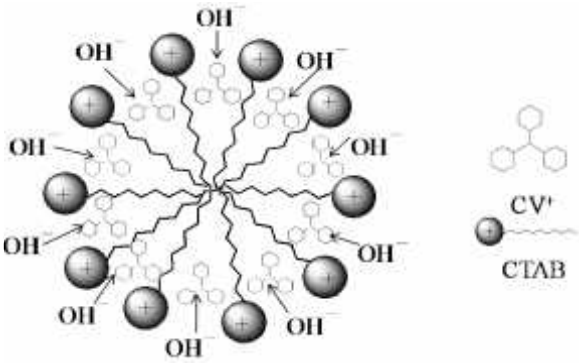

Scheme 4.1. Catalysis of the reaction of CV^+ with OH^- in presence of CTAB micelles.

With further increasing [CTAB] (at far above the CMC), the k' vs. [CTAB] plot reaches a maximum at [CTAB] = ca. 15.0 mM, after which the rate constant has been found to decrease gradually. This may be due to two facts. *Firstly*, the number of micelles increases with increase in [CTAB]. When the number of micelles exceeds that required solubilizing all of CV^+, there is a dilution of the concentration of CV^+ per micelle as the [CTAB] is increased further (Scheme 4.2a). This causes a reduction in the rate constant. *Secondly*, the charged surface of a CTAB micelle in aqueous solution may cause the adsorption of an oppositely-charged reactant (OH^-) on it, or even the solubilization of the OH^- into the micelle. Such adsorption or solubilization of the OH^- will result in a decrease in its activity in the solution phase (Scheme 4.2b). An increase in the [CTAB] over that required to effect substantially complete solubilization of the CV^+ may therefore result in decrease in the rate constant, even in those cases where rate enhancement by micelles occurs [42].

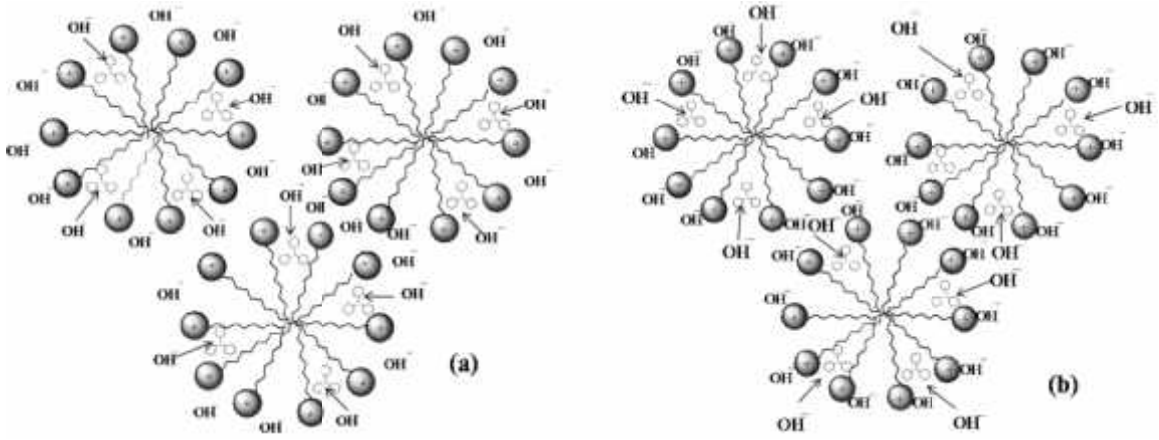

Scheme 4.2. Inhibition of the reaction of CV^+ with OH^- in presence of CTAB micelles at far above the CMC: (a) dilution of the concentration of CV^+ per micelle and (b) adsorption or solubilization of the OH^- on charged surface of CTAB micelles.

4.3.1.4. Hydrolysis in Presence of SDBS

The k' vs. [SDBS] [17] profile for alkaline hydrolysis of CV in is shown in Figure 4.3.2 at $[OH^-]$ = 0.122 M. The addition of SDBS retards the rate of the reaction for concentration of SDBS below the CMC and after the CMC the rate of reaction is accelerated slightly which indicates that micelle of SDBS is responsible for the change in rate constant. From Figure it has been shown that, the rate constant exhibits a decreasing trend and reaches a minimum at [SDBS] = 1.84 mM (below the CMC) initially after which the rate constant has been found to increase gradually with increase in [SDBS]. The sharp decrease in the rate constants is probably caused by the interaction of the CV^+ with anions of SDBS, which leads to the redistribution of the charge in cation and the lowering of positive charge on the CV^+. Also, the carbinol formation may be decelerated because the CV cations are hidden in the clusters of ionic pairs, CV^+DBS^- (Scheme 4.3) [49].

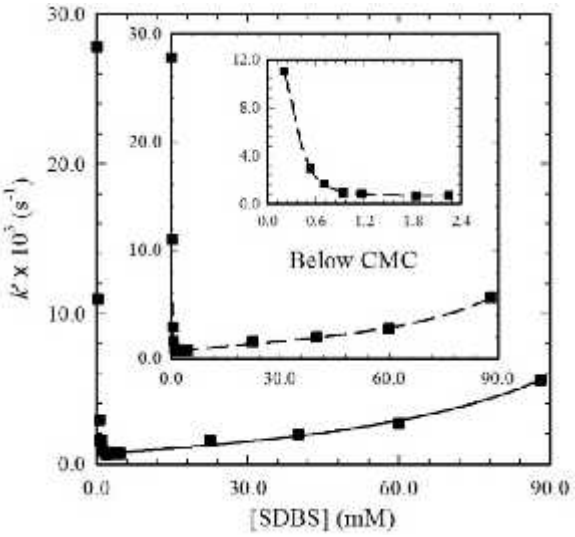

Figure 4.3.2. The k' for alkaline hydrolysis of 1.25×10^{-5} M CV as a function of [SDBS] at $[OH^-] = 0.122$ M. Inset shows the value of k' at below the CMC of SDBS. Solid and dash line drawn using calculated values according to PPIE and Piszkiewicz's model, respectively.

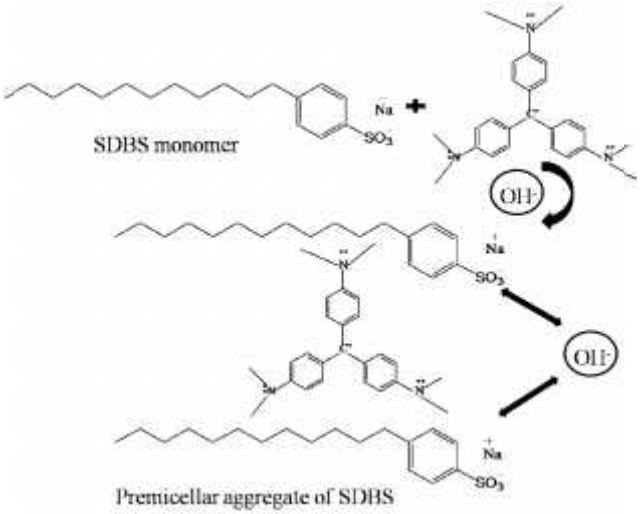

Scheme 4.3. Involvement of premicellar clusters during the reaction in presence of SDBS.

Above the CMC, as both the hydrophobic and electrostatic interactions between the CV^+ and anionic SDBS micelles are favorable to each other, the CV^+ are strongly bound to the SDBS micelles. The cores of SDBS micelles are hydrocarbon-like and due to the high hydrophobicity of the CV^+, it is solubilized into the micellar aggregate. It is also favored by the electrostatic interaction between the positively charged CV^+ and negatively charged SDBS micelles (Scheme 4.4). The OH^- which lacks hydrophobicity and bearing charge similar to that of SDBS micellar surface (or head group) is excluded from the micellar aggregates containing the CV^+. Thus, in presence of SDBS micelles, an

inhibitory effect is observed due to non-approachability of the nucleophile to the strongly bound CV^+ in the negatively charged SDBS aggregate [49].

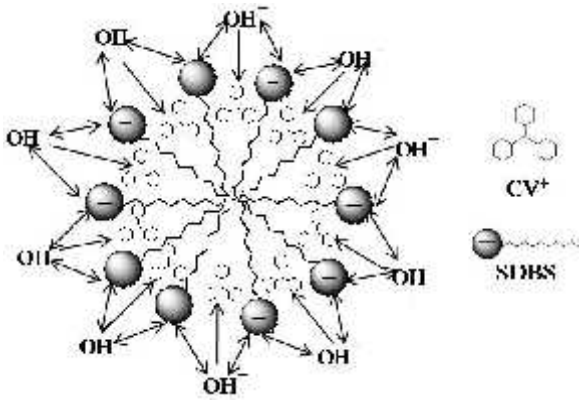

Scheme 4.4. Interaction of CV^+ with OH^- in presence of SDBS micelles.

4.3.1.5. Hydrolysis in Presence of TX-100

The *k*' vs. [TX-100] profile for the hydrolysis of CV is shown in Figure 4.3.3 at $[OH^-]$ = 0.011 M. With increasing [TX-100], the *k*' increases up to [TX-100] = 0.73 mM and then gradually decreases while the CMC of TX-100 is 0.22 mM [43]). With further increase in [TX-100], the rate constants are almost constant.

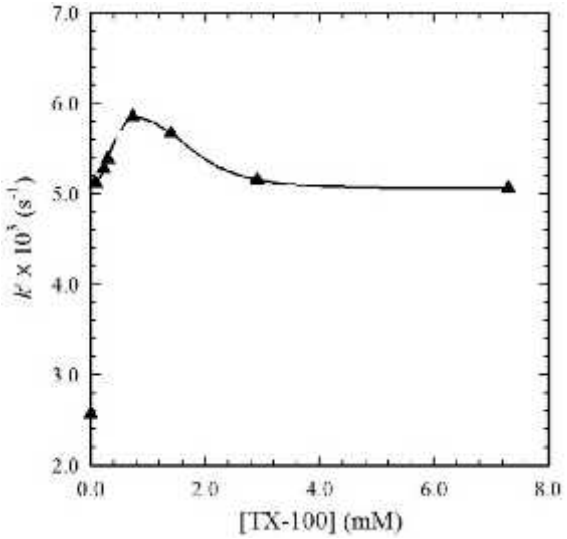

Figure 4.3.3. The *k*' for alkaline hydrolysis of 1.54×10^{-5} M CV as a function of [TX-100] at $[OH^-]$ = 0.01 M. Dashed and solid lines are drawn using calculated values according to Piszkiewicz's model for below and above the CMC of TX-100, respectively.

TX-100 is a nonionic surfactant. Unlike typical ionic surfactants, its hydrophilic counterpart, polyoxyethylene (POE) has a chain length longer than the hydrophobic part. The interaction of TX-100 with CV^+ is weak and cannot result in a remarkable effect on the alkaline rate constant. In micelles of TX-100, the hydrophobic parts having shorter

chain length are in interior (the micelle core) and the hydrophilic parts having longer chain length are in the exterior. As CV^+ is easily solubilized in the micelle core of TX-100 by hydrophobic interaction, the *k*' of the alkaline hydrolysis of CV increases up to 0.73 mM of TX-100 (Scheme 4.5). If [TX-100] is further increased, the value of *k*' slightly decreases which might be due to the hydrophobic repulsion between the different micelles of TX-100. At concentrations far above the CMC of TX-100, as TX-100 is non ionic, there is no electrostatic attraction and repulsion in between the CV^+ and nonionic POE counterpart results the constant values of *k*'.

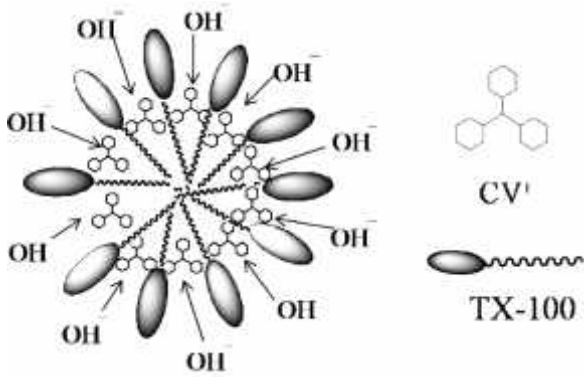

Scheme 4.5. Catalysis of the reaction of CV^+ with OH^- in presence of nonionic TX-100 micelles.

4.3.1.6. Application of Different Models on Micellar Catalysis

In order to understand the mechanism by which micelles catalyze reactions, many efforts have been made to study simpler model chemical reactions [50, 51]. Reactions catalyzed or inhibited by micelles have thus been viewed as models for enzyme catalyzed reactions [1, 52]. This analogy, though far from perfect, is based on the observation that micelles and enzymes are structurally and functionally similar. Both micelles and enzymes have hydrophobic cores with polar regions on their surfaces. Both bind substrate in a noncovalent manner. The kinetics of micellar catalysis also resembles that of enzyme catalysis as described in various investigations [1, 52, 53, 54]. The micellar catalysis of hydrolysis of CV by CTAB, SDBS and TX-100 were treated by Piszkiewicz and the PPIE model.

4.3.1.6.1. Analysis of Kinetic Data by Piszkiewicz Model

The Piszkiewicz model [53] analogous to the Hill model applied to the enzyme-catalyzed reactions may be considered with some modifications. According to this model, it is assumed that substrate, CV^+, in this work, associates with *n* number of surfactants, S to form critical micelle CV^+- S_n which may react as follows (Scheme 4.6)

$$CV^+ + nS \xleftrightarrow{K_S} S_n - CV^+$$

$$S_n - CV^+ \xrightarrow{k_M} \text{Product}$$

$$S \xrightarrow{k_W} \text{Product}$$

Scheme 4.6. The Piszkiewicz's model of premicellar catalysis.

The model gives the following rate equation:

$$k_{obs} = \frac{k_M[S]^n + k_W K_S}{K_S + [S]^n} \text{----------(4.2)}$$

where K_S is the dissociation constant of micellized surfactant-substrate compound back to its components (its reciprocal is the binding constant) and [S] gives the total surfactant concentration. Here, k_W is the reaction rate without any surfactant, and k_M is the reaction rate with the maximum amount of surfactant concentration within the given range and if reaction is inhibited by adding surfactant, $k_M = 0$. n is known as the cooperativity index which is a measure of the association of additional surfactants to an aggregate in the whole surfactant concentration range. If $n > 1$, cooperativity of interaction is positive, if $n < 1$, cooperativity of interaction is negative and if $n = 1$, interaction is noncooperative [53]. It is clear that equation (4.2), a two-parameter equation, can not fit properly the data of different types of surfactant-substrate interactions. The equation (4.3) may be rearranged to give,

$$\log \frac{k_w - k_{obs}}{k_{obs} - k_m} = n \log[S] - \log K_S \text{-----(4.3)}$$

According to equation (4.3), a plot of $\log[(k_w - k_{obs})/(k_{obs} - k_m)]$ versus log[S] should be linear with a slope of 'n' and an intercept of '$-\log K_S$'. Table 4.1 represents the n and K_S values obtained from Piszkiewicz model for interaction of CV^+ with CTAB, SDBS and TX-100.

Table 4.1. The n and K_S values obtained from Piszkiewicz model for interaction of CV^+ with CTAB, SDBS and TX-100.

	Premicellar region (below the CMC)			Postmicellar region (above the CMC)		
Surfactants	K_S	n	r^2	K_S	n	r^2
CTAB	2.66	1.20	1.00	---	---	---
SDBS	0.02	2.57	0.99	3.17	0.23	0.99
TX-100	0.09	2.54	1.00	12.5	4.24	1.00

It has been reported [53, 55] that for a given reaction '*n*' varies with the nature of the surfactant. At concentrations below the CMC of different surfactant, the evaluated values of *n* (>1, between 1 and 3) are in agreement with earlier observations [53, 55]. These '*n*' values are far less than the number of CTAB, SDBS and TX-100 found in the normal micelle (the aggregation number of CTAB, SDBS and TX-100 are 61 [56], 60 [57, 58] and 100-155 [59], respectively). The values of '*n*' are reported to be an indication of premicellar aggregates [53]. Since the values of K_S are very small for all surfactants, it indicates that the extent of dissociation of premicellar complex back to its free components is negligible. Before the formation of pre-micelles, CV^+ and the surfactant monomer may be considered to be in hydrated forms. However, in the pre-micellar aggregates, these surfactants interact with CV^+ in a stronger manner through hydrophobic as well as electrostatic interactions. These interaction forces are possibly stronger than the hydration interactions of the individual species, which may account for the small values of K_S for CTAB, SDS and TX-100 [49].

4.3.1.6.2. Analysis of Kinetic Data by PPIE Model

The PPIE model based on the effect of the competition between counterions and other ions of similar charge for ionic micellar surface on reaction rate. It suggests that both negatively charged species (reagent, OH^- and counterion of surfactants, Br^-) can bind to the positively charged CTAB micelles. Therefore, both the species compete with each other for inclusion in the micellar aggregate. Thus due to the exchange between OH^- and Br^- species between micellar (M) phase and bulk aqueous (W) phase, the OH^- ions are replaced from micellar surface. The exchange process may be represented as:

$$[OH^-]_M + [Br^-]_W \Leftrightarrow [Br^-]_M + [OH^-]_W$$

The observed effect of counterions on micellar catalysis cannot be attributed to the replacement of substrate from the micellar phase to the bulk phase, as the hydrophobic substrate is fully incorporated into micelles. The counterion, Br- does not compete with substrate or alter its distribution between micellar and bulk phase. According to this model, the binding constants of the interaction of surfactant with CV^+ and the observed rate constants, *k*' were calculated by using the following equation (4.4) [42]

$$k' = \frac{k_W[OH^-] + (k_M K_S - k_W) m_{OH}[M]}{1 + K_S[M]} \text{ - - - - - - - - - - (4.4)}$$

Here, [M] is the concentration of micellized surfactant given by, [M] = ([S] - CMC)/*N*, where [S] is the analytical concentration of the surfactant and *N* is the aggregation number (61 for CTAB in aqueous solution at 25 ^oC). The k_M refers to the second order rate constant in the micellar pseudopahse. The K_X^Y and K_S are the ion exchange equilibrium constant and the binding constant of the substrate to the micelles,

respectively. The fraction of micellar head groups neutralized by OH^- ions (m_{OH}) were obtained by solving equation 4.5 [37]. For aqueous solution of CTAB or SDBS,

$$m_{OH}^2 + m_{OH}\{\frac{[OH^-] + K_{Na}^{OH}[Na^+]}{(K_{Na}^{OH} - 1)[M]} - \beta\} - \frac{\beta[OH^-]}{(K_{Na}^{OH} - 1)[M]} = 0$$

or,

$$m_{OH}^2 + m_{OH}\{\frac{[OH^-] + K_{Br}^{OH}[Br^-]}{(K_{Br}^{OH} - 1)[M]} - \beta\} - \frac{\beta[OH^-]}{(K_{Br}^{OH} - 1)[M]} = 0 \qquad \text{- - - - - - (4.5)}$$

As this model cannot study the surfactant-substrate interactions below the CMC value of surfactants, the experimental data of alkaline hydrolysis of CV catalyzed by CTAB and SDBS only for above were fitted to both the equations 4.4 and 4.5 simultaneously, using k_M, K_S and K_{Br}^{OH} or K_{Na}^{OH} as adjustable parameters. The value of k_M, K_S and K_{Br}^{OH} or K_{Na}^{OH} obtained with best fitting at $[OH^-] = 0.01$ M, is shown in Table 4.2. The PPIE model is based on the counterion competition with the reactants of the reactions and fitting kinetic data is only possible for ionic surfactants.

Table 4.2. k_M, K_s and K_{Br}^{OH} or K_{Na}^{OH} values obtained from PPIE model for interaction of CV^+ with CTAB, and SDBS.

Surfactants	k_M (s^{-1})	K_X^Y	K_S	r^2
CTAB	0.14	1.0	54.81	0.99
SDBS	2.72×10^{-5}	0.1	416.0	0.98

From Table 4.2, it has been shown that the value of k_M for SDBS is lower than that for CTAB. The inhibitory effect on rate due to SDBS micelles can be explained by considering both electrostatic and hydrophobic interactions which operates simultaneously in the reaction system. In presence of SDBS micelles, as OH^- bears similar charge as that of anionic micelles, so they are unable to approach the strongly bound CV^+ with negatively charged SDBS micelles as effectively as it can do in absence of SDBS micelles, thus exhibiting inhibitory effect. But, in presence of CTAB, OH^- being negatively charged has favorable interaction with positively charged CTAB micellar aggregates containing hydrophobic substrate. Thus, the approach of OH^- is facilitated towards CV^+ and local concentration of OH^- increases round the micellar aggregates, leading to catalytic effect by CTAB [47].The calculated K_S for CV^+ with anionic surfactant, SDBS is much more than cationic surfactant, CTAB that is in accordance with the existing electrostatics and hydrophobic interaction in the reaction system (both interactions are favorable for SDBS, but only hydrophobic interaction is favorable for CTAB). Thus, the interaction of CV^+ with SDBS is stronger due to electrostatic-hydrophobic environment in SDBS micellar systems [47].

4.3.2 Hydrolysis of CV Catalyzed by Reverse Micelles and Microemulsions of CTAB

4.3.2.1. Spectral Behavior of CV in Aqueous Solution and Micelles, Reverse Micelles and Microemulsions of CTAB

Figure 4.3.4 shows spectra of 9.1×10^{-6} M CV in aqueous solution, 1-butanol, micelles (20 %wt. of CTAB in aqueous solution) and reverse micelles (20 %wt. of CTAB in 1-butanol).

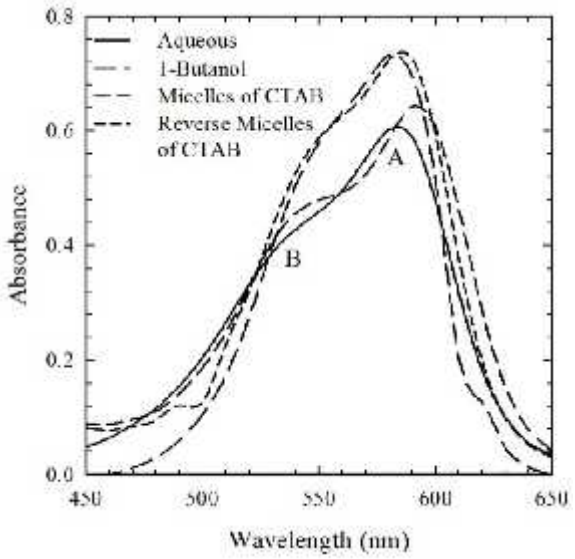

Figure 4.3.4. Spectra of 9.1×10^{-6} M CV in aqueous solution, 1-butanol, micelles (20 %wt. of CTAB in water) and reverse micelles (20 %wt. of CTAB in 1-butanol).

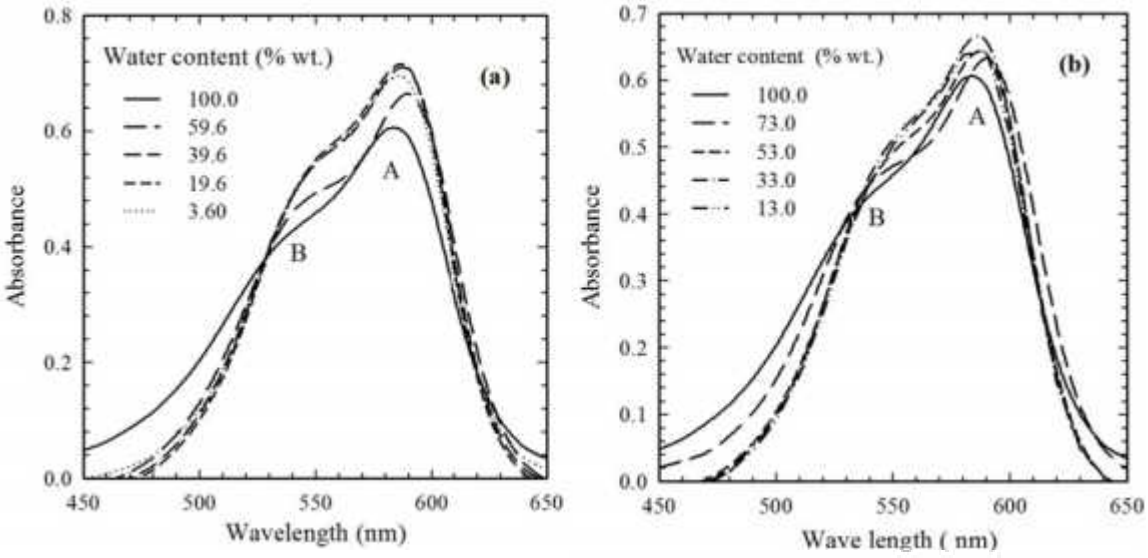

Figure 4.3.5. Spectra of 9.1×10^{-6} M CV in aqueous solution in comparison with (a) CTAB/cyclohexane/1-butanol/water microemulsions with 20 %wt. of CTAB, 3.4 %wt. of cyclohexane and different 1-butanol/water content and (b) CTAB/ 1-butanol/ water reverse micelles with 20 %wt. of CTAB and different 1-butanol/water content.

Upon addition of CTAB, the position of the λ_{max} shifts towards higher wavelength to 592 nm (A) with the shoulder at 541 nm (B). In 1-butanol and 20 %wt. CTAB in 1-butanol solution, the dielectric constant value is smaller and the A band had only a slight shift and the shoulder (B band) becomes less marked. The equilibrium between two isomers of the CV depends on the dielectric constant of the solvents in agreement with literatures [44]. Figure 4.3.5 shows the spectra of 9.1×10^{-6} M CV solutions in different CTAB/cyclohexane/1-butanol/water microemulsions and CTAB/1-butanol/water reverse micelles. As the content of water decreases, the A band shifted slightly to lower wavelength and the shoulder (B band) nearly disappeared indicating a change in the dielectric constant of the medium.

4.3.2.2. Hydrolysis in 1-Butanol

The values of *k*' of the reaction in aqueous solution shows a strong dependence on the dielectric constant of the medium [27, 44]. 1-butanol has lower dielectric constant (18.3 at 25 ^{o}C) compared to water (80.0 at 25 ^{o}C). The *k*' of the alkaline hydrolysis of CV with $[OH^-]$ = 7.4 mM in aqueous solution is 1.73×10^{-3} s^{-1} and in 1-butanol is 17.70×10^{-3} s^{-1}. This indicates that a solvent having lower dielectric constant, favors the hydrolysis reaction of CV compared to that with a high value [40]. The *k*' value for the title reaction under identical experimental conditions using water with 20 %wt. of CTAB was also found to be much lower (1.17×10^{-3} s^{-1}) than that in 1-butanol with 20 %wt. of CTAB (8.79×10^{-3} s^{-1}). This correspond to the fact that in 1-butanol with 20%wt. of CTAB, CTAB/1-butanol reverse micelles are formed where the hydrophilic part of CTAB form the core of reverse micelles and the hydrophobic parts are in the bulk. Thus, the reagent, OH^- is solubilized in the core of reverse micelles and easily reacts with the CV^+ which is in contact with the hydrophobic part of CTAB. The schematic diagram of the alkaline hydrolysis of CV^+ in CTAB/1-butanol reverse micelles is shown in Scheme 4.7.

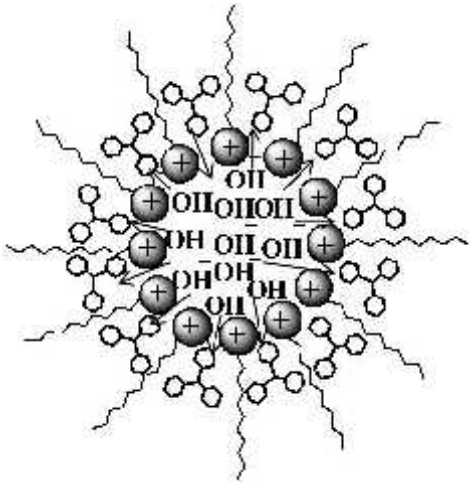

Scheme 4.7. Alkaline hydrolysis of CV in CTAB/1-butanol reverse micelles.

On the other hand, in water with 20 %wt. CTAB, the CTAB/water micelles are formed and the number of micelles are high enough to solubilize CV (discussed in Section 4.3.1.3.) resulting in the dilution of CV in each hydrophobic core of micelles. So, the rate constant value in water with 20 %wt. of CTAB is lower than that of the corresponding value in aqueous solution under identical conditions.

4.3.2.3. Hydrolysis in Presence of Reverse Micelles and Microemulsions of CTAB

Figure 4.3.6. represents the k' vs. ϕ_W profiles for alkaline hydrolysis of CV using [OH^-] = 7.4 mM in CTAB/1-butanol/water reverse micelles and CTAB/1-butanol/cyclohexane/water microemulsions with 0 and 3.4 %wt. cyclohexane, respectively. As ϕ_W in reverse micelles and microemulsion increases, the k' decreases first and then gradually increases; however, at lower water content (ϕ_W < 0.20) a sharp increase is apparent. The rate constant attains value much higher than the corresponding value in aqueous solution under identical experimental conditions. This is a clear indication of catalysis of the title reaction by microemulsions and reverse micelles.

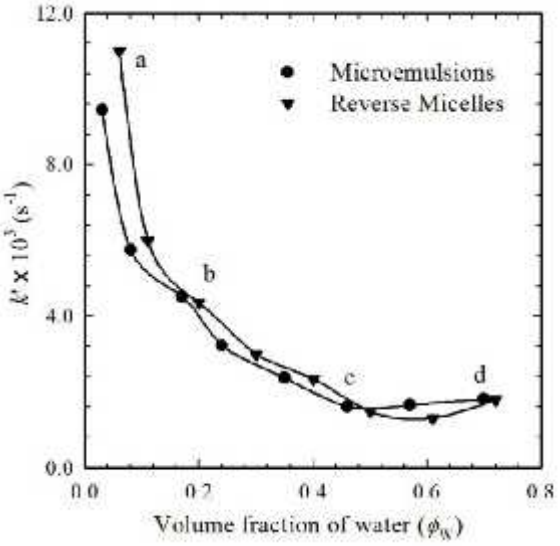

Figure 4.3.6. The k' vs. ϕ_W for alkaline hydrolysis of 9.1×10^{-6} M CV in CTAB/1-butanol/water reverse micelles and CTAB/1-butanol/cyclohexane/water microemulsions at [OH^-] = 7.4 mM.

It is not surprising that microemulsions and reverse micelles affect chemical reaction rates. It is, however, difficult to give a quantitative explanation for the kinetic data since different factors influence micellar catalysis or inhibition. Since water is one of the major components of the microemulsions and reverse micelles, the influence of water on the title reaction in surfactant solutions was studied to understand the effects of the micellar systems on chemical reactivity**.**

The kinetic rate constants (Figure 4.3.6) may be further analyzed to have a deeper understanding of the mechanism of catalysis by microemulsions and reverse micelles. In

region '*ab* ' of the Figure 4.3.6, there is a decrease in rate constant with ϕ_W and it corresponds to the region of direct CTAB/1-butanol reverse micelle where water incorporation into the CTAB reverse micelles and inhibit the reaction [27]. Region '*cd* ' of Figure 4.3.6, corresponds to the reaction in CTAB/water micelle where an increase in the ϕ_W is related to a structured water phase with lower dielectric constant that produces a slightly increase in the reaction rate [22]. Region '*bc* ' of the Figure 4.3.6**,** may well correspond to a transition phase from the direct CTAB/1-butanol reverse micelles to CTAB/water micelles with increasing ϕ_W. In this region the water is not structured and the rate constant has nearly the same value as the second order rate constant for the reaction in water [46], $k = 0.234\ M^{-1}s^{-1}$.

4.3.3. Hydrolysis of CV Catalyzed by Reverse Micelles and Microemulsions of SDS

4.3.3.1. Spectral Behavior of CV in Aqueous Solution and Micelles, Reverse Micelles and Microemulsions of SDS

Figure 4.3.7 shows spectra of 1.56×10^{-5} M CV in aqueous solution and micelles of SDS (15%wt. of SDS in water). Upon addition of 15 %wt. of SDS, the position of the λ_{max} shifted towards higher wavelength to 595 nm (A) with the shoulder at 544 nm (B).

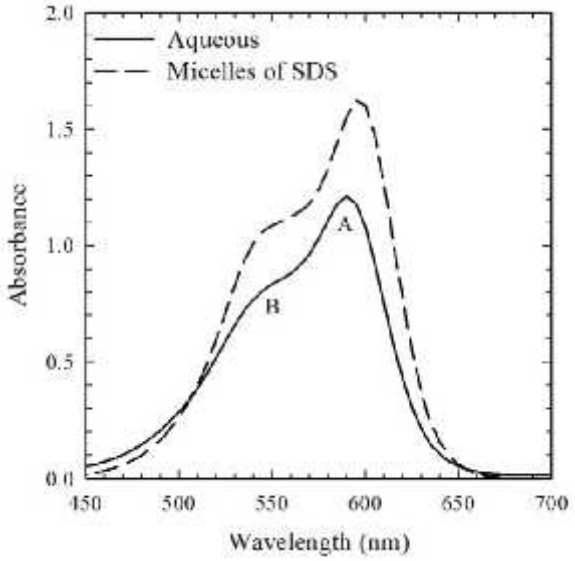

Figure 4.3.7. Spectra of 1.56×10^{-5} M CV solutions in aqueous solution and micelles of SDS (15%wt. of SDS in aqueous solution).

Figure 4.3.8 shows the spectra of 1.56×10^{-5} CV solutions in different SDS/cyclohexane/1-butanol/water and SDS/1-butanol/water microemulsion systems. As the water content increases, the A band and the shoulder (B band) shifted slightly to higher wavelength that may be due to the different dielectric constant values in different reverse micelles and microemulsions.

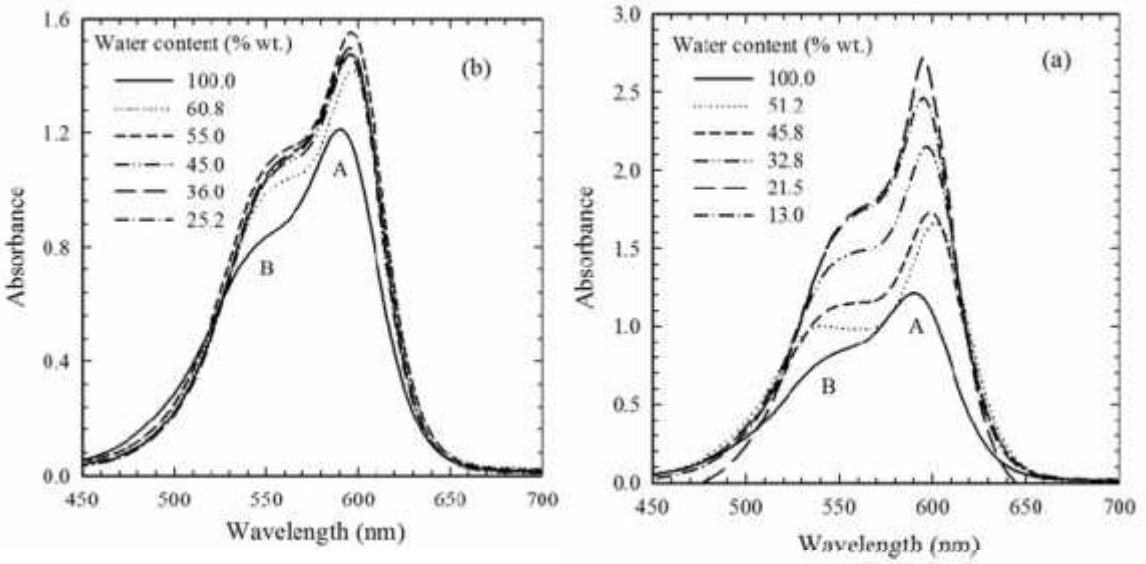

Figure 4.3.8. Spectra of 1.56×10^{-5} M CV in aqueous solution in comparison with (a) SDS/cyclohexane/1-butanol/water microemulsions with 15 %wt. of SDS, 20 %wt. of cyclohexane and different 1-butanol/water content and (b) SDS/1-butanol/ water reverse micelles with 15 %wt. of SDS and different 1-butanol/water content.

4.3.3.2. Hydrolysis in Micellar Solution of SDS

The k' for alkaline hydrolysis of CV in absence of SDS at $[OH^-] = 0.25$ M is about 0.036 s^{-1}, but in presence of 1×10^{-4} M SDS, the k' reduces to 8.84×10^{-3} s^{-1}. So, SDS inhibits the hydrolysis reaction at all concentrations and serves as a negative catalyst which is in agreement with the results obtained by Talman et al [10] and Datta et al [11]. The k' vs. [SDS] profile for the alkaline hydrolysis of CV in the presence of SDS shows interesting behavior. The rate constants of the reaction initially decreases and after passing through a minimum the rate constant almost constant with increasing [SDS] [17]. Above the CMC of SDS, self association results in the formation of micelles. This leads to the solubilization of CV in the hydrophobic core of micelles and the number of CV^+ existing as monomers/dimers in the bulk solution interacting with the SDS decreases. The binding of the reagents, OH^- within micelles and hence enhancement of their concentration in the micellar phase occurs. Thus, the rate constant above the CMC for SDS system in aqueous solution remains almost constant.

In the kinetic runs for microemulsions, 15 %wt. of SDS was used (*vide infra*). The kinetics of alkaline hydrolysis of CV has, therefore, been also studied in aqueous solution using 15 %wt. of SDS and the result has been compared with that in aqueous solution without added SDS. Table 4.3 shows k' for hydrolysis of 1.56×10^{-5} M CV in aqueous and micellar solution of SDS (15 %wt. of SDS in aqueous solution) at $[OH^-] = 0.012$ M.

Table 4.3. The k' for hydrolysis of 1.56×10^{-5} M CV in aqueous and micellar solution of SDS (15 %wt. of SDS in aqueous solution) at $[OH^-] = 0.012$ M.

Media	$k'\times10^3(s^{-1})$	$k_w\ (M^{-1}s^{-1})$
Water	2.8969	0.242
15 %wt. of SDS in water	0.0363	3.1328×10^{-3}

The k' in 15 %wt. of SDS in aqueous solution was lower than the corresponding value without SDS in aqueous solution under identical experimental conditions. The reason for this may be, when CV is mixed with SDS, strong interaction between SDS and CV^+ prevails and when OH^- is added to the reaction mixture, OH^- cannot approach to the CV^+ easily which are already under strong interaction with SDS. The rate of hydrolysis reaction is therefore inhibited. The significant change in the rate constant may also be ascribed to a change in solubilization originating from the change in micellar structure: from sphere to rod at extremely high concentrations.

4.3.3.3. Hydrolysis in Reverse Micelles and Microemulsions of SDS

Figure 4.3.9 represents the k' vs. ϕ_W profiles for the alkaline hydrolysis of 1.56×10^{-5} M CV using $[OH^-] = 0.012$ M in SDS/1-butanol/cyclohexane/water microemulsions and SDS/1-butanol/water reverse micelles with 20 and 0 %wt. cyclohexane, respectively.

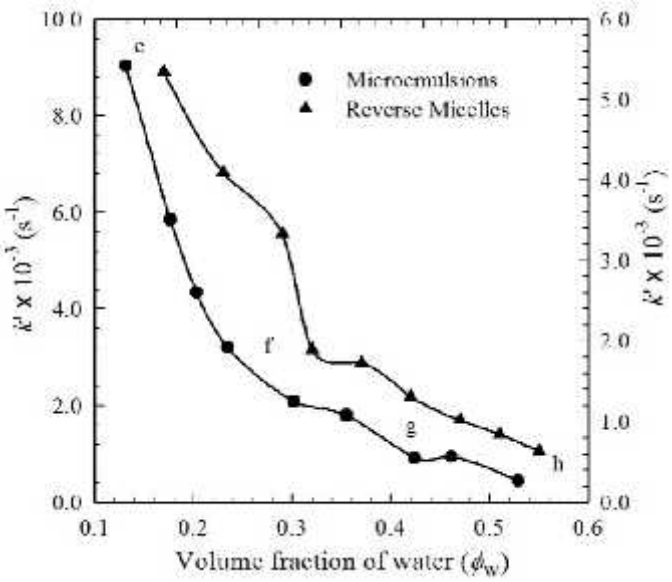

Figure 4.3.9. The k' vs. ϕ_W for alkaline hydrolysis of 1.56×10^{-5} M CV in SDS/1-butanol/water reverse micelles and SDS/1-butanol/cyclohexane/water microemulsions with $[OH^-] = 0.012$ M. The values of k' in right and left side are for SDS/1-butanol/water reverse micelles and SDS/1-butanol/cyclohexane/water microemulsions, respectively.

As ϕ_W increases, the k' decreases sharply and then gradually decreases. The proportion of bound water decreases with the increase of ϕ_W; therefore, the electrostatic repulsion

between OH^- and head groups of SDS becomes more significant which reduces the effective concentration of OH^- near the interface where the reaction takes place and decrease the reaction rate.

For a deeper understanding about the mechanism of catalysis by SDS/1-butanol/water reverse micelles and SDS/1-butanol/cyclohexane/water microemulsions, the kinetic rate constants (Figure 4.3.9) may be further analyzed. In Figure 4.3.9, there is a sharp decrease in rate constant with ϕ_W in part '*ef*' and it corresponds to the region of direct SDS/1-butanol reverse micelle in 1-butanol where the OH^- group are in hydrophillic core of SDS and the incorporation of water swell the reverse micelle core results decrease in rate of the reaction [27]. In part '*gh* ' of Figure 4.3.9, an increase in the ϕ_W changes the orientation of SDS by forming SDS/water micelle in water where the CV is in the core of the micelle and OH^- does not react with CV due to strong repulsion between the hydrophilic part of SDS and OH^- [22]. As a result, reaction rate decreases gradually. Part '*fg* ' of the Figure 4.3.9 may correspond to a transition phase (such as bicontinuous phase) from the direct SDS/1-butanol reverse micelles in 1-butanol to SDS/water micelles in water [60].

4.3.4. Hydrolysis of CV Catalyzed by Reverse Micelles and Microemulsions of TX-100

4.3.4.1. Spectral Behavior of CV in Aqueous Solution and Micelles, Reverse Micelles and Microemulsions of TX-100

Figure 4.3.10 shows spectra of 1.54×10^{-5} M CV in aqueous solution, 1-butanol, micelles (20 %wt. of TX-100 in aqueous solution) and reverse micelles (20 %wt. of TX-100 in 1-butanol) of TX-100.

Upon addition of TX-100, the position of the λ_{max} shifted towards higher wavelength to 600 nm (A) with the shoulder at 560 nm (B). In 1-butanol and 20 %wt. of TX-100 in 1-butanol solution, the dielectric constant value is smaller and the A band had only a slight shift and the shoulder (B band) becomes less marked.

Figure 4.3.11 shows the spectra of 1.54×10^{-5} M CV solutions in different TX-100/1-butanol/water (micelle rich) microemulsions and TX-100/1-butanol/cyclohexane/water (reverse micelle rich) microemulsions. As the content of water decreases, the A band shifts slightly to lower wavelength and the shoulder (B band) nearly disappears indicating a change in the dielectric constant of the medium.

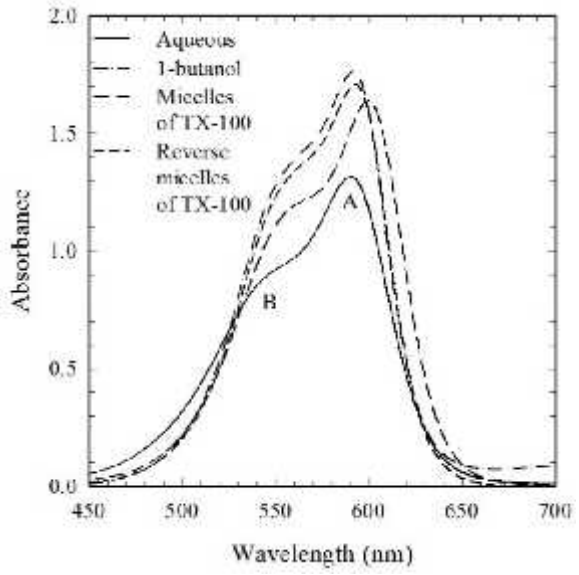

Figure 4.3.10. Spectra of 1.54×10^{-5} M CV in aqueous solution, 1-butanol, micelles (20 %wt. of TX-100 in aqueous solution) and reverse micelles (20 %wt. of TX-100 in 1-butanol).

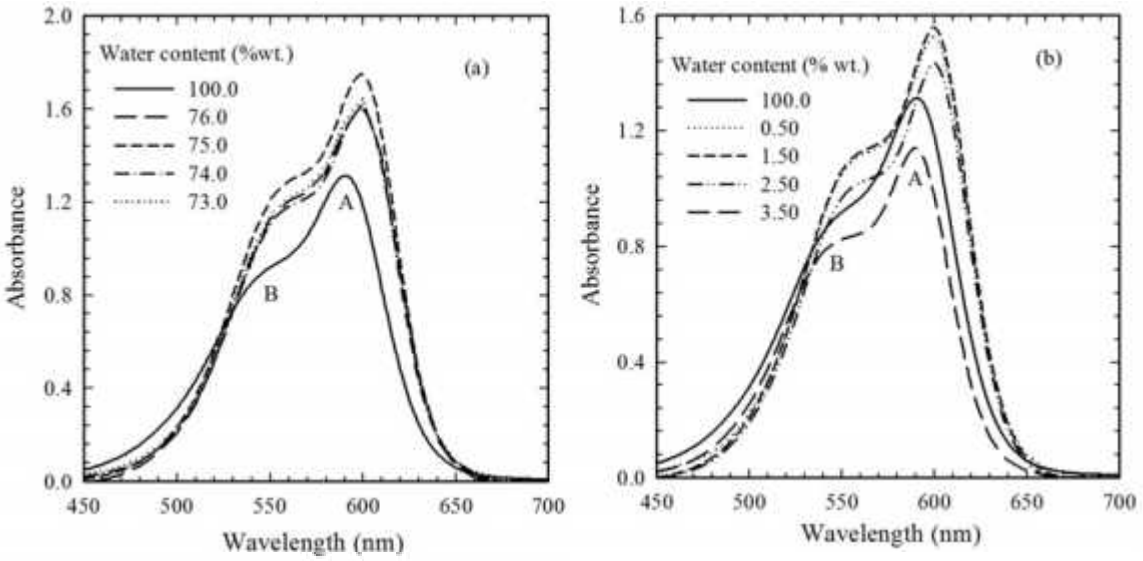

Figure 4.3.11. Spectra of 1.54×10^{-5} M CV in aqueous solution in comparison with (a) TX-100/1-butanol/water microemulsions with 20 %wt. of TX-100 and different 1-butanol/water content (micelle rich) and (b) TX-100/1-butanol/cyclohexane/water (reverse micelle rich) microemulsions with 20 %wt. of TX-100, 72 %wt. of cyclohexane and different 1-butanol/water content.

4.3.4.2. Hydrolysis in Reverse Micelles and Microemulsions of TX-100

Figure 4.3.12 represents the k' vs. ϕ_W profiles for alkaline hydrolysis of 1.54×10^{-5} M CV using $[OH^-]$ = 0.011 and 0.030 M in TX-100/1-butanol/cyclohexane/water (reverse micelle rich) microemulsions and TX-100/1-butanol/water (micelle rich) microemulsions

with 72 and 0 %wt. cyclohexane. In reverse micelle rich microemulsions of TX-100, as ϕ_W increases, the *k*' at first increases gradually and then a sharp increase is noticeable; after a certain region the value of *k*' sharply decreases. In micelle rich microemulsions of TX-100, the *k*' decreases initially, then sharply increases and after that a slight increase in *k*' is apparent with increasing ϕ_W.

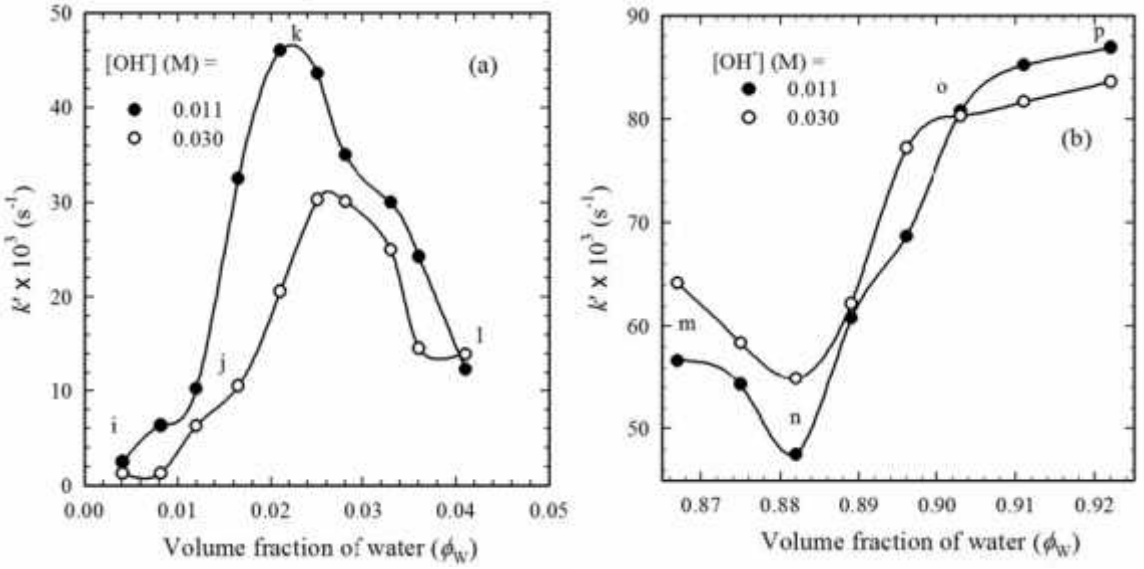

Figure 4.3.12. The *k*' vs. ϕ_W for alkaline hydrolysis of 1.54×10^{-5} M CV in (a) TX-100/1-butanol/cyclohexane/water (reverse micelles rich) and (b) TX-100/1-butanol/water (micelles rich) microemulsions.

From Figure 4.3.12 (a), it is clear that the *k*' vs. ϕ_W profiles give three different patterns in various regions for both the reverse micelle rich and micelle rich microemulsions. Thus, the rate constant for this reaction is mainly related to the content of water in microemulsions, in accordance with the results in dodecylammonium propaniate microemulsions obtained by Miyoshi et al [61] where the *k*' decreases as the amount of water increases. In the region '*ij*'(Figure 4.3.12 (a)), the increase in *k*' might be due to the direct TX-100/1-butanol reverse micelles where incorporation of water helps to accelerate the reaction. The decrease of *k*' in region '*kl*' (Figure 4.3.12 (a)), corresponds to the formation of TX-100/water micelles. In the middle region '*jk*'(Figure 4.3.12 (a)), the sharp increase in *k*' indicates the formation of *BC* microemulsion as the structures of microemulsions change with increasing ϕ_W [38].

Alkaline hydrolysis of CV is strongly dependent on the dielectric constant of the reaction medium [27]. Consequently, in reverse micelle rich microemulsions of TX-100 (Figure 4.3.12 (a)), the increase in the rate constant in region '*ij*' to '*jk*' can also be related to the lower dielectric constant in the reverse micelles water pool, as compared to the higher dielectric constant value in pure water.

From the profile of k' vs. ϕ_W of CV hydrolysis in micelle rich microemulsions of TX-100 (Figure 4.3.12 (b)), it can be seen that the different microemulsion structures have different effects on k'. The rates are much higher in TX-100/1-butanol reverse micelles; *w*/*o* microemulsions and decrease with increasing ϕ_W. For $\phi_W < 0.88$, the reaction rates decrease and for $\phi_W > 0.90$, the reaction rates increase slightly with increasing ϕ_W. The variations observed in Figure 4.3.12 (b) indicate two transition points, at $\phi_W = 0.88$ and $\phi_W = 0.90$, at which the reaction rates of CV hydrolysis are changed. Significantly, the two points correspond to the transitions of the structures of microemulsions from TX-100/1-butanol (*w*/*o*) reverse micelles to *BC* and from BC to TX-100/water (*o*/*w*) microemulsions.

4.4. Hydrolysis of CV Catalyzed by Microemulsions of CTAB, SDS and TX-100

In microemulsion systems, chemical reactions are considered to occur at the phase structure interface of the microemulsions [62]. In *w*/*o* microemulsions, CV is solubilized in the inner (water phase) and outer (oil) phase. The concentration of OH^- in the inner core of the microemulsions is high; the probabilities of collisions between OH^- ions and the CV^+ are high, and so the hydrolysis reaction rates are much higher. In addition, the reaction rates of hydrolysis of CV in microemulsions are high compared to the rate in pure water, because the amount of solubilization of CV in the inner core of the microemulsions is much higher than the solubility of CV^+ in pure water [63]. With the increase in the water content, however, the microdrops of the *w*/*o* microemulsions increase in size and the relative concentrations of OH^- decrease, which gradually results in a decrease in the rates of CV hydrolysis. After first critical point, the structures of the microemulsions are changed from *w*/*o* to *BC* where water and oil phases intersect each other [64, 65] and the collisions between OH^- ions and CV become less or more frequent depending on the type or structure of the surfactant, which results in an increase or decrease in the rates of CV in *BC* microemulsions. Again, after second critical point, the microemulsion structure is changed to *o*/*w*. The microdrops of the microemulsions are much bigger, the surface electric charges for ionic microemulsions are higher than in the *w*/*o* microemulsions, the concentration of CV are higher in the core of microemulsion and OH^- submerged into 'the surface layers" of the microemulsions, the collisions between CV^+ and OH^- are not easy and the rates of CV hydrolysis decrease or are almost constant. For nonionic surfactant, there are no electric charges on the surface layer and therefore there is no electrostatic interaction with the OH^-; the collision between CV^+ and OH^- are easier compared to that in ionic surfactants. Thus, the rates of hydrolysis of CV in *o*/*w* microemulsions are higher and almost constant with increasing ϕ_W.

4.5. Conclusions

Alkaline hydrolysis of CV is catalyzed by micelles, reverse micelles and microemulsions of CTAB, SDS/SDBS and TX-100. The reaction is accelerated by the micelles of CTAB and TX-100 and inhibited by the micelles of SDBS/SDS with increasing concentration of

surfactants. However, the rate of the reaction at extremely high [CTAB] has been found to decrease due to the increased electrostatic repulsion between the micellar head groups and positively charged CV, which discourages further solubilization of CV in the micelle core. In addition, the decrease in rate constant in presence of SDBS/SDS corresponds to premicellar aggregation of CV and SDBS/SDS. The acceleration and inhibition effect of the CTAB, SDBS/SDS and TX-100 on the reaction at concentrations below the CMC has been satisfactorily explained with the help of Piszkiewicz model via formation of premicellar aggregates. The kinetic results in presence of CTAB and SDS also show good fit to the PPIE model for the reaction with reasonable values of the parameters. The k' vs. ϕ_W profiles for reverse micelles and microemulsions of CTAB showed an initial decrease in the k' followed by a gradual increase and for reverse micelles and microemulsions of SDS, the k' initially sharply decreases and then a gradual decrease is apparent. Additionally, in reverse micelle rich microemulsions of TX-100, as the ϕ_W increases, the k' at first increases gradually and then a sharp increase is noticeable; after a certain region the value of k' sharply decreases while in micelle rich microemulsions of TX-100, the k' decreases initially, then sharply increases and after that the k' becomes almost constant with increasing ϕ_W. This change in k' with ϕ_W may be ascribed to the increased amount of micelles of CTAB, SDS and TX-100 in the microemulsions and reverse micelles. Microemulsions and reverse micelles can thus influence the rate of the reaction by formation of micelles in water phase and reverse micelles in oil phase.

References

[1] J. H. Fendler, E. J. Fendler, *Catalysis in micellar and macromolecular system*, Academic Press, New York, 1975.

[2] M. N. Khan, *Micellar catalysis (Surfactant series),* CRC Press, 2006.

[3] N. Singh, K. K. Ghosh, J. Marek, K. Kuca, *Hydrolysis of carboxylate and phosphate esters using monopyridinium oximes in cationic micellar media*, International Journal of Chemical Kinetics, 2011, 43, 569-578.

[4] Y. S. Simanenko, A. F. Popov, T. M. Prokopeva, E. A. Karpichev, I. A. Belousova, V. A. Savelova, *Micellar effects of cationic detergents in the decomposition of ecotoxic substrates by hydroxide ion*, Theoretical and Experimental Chemistry, 2002, 38, 242-249.

[5] C. O. R. Yagui, A. P. Junior, *Micellar solubilization of drugs*, Journal of Pharmaceutical Science, 2005, 8, 147-165.

[6] F. Monica, V. Carmen, *The study of the influence of surfactant charge on alkaline hydrolysis reactions of acetylsalicylic acid (ASA) and triflusal (TFL) using spectrophotometric methods*, European Journal of Pharmaceutical Science, 2007, 31, 211-220.

[7] M. N. Khan, P. C. Gleen, Z. Arifin, *Effects of inorganic salts and mixed aqueous-organic solvents on the rates of alkaline hydrolysis of aspirin*, Indian Journal of Chemistry, 1996, 35, 758-765.

[8] M. E. Moro, J. N. Fertrell, M. M. Velazquez, L. J. Rodriguez, *Kinetics of the acid hydrolysis of diazepam, bromazepam, and flunitrazepam in aqueous and micellar systems*, Journal of Pharmaceutical Sciences, 1991, 80, 459-468.

[9] L. Mukherjee, N. Mitra, P. K. Bhattacharya, S. P. Moulick, *Kinetics in microemulsion medium. 4. Alkaline fading of crystal violet in aqueous (H_2O/aerosol OT/isooctane and H_2O/aerosol OT/decane) and nonaqueous (ethylene glycol/ aerosol OT/isooctane)* microemulsions, *Langmuir*, 1995, 11, 2866-2871.

[10] R.Y. Talman, S. Gokturkand, M. Tuncay, *Kinetic cosolvent effects on the alkaline fading of crystal violet in the presence of sodium dodecyl sulfate micelles*, Colloids and Surfaces A: Physicochemical and Engineering Aspects, 2005, 270, 72-77.

[11] J. Datta, A. Bhattiacharya, K. Kundu, *Effect of surfactants on the kinetics of alkaline fading of crystal violet and acid-catalyzed inversion of sucrose,* Indian Journal of Chemistry,1988, 27, 115-122.

[12] C. Dolect, E. Rodenas, *Hydroxide ion specific adsorption on cetyltrimethylammonium bromide micelles explains kinetic data,* Colloids and Surfaces A: Physicochemical and Engineering Aspects, 1993, 75, 39-50.

[13] E. F. J. Duynstee, E. Grunwald, *Organic reactions occurring in or on micelles. I. Reaction rate studies of the alkaline fading of triphenylmethane dyes and sulfonphthalein indicators in the presence of detergent salts*, Journal of the American Chemical Society, 1959, 81, 4540-4542.

[14] M. Isabel, M. L. Sierra, M. Valiente, E. Rodenas, *Physical properties of cetylpyridinium chloride micelles and their behaviour as reaction media*, Journal of the Chemical Society, Faraday Transactions, 1996, 92, 59-63.

[15] O. Olanrewaju, J. Ige, O. Soriyan, O. Grace, O. Segun Esan, O. Olanrewaju, *Kinetics and mechanism of the alkaline fading of brilliant green in aqueous solutions of a double-tailed and some single-tailed cationic surfactants*, Acta Chimica Slovenica, 2007, 54, 370-374.

[16] B. Samiey, F. Ashoori, *Kinetics of crystal violet fading in the presence of TX-100, DTAB and SDS*, Acta Chimica Slovenica, 2011, 58, 223-232.

[17] A. R. Kabir, M. A. B. H. Susan, *Kinetics of the alkaline hydrolysis of crystal violet in aqueous solution influenced by anionic surfactants,*Journal of Saudi Chemical Society, 2008, 12, 543-554.

[18] M. L. Sierra, E. Rodenas, *CTAB/poly(propylene glycol) mixed micelles: characterization and its properties as a reaction medium*, The Journal of Physical Chemistry, 1993, 97, 12387-12392.

[19] L. G. Río, J. R. Leis, J. C. Mejuto, A. N. Vázquez, J. P. Juste, P. R. Dafonte, *Basic hydrolysis of crystal violet in β-cyclodextrin/surfactant mixed systems*, Langmuir, 2004, 20, 606-613.

[20] M. Valiente, E. Rodenas, *Influence of mixed micelles CTAB/1-hexanol and CTAB/1-octanol on the basic hydrolysis of crystal violet: Different theoretical approaches*, Langmuir, 1990, 6, 775-782.

[21] J. R. Leis, J. C. Mejuto, M. E. Pena, *Comparison between the kinetics of the alkaline fading of carbocation dyes in water/sodium bis(2-ethylhexyl) sulfosuccinate/isooctane microemulsions and in homogeneous media*, Langmuir, 1993, 9, 889-893.

[22] M. Valiente, E. Rodenas, *Reverse CTAB micelles in alkanols: Influence on the basic hydrolysis of crystal violet*, The Journal of Physical Chemical, 1991, 95, 3368-3370.

[23] L. Mukhopadhyay, N. Mitra, P. K. Bhattacharya, S. P. Moulcik, *Thermodynamics of formation of biological microemulsion (with cinnamic alcohol, aerosol ot, tween 20, and water) and kinetics of alkaline fading of crystal violet in them*, Journal of Colloid and Interface Science, 1997, 186, 1-8.

[24] M. Valiente, E. Rodenas, E. P. Benito, *Reactants Location in L2 Phase*, Tenside, surfactants, detergents, 1994, 21, 168-136.

[25] C. Izquierdo, J. Casado, A. Rodriguez, M. L. Moya, *Microemulsions as a medium in chemical kinetics. II: The $I^- + S_2O_8^=$ and crystal violet + OH^- reactions in different surfactant/oil/water microemulsions*, International Journal of Chemical Kinetics 1992, 24, 19-30.

[26] Y. Ikushima, Z. Shervani, *The promotion of hydrolysis of acetylsalicylic acid in AOT/near-critical propane microemulsion*, Chemical Communication, 2001, 2506-2507.

[27] M. Valiente, E. Rodenas, *Influence of CTAB/1-Butanol micelles on crystal violet basic hydrolysis,* Journal of Colloid and Interface Science, 1989, 127, 522-531.

[28] M. Valiente, E. Rodenas, *Benzene, toluene and cyclohexane incorporation into CTAB micelles: effects on the basic hydrolysis of crystal violet*, Journal of Colloid Interface Science, 1990, 138, 299-306.

[29] E. Rodenas, C. Dolcet, M. Valiente, E. C. Valeron, *Physical properties of dodecyltrimethylammonium bromide (DTAB) micelles in aqueous solution and their behavior as the reaction medium*, Langmuir 1994, 10, 2088-2094.

[30] M. Häger, F. Currie, K. Holmberg, *A nucleophilic substitution reaction in microemulsions based on either an alcohol ethoxylate or a sugar surfactant*, Colloids and Surfaces A: Physicochemical and Engineering Aspects, 2004, 250,163-170.

[31] K. K. Ghosh, M. L. Satnami, *Nucleophilic substitution reaction of carboxylate and phosphate esters with hydroxamate ions in microemulsions*, Colloids and Surfaces A: Physicochemical and Engineering Aspects, 2006, 274, 125-129.

[32] C. A. Bunton, L. Robinson, *Micellar effects upon nucleophilic aromatic and aliphatic substitution*, Journal of the American Chemical Society , 1968, 90, 5972-5979.

[33] A. B. Mirgorodskaya, F. G. Valeeva, L. A. Kudryavtseva, N. N. Vylegzhanina, Yu. F. Zuev, *Reaction of carboxylic acid esters with phenolates in oil-in-water microemulsions based on cetyltrimethylammonium bromide*, Russian Journal of General Chemistry, 2006, 76, 590-595.

[34] Y. Miyake, T. Owari, K. Matsuura, M. Teramoto, *Enzymatic reaction in water-in-oil microemulsions. Part 2.—Rate of hydrolysis of a hydrophobic substrate, 2-naphthyl acetate*, Journal of the Chemical Society, Faraday Transactions, 1994, 90, 979-986.

[35] Y. Miyake, T. Owari, F. Ishiga, M. Teramoto, *Enzymatic reaction in water-in-oil microemulsions. Part 1.-Rate of hydrolysis of a hydrophilic substrate: acetylsalicylic acid*, Journal of the Chemical Society, Faraday Transactions, 1993, 89, 1993-1999.

[36] H. Jingcheng, *Studies on chemical reactions in microemulsion media (I) hydrolysis kinetics studies in microemulsion system for CTAB/n-butanol/25%n-octane/water*, Journal of Dispersion Science and Technology, 2000, 21, 19-30.

[37] F. Tafesse, K. Eguzozie, *Efficient hydrolysis of 4-nitrophenylphosphate catalyzed by copper bipyridyl in microemulsions*, Ecotoxicology and environmental safety, 2009, 72, 954-959.

[38] J. Hao, *Effect of the structures of microemulsions on chemical reactions*, Colloid and Polymer Science, 2000, 278,150-154.

[39] Z. Y. Chen, J. H. Zhao, W. He, X. Qinan, W. G. Shen, *Study of association thermodynamics between crystal violet and sodium bis(2-ethylhexyl)sulfosuccinate and kinetics of basic fading of crystal violet in microemulsions*, International Journal of Chemical Kinetics, 2008, 40, 294-300.

[40] M. Valientie, E. Rodenas, *Influence of CTAB/alkanol/cyclohexane w/o microemulsions on the basic hydrolysis of crystal violet*, Colloid and Polymer Science, 1993, 271, 494-498.

[41] P. Ekwall, L. Mandell and K. Fontell*, The cetyltrimethylammonium bromide-hexanol-water system,* Journal of Colloid and Interface Science, 1969, 29, 639-695.

[42] L. Arzuman, S. N. Karobi, M. J. Islam, G. Ara, M. M. Rahman, M. Y. A. Mollah, M. A. B. H. Susan, *Effect of urea on the kinetics of the alkaline hydrolysis of crystal violet catalyzed by aqueous micellar solutions of cetyltrimethylammonium bromide*, Synthesis and Reactivity in Inorganic, Metal-Organic and Nano-Metal Chemistry, 2015, 45, 764-769.

[43] J. Aguiar, P. Carpena, J. A. Molina-Bolívar, C. C. Ruiz, *On the determination of the critical micelle concentration by the pyrene 1:3 ratio method*, Journal of Colloid and Interface Science, 2003, 258,116-122.

[44] G. N. Lewis, T. T. Magel, D. Lipkin, *Isomers of crystal violet ion: their absorption and remission of light*, Journal of American Chemical Society*,* 1942*,* 64, 1774-1782.

[45] W. Caetano, M. Tabak, *Interaction of chlorpromazine and trifluoperazine with anionic sodium dodecyl sulfate (SDS) micelles: electronic absorption and fluorescence studies*, Journal of Colloid and Interface Science, 2000, 225, 69-81.

[46] C. D. Ritchi, *Cation-anion combination reactions. XIII. Correlation of the reactions of nucleophiles with esters*, Journal of American Chemical Society, 1975, 97, 1170 -1179.

[47] V. C. Reinsborough, *Micellar catalysis,* in Interfacial catalysis, A. G. Volkov, CRC Press, Taylor and Francis group, 2003.

[48] S. K. Srivastava, S. S. Katiyar, *Quantitative treatment of the effect of counterions on CTAB-catalyzed reactions of stabilized carbonium ions with cyanide ion*, International Journal of Chemical Kinetics, 1982, 14, 1007-1015.

[49] P. K. Sena, S. Talukder, B. Palba, *Specific interactions of anions and pre-micelles in the alkaline fadingof crystal violet carbocation*, Colloids and Surfaces A: Physicochemical Engineering Aspects, 2015, 467, 259-269.

[50] T. C. Bruice, S. J. Benkovic, *Bioorganic mechanism*, Benjamin, New York, 1966.

[51] W. P. Jencks, *Catalysis in chemistry and enzymology*, Mc Graw Hill, New York, 1969.

[52] J. H. Fendler, *Membrane mimetic chemistry*, John Wiley, New York, 1982.

[53] D. Piszkiewicz, *Positive cooperativity in micelle-catalyzed reactions*, Journal of the American Chemical Society, 1977, 99, 1550-1557.

[54] S. K. Srivastava, S. S. Katiyar, in *Surfactants in solution*, K. L Mittal (ed) V 9, Plenum Press, New York, 1989.

[55] E. H. Cordes, R. B. Dunlap, *Kinetics of organic reactions in micellar system*, Accounts of Chemical Research, 1969, 11, 329-337.

[56] E. S. Anachkov K. D. Danov, E. S. Basheva, P. A. Kralchevsky, K. P. Ananthapadmanabhan, *Determination of the aggregation number and charge of ionic surfactant micelles from the stepwise thinning of foam films*, Advances in Colloid and Interface Science, 2012, 183, 55-67.

[57] P. Ferruccio, C. Matteo, Z. Francesco, *A molecular dynamics investigation of structure and dynamics of SDS and SDBS micelles*, Soft Matter, 2011, 7, 9148-9156.

[58] D. J. Jobe, *Sodium dodecyl sulfate micellar aggregation numbers in the presence of cyclodextrins*, Langmuir 1995, 11, 2476-2479.

[59] J. Das, K. Ismail, *Aggregation, adsorption, and clouding behaviors of Triton X-100 in formamide*, Journal of Colloid and Interface Science, 2009, 337, 227-33.

[60] B. S. Valaulikar, *Reactions in microemulsion formed by sodium dodecyl sulfate, water, and hexanol, Journal of Colloid and Interface Science,* 1993,161, 268-269.

[61] N. Miyoshi, G. Tomita, *Generation of tris(4-dimethylaminophenyl)methanol (crystal violet carbinol) in reversed micelles*, Australian Journal of Chemistry, 1981, 34, 1545-1550.

[62] R. J. Schomacker, K. Stickdorn, R. Schomacker, *Microemulsions in technical processes*, Chemical Review 1995, 95, 849-864.

[63] L. Ganzuo, X. Rui, S. Dasheng, Z. Xian-cheng, D. Yu, *Studies on thermokinetics (xiv) the alkaline hydrolysis of aspirin in miceliar solution*, Journal of Dispersion Science and Technology, 1992, 13, 201-208.

[64] S. E., Friberg, I. Lapczynske, G. Gillberg, *Microemulsions containing nonionic surfactants-The importance of the PIT value*, Journal of Colloid and Interface Science, 1976, 56, 19-32.

[65] L. E. Scriven, *Equilibrium bicontinuous structure*, Nature, 1976, 263, 123-125.

Abstract

Kinetics of hydrolysis of Bz has been investigated in aqueous solution and micellar solutions of SDBS/SDS, CTAB and TX-100 and reverse micelles and microemulsions of CTAB using spectrophotometric method under pseudo first order conditions. In aqueous solution, the k' for acid hydrolysis of Bz increases non linearly with increasing $[H^+]$. The presence of SDBS/SDS and TX-100 produced an inhibitory effect while addition of CTAB has been found to enhance the rate of hydrolysis of Bz at concentrations below the CMC. Above the CMC, the k' increases slightly for some concentration of SDBS/SDS whereas for TX-100, the k' was almost constant. As [CTAB] increases at low $[H^+]$, the rate constant attains a limiting value; while at high $[H^+]$, the rate constant passes through a maximum and then decreases. This enhancement and inhibition of the rate of hydrolysis of Bz by CTAB, SDBS/SDS and TX-100 micelles were treated by Piszkiewicz and PPIE model to obtain the binding constant of Bz with CTAB, SDBS/SDS and TX-100 and other kinetic parameters. In CTAB/cyclohexane/1-butanol/water microemulsions, at $[H^+]$ = 0.001 M, the k' of acid hydrolysis of Bz decreases sharply followed by a slight increase while at $[H^+]$ = 0.01 M, k' increases first followed by a sharp decrease with increasing ϕ_W increases.

5.1. Introduction

Bromazepam (Bz, 7-bromo-1,3-dihydro-5-(2-pyridyl)-2*H*-1,4- benzodiazepin-2-one) is the group of 1,4- benzodiazepines drugs that are widely used to treat insomnia, anxiety, panic attacks, muscule spasms, and seizure disorders in everyday medical practice [1]. It has unique physicochemical properties as the consequence of the pyridine moiety. The molecular structure of Bz changes in aqueous solution through acid-base reaction and hydrolytic degradation. The acid hydrolysis of Bz occurs in two stages (Figure 1.13, Chapter 1) [2]. In the *first* stage, breakage of the ring is produced at the 1, 2-amidic bonds, which is considered to be reversible. The *second* stage consists of the rupture of the remaining bond, rise to derivative of glycine. The difference in the type and extent of products changes with change in $[H^+]$ and as a whole in the reaction environment.

Nudelman et al [3] studied the kinetics of the reaction of 2-(n-methylamino)-5-chlorobenzophenone, with hydrochloric acid in methanol-water and isolated several unexpected products. The kinetics of the hydrolysis of diazepam and structural identification of some intermediate products indicated an initial hydroxide attack at the C2-carbonyl carbon of diazepam, resulting in the formation of a dioxide (**7**, 7-chloro-1,3-dihydro-1-methyl-5-phenyl-2H-1,4-benzodiazepin-2,2-dioxide) [4]. Smyth et al [5] studied the acid-base and complexing behavior of Bz by spectral and polarographic measurements and discussed acid-base equilibrium reactions with reference to the hydrolysis and complexing properties of this compound. The hydrolytic reaction of diazepam in acid solution at body temperature was studied spectrophotometrically and the rate of ring closure was found to be greater than that of ring opening, indicating that

the concentration at equilibrium of the closed-ring compound is larger than the open-ring species [6]. Hong et al [7] studied that the behavior of some pyrazolodiazepinones in aqueous solution forms stable equilibrium mixtures consisting of ring and opened forms. The hydrolysis of nitrazepam involves an uncatalyzed reaction, specific acid-base catalysis, and general acid-base catalysis for acetate and phosphate buffers [8]. The hydrolysis kinetics of oxazepam and diazepam leading to a benzophenone product and a glycine derivative were quantified from pH 1 to 11 [9].

It is well known that micelles, reverse micelles and microemulsions are self-organized media of surfactants formed by the spontaneous and reversible association of surfactants under equilibrium conditions into stable, structurally well-defined aggregates joined by non-covalent bonds [10]. These organizations from molecular self-assemblies to controllable architectures and materials with advanced functions may meet the requirement of many objectives in science and technology such as catalysis of chemical reactions, sensors, electronic and electromechanical devices [11-16]. The rate of a chemical reaction significantly changes in those surfactant-based organized media involving hydrophobic interactions. This has resulted in a surge of interest in the kinetics of reactions involving different substrates solubilized in such organized media with a view to the fundamental understanding of the mechanism of reaction in different environments for their potential applications.

There have been numerous attempts to explore the catalysis of hydrolysis reactions by supramolecular self-assembled systems such as: micelles, reverse micelles and microemulsions using a wide variety of substrates, including esters [17, 18], dyes [19-28] and drugs [2, 29-43]. Sodium decyl (SdeS), dodecyl (SDS) and tetradecyl (STS) sulfate have been reported to produce an inhibitory effect in the kinetics of the acid hydrolysis of aqueous diazepam, Bz and flunitrazepam drugs; while negligible effects were observed in the cases of polyoxy ethylene-23-dodecanol and CTAB [2]. The presence of *N*-cetyl-*N*-ethyl-*N*, *N*-dimethylammonium bromide has been found to cause inhibition of the basic hydrolysis of triflusal [33]. The hexadecylphosphocholine micelles inhibit the basic hydrolysis of the indomethacin and acemetacin [34]. The presence of CTAB micelles enhances the rate of alkaline hydrolysis of penicillin [35]. The rate - [surfactant] profiles for the hydrolysis of indomethacin provide rate inhibition in the presence of SDS and rate enhancement in the presence of CTAB [36]. At pH 13, curcumin undergoes rapid degradation by alkaline hydrolysis in the SDS micelles whereas greatly suppressed in the presence of either CTAB or dodecyltrimethylammonium bromide micelle [37]. The effect of cationic surfactants with varying hydrophobic chains and with different headgroups and anionic surfactant (SDS) on the rate of alkaline hydrolysis of the carsalam and its *N*-substituted derivatives have been investigated by Abdullah et al [38]. The plots of observed rate constant vs. [surfactants] for degradation of indomethacin under alkaline condition were curved with negative slopes for ethoxylated lanolin,

polysorbate 80; but with the cetrimonium bromide, the plots showed a marked positive change in k_{obs} as the [surfactant] passed through the CMC [39]. The intramolecular degradation of cephaclor was catalyzed 25-fold by micelles of CTAB [40]. The rate of the hydrolysis of isatin and its derivatives of different hydrophobicities increased on increasing the [cetyltrimethylamonium chloride] and after reaching a maximum, it started decreasing: conversely, micelles of SDS inhibited the rate of hydrolysis of isatin and its derivatives [41]. Cationic micelles showed a catalytic effect on alkaline hydrolysis of acetylsalicylic acid and triflusal at low surfactant concentrations while was inhibited at high surfactant concentrations and in anionic micelles, a catalytic effect occurs, while in zwitterionic and non-ionic micelles there is an inhibitory effect [42]. The basic hydrolysis of carbofuran was catalyzed in the presence of colloidal aggregates with positive surface charge and large inhibition by anionic and nonionic surfactants [43].

Till to date, there have been no reports on the investigation of the kinetics of the acid hydrolysis of Bz in reverse micelles and microemulsions. To understand the mechanism of this reaction under different reaction environments, microemulsion may serve as a very potential medium and kinetic studies need to be systematically and intensively conducted. In the present work, we investigated the kinetics of the acid hydrolysis of Bz in absence and presence of micelles CTAB, SDBS/SDS and TX-100 in aqueous solution and also in reverse micelles and microemulsions of CTAB and the kinetic results in these different media have been compared with those in aqueous solution. In addition, kinetic profiles for the reaction catalyzed by CTAB, SDBS/SDS and TX-100 were treated quantitatively by Piszkiewicz and PPIE model.

5.2. Experimental

5.2.1. Materials and Methods

Bz (ACI), CTAB (BDH), SDBS/SDS (E. Merck), TX-100 (Sigma), NaOH and HCl solution, each were reagent grade materials; and were used as received without further purification. As Bz is sparingly soluble in aqueous solution, the stock solutions of Bz were prepared in aqueous solution with few drops of ethanol. The CMCs of CTAB, SDS/SDBS and TX-100 in pure water at 25 °C were reported in Section 4.2.1 in Chapter 4.

5.2.2. Kinetic Measurements

Kinetic measurements and spectral analysis were carried out in a double beam Shimadzu UV-visible spectrophotometer model UV1650C. It was equipped with spectral data processing facilities. The sensitivity of the equipment was 0.001 absorbance unit at a signal to noise ratio of 1. Rectangular quartz cells of path length 1 cm were used throughout the investigation.

The rate of acid hydrolysis of Bz in aqueous solution was measured spectrophotometrically by monitoring the absorbance, at the λ_{max} (= 235 nm) of Bz with the progress of the reaction. In the cases of kinetic measurements absorbance at the λ_{max}

of Bz in micelles of CTAB, SDBS/SDS and TX-100 was monitored. The kinetic studies were conducted at ambient temperature (ca. 25 ^{o}C). Rectangular quartz cells of path length 1 cm were used throughout the investigation. In all kinetic runs, the initial Bz concentration of 2.21 × 10^{-5} M was used and the hydrolysis was carried out by using a large excess of [H^{+}] (more than 10-fold). The observed pseudo-first-order rate constants, k', were obtained from the slopes of the dependence of $\ln\frac{(A_0 - A_\infty)}{(A - A_\infty)}$ vs. t using the following equation,

$$\ln\frac{(A_0 - A_\infty)}{(A - A_\infty)} = k't \text{ - - - - - - - - - - - - - (5.1)}$$

where A_0 and A_∞ are the absorbencies at t = 0 and t = ∞, respectively that depend on the molar absorptivities and on the initial and final concentrations of the species. A is the absorbance at any time, t.

5.3. Results and Discussion

5.3.1. Spectral Behavior of Bz in Aqueous Solution

Figure 5.3.1 shows the absorption spectra of aqueous solutions of Bz at different concentrations in the range of (0.221-4.42) ×10^{-5} M. The λ_{max} does not show any appreciable change with change in [Bz].

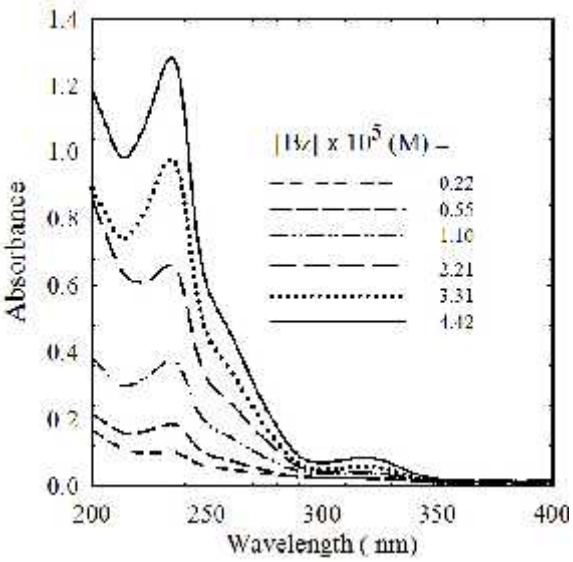

Figure 5.3.1. Absorption spectra of Bz at different concentrations in aqueous solution.

Molar extinction co-efficient (ε) of Bz has therefore been determined at 235 nm by measuring the absorbance at this wavelength of aqueous solutions of several concentrations. The slope of the straight line (according to Beer-Lambert law) evaluated by the least square method gave a value of 29.47×10^{6} mol^{-1} cm^{2} for the ε of Bz at 235 nm, in agreement with literature data [1, 2].

5.3.2. Hydrolysis of Bz in Aqueous Solution

In aqueous solution, acid hydrolysis of Bz follows second order kinetics. The bimolecular rate constant k_w for the title reaction in water could not be evaluated from the plots of the k' vs. $[H^+]$ (Figure 5.3.2), since k' shows a non-linear increase with increasing $[H^+]$. Under pseudo first order conditions i.e. $[H^+] >> [Bz]$, the k' for each individual kinetic run has been evaluated from, $k' = k_w [H^+]$. While a rapid formation of the hydrolyzed product, BZH^+(II) depending on acid concentration, i.e. pH is apparent, at high $[H^+]$ i.e. under more vigorous condition, rise in k' with $[H^+]$ can be ascribed to be due to the formation of the final product, BZH^+(II) benzoyl-pyridine derivative (Figure 1.13., Chapter 1) [2].

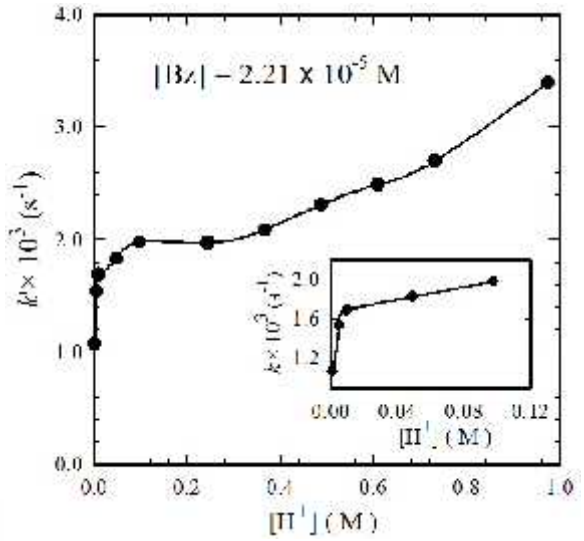

Figure 5.3.2. The k' vs. $[H^+]$ for acid hydrolysis of Bz in aqueous solution. Inset shows the values of the k' at lower $[H^+]$.

5.3.3. Spectral Behavior of Bz in Presence of CTAB in Aqueous Solution

Figure 5.3.3 (a) represents the spectra of 2.21×10^{-5} M Bz solution in presence of CTAB at various concentrations. Upon addition of CTAB, the position of absorption maximum shifts towards a higher wavelength and at concentrations close to the CMC the λ_{max} attains an almost constant value (Figure 5.3.3 (b)). Figure 5.3.3 (b) also shows the variation of absorbance of 2.21×10^{-5} M Bz in aqueous solutions with [CTAB] at their respective λ_{max}. With increasing [CTAB], absorbance at the λ_{max} increases first followed by a decrease to attain a limiting absorbance at concentrations close to the value of the CMC.

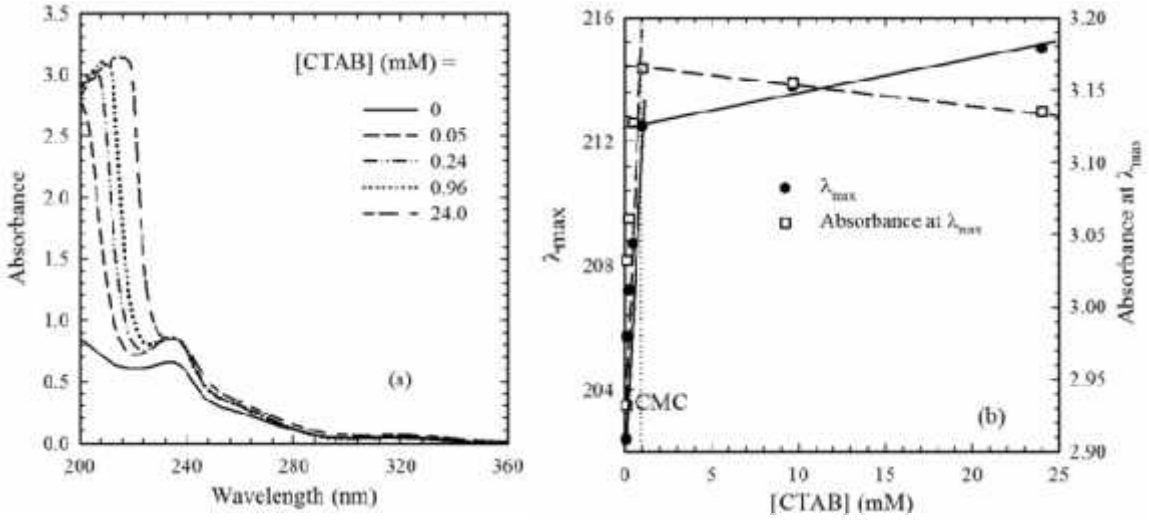

Figure 5.3.3. (a) Absorption spectra and (b) the λ_{max} and absorbance at the respective λ_{max} of 2.21×10^{-5} M Bz as a function of [CTAB] in aqueous solution.

5.3.4. Hydrolysis in Presence of CTAB

The *k*' vs. [CTAB] profile for acid hydrolysis of Bz in presence of CTAB is shown in Figure 5.3.4 for $[H^+]$ = 0.001 and 0.01 M. From Figure 5.3.4, it is apparent that below the CMC, the *k*' increases for both low and high $[H^+]$. For low $[H^+]$, at high [CTAB] (up to the CMC), the *k*' becomes almost constant; however, for high $[H^+]$, the *k*' decreases as [CTAB] increases further.

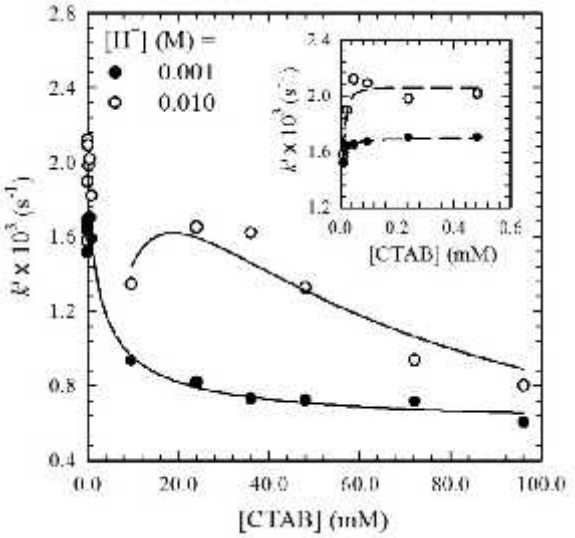

Figure 5.3.4. The *k*' as a function of [CTAB] for acid hydrolysis of 2.21×10^{-5} M Bz. Inset shows the values of the *k*' at [CTAB] below the CMC. Solid and dash line drawn using calculated values according to PPIE and Piszkiewicz's model, respectively.

Above the CMC, the *k*' shows an initial decrease for both low and high $[H^+]$. As the [CTAB] continues to increase above the CMC, the *k*' at low $[H^+]$ attains an almost

constant value; while at high [H^+], the *k*' passes through a maximum and then decreases. This corresponds to the change in reaction mechanism during the course of the reaction depending on [H^+]. In fact, the mechanism of the hydrolysis of Bz changes with change in pH. At high pH i.e. low [H^+], the breakage of the ring occurs at the 1, 2-amidic bonds, which is considered to be reversible and at low pH i.e. high [H^+], the rupture takes place in the remaining 1, 2-amidic or 4, 5-azomethine group and the final hydrolysis products, the 2-amino-5-substituted benzophenones and glycine derivatives [2] are formed.

The *k*' for acid hydrolysis of Bz in aqueous solution at [H^+] = 0.001 and 0.01 M are 1.07×10^{-3} s^{-1} and 1.69×10^{-3} s^{-1}, respectively. Under identical experimental conditions, the *k*' has the value of 1.58×10^{-3} s^{-1} and 1.82×10^{-3} s^{-1} in the presence of 0.96 mM CTAB (just above the CMC), while the *k*' has the value of 1.70×10^{-3} s^{-1} and 2.02×10^{-3} s^{-1} for 0.49 mM CTAB (below the CMC), for [H^+] = 0.001 and 0.01 M, respectively. It is clear that the values of the *k*' in presence of CTAB are higher than in aqueous solution. CTAB, thereby, enhances the acid hydrolysis of Bz and serves as a positive catalyst both below and above the CMC. The interactions of Bz and H^+ with different concentrations of CTAB during hydrolysis of Bz is shown in scheme 5.1.

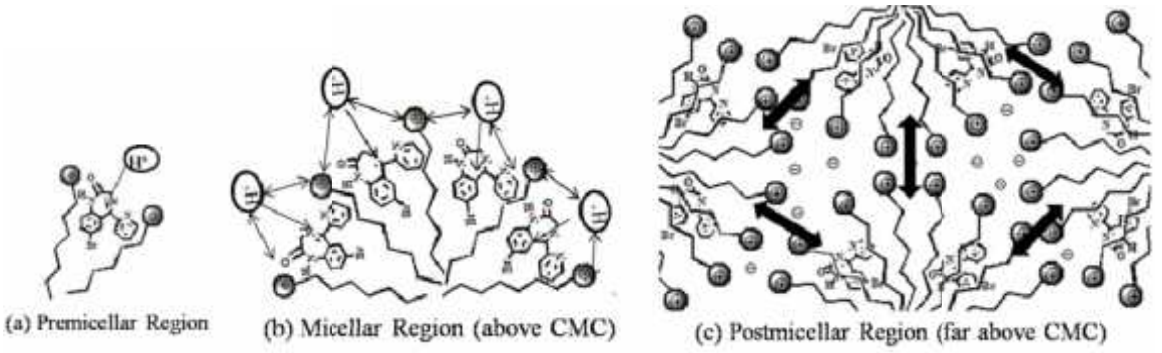

Scheme 5.1. Different interactions of Bz and H^+ with increasing [CTAB] ((a) premicellar (b) Micellar (above the CMC) and (c) postmicellar (far above the CMC) during hydrolysis of Bz.

The initial increase in *k*' with increase in [CTAB] is due to a catalytic effect of the CTAB monomers present in the solution which form a catalytic premicelle by aggregation with Bz. Such aggregation possibly sterically or entropically favors the reaction and enhances the reaction rate. Several works are reported wherein the rates of reactions were found to be influenced by the different surfactants in the premicellar region (Scheme 5.1. (a)) [44, 45]. Piszkiewicz [46] analyzed a large number of published data on the dependence of rate constants on the surfactant concentration especially on surfactant concentration at premicellar region.

Above the CMC of CTAB, at [H^+] = 0.001 M, the values o *k*' decreases initially then becomes almost constant. This should correspond to the electrostatic repulsion between

the reactant, H^+ and the hydrophilic trimethylammonium ions of CTAB which reduces the possibilities to react H^+ with Bz (Scheme 5.1 (b)). Additionally, at $[H^+] = 0.01$ M, the *k*' slightly increases at some concentration of CTAB might be due to different extent of binding of Bz with CTAB.

At very high [CTAB], the values of the *k*' have been found to be smaller than the corresponding value in aqueous solution for both at high and low $[H^+]$. This indicates that at concentrations far above the CMC of CTAB, the rate of reaction is ultimately inhibited. This may be explained in terms of two facts. *Firstly*, with increasing [CTAB], the number of micelles increases and when the number of micelles exceeds that required to solubilize all of Bz, there is a dilution of the concentration of Bz per micelle as the [CTAB] is increased further. This causes a reduction in the rate constant. *Secondly*, the charged surface of CTAB in aqueous solution may cause the repulsion of similar-charged reactant, H^+ (Scheme 5.1. (c)) or even the solubilization of the H^+ into the micelle. Such repulsion or solubilization of the H^+ will result in a decrease in its activity in the solution phase. An increase in the [CTAB] over that required to affect complete solubilization of the Bz may therefore result in a decrease in the rate constant, even for the cases where rate enhancement by micelles occurs.

5.3.5. Spectral Behavior of Bz in Presence of TX-100 in Aqueous Solution

Figure 5.3.5 (a) represents the spectra of 2.21×10^{-5} M Bz in presence of TX-100 at various concentrations. The position of absorption maximum shifts towards a higher wavelength upon addition of TX-100 and at concentrations below the CMC the λ_{max} attains an almost constant value (Figure 5.3.5 (b)).

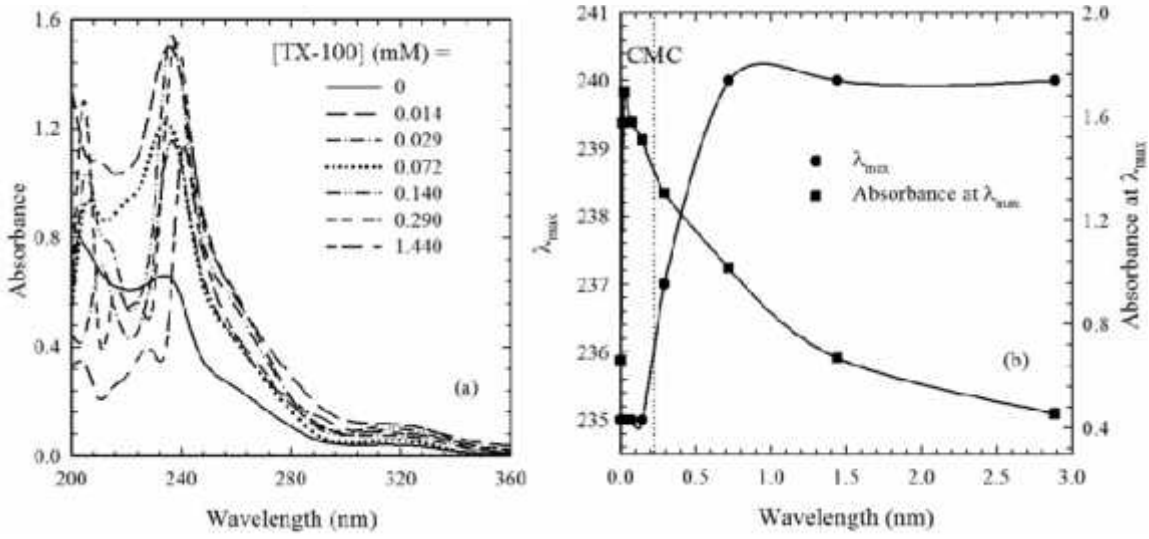

Figure 5.3.5. (a) Absorption spectra and (b) the λ_{max} and absorbance at the respective λ_{max} of 2.21×10^{-5} M Bz as a function of [TX-100] in aqueous solution.

At concentrations close to the CMC, the λ_{max} increases while at concentrations far above the CMC, the values of λ_{max} are constant. Figure 5.3.5 (b) also shows the variation of absorbance of 2.21×10^{-5} M Bz aqueous solutions with [TX-100] at their respective λ_{max}. The absorbance at the λ_{max} increases first then decreases with increasing [TX-100].

5.3.6. Hydrolysis in Presence of TX-100

Figure 5.3.6 shows the k' vs. [TX-100] profile for the acid hydrolysis Bz at $[H^+]$ = 0.001 and 0.01 M. The k' initially decreases and then becomes almost constant with increasing [TX-100] at concentrations below the CMC and at concentrations above the CMC, k' slightly increases and then becomes almost constant with increasing [TX-100]. From Figure 5.3.6, it has been also shown that the rate constant values at concentrations below and above the CMC of TX-100 are lower than in aqueous solution under identical conditions. Thus, TX-100 acts as a negative catalyst for acid hydrolysis of Bz.

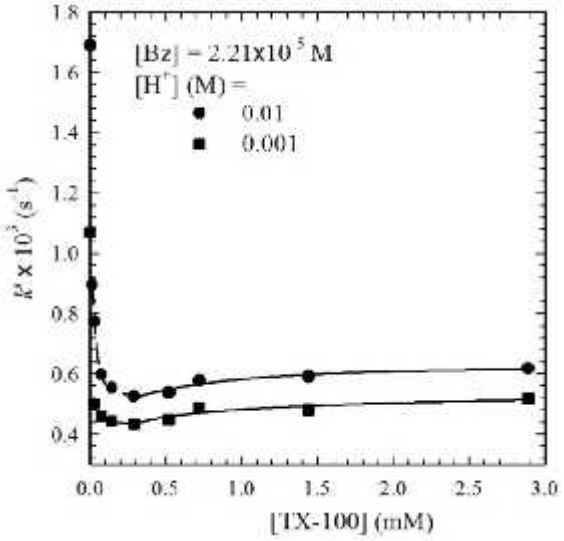

Figure 5.3.6. The k' for acid hydrolysis of Bz as a function of [TX-100] at different $[H^+]$. Dashed and solid lines represent the Piszkiewicz's model fitting results for concentrations below and above the CMC of TX-100, respectively.

The k' vs. [TX-100] plot reaches a minimum at 0.15 mM for both high and low $[H^+]$ (0.001 and 0.01 M), after which the rate constants have been found to increase slightly with increase in [TX-100] (Figure 5.3.6.). The interactions of Bz with different concentrations of TX-100 during hydrolysis of Bz is shown in Scheme 5.2. As Bz is hydrophobic in nature, it binds itself to TX-100 diluting the concentration of Bz in the bulk solution resulting in reducing the chance by which the two reactants can meet and the rate constant decreases (Scheme 5.2 (a)).

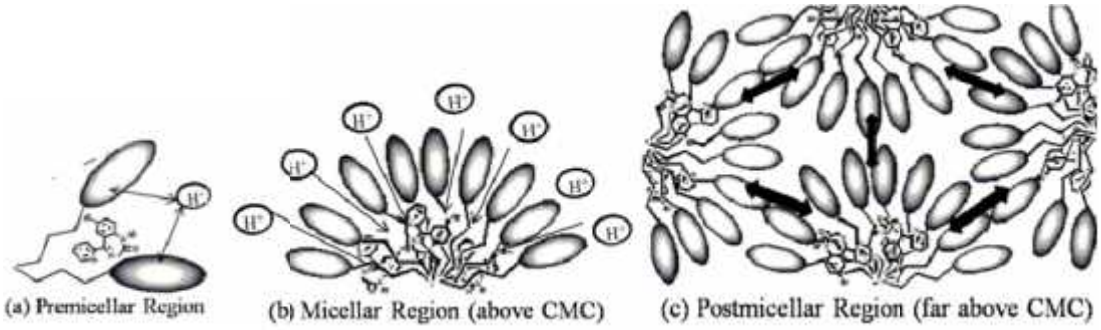

Scheme 5.3. Different interactions of Bz and H^+ with increasing [TX-100]: ((a) premicellar (b) micellar (above the CMC) and (c) postmicellar (far above the CMC) solutions during hydrolysis of Bz.

When the concentration of TX-100 reaches the CMC, self-aggregation of the TX-100 results in the formation of micelles where the Bz solubilizes in the hydrophobic core of micelles and the number of Bz in the bulk solution decreases. The binding of the H^+ within the neutral micelles of TX-100 and hence enhancement of their concentration in the micellar phase occurs. This increased concentration of Bz within the micellar phase makes the hydrolysis of Bz feasible, when H^+ approaches in close contact of Bz within the micellar phase and also at the interface between the micellar pseudo-phase and the aqueous phase. Also, as the micellization commences at the CMC, micelles lowering the concentration of TX-100 in the bulk; the reactivity of Bz in aqueous phase is changed and the rate of alkaline hydrolysis of Bz is slightly increased. At concentrations far above the CMC of TX-100, the steric repulsion between micellar interfaces of TX-100 results constant values of rate constants.

5.3.7. Spectral Behavior of Bz in Presence of SDBS in Aqueous Solution

Figure 5.3.7(a) represents the spectra of 2.21×10^{-5} M Bz in presence of SDBS at various concentrations. Addition of SDBS shifts the position of absorption maximum towards a higher wavelength and at concentrations close to the CMC the λ_{max} attains an almost constant value (Figure 5.3.7 (b)). Figure 5.3.7(b) also shows the variation of absorbance of 2.21×10^{-5} M Bz aqueous solutions with varying concentrations of SDBS at their respective λ_{max}. With increasing [SDBS], absorbance at the λ_{max} increases first followed by a decrease to attain a limiting absorbance at concentrations close to the value of the CMC.

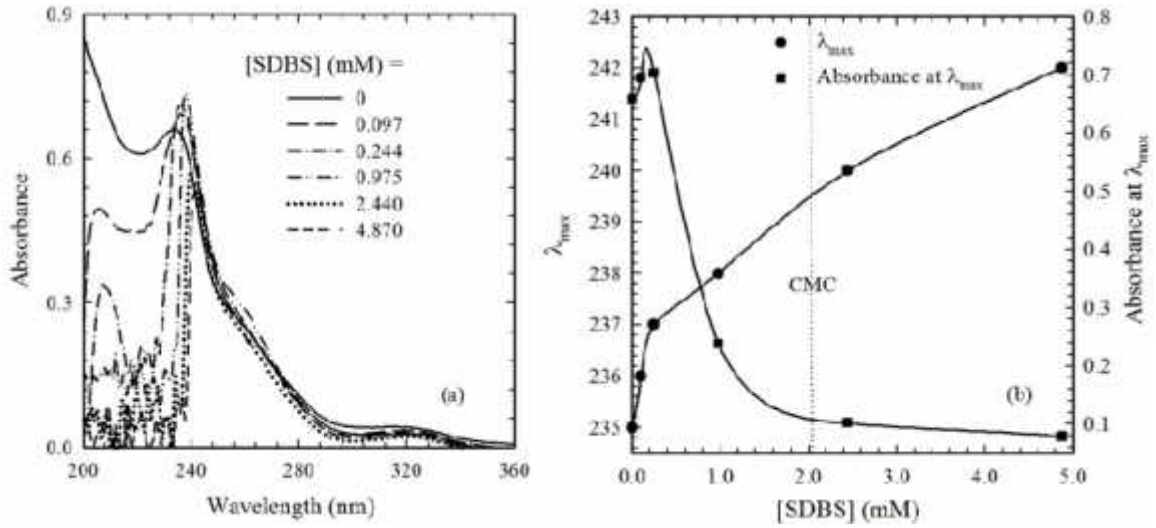

Figure 5.3.7. (a) Absorption spectra and (b) the λ_{max} and absorbance at the respective λ_{max} of 2.21×10^{-5} M Bz as a function of [SDBS] in aqueous solution.

5.3.8. Hydrolysis in Presence of SDBS

Figure 5.3.8 shows the k' vs. [SDBS] profile for acid hydrolysis of Bz at $[H^+]$ = 0.01 and 0.1 M. The k' for the acid hydrolysis of Bz in aqueous solution in the absence of SDBS at $[H^+]$ = 0.01 M is 1.69×10^{-3} s^{-1}. Under identical experimental conditions, the rate constant has the value of 1.55×10^{-3} s^{-1} in presence of 2.44 mM SDBS (above the CMC), while the k' has the value of 1.63×10^{-4} s^{-1} for 0.48 mM SDBS (below the CMC). It is clear that the value of k' in presence of SDBS are smaller than the value in absence of SDBS in both cases. SDBS, thereby, inhibits the acid hydrolysis reaction and serves as a negative catalyst both below and above the CMC.

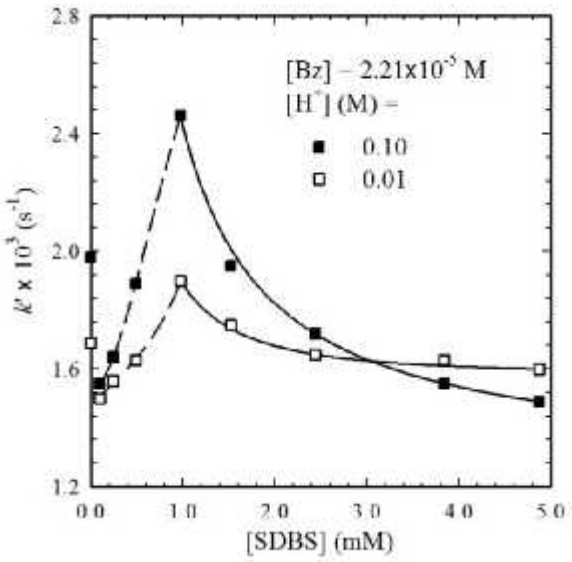

Figure 5.3.8. The k' for acid hydrolysis of Bz as a function of [SDBS] at different $[H^+]$. Dash and solid lines represents the Piszkiewicz's model fitting results for below and above the CMC of SDBS, respectively.

The k' for acid hydrolysis of Bz at some [SDBS] increases than the corresponding value in absence of SDBS at $[H^+]$ = 0.01 and 0.1 M. This should correspond to change in reaction mechanism during the course of reaction. It is noticeable from Figure 5.3.8 that the k' increases with increasing [SDBS] at concentrations below the CMC and decreases with increasing [SDBS] at concentrations above the CMC. The maximum inhibition occurs at SDBS concentration far below the CMC. At very high [SDBS], precipitation occurs and Bz solution turns to white precipitates. Therefore, kinetic measurements could not be conducted at very high [SDBS] above the CMC. The interactions of Bz and H^+ with different concentrations of SDBS during hydrolysis of Bz is shown in Scheme 5.3.

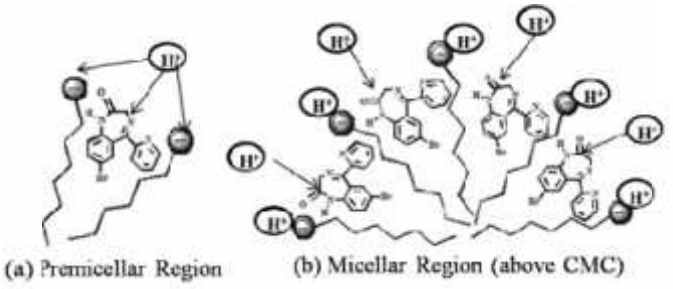

Scheme 5.3. Different interactions of Bz and H^+ with increasing [SDBS] ((a) premicellar and (b) micellar (above the CMC) solutions during hydrolysis of Bz.

When Bz is mixed with SDBS, strong interaction between SDBS and Bz prevails and when H^+ is added to the reaction mixture H^+ cannot come closer approach to Bz easily which are already under interaction with SDBS (Scheme 5.3(a)). The rate of hydrolysis reaction is therefore inhibited. As the [SDBS] increases, the k' increases and passes through a maximum. This may be correlated with change in binding constant between Bz and SDBS, and acid dissociation constant of Bz [26].

The micellar effect on the chemical reactivity is fairly independent of the size and volume of the aggregate when the reaction occurs at the level of the micellar interphase. The rate constant in the micellar phase seems to be independent of the $[H^+]$. However, the hydrophobic nature of SDBS would facilitate the penetration of the Bz into the micelle and since the H^+ is hydrophilic and tends to reside close to the stern layer of SDBS micelle, the reaction rate at concentrations above the CMC is likely to be lowered (Scheme 5.3 (b)).

5.3.9. Hydrolysis in Presence of SDS

Rodriguez and coworkers [2] reported that the presence of anionic micelles of SDS leads to a considerable decrease in the rate constant when the [SDS] is increased. They studied the rate constant of this reaction for only one concentration of SDS at below the CMC. In this work, the rate constants were determined for a number of concentration of SDS (below the CMC). Figure 5.3.9. shows the k' vs. [SDS] profile for the acid hydrolysis Bz

at $[H^+]$ = 0.1 M. With increasing [SDS], the *k*' initially decreases and then increases passing through a maximum at concentrations below the CMC and at concentrations above the CMC, the *k*' decreases and then becomes almost constant. Thus, SDS also serves as negative catalyst for the acid hydrolysis Bz as like as SDBS.

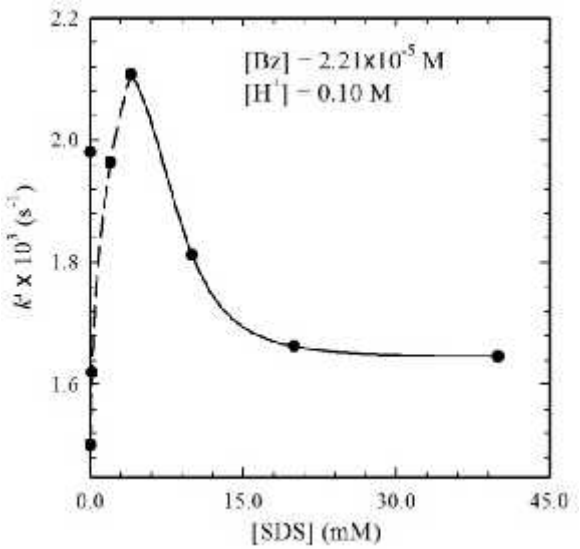

Figure 5.3.9. The *k*' for acid hydrolysis of Bz with [SDS] at $[H^+]$. Dash and solid lines represents the Piszkiewicz's model fitting results for below and above the CMC of SDS, respectively.

When the concentration of SDS reaches the CMC, self aggregation of SDS results in the formation of micelles. This leads to the solubilization of Bz in the hydrophobic core of SDS micelles and number of Bz existing in the bulk solution interacting with SDS species decreases. The binding of Bz within micelles and hence enhancement of their concentration in the micellar phase occurs as noted for SDBS. However, since SDS is also an anionic surfactant, the negatively charged micellar head groups discourage the closer approach of H^+ and Bz, which is solubilized inside the hydrophobic core of micelle. This increased concentration of Bz within the micellar phase makes hydrolysis of Bz feasible, when H^+ approaches in close contact of Bz within the micellar phase and also at the interface between the micellar pseudo-phase and aqueous phase. The fact that the rate constant decreases and then almost constant at above the CMC, in contrast to SDBS system indicates that solubilization of Bz inside the core of micelle is relatively less prominent for SDS compared to that for SDBS. This is not surprising since a phenyl group in the hydrobphobic moiety of SDBS makes it more hydrophobic and a more hydrophobic core of micelle for SDBS compared to SDS is likely above their CMCs.

5.3.10. Analysis of the Kinetic Results by Piszkiewicz's Model

The Piszkiewicz's model [46–48] is based on the mechanism described in Scheme 5.4.

$$Bz + H^+ \xrightarrow{k_W} Bz - H$$

$$Bz + nS \xleftrightarrow{K_D} S_n - Bz$$

$$S_n - Bz + H^+ \xrightarrow{k_m} Bz - H$$

Scheme 5.4. Acid hydrolysis of Bz in presence of surfactant.

From Scheme 5.4, it has been apparent that the kinetic mechanism of reaction of acid hydrolysis of Bz in aqueous solution in presence of surfactant includes three steps: *(1)* the interaction of the free Bz and H^+ with the formation of the product (Bz-H) in water; k_w is the second-order rate constant for this process. *(2)* the equilibrium of the binding of the Bz with several numbers of surfactants (n) with the formation of catalytic micelles (S_n−Bz); K_D is the equilibrium constant of dissociation of the free Bz and surfactant, $K_D = [Bz]\,[S]_n / [S_n - Bz]$. *(3)* the interaction of the Bz bound by catalytic micelle and H^+ with the formation of the same product; k_m is the second-order rate constant for this reaction. It follows from scheme 5.6, that for the observed rate constant as a function of the surfactant concentration [46-48]

$$k_{obs} = \frac{k_m[D]^n + k_w K_D}{K_D + [D]^n} \text{ - - - - - - - - - - - - (5.2)}$$

The kinetic results of this reaction in presence of CTAB, TX-100 and SDBS/ SDS have been analyzed by applying the Piszkiewicz's model in the form of equation (2) for describing the variation of the rate constants along with the concentration of CTAB, TX-100 and SDBS/ SDS in solution below and above the CMC values. The nonlinear method of the least squares was used for calculation and the corresponding values of n and K_D thus obtained is shown in Table 5.1.

Table 5.1. Values of n and K_D obtained from Piszkiewicz's model for interaction of Bz with CTAB, TX-100 and SDBS/SDS at 25 ^oC.

		Below the CMC			Above the CMC		
Surfactant	$[H^+]$ (M)	K_D	n	r^2	K_D	n	r^2
CTAB	0.001	50.0	1.00	0.99	0.43	0.80	0.99
	0.01	53×10^2	1.96	0.98	- - - -	- - -	- - -
SDBS	0.01	0.98	0.03	0.99	5.01	1.81	1.00
	0.1	1.32	1.89	1.00	16.42	1.01	1.00
SDS	0.1	3.09	0.52	1.00	3.2×10^3	3.78	1.00
TX-100	0.001	242.8	1.23	1.00	1.42	0.04	0.93
	0.01	743.9	1.92	0.99	0.50	1.71	0.97

5.3.11. Analysis of the Kinetic Results by PPIE Model

The enhancement and inhibition of the rate of the hydrolysis of Bz by CTAB micelles were treated by PPIE model [49]. According to PPIE model the apparent rate constant is given by equation (5.3),

$$k' = \frac{k_W[H^+] + (k_M K_S - k_W) m_H[M]}{1 + K_S[M]} \text{ - - - - - - - - - (5.3)}$$

Here, [M] is the concentration of micellized surfactant whose is given by, [M] = ([S] - CMC)/*N*, where [S] is the concentration of the surfactant and *N* is the aggregation number (61 for CTAB [50] in aqueous solution at 25 ^oC). The k_M refers to the second order rate constant in the micellar pseudophase. The K_{Br}^H and K_S are the ion exchange equilibrium constant and the binding constant of the substrate, Bz to the micelles, respectively. The fraction of micellar head groups neutralized by H^+ ions (m_H) were obtained by solving equation 5.4 [49]

$$m_H^2 + m_H\{\frac{[H^+] + K_{Br}^H[Br^-]}{(K_{Br}^H - 1)[M]} - \beta\} - \frac{\beta[H^+]}{(K_{Br}^H - 1)[M]} = 0 \text{ - - - - - - - - - (5.4)}$$

The experimental data were fitted to both the equations 1 and 2 simultaneously, using k_M, K_S and K_{Br}^H as adjustable parameters. Results of computer simulation for the data at the concentration of H^+ = 0.001 and 0.01 M is shown in Figure 5.3.4. The values of k_M, K_S and K_{Br}^H obtained with best fitting at $[H^+]$ = 0.001 and 0.01 M are shown in Table 5.2.

Table 5.2. The optimized values of k_M, K_S and K_{Br}^H for $[H^+]$ = 0.001 and 0.01 M for acid hydrolysis of 2.21×10^{-5} M Bz in micellar solutions of CTAB using PPIE model.

$[H^+]$ (M)	k_M (s^{-1})	K_{Br}^H	K_S (M^{-1})
0.010	0.016	1.00	200
0.001	0.370	1.00	187

From Table 1, it is apparent that the values of K_{Br}^H are independent of $[H^+]$ and the K_s and k_M depend on the $[H^+]$. This may be due to the fact that as the concentration of Bz is constant, at low and high $[H^+]$, the concentration of the reactant, H^+ are different in the micellar pseudophase and the bulk phase.

5.3.12. Spectral Behavior of Bz in Reverse Micelles and Microemulsions of CTAB

Figure 5.3.10 shows the spectra of 2.21×10^{-5} M Bz solutions in CTAB/cyclohexane/1-butanol/water microemulsions and CTAB/1-butanol/water reverse micelles. As the content of water decreases, the λ_{max} slightly shifts to higher wavelength for both reverse micelles and microemulsions.

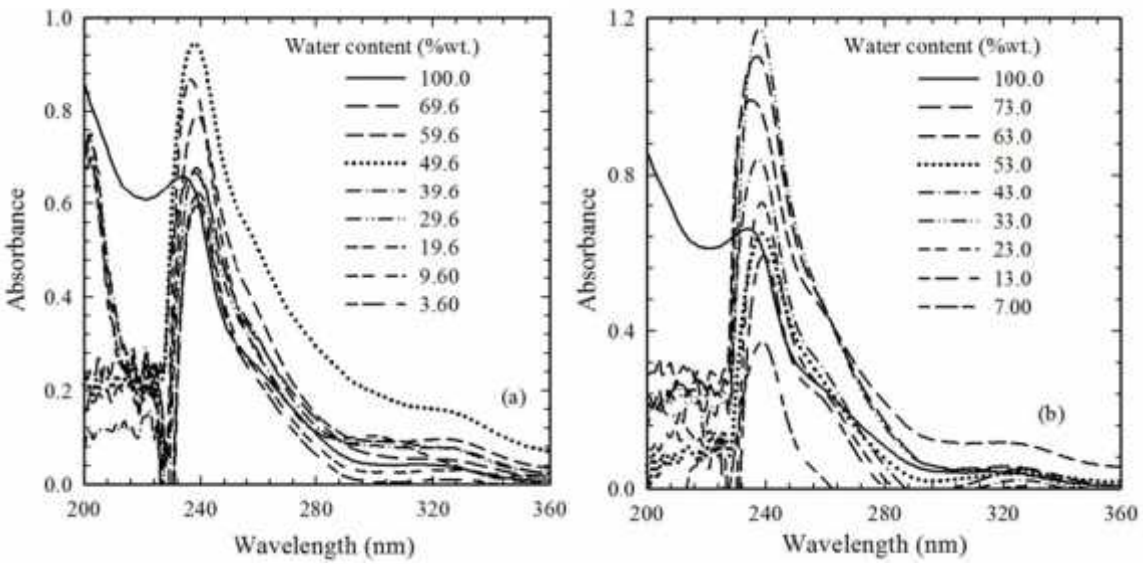

Figure 5.3.10. Spectra of 2.21×10^{-5} M Bz in aqueous solution in comparison with (a) CTAB/cyclohexane/1-butanol/water microemulsions with 20 %wt. of CTAB, 3.4 %wt. of cyclohexane and different 1-butanol/water content and (b) CTAB/ 1-butanol/ water reverse micelles with 20 %wt. of CTAB and different 1-butanol/water content.

5.3.13. Hydrolysis in Reverse Micelles and Microemulsions of CTAB

Figure 5.3.11 represents the k' vs. ϕ_W profiles for CTAB/1-butanol/cyclohexane/water microemulsions and CTAB/1-butanol/water reverse micelles at $[H^+] = 0.001$ M. Figure 5.3.11 shows that the rate constants are greatly affected by CTAB/cyclohexane/1-butanol/water microemulsions and CTAB/1-butanol/water reverse micelles, which is clear indication of catalysis of the acid hydrolysis of Bz by these organized media. As ϕ_W in CTAB/cyclohexane/1-butanol/water microemulsions and CTAB/1-butanol/water reverse micelles increases, the k' sharply decreases first and then becomes almost constant; however, at higher value of the ϕ_W (> 0.46) a gradual increase is apparent. The rate constants attain value much higher than the corresponding value in aqueous solution under identical experimental conditions.

From Figure 5.3.11, in the region '*ab*' of the curve (ϕ_W < 0.20), the rate constant decreases with increasing ϕ_W which should correspond to the region of CTAB/1-butanol reverse micelles where the incorporation of water into the core inhibit the reaction. Part '*cd*' of the curve (ϕ_W > 0.46) should correspond to the reaction in CTAB/water micelles where a decrease in 1-butanol produces a slight increase in the rate of reaction. Part '*bc*' of the curve (ϕ_W = 0.2~0.46) should correspond to the cluster formation by the aggregation of CTAB reverse micelles (*w*/*o* microemulsions) in 1-butanol and CTAB micelles (*o*/*w* microemulsions) in water that is *BC* microemulsions [51].

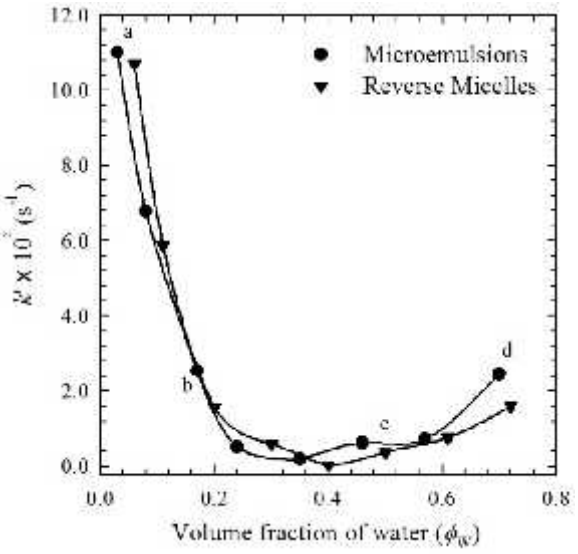

Figure 5.3.11. The k' vs. ϕ_W profiles for acid hydrolysis of 2.21×10^{-5} M Bz in CTAB/1-butanol/cyclohexane/water microemulsions and CTAB/1-butanol/water reverse micelles at $[H^+] = 0.001$ M.

At high $[H^+]$ (= 0.01 M) (Figure 5.3.12), with increasing ϕ_W in microemulsions, the k' increases first followed by a sharp decrease. However, the sharp increases in k' at $\phi_W <$ 0.20~0.25 indicates the CTAB/1-butanol reverse micelles (*w*/*o*) [52] and after $\phi_W >$ 0.40~0.45, the k' decreases for CTAB/water micelles (*o*/*w*) in reverse micelles and microemulsions. At ϕ_W = 0.20~0.45, the change in k' is due to the formation of *BC* microemulsions.

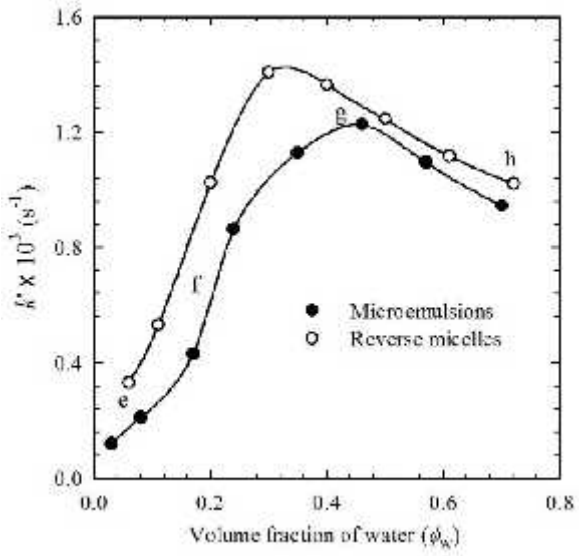

Figure 5.3.12. The k' vs. ϕ_W profiles for acid hydrolysis of 2.21×10^{-5} M Bz in CTAB/1-butanol/cyclohexane/water microemulsions and CTAB/1-butanol/water reverse micelles at $[H^+] = 0.01$ M.

It worth mentioning that k' vs. ϕ_W in reverse micelles and microemulsions profiles for low $[H^+]$ (= 0.001 M) (figure 5.3.11) and high $[H^+]$ (= 0.01 M) (Figure 5.3.12) are entirely different. The difference should be originated from the change in reaction mechanism with different pH. The binding constant of Bz to microemulsions of CTAB (both *w*/*o* and *o*/*w*) as well as interaction of reaction products, BZH^+(II) benzoyl-pyridine derivative with the organized species in high $[H^+]$ are expected to have significant changes which shows the different profile in reverse micelles and microemulsions of CTAB with same composition.

5.4. Conclusions

The acid hydrolysis of Bz is catalyzed by the micellar solution of CTAB, SDBS/SDS and TX-100. The addition of CTAB has been found to enhance the rate of the hydrolysis of Bz while presence of SDBS/SDS and TX-100 produced an inhibitory effect at concentrations below the CMC. Above the CMC, the rate constant increases slightly for some concentration of SDBS/SDS whereas for TX-100, the k' was almost constant. As the [CTAB] increases at low $[H^+]$, the rate constant attains a limiting value; while at a high $[H^+]$, the rate constant passes through a maximum and then decreases. The acceleration and inhibition effect of the CTAB, SDBS/SDS and TX-100 on the reaction at concentration below the CMC has been satisfactorily explained with the help of Piszkiewicz model via formation of premicellar aggregates between the Bz and a small number of different surfactant monomers with hydrophobic interactions. The kinetic results in presence of CTAB also showed good fit to the PPIE model for the reaction with reasonable values of the parameters. Moreover, the kinetic profiles vary depending on the change in the reaction environment due to different assembly and orientation of the surfactants in micelles, reverse micelles and microemulsions. The k' vs. ϕ_W profiles for CTAB/cyclohexane/1-butanol/water microemulsions and CTAB/1-butanol/water reverse micelles show special patterns for both $[H^+]$ (0.001 and 0.01 M) (depending on the change in reaction mechanism with different pH) with increasing ϕ_W indicating a transition from *w*/*o* to *o*/*w* via *BC* microemulsions. Thus, the kinetic profiles also exhibit pH dependence in micelles, reverse micelles and microemulsions like that in aqueous solution.

References

[1] T. Damjanovi, G. Popovi, S. Verbi, L. Pfendt, *Study of acid hydrolysis of bromazepam*, Canadian Journal of Chemistry, 2004, 82, 1260-1265.

[2] M. E. Moro, J. N. Fertrell, M. M. Velazquez, L. J. Rodriguez, *Kinetics of the acid hydrolysis of diazepam, bromazepam, and flunitrazepam in aqueous and micellar systems*, Journal of Pharmaceutical Science, 1991, 80, 459-466.

[3] N. S. Nudelman, R. G. Waisbaum, *Acid hydrolysis of diazepam: Kinetic study of the reactions of 2-(N-methylamino)-5-chlorobenzophenone, with HCl in MeOH-H_2O,* Journal of Pharmaceutical Science, 1995, 84, 998-1004.

[4] K. Y. Shen, *Mechanism of alkaline hydrolysis of diazepam*, Journal of the Chinese Chemical Society, 1998, 45, 277-284.

[5] R. Smyth, T. S. Beng, W. F. Smyth, *A spectral and polarographic study of the acid-base and coxiplexing behaviour of bromazepam*, Analytica Chimica Acta, 1977, 92, 129-138.

[6] M. Nakano, N. Inotsume, N. Kohri, T. Arita, *Reversible ring-opening reaction of diazepam in acid media around body temperature*, International Journal of Pharmaceutics, 1979, 3, 195-204.

[7] W. H. Hong, C. Johnston, D. Szulczewski, *Equilibrium reaction of pyrazolodiazepinones in aqueous solution,* Journal of Pharmaceutical Science, 1977, 66, 1703-1708.

[8] W. W. Han, G. J. I. Yakatan, D. D. Maness, *Kinetics and mechanisms of hydrolysis of 1, 4-benzodiazepines III: Nitrazepam*, Journal of Pharmaceutical Science, 1977, 66, 795-798.

[9] W. W. Han, G. J. I. Yakatan, D. D. Maness, *Kinetics and mechanisms of hydrolysis of 1, 4-benzodiazepines II: Oxazepam and diazepam*, Journal of Pharmaceutical Science, 1977, 66, 573-577.

[10] G. M. Whitesides, B. Grzybowski, *Self-assembly at all scales*, Science, 2002, 295, 2418-2421.

[11] C. M. Drain, *Self-organization of self-assembled photonic materials into functional devices: Photo-switched conductors*, Proceedings of the National Academy of Sciences of the United States of America, 2002, 99, 5178-5182.

[12] C. Du, G. Falini, S. Fermani, C. Abbott, J. Moradian-Oldak, *Supramolecular assembly of amelogenin nanospheres into birefringent microribbons*, Science, 2005, 307, 1450-1454,

[13] D. G. Kurth, P. Lehmann, M. Schutte, *A route to hierarchical materials based on complexes of metallosupramolecular polyelectrolytes and amphiphiles*, Proceedings of the National Academy of Sciences of the United States of America, 2000, 97, 5704-5707.

[14] S. H. Park, J. H. Lim, S.W. Chung, C. A. Mirkin, *Self-assembly of macroscopic metal- polymer amphiphiles*, Science, 2004, 303, 348-351.

[15] E. Winfree, F. Liu, L. A. Wenzler, N. C. Seeman, *Design and self-assembly of two-dimensional DNA crystals*, Nature, 1998, 394, 539-544.

[16] D. M. Vriezema, M. C. Aragones, A. E. Rowan, R. J. M. Nolte, *Self-assembled nanoreactors*, Chemical Review, 2005, 105, 1445-1489.

[17] G. Stinga, D. M. Mihai, A. Iovescu Baran A., D. F. Anghel, *Effect of organic solvents upon the basic hydrolysis of acetylsalicylic acid in aqueous-micellar solutions,* Romanian Journal of Chemistry, 2005, 50, 767-775.

[18] Y. S. Simanenko, A. F. Popov, T. M. Prokopeva, E. A. Karpichev, I. A. Belousova, V. A. Savelova, *Micellar effects of cationic detergents in the decomposition of ecotoxic substrates by hydroxide ion*, Journal of Theoretical and Experimental Chemistry, 2002, 38, 242-249.

[19] L. Mukherjee, N. Mitra, P. K. Bhattacharya, S. P. Moulick, *Kinetics in microemulsion medium. 4. Alkaline fading of crystal violet in aqueous (H_2O/aerosol OT/isooctane and H_2O/aerosol OT/decane) and nonaqueous (ethylene glycol/ aerosol OT/isooctane) microemulsions*, Langmuir, 1995, 11, 2866-2871.

[20] R.Y. Talman, S. Gokturkand, M. Tuncay, *Kinetic cosolvent effects on the alkaline fading of crystal violet in the presence of sodium dodecyl sulfate micelles*, Colloids and Surfaces A: Physicochemical and Engineering Aspects, 2005, 270, 72-77.

[21] J. Datta, A. Bhattiacharya, K. Kundu, *Effect of surfactants on the kinetics of alkaline fading of crystal violet and acid-catalyzed inversion of sucrose,* Indian Journal of Chemistry,1988, 27, 115-122.

[22] C. Dolect, E. Rodenas, *Hydroxide ion specific adsorption on cetyltrimethylammonium bromide micelles explains kinetic data,* Colloids and Surfaces A: Physicochemical and Engineering Aspects, 1993, 75, 39-50.

[23] E. F. J. Duynstee, E. Grunwald, *Organic reactions occurring in or on micelles. I. Reaction rate studies of the alkaline fading of triphenylmethane dyes and sulfonphthalein indicators in the presence of detergent salts*, Journal of the American Chemical Society, 1959, 81, 4540-4542.

[24] M. Isabel, M. L. Sierra, M. Valiente, E. Rodenas, *Physical properties of cetylpyridinium chloride micelles and their behaviour as reaction media*, Journal of the Chemical Society, Faraday Transactions, 1996, 92, 59-63.

[25] Z. Yuanqin, L. Xiaoyan, L. Jing, Z. Xiancheng, *Micellar catalysis of composite reactions-The effect of SDS micelles and premicelles on the alkaline fading of crystal violet and malachite green*, Journal of Dispersion Science and Technology, 2002, 23, 473-481,

[26] A. R. Kabir, M. A. B. H. Susan, *Kinetics of the alkaline hydrolysis of crystal violet in aqueous solution influenced by anionic surfactants,* Journal of Saudi Chemical Society, 2008, 12, 543-554.

[27] L. Arzuman, S. N. Karobi, M. J. Islam, G. Ara, M. M. Rahman, M. Y. A. Mollah, M. A. B. H. Susan, *Effect of urea on the kinetics of the alkaline hydrolysis of crystal violet catalyzed by aqueous micellar solutions of cetyltrimethylammonium bromide*, Synthesis and Reactivity in Inorganic, Metal-Organic and Nano-Metal Chemistry, 2015, 45, 764-769.

[28] F. Begum, M. Y. A. Mollah, M. M. Rahman, M. A. B. H. Susan, *Kinetics of the alkaline hydrolysis of crystal violet in micelles, reverse micelles and microemulsions of cetyltrimethylammonium bromide*, Journal of Bangladesh Chemical Society, 2011, 24, 173-184,

[29] C. O. R. Yagui, A. P. Junior, *Micellar solubilization of drugs*, Journal of Pharmaceutical Science, 2005, 8, 147-163.

[30] F. Begum, M. Y. A. Mollah, M. M. Rahman, M. A. B. H. Susan, *Acid hydrolysis of bromazepam catalyzed by micelles, reverse micelles, and microemulsions*, Journal of Chemistry, 2015, 2015, 1-10.

[31] P. C. Mohr, A Mohr, T. P. Vila, H. G. Korth, *Localization of hydrophobic N-diazeniumdiolates in aqueous micellar solution*, Langmuir, 2010, 26, 12785-12793.

[32] M. N. Khan, P. C. Gleen, A. Zainudin, *Effects of inorganic salts and mixed aqueous-organic solvents on the rates of alkaline hydrolysis of aspirin*, Indian Journal of Chemistry, 1996, 35, 758-765.

[33] M. Ferrit, C. D. Valle, M. L. Pez, R. Luque, F. M. Nez, *The stability of 2-acetoxy-4-trifluoromethylbenzoic acid (Triflusal) in micellar pseudophase*, Journal of Pharmaceutical Sciences, 2004, 93, 461-469.

[34] C. Matos, H. Chaimovich, J. L. Lima, I. M. Cuccovia, S. Reis, *Effect of liposomes on the rate of alkaline hydrolysis of indomethacin and acemetacin*, Journal of Pharmaceutical Sciences, 2001, 90, 298-309.

[35] N. P. Gensmantel, M. I. Page, *The micelles catalyzed hydrolysis of penicillin derivatives (Part I) and the effect of increasing the hydrophobicity of penicillin on its micelle-catalyzed hydrolysis (Part II)*, Journal of the Chemical Society Perkin Transactions, 1982, 2, 147-155,

[36] A. Cipiciani, C. Ebert, R. Germani, P. Linda, M. Lovrecich, F. Rubessa, G. Savelli, *Micellar effects on the basic hydrolysis of indomethacin and related compounds*, Journal of Pharmaceutical Sciences, 1985, 74, 1184-1187.

[37] H. Mandy, M. Leung, C. Hannah, W. K. Tak, *Encapsulation of curcumin in cationic micelles suppresses alkaline hydrolysis*, Langmuir, 2008, 24, 5672-5675.

[38] S. A. Abdullah, S. A. Mohd, A. A. Hamad, M. A. Adel, A. I. Zuheir, *Effect of alkyl length head group and nature of the surfactant on the hydrolysis 0f 1,3-benzoxazine-2,4-dione and its derivatives,* Journal of Colloid and Interface Science, 2011, 361, 205-211.

[39] J. E. Dawson, B. R. Hajratwala, H. Taylor, *Kinetics of indomethacin degradation II: Presence of alkali plus surfactant*, Journal of Pharmaceutical Science, 1977, 66, 1259-1263.

[40] A. G. Oliveira, I. M. Cuccovia, H. Chaimovich, *Micellar modification of drug stability: Analysis of the effect of hexadecyltrimethylammonium halides on the rate of degradation of cephaclor*, Journal of Pharmaceutical Science, 1990, 79, 37-42.

[41] A. S. Al-Ayed, M. S. Ali, H. A. Al-Lohedan, A. M. Al-Sulaim, Z. A. Issa, *Micellar effects on the alkaline hydrolysis of isatin and its derivatives*, Journal Colloid and Interface Science, 2011, 357, 393-399.

[42] M. Ferrit, C. Valle, F. Martinez, *The study of the influence of surfactant charge on alkaline hydrolysis reactions of acetylsalicyclic acid and triflusal using spectrophotometric methods*, European Journal of Pharmaceutical Sciences, 2007, 31, 211-220.

[43] L. Garciario, J. C. Mejuto, D. P. Rodriguez, G. J. Simal, *Influence of micelles on the basic degradation of carbofuran*, Journal of Agricultural and Food Chemistry, 2005, 53, 7172-7178.

[44] T. C. Bruice, J. Katzhendler, L. R. Fedor, *Nucleophilic micelles. II. Effect on the rate of solvolysis of neutral, positively, and negatively charged esters of varied chain length when incorporated into nonfunctional and functional micelles of neutral, positive and negative charge*, Journal of the American Chemical Society, 1968, 90, 1333-1348.

[45] J. H. Fendler, E. J. Fendler, R. T. Medary, V. A. Woods, *Catalysis by reversed micelles in nonpolar solvents: Mutarotation of 2, 3,4 ,6-tetramethyl-α-d-glucose in benzene and in cyclohexane*, Journal of the American Chemical Society, 1972, 94, 7288-7295.

[46] D. Piszkiewicz, *Cooperativity in bimolecular micelle-catalyzed reactions - inhibition of catalysis by high-concentrations of detergent*, Journal of the American Chemical Society 1977, 99, 7695-7697.

[47] D. Piszkiewicz, *Micelle catalyzed reactions are models of enzyme catalyzed reactions which show positive homotropic interactions*, Journal of the American Chemical Society, 1976, 98, 3053-3055.

[48] D. Piszkiewicz, *Positive cooperativity in micelle-catalyzed reactions*, Journal of the American Chemical Society, 1977, 99, 1550-1557.

[49] M. N. Khan, *Micellar catalysis*, Surfactant science, CRC Press: Florida, 2006.

[50] E. S. Anachkov K. D. Danov, E. S. Basheva, P. A. Kralchevsky, K. P. Ananthapadmanabhan, *Determination of the aggregation number and charge of ionic surfactant micelles from the stepwise thinning of foam films*, Advances in Colloid and Interface Science, 2012, 183, 55-67.

[51] J. Hao, *Effect of the structures of microemulsions on chemical reactions*, Colloid and Polymer Science, 2000, 278,150-154.

[52] Y. Miyake, T. Owari, K. Matsuura, M. Teramoto, *Enzymatic reaction in water-in-oil microemulsions, part 1.-Rate of hydrolysis of a hydrophilic substrate: Acetylsalicylic acid*, Journal of the Chemical Society, Faraday Transactions, 1993, 89, 1993-1999.

Abstract

Kinetic studies of hydrolysis of CV and Bz have been compared with those in aqueous solution and micelles, reverse micelles and microemulsions of CTAB, SDS and TX-100. The hydrolysis of CV was carried out under alkaline conditions; while that of Bz was followed under acidic conditions. The *k*'-[CTAB] profiles for hydrolysis of CV show a maximum at ca. 10 mM of CTAB concentration, after which *k*' gradually decreases with increasing [CTAB]; while for the hydrolysis of Bz, the addition of CTAB has been found to enhance the rate of the hydrolysis of Bz at concentrations below the CMC. Above the CMC of CTAB, at a low [H^+], as [CTAB] increases the rate constant to attain a limiting value; while at a high [H^+], the rate constant passes through a maximum and then decreases. SDBS produced an inhibitory effect on the reaction rate for both reactions. Micellar solution of TX-100 accelerates and inhibits hydrolysis of CV and Bz, respectively. The rate constants of the reactions are also greatly affected by reverse micelles and microemulsions of CTAB, SDS and TX-100 under identical experimental conditions. The rates are higher in *w*/*o* microemulsions and decrease with ϕ_W while rates are almost constant in BC microemulsions and decrease in *o*/*w* microemulsions.

6.1. Introduction

The rates of chemical reactions are known to be changed by self-organized assemblies of surfactants, containing both hydrophobic (nonpolar) and hydrophilic (polar) parts in its structure such as micelles, reverse micelles and microemulsions [1-10]. These self organized media are often found to catalyze or inhibit the rates of different chemical reactions owing to electrostatic and hydrophobic interactions [4, 7-10]. The accelerating effect of these media has been attributed to the fact that they increase the local concentration of reactants [9-11]. However, the retarding effect may be explained owing to the adsorption of one reactant on the micellar or reverse micellar surface and repulsion of the other by the same [10, 11]. This phenomenon has received considerable attention in recent past [7-27] Investigations provided evidence that surfactant aggregates can be utilized in controlling the rate of chemical reactions and as probes for studying reaction mechanisms [28-30].

It may be worth mentioning that inhibitory/accelerating effects on reaction rates by different surfactants have also been observed for different reactions such as enzymatic reaction, nucleophillic addition reaction, hydrolysis reaction [31-41] etc. Acceleration or inhibition of reaction rates in micelles, reverse micelles and microemulsions arises from different rates of reaction of the reactants in the micellar pseudophase and in the aqueous pseudophase and the distribution of the reactants in these two pseudophases [40]. Basically, these acceleration or retardation of reaction rates can be attributed to electrostatic and/or hydrophobic interactions between the reactants and the surfactant aggregates and in some cases to alterations in the structure of the surrounding water molecules [6].

Numerous attempts have been made to investigate the change of the rate constants of different reactions by micelles, reverse micelles and micremulsions of different surfactants. Micelles and reverse micelles affect the rate of reactions due to: (i) enhancement of reagents within their volume; (ii) stabilization or destabilization of substrates, intermediates, and products; (iii) specific orientation of reagents that changes their physicochemical properties [1]. They provide microreaction media that is similar to that for many biochemical processes. Micellar kinetic effects depend on the nature of the surfactants hydrophobic and hydrophilic groups [8, 31-41], and on the counter-ion [42].

Owoyomi et al [41] reported that the variation in k' with [surfactant] for alkaline hydrolysis of brilliant green (BG) shows a sigmoid shaped curve with different cationic surfactants; dodecyltrimethylammoniumbromide (DTAB), didodecyldimethylammonium bromide (DDAB) and CTAB at 25 °C, which is analogous to the positive cooperativity in enzymatic reactions. Samiey et al reported kinetic results for a number of carbocationic dye, CV [35], malachite green [36] and BG [37] in aqueous solution with different surfactants; TX-100, DTAB and SDS and showed that the reaction rates for all dyes increase in presence of TX-100 and DTAB and decrease in presence of SDS. The alkaline hydrolysis of CV was inhibited by both of SDS and SDBS [8] while catalyzed by micelles of CTAB and addition of urea caused a gradual decrease in the rate of the reaction [9, 10]. The values of k' for this reaction has been found to decrease upon incorporation of 1-butanol to CTAB micelles and in reverse micelles and microemulsions of CTAB, the k' vs. % wt. of 1-butanol profiles show an initial decrease in the k' followed by a gradual increase and finally, to a sharp increase with increasing 1-butanol content [10]. Both ethylene glycol (EG) and its microemulsion (EG/Aerosol OT (AOT)/isooctane) accelerate the hydrolysis of CV and the k' in the H_2O/AOT/isooctane and H_2O/AOT/decane microemulsion media is inversely proportional to the water/AOT or the ethylene glycol/AOT mole ratio; significant increases in rates occur at ratio less than 8 in the former and less than 4 in the latter case [7].

Sodium decyl (SdeS), dodecyl (SDS) and tetradecyl (STS) sulfate have been reported to produce an inhibitory effect in the kinetics of the acid hydrolysis of aqueous diazepam, Bz and flunitrazepam drugs; while negligible effects were observed in the cases of polyoxy ethylene-23-dodecanol and CTAB [43]. The presence of *N*-cetyl-*N*-ethyl-*N*, *N*-dimethylammonium bromide has been found to cause inhibition of the basic hydrolysis of triflusal [44]. The hexadecylphosphocholine micelles inhibit the basic hydrolysis of the indomethacin and acemetacin [45]. The presence of CTAB micelles enhances the rate of alkaline hydrolysis of penicillin [46]. The rate - [surfactant] profiles for the hydrolysis of indomethacin provide rate inhibition in the presence of SDS and rate enhancement in the presence of CTAB [47]. At pH 13, curcumin undergoes rapid degradation by alkaline hydrolysis in the SDS micelles; whereas is greatly suppressed in the presence of either CTAB or DTAB micelle [48]. The effect of cationic surfactants with varying

hydrophobic chains and with different headgroups and anionic surfactant, SDS on the rate of alkaline hydrolysis of the carsalam and its *N*-substituted derivatives have been investigated by Abdullah et al [49]. The plots of observed rate constant vs. [surfactants] for degradation of indomethacin under alkaline condition were curved with negative slopes for ethoxylated lanolin, polysorbate 80; but with the cetrimonium bromide, the plots showed a marked positive change in k_{obs} as the [surfactant] passed through the CMC [50]. The intramolecular degradation of cephaclor was catalyzed 25-fold by micelles of CTAB [51]. The rate of the hydrolysis of isatin and its derivatives of different hydrophobicities increased on increasing the [cetyltrimethylamonium chloride] and after reaching a maximum, it started decreasing: conversely, micelles of SDS inhibited the rate of hydrolysis of isatin and its derivatives [52]. Cationic micelles showed a catalytic effect on alkaline hydrolysis of acetylsalicylic acid and triflusal at low surfactant concentrations while was inhibited at high surfactant concentrations and in anionic micelles, a catalytic effect is observed, while in zwitterionic and non-ionic micelles there is an inhibitory effect [53]. The basic hydrolysis of carbofuran was catalyzed in the presence of colloidal aggregates with positive surface charge and large inhibition by anionic and nonionic surfactants [54].

In spite of numerous studies, there have been no reports on the comparative study of the kinetics of the alkaline hydrolysis of CV and the acid hydrolysis of Bz in aqueous solution and also in micelles, reverse micelles and microemulsions with different nature of surfactants. To understand the mechanism of those reactions under different reaction environments in micelles, reverse micelles and microemulsions depending on nature of surfactants, kinetic studies need to be systematically and intensively conducted. In present work, the kinetic results of hydrolysis of CV and Bz in micelles, reverse micelles and microemulsions have been compared with those in aqueous solution and also compared in different surfactants depending on their nature.

6.2. Experimental

6.2.1. Materials and Methods

Materials used and methods followed have been described in detail in Section 4.2.1 and 5.2.1.

6.3. Results and Discussion

6.3.1 Comparative Study of Alkaline Hydrolysis of CV

6.3.1.1 Hydrolysis in Presence of CTAB, SDBS and TX-100

Figure 6.3.1 shows the comparison of the k' vs. concentration profiles for CTAB, SDBS and TX-100 for alkaline hydrolysis of CV with $[OH^-]$ = 0.01 M. The CMC's of CTAB, SDBS and TX-100 were reported in Section 4.2.1. It should be noted here that the kinetic rate constants used in Figure 6.3.1 are for CTAB, SDBS and TX-100 with $[OH^-]$ = ca. 0.01 M. Although the pseudo first order rate constant does not follow, $k' = k_w [OH^-]$ in the presence of SDBS, the rate constants using $[OH^-]$ = 0.1 M (Figure 4.3.2, Chapter 4) have

been divided by 10 for the sake of comparison with the experimental results in presence of CTAB and SDBS for which the kinetic studies were conducted with $[OH^-] = 0.01$ M.

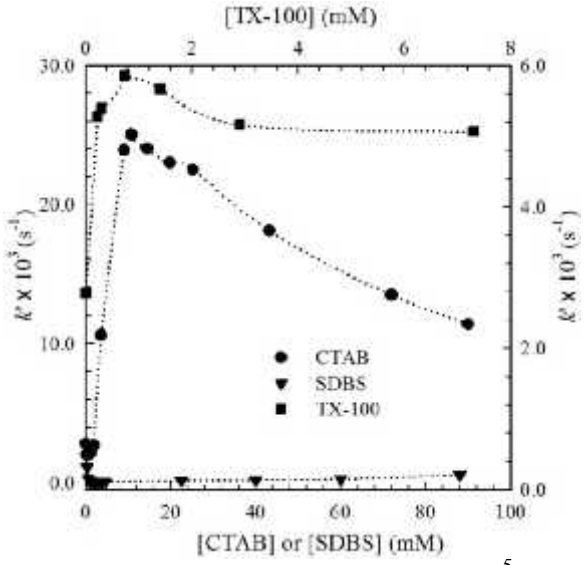

Figure 6.3.1. The k' for alkaline hydrolysis of 1.00×10^{-5} M CV with $[OH^-] = 0.01$ M as function of concentration of different surfactants, CTAB, SDBS and TX-100. For clarity, the values of k' are shown in the right side for TX-100.

The rate of alkaline hydrolysis of CV is accelerated in the presence of cationic, CTAB and nonionic TX-100 (section 4.3.3 and 4.3.5, Chapter 4) while it is inhibited by anionic, SDBS (section 4.3.4, Chapter 4). Below the CMC, the rate constant increases with increase in [CTAB]. Above the CMC (0.87 mM), a pronounced sharp increase in the rate constant is observed and the rate is enhanced up to more than 10-fold in micellar solutions of CTAB. As the [CTAB] is further increased (far above the CMC), the electrostatic repulsion between the micellar head groups, trimethylammonium ions and CV^+ increases discouraging further solubilization of CV in the micelle core. The ultimate result is a smaller value of the k' at very high [CTAB] than the value of k' in aqueous solution. On the other hand, addition of SDBS retards the rate of reaction at a galloping rate for below the CMC of SDBS and after the CMC. The k' is slightly increased but still the rate constant remains smaller than the corresponding value in aqueous solution. The sharp decrease in the rate constant at premicellar concentration of SDBS is due to the decrease in concentration of the CV for hydrolysis due to the strong CV-SDBS interaction in this case. Additionally, with increasing [TX-100], the k' increases up to 0.73 mM of TX-100 and then gradually decreases. With further increase in [TX-100], the rate constants are almost constant. The increases in k' is due to the increase in concentration of CV^+ in the micelle core of TX-100 which accelerates the reaction. With further increase in the [TX-100], the values of k' slightly decreases due to the hydrophobic repulsion between the different micelles of TX-100. At concentrations far above the CMC of TX-100, as TX-100 is non ionic, there was no electrostatic attraction

and repulsion between the CV^+ and nonionic POE counterparts resulting in the constant values of *k*'.

6.3.1.2 Hydrolysis in Aqueous Solution, 1-Butanol and Micelles, Reverse Micelles and Microemulsions of CTAB

Figure 6.3.2 compares the values of *k*' for alkaline hydrolysis of CV in 1-butanol and different organized media based on CTAB at identical [CTAB] with that in aqueous solution under identical experimental conditions. The values of *k*' of the reaction in aqueous solution shows a strong dependence on the dielectric constant of the medium [55, 56]. 1-Butanol has lower dielectric constant (18.3 at 25 ^oC) compared to water (80.0 at 25 ^oC). The *k*' of the alkaline hydrolysis of CV in aqueous solution is 1.73×10^{-3} s^{-1} and in 1-butanol is 17.70×10^{-3} s^{-1}. This indicates that a solvent having lower dielectric constant, favors the hydrolysis reaction of CV compared to that with a high value [57].

It is apparent from Figure 4.3.1, Chapter 4 that the *k*' in micellar solution of very high [CTAB] (far above the CMC) has a lower value than that in aqueous solution. This is due to the fact that as the [CTAB] is increased, the electrostatic repulsion between the micellar head groups and CV^+ increases discouraging further solubilization of CV in the micelle core. It is the reduction in the concentration of CV^+ in the micelle core that causes a gradual decrease in the rate of the hydrolysis in the system.

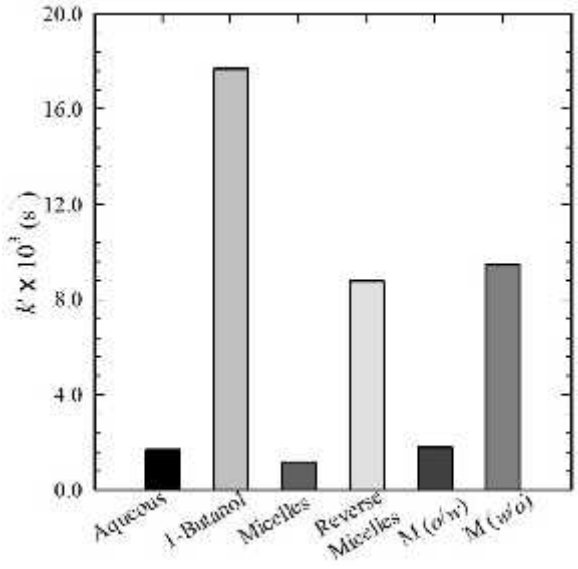

Figure 6.3.2. The *k*' for alkaline hydrolysis of 9.1×10^{-6} M CV with $[OH^-]$ = 7.4 mM in aqueous solution, 1-butanol and different organized media based on CTAB at [CTAB] = ca. 0.5 M. Micelle (20 %wt. of CTAB in water); Reverse micelle (20 %wt. of CTAB in 1-butanol); Microemulsion, M (*o*/*w*) (ϕ_W = 0.68) and microemulsion, M (*w*/*o*) (ϕ_W = 0.03).

For CTAB/1-butanol reverse micelles (20 %wt. of CTAB in 1-butanol), the value of *k*' is higher than in 20 %wt. of CTAB in aqueous solutions. This corresponds to the fact that in CTAB/1-butanol reverse micelles, the hydrophilic part of CTAB form the core of reverse micelles and the hydrophobic parts were in the bulk. Thus, the reagent, OH^- is solubilized in the core and easily reacts with the CV^+ and produces an increase in the reaction rate.

In *o*/*w* microemulsion (ϕ_W =0.68), the rate constant is similar as compared to aqueous solution, but higher than the corresponding micelles and it should correspond to the region of direct CTAB micelle in water where the 1-butanol incorporation into the CTAB micelles influences the reaction. On the other hand, in *w*/*o* microemulsion (ϕ_W = 0.03), the reverse micelles are dominating because of high 1-butanol content and the rate constant of the reaction is high.

6.3.1.3 Hydrolysis in Aqueous Solution, Micelles, Reverse Micelles and Microemulsions of SDS

Figure 6.3.3 compares the values of *k*' for alkaline hydrolysis of CV in different organized media based on SDS at identical [SDS] with that in aqueous solution under identical experimental conditions.

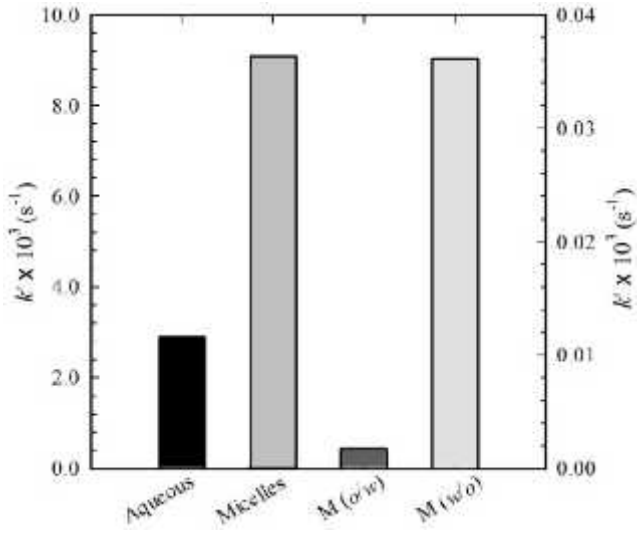

Figure 6.3.3. The *k*' for alkaline hydrolysis of 1.54×10^{-5} M CV with $[OH^-]$ = 0.012 M in aqueous solution and different organized media based on SDS at [SDS] = 1.88 M. Micelle (15 %wt. of SDS in water); Microemulsion, M (*o*/*w*) (ϕ_W = 0.50) and microemulsion, M (*w*/*o*) (ϕ_W = 0.11). For clarity, the value of *k*' is shown in the right side for micelles (15 %wt. of SDS in water).

It is apparent (section 4.3.3.2, Chapter 4) that the *k*' in micellar solution of SDS (15 %wt. of SDS in aqueous solution) at $[OH^-]$ = 0.012 M has very lower value than that in aqueous solution. This is due to the strong interaction between SDS and CV^+. OH^- cannot approach to CV^+ easily during hydrolysis reaction. The rate of hydrolysis reaction is

therefore inhibited. The significant change in the rate constant may also be ascribed to a change in solubilization originating from the change in micellar structure: from sphere to rod at extremely high concentrations.

In *o*/*w* microemulsion (ϕ_W = 0.50), the rate constant has lower value as compared to aqueous solution but higher than the corresponding micelles of SDS. This correspond to the region of direct SDS micelle in water where the 1-butanol incorporation into the SDS micelles slightly influences the reaction. On the other hand, in *w*/*o* microemulsion, (ϕ_W = 0.11), the SDS reverse micelles in 1-butanol are dominating because of high 1-butanol content and the rate constant of the reaction is high.

6.3.1.3 Hydrolysis in Aqueous Solution, Micelles, Reverse Micelles and Microemulsions of TX-100

Figure 6.3.4 compares the values of *k*' for alkaline hydrolysis of CV in different organized media based on TX-100 at identical [TX-100] with that in aqueous solution under identical experimental conditions.

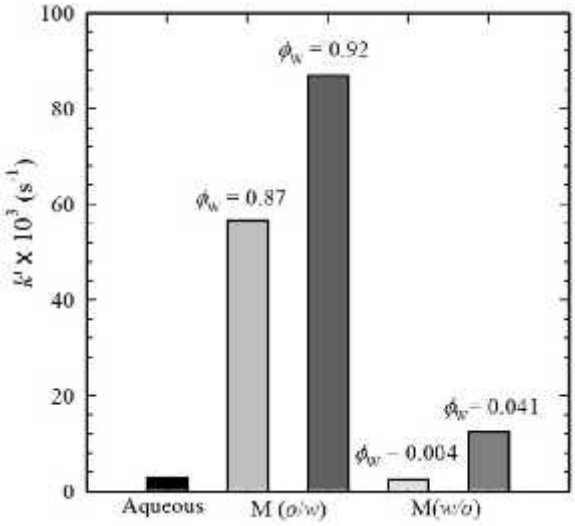

Figure 6.3.4. The *k*' for alkaline hydrolysis of 1.54×10^{-5} M CV with [OH^-] = 0.011 M in different organized media based on TX-100 at [TX-100] = 3.2 M. Microemulsion, M (*o*/*w*) (ϕ_W = 0.87 and 0.92) and microemulsion, M (*w*/*o*) (ϕ_W = 0.004 and 0.041).

In *o*/*w* microemulsion, the rate constant has higher value for both ϕ_W = 0.87 and 0.92 as compared to aqueous solution. These are the micelle rich microemulsions where with increasing ϕ_W, the rate of the reaction increases. When ϕ_W = 0.92, the value of *k*' is higher than that of ϕ_W = 0.87, which correspond to higher concentration of CV^+ in the aqueous solution.

On the other hand, in *w*/*o* microemulsion, the values of *k*' is almost same to that in aqueous solution for ϕ_W = 0.004; but slightly higher for the ϕ_W = 0.041. This is attributed

to the region of direct TX-100 reverse micelle in 1-butanol where the water incorporation into the TX-100/1-butanol reverse micelles slightly influences the reaction.

6.3.2 Comparative Study of Acid Hydrolysis of Bz

6.3.2.1 Hydrolysis in Presence of CTAB, SDBS and TX-100

Figure 6.3.5 shows the comparison of the *k*' vs. concentration of CTAB, SDBS and TX-100 for acid hydrolysis of Bz with $[H^+]$ = 0.01 M. CTAB, TX-100 and SDBS retards the hydrolysis reaction initially with addition of the surfactant. Thus, they play an inhibitory catalytic role in the acid hydrolysis of Bz.

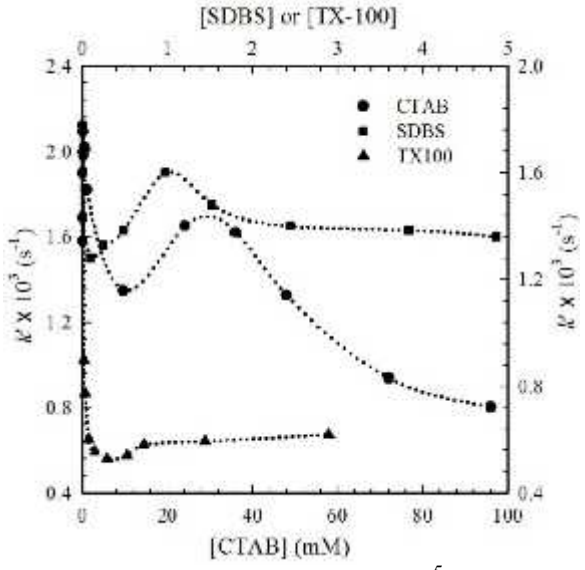

Figure 6.3.5. The *k*' for acid hydrolysis of 2.21×10^{-5} M Bz with $[H^+]$ = 0.01 M as a function of concentration of different surfactants, CTAB, SDBS and TX-100. Form clarity the values of *k*' are shown in the right side for TX-100.

It is apparent from the *k'* vs. [SDBS] plot, that after initial inhibition the apparent rate constant increases with increasing [SDBS]. For SDBS the rate constant passes through a maximum (Figure 5.3.8, Chapter 5) after which the rate constant decreases. It should be noted that the rate of the reaction is catalyzed at some concentrations close to the CMC of SDBS. For CTAB (Figure 5.3.4, Chapter 5), on the other hand, as the [CTAB] increases, the rate constant slightly increases at concentrations below the CMC due to catalytic effect of CTAB monomers present in the solution which form a catalytic premicelle by aggregation with Bz. This favors the reaction and enhances the reaction rate. At concentrations higher than the CMC, the rate constant increases and passes through a maximum and then decreases. The increase in *k*' at some concentration of CTAB might be due to different extent of binding of Bz with CTAB. In addition, the rate constant sharply decreases and then becomes almost constant with increasing [TX-100] (Figure 5.3.6, Chapter 5).

Above the CMC of CTAB, SDBS and TX-100, self-association results in the formation of micelles. This leads to the solubilization of Bz in the hydrophobic core of micelles and the number of Bz in the bulk solution interacting with the surfactants decreases. The binding of the reagent within micelles and hence enhancement of their concentration in the micellar phase occurs. The fact that the rate constant above the CMC for CTAB and TX-100 is smaller than that in the presence of SDBS at similar concentrations indicates that solubilization of Bz inside the core of micelle is relatively less prominent for CTAB and TX-100 compared to that for SDBS.

6.3.2.2. Hydrolysis in Presence of SDBS and SDS

Figure 6.3.6 shows the comparison of the *k*' vs. concentration of two anionic surfactants, SDBS and SDS for acid hydrolysis of Bz with $[H^+]$ = 0.1 M. Both the surfactants lowers the reaction rate. So, SDBS and SDS, both play an inhibitory role in the acid hydrolysis of Bz. It is apparent from the *k*' vs. [SDBS] profile that after initial inhibition the rate constant increases with increasing [SDBS] and passes through a maximum (Figure 5.3.8, Chapter 5), after which the rate constant further decreases.

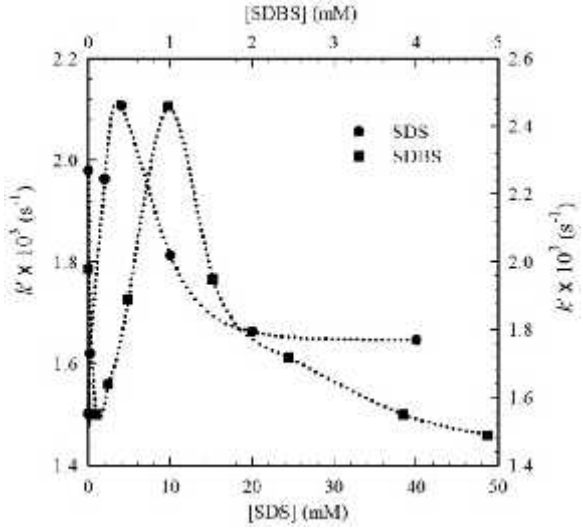

Figure 6.3.6. The *k'* for hydrolysis of Bz with [SDS] and [SDBS] at $[H^+]$ = 0.1 M. The values of *k*' in left and right side are for SDS and SDBS, respectively.

For SDS system (Figure 5.3.9, Chapter 5), on the other hand, the rate constant initially decreases and then increases gradually with increasing [SDS] at concentrations below the CMC and after passing through a maximum, the *k*' decreases at concentrations above the CMC. Additionally, at concentrations far above the CMC, the rate constant does not show appreciable change. Above the CMC of SDS and SDBS, self association results in the formation of micelles. This leads to solubilization of Bz in the hydrophobic core of micelles and the number of Bz in the bulk solution interacting with the surfactants decreases. The binding of Bz within micelles increases and hence enhancement of their concentration in the micellar phase occurs. The fact that the rate constant far above the

CMC for SDS system in aqueous solution remains almost constant, indicates that solubilization of Bz inside the core of micelle is relatively less prominent for SDS compared to that for SDBS. This is, as discussed earlier, due to the presence of a phenyl group in the hydrobphobic part of the structure of SDBS, which renders it more hydrophobic and a more hydrophobic core of micelle for SDBS compared to SDS is likely above the CMC.

As the CMCs of SDS (8.75 mM) and SDBS (2.07 mM) [8] are different, to compare the k' from the Figures 5.3.8, and 5.3.9, Chapter 5, the concentration of micelle [M] for both SDBS and SDS, are calculated using equation 6.1,

$$[\mathrm{M}] = \frac{[\mathrm{S}]_0 - \mathrm{CMC}}{N} \text{ - - - - - - - - (6.1)}$$

where, [M] = The concentration of micelle, $[\mathrm{S}]_0$ = The total concentration of surfactant that is above the CMC and N = The mean aggregation number (62 [57] and 60 [58] for SDS and SDBS at 25 ^{o}C, respectively). Table 6.1 shows the calculated [M] and the rate of the reaction k' for both SDBS and SDS.

Table 6.1. The calculated [M] and the rate of the reaction k' for both SDBS and SDS.

$[S]_0$ (mM)		[M] (mM)		$k' \times 10^3 (s^{-1})$	
SDS	SDBS	SDS	SDBS	SDS	SDBS
10.0	2.44	0.054	0.006	1.81	1.72
20.0	4.87	0.220	0.040	1.66	1.49

It can be seen from Table 6.1 that for SDBS at [M] = 0.006 mM, the value of the k' is 1.72×10^{-3} s^{-1} while the same value of k' is found at [M] = 0.125 mM for SDS. Since the CMC of SDBS is lower than the SDS due to the presence a phenyl ring in its structure, the rate constants are similar at lower concentrations of micelles of SDBS than SDS.

6.3.2.3. Hydrolysis in Presence of Micelles, Reverse Micelles and Microemulsions of CTAB

Figure 6.3.7 compares the values of k' for different media based on CTAB at [CTAB] = ca. 0.5 M with that in aqueous solution under identical experimental conditions. From the Figure 6.3.7, it can be seen that the k' in micellar solution has lower value for very high concentration of CTAB (far above the CMC) than the corresponding value in aqueous solution. The charged surface of CTAB in aqueous solution may cause the repulsion of similar-charged reactant, H^+ or even the solubilization of the H^+ into the micelle. Such repulsion or solubilization of the H^+ will result in a decrease in its activity in the solution phase.

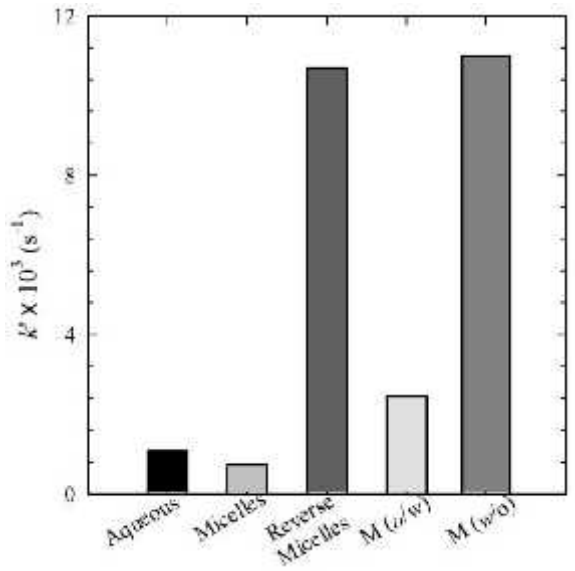

Figure 6.3.7. The k' for different media based on CTAB at [CTAB] = ca. 0.5 M concentration; [Bz] = 2.21×10^{-5} M and [H^+] = 0.001 M. Micelle (20 %wt. of CTAB in water); Reverse micelle (ϕ_W = 0.06); Microemulsion, M (*o*/*w*) (ϕ_W = 0.68) and microemulsion, M (*w*/*o*) (ϕ_W = 0.03).

The reverse micelle (ϕ_W = 0.06) has been found to bring about an increase in the reaction rate. In reverse micelles, a decrease in the water content is related to a structured water phase with lower dielectric constant. The rate constant is significantly increased due to the incorporation of 1-butanol to cationic CTAB micelles, which displaces the substrate from the micellar into the aqueous phase.

In *o*/*w* microemulsions (ϕ_W = 0.68), the rate constant is higher as compared to aqueous solution and the corresponding micelles and it should correspond to the region of direct CTAB micelle in water where the 1-butanol incorporation into the CTAB micelles inhibits the reaction. On the other hand, in *w*/*o* microemulsions, (ϕ_W = 0.03), the CTAB reverse micelles in 1-butanol are dominating because of high 1-butanol content and the rate constant of the reaction is high.

6.4. Conclusions

The alkaline hydrolysis of CV is catalyzed by CTAB and TX-100 and inhibited by SDBS in aqueous solution. The k' of alkaline hydrolysis of CV in 1-butanol is much higher than in aqueous solution under identical conditions which indicates that 1-butanol having lower dielectric constant favors the reaction. In CTAB/water (20 %wt. of CTAB in aqueous solution) and SDS/water (15 %wt. of SDS in aqueous solution) micelles, the k' has a lower value than that in aqueous solution due to the electrostatic repulsion between the micellar head groups of CTAB and CV^+ as well as the strong interaction between SDS and CV^+. The higher value of k' in the CTAB/1-butanol reverse micelles (20 %wt. of CTAB in 1-butanol) than in CTAB/water micelles corresponds to the increase in the

solubilization of the reagent, OH^- in the core of the reverse micelle. Thereby the reaction occurs with ease and results an increase in the reaction rate is observed. In oil-in-water microemulsion, the *k*' is similar to that in aqueous solution, but higher than the corresponding micelles due to the incorporation of 1-butanol in CTAB/water or SDS/water. On the other hand, in water-in-oil microemulsion, the rate constant of the reaction is high for both CTAB and SDS because of the higher content of 1-butanol having lower dielectric constant. Moreover, CTAB, SDBS and TX-100 inhibit acid hydrolysis of Bz. The *k*' in CTAB/water micelles (20 %wt. of CTAB in aqueous solution) has lower value than the corresponding value in aqueous solution due to the repulsion between the charged surface of CTAB and similar-charged reactant, H^+ (or even the solubilization of the H^+ into the micelle core) which decrease its activity in the solution phase. In oil-in-water microemulsions, the *k*' is similar to that in aqueous solution but higher than the corresponding micelles and in water-in-oil microemulsion. The rate constant of this reaction is very high as is observed for the alkaline hydrolysis of CV.

References

[1] E. J. Fendler, J. H. Fendier, *Micellar catalysis in organic reactions: Kinetic and mechanistic implications*, Advances in Physical Organic Chemistry, 1970, 8, 271-406.

[2] K. Das, B. Jain, H. S. Patel, *Nile blue in Triton-X 100/benzene-hexane reverse micelles: A fluorescence spectroscopic study*, Spectrochimica Acta Part A: Molecular and Biomolecular Spectroscopy, 2004, 60, 2059-2064.

[3] T. Hadara, N. Nishikido, Y. Moroi, R. Matuura, *Effect of surfactant micelles on the rate of reaction of tetranitromethane with hydroxide ion*, Bulletin of the Chemical Society of Japan, 1981, 54, 2592-2597.

[4] H. C. Hung, T. M. Hung, G. G. Chang, *Reverse micelles as a model system with which to study leaving group effects on alkaline phosphatase-catalysed hydrolysis*, Journal of the Chemical Society, Perkin Transactions 2, 1997, 2757-2760.

[5] F. Merino, S. Rubio, D. Perez-Bendito, *Determination of dialkyldimethylammonium surfactants in sewage based on the formation of premicellar aggregates*, Analyst, 2001, 126, 2230-2234.

[6] J. H. Fendler, E. J. Fendler, *Catalysis in micellar and macromolecular system*, Academic Press, New York, 1975.

[7] L. Mukherjee, N. Mitra, P. K. Bhattacharya, S. P. Moulick, *Kinetics in microemulsion medium. 4. Alkaline fading of crystal violet in aqueous (H_2O/aerosol OT/isooctane and H_2O/aerosolOT/decane) and nonaqueous (ethylene glycol/ aerosol OT/isooctane) microemulsions*, Langmuir, 1995, 11, 2866-2871.

[8] A. R. Kabir, M. A. B. H. Susan, *Kinetics of the alkaline hydrolysis of crystal violet in aqueous solution influenced by anionic surfactants,* Journal of Saudi Chemical Society, 2008, 12, 543-554.

[9] L. Arzuman, S. N. Karobi, M. J. Islam, G. Ara, M. M. Rahman, M. Y. A. Mollah, M. A. B. H. Susan, *Effect of urea on the kinetics of the alkaline hydrolysis of crystal violet catalyzed by aqueous micellar solutions of cetyltrimethylammonium bromide*, Synthesis and Reactivity in Inorganic, Metal-Organic and Nano-Metal Chemistry, 2015, 45, 764-769.

[10] F. Begum, M. Y. A. Mollah, M. M. Rahman, M. A. B. H. Susan, *Kinetics of the alkaline hydrolysis of crystal violet in micelles, reverse micelles and microemulsions of cetyltrimethylammonium bromide*, Journal of Bangladesh Chemical Society, 2011, 24, 173-184.

[11] P. K. Sen, N. Gani, B. Pal, *Effects of microheterogeneous environments of SDS,TX-100 and Tween 20 on the electron transfer reaction between l-Leucine and* $AuCl_4^-/AuCl_3(OH)^-$, Industrial and Engineering Chemistry Research, 2013, 52, 2803-2813.

[12] T. Kunitake, Y. Okahata, R. Ando, S. Shinkai, S. Hirakawa, *Decarboxylation of 6-nitrobenzisoxazole-3-carboxylate catalyzed by ammonium bilayer membranes. a comparison of the catalytic behavior of micelles, bilayer membranes, and other aqueous aggregates*, Journal of the American Chemical Society, 1980, 102, 7877-7881.

[13] C. A. Bunton, E. J. Fendler, J. H. Fendler, *The hydrolysis of dinitrophenyl phosphates*, Journal of the American Chemical Society ,1967, 89, 1221-1230.

[14] C. A. Bunton, E. J. Fendler, K. U. Sepulveda, J. Yang, *Micellar-catalyzed hydrolysis of nitrophenyl phosphates*, Journal of the American Chemical Society, 1968, 90, 5512-5518.

[15] J. Albrizzio, J. Archilla, T. Rodulfo, E. H Cordes, *Secondary valence force catalysis. XIII. Kinetics of the alkaline fading of crystal violet in the presence of cationic surfactants,* Journal of Organic Chemistry, 1972, 37, 871-874.

[16] C. A. Bunton, N. Carrasco, S. K. Huang, C. H. Paik, L. S. Romsted, *Reagent distribution and micellar catalysis of carbocation reactions*, Journal of the American Chemical Society, 1978, 100, 5420-5425

[17] D. J. Jobe, V. C Reinsborough, *Surfactant structure and micellar rate enhancements: Comparison within a related group of one-tailed, two-tailed and two-headed anionic surfactants*, Australian Journal of Chemistry, 1984, 37, 1593-1599.

[18] F. M. Menger, C. E. Portnoy, *Chemistry of reactions proceeding inside molecular aggregates*, Journal of the American Chemical Society, 1967, 89, 4698-4703.

[19] E. Pandey, S. K. Upadhyay, *Effect of micellar aggregates on the kinetics of oxidation of α-aminoacids by chloramine-T in perchloric acid medium*, Colloids and Surfaces A: Physicochemical and Engineering Aspects,2005, 269, 7-15.

[20] F. Sanchez, L. M. Moya, A. Rodrigues, R. Jimenez, H. C. Gomez, M. C. Carmona, C. P. Lopez, *Micellar, microemulsion, and salt kinetic effects upon the reaction* $Fe(CN)_2(bpy)_2 + S_2O_8^{2-}$, Langmuir, 1997, 13, 3084-3089.

[21] G. P. Panigrahi, B. P. Sahu, *Effect of cetylpyridinium chloride on the electron transfer reactions of acetophenones with Ce(IV)*, International Journal of Chemical Kinetics, 1993, 25, 595-607.

[22] M. Akram, N. H. Zaidi, Kabir-ud-Din, *Kinetics and mechanism of interaction of dipeptide (glycyl–glycine) with ninhydrin in aqueous micellar media*, International Journal of Chemical Kinetics, 2006, 38, 643-650.

[23] M. Akram, A. A. M. Saeed, Kabir-ud-Din, *Cationic micellar effect on the reaction between dipeptide glycyl-alanine (gly-ala) and ninhydrin with and without salt additives*, European Chemical Bulletin, 2014, 3, 119-126.

[24] A. H. Gemeay, I. A. Mansour, G. R. El-Sharkawy, B. A. Zaki, *Catalytic effect of supported metal ion complexes on the induced oxidative degradation of pyrocatechol violet by hydrogen peroxide*, Journal of Colloid Interface Science, 2003, 263, 228-236.

[25] V. W. Bhagwat, J. Tiwari, A. Choubey, B. Pare, *Kinetics and mechanism of cetyltrimethylammonium bromide catalyzed oxidation of diethylene glycol by chloramine-T in acidic medium*, Journal of Serbian Chemical Society, 2003, 68, 535-542.

[26] O. Olanrewaju, J. Ige, S. O. Omopariola, *Alkaline hydrolysis of brilliant green in mixed cationic surfactant systems*, Central European Journal of Chemistry, 2011, 9, 106-111.

[27] O. Owoyomi, J. Ige, M. S. Akanni, O. Soriyan, M. K. Morakinyo, *Interaction between sodium dodecyl sulfate and Triton X-100: Molecular properties and kinetic investigations*, Journal of Applied Science, 2005, 5, 729-734.

[28] C. A. Bunton, Y. S. Hong, L. S. Romsted, C. Quan, *Micellar catalysis of dephosphorylation by benzimidazolide and naphth-2,3-imidazolide ions*, Journal of the American Chemical Society, 1981, 103, 5784-5788.

[29] R. A. Moss, H. Zhang, S. Chatterjee, K. Krogh-Jerpersen, *Iodosonaphthoate catalysts for the cleavage of a reactive phosphate*, Tetrahedron Letters, 1993, 34, 1729-1732.

[30] J. Ige, O. Soriyan, *Micellar inhibition of the aquation of tris-(3,4,7,8-tetramethyl-1,10-phenanthroline)iron(II) by sodium dodecyl sulphate in aqueous acid medium*, Journal of Chemical Society, Faraday Transactions I, 1986, 82, 2011-2023.

[31] N. Singh, K. K. Ghosh, J. Marek, K. Kuca, *Hydrolysis of carboxylate and phosphate esters using monopyridinium oximes in cationic micellar media*, 2011, 43, 569-578.

[32] Y. S. Simanenko, A. F. Popov, T. M. Prokopeva, E. A. Karpichev, I. A. Belousova, V. A. Savelova, *Micellar effects of cationic detergents in the decomposition of ecotoxic substrates by hydroxide ion*, Theoretical and Experimental Chemistry, 2002, 38, 242-249.

[33] R.Y. Talman, S. Gokturkand, M. Tuncay, *Kinetic cosolvent effects on the alkaline fading of crystal violet in the presence of sodium dodecyl sulfate micelles*, Colloids and Surfaces A: Physicochemical and Engineering Aspects, 2005, 270, 72-77.

[34] E. F. J. Duynstee, E. Grunwald, *Organic reactions occurring in or on micelles. I. Reaction rate studies of the alkaline fading of triphenylmethane dyes and sulfonphthalein indicators in the presence of detergent salts*, Journal of the American Chemical Society, 1959, 81, 4540-4542.

[35] B. Samiey, F. Ashoori, *Kinetics of crystal violet fading in the presence of TX-100, DTAB and SDS*, Acta Chimica Slovenica, 2011, 58, 223-232.

[36] B. Samiey, A. R. Toosi, *Kinetics study of malachite green fading in the presence of TX-100, DTAB and SDS*, Bulletin of the Korean Chemical Society, 2009, 30, 2051-2056.

[37] B. Samiey, M. R. Dargahi, *Kinetics of brilliant green fading in the presence of TX-100, DTAB and SDS*, Reaction Kinetics, Mechanisms and Catalysis, 2010, 101, 25-39.

[38] D. Piszkiewicz, *Positive cooperativity in micelle-catalyzed reactions*, Journal of the American Chemical Society, 1977, 99, 1550-1557.

[39] E. H. Cordes, R.B. Dunlap, *Kinetics of organic reactions in micellar system*, Accounts of Chemical Research, 1969, 2 329-337.

[40] L. Brinchi, P. D. Profio, R. Germani, V. Giacomini, G. Savelli, C.A. Bunton, *Surfactant effects on decarboxylation of alkoxynitrobenzisoxazole-3-carboxylateions: Acceleration by premicelles*, Langmuir, 2000, 16, 222-226.

[41] O. Olanrewaju, J. Ige, O. Soriyan, O. Grace, O. S. Esan, O. Olanrewaju, *Kinetics and mechanism of the alkaline fading of brilliant green in aqueous solutions of a double-tailed and some single-tailed cationic surfactants*, Acta Chimica Slovenica, 2007, 54, 370-374.

[42] S. K. Srivastava, S. S. Katiyar, *Quantitative treatment of the effect of counterions on CTAB-catalyzed reactions of stabilized carbonium ions with cyanide ion*, International Journal of Chemical Kinetics, 1982, 14, 1007-1015.

[43] M. E. Moro, J. N. Fertrell, M. M. Velazquez, L. J. Rodriguez, *Kinetics of the acid hydrolysis of diazepam, bromazepam, and flunitrazepam in aqueous and micellar systems*, Journal of Pharmaceutical Sciences, 1991, 80, 459-468.

[44] M. Ferrit, C. D. Valle, M. L. Pez, R. Luque, F. M. Nez, *The stability of 2-acetoxy-4-trifluoromethylbenzoic acid (Triflusal) in micellar pseudophase*, Journal of Pharmaceutical Sciences, 2004, 93, 461-469.

[45] C. Matos, H. Chaimovich, J. L. Lima, I. M. Cuccovia, S. Reis, *Effect of liposomes on the rate of alkaline hydrolysis of indomethacin and acemetacin*, Journal of Pharmaceutical Sciences, 2001, 90, 298-309.

[46] N. P. Gensmantel, M. I. Page, *The micelles catalyzed hydrolysis of penicillin derivatives (Part I) and the effect of increasing the hydrophobicity of penicillin on its micelle-catalyzed hydrolysis (Part II)*, Journal of the Chemical Society Perkin Transactions, 1982, 2,147-155.

[47] A. Cipiciani, C. Ebert, R. Germani, P. Linda, M. Lovrecich, F. Rubessa, G. Savelli, *Micellar effects on the basic hydrolysis of indomethacin and related compounds*, Journal of Pharmaceutical Sciences, 1985, 74, 1184-1187.

[48] H. Mandy, M. Leung, C. Hannah, W. K. Tak, *Encapsulation of curcumin in cationic micelles suppresses alkaline hydrolysis*, Langmuir, 2008, 24, 5672-5675.

[49] S. A. Abdullah, S. A. Mohd, A. A. Hamad, M. A. Adel, A. I. , *Effect of alkyl length head group and nature of the surfactant on the hydrolysis 0f 1,3-benzoxazine-2,4-dione and its derivatives*, Journal of Colloid and Interface Science, 2011, 361, 205-211.

[50 J. E. Dawson, B. R. Hajratwala, H. Taylor, *Kinetics of indomethacin degradation II: Presence of alkali plus surfactant*, Journal of Pharmaceutical Science, 1977, 66, 1259-1263.

[51] A. G. Oliveira, I. M. Cuccovia, H. Chaimovich, *Micellar modification of drug stability: analysis of the effect of hexadecyltrimethylammonium halides on the rate of degradation of cephaclor*, Journal of Pharmaceutical Science, 1990, 79, 37-42.

[52] A. S. Al-Ayed, M. S. Ali, H. A. Al-Lohedan, A. M. Al-Sulaim, Z. A. Issa, *Micellar effects on the alkaline hydrolysis of isatin and its derivatives*, Journal Colloid and Interface Science, 2011, 357, 393-399.

[53] M. Ferrit, C. Valle, F. Martinez, *The study of the influence of surfactant charge on alkaline hydrolysis reactions of acetylsalicyclic acid (ASA) and triflusal (TFL) using spectrophotometric methods*, European Journal of Pharmaceutical Sciences, 2007, 31, 211-220.

[54] L. Garciario, J. C. Mejuto, D. P. Rodriguez, G. J. Simal, *Influence of micelles on the basic degradation of carbofuran*, Journal of Agricultural and Food Chemistry, 2005, 53, 7172-7178.

[55] M. Valiente, E. Rodenas, *Influence of CTAB/1-Butanol micelles on crystal violet basic hydrolysis,* Journal of Colloid and Interface Science*,* 1989, 127, 522-531.

[56] G. N. Lewis, T. T. Magel, D. Lipkin, *Isomers of crystal violet ion: their absorption and remission of light*, Journal of American Chemical Society*,* 1942*,* 64, 1774-1782.

[57] M. Valientie, E. Rodenas, *Influence of CTAB/alkanol/cyclohexane w/o microemulsions on the basic hydrolysis of crystal violet*, Colloid and Polymer Science, 1993, 271, 494-498.

[58] P. Ferruccio, C. Matteo, Z. Francesco, *A molecular dynamics investigation of structure and dynamics of SDS and SDBS micelles*, Soft Matter, 2011, 7, 9148-9156.

Abstract

Electrochemical behavior of different metal ions: Co^{2+}, Cu^{2+}, Zn^{2+}, Ni^{2+} and Sn^{2+} has been studied in aqueous solution and reverse microemulsions of CTAB and SDS with different w_o on CuE by cyclic voltammetry. The electrochemical reduction of different metal ions to metals has been found to occur easily on CuE in aqueous solution. Electrodeposition of different metals was therefore performed from aqueous solution at a fixed potential below the reduction potential using constant potential electrolysis method on CuE. In reverse microemulsions with different w_o, electrodeposition of different metals on CuE has been performed at different reduction potentials. Morphology and microstructures of the electrodeposited metals were examined by scanning electron microscopy; while elemental characterization was carried out by energy dispersive x-ray spectroscopic method. From aqueous medium, electrodeposition of metals occurs very fast and a gross deposition of bulk metal results without any definite morphology. In CTAB/1-butanol/water and SDS/1-butanol/water reverse microemulsions with fixed w_o, deposition rate varies with change in applied potentials and thickness of deposited metals only changed with change in deposition potential. The variation of w_o of reverse microemulsions brings about changes in size distribution of reverse microemulsions as revealed by dynamic light scattering measurements and consequently influences morphology of electrodeposited metals. SEM images show that deposition of metals occurs with definite size and shape; even the shape changes with w_o of reverse microemulsions. Electrodeposits from reverse microemulsions of CTAB and SDS with different w_o were compared to judge the suitability of the reverse microemulsions for electrodeposition of metal with tunable morphology.

7.1 Introduction

Electrodeposition is a fascinating phenomenon [1-2] where one can put a shiny coating of one metal on another simply by donating electrons to ions in a solution. There have been remarkable attention on this process, and studies at an atomic level continue to yield surprises. It is exceptionally versatile, and valuable applications keep being invented: to protect and enhance the functionality of parts used in many diverse industries including home appliances, jewelry, automotive, aircraft/aerospace, and electronics−in both decorative and engineering applications [3].

Although decorative applications have diminished somewhat primarily due to added expenses and problems associated with plant effluent control and waste treatment, its applications in engineering, electroforming, and electronics have increased. The emphasis is on the latter applications, and the structures and properties of deposits [1].

Co, Cu, Zn, Ni and Sn have great importance due to their several properties and manifold applications:

- Co is one of the important constituents of magnetic, corrosion and wear resistant alloys. It has been used for the production of sensors, [4, 5] heterogeneous catalysts [6-9] and intercalation compounds for energy storage [10-12].
- Cu is widely used metal with extensive industrial applications, especially in the semiconductor industry due to its low electrical resistance, good mechanical properties and high corrosion resistance [13]. It has been also suitable to decorative uses such as jewellery, statues and parts of buildings, for making pipes, electrical cables, saucepans, radiators, in special tools and military applications and its alloys were well suited to being used for tools and weapons.
- Zn and its alloys are good materials for corrosion-resistant coatings and they are widely used in the automobile industry [13].
- Ni is ferromagnetic and is also a fair conductor of heat and electricity like Zn. It has the potential for use including in corrosion-resistant alloys, such as stainless steel, batteries - for example, nickel-cadmium rechargeable batteries and magnets, nuclear power systems, aircraft gas turbines, medical applications, and the chemical and petrochemical industries.
- Tin is a moderately corrosion resistant material that is widely used in tinplate for food beverage [14]. Alloys of tin are commercially important in soft solder, pewter, bronze, dyeing textiles and phosphor bronze.

Research to date includes numerous attempts that have been made to study the electrodeposition of Co [15-19], Cu [20-26], Zn [27-31], Ni [32-34], and Sn [26, 35-40] from aqueous solution. The metal electrodeposition from aqueous solution sometime involves the hydrogen evolution simultaneously which makes difficult to analyze the current transients and the morphology of the electrodeposited metal. Thus, although these metals were deposited from aqueous solution, for specific requirements (deposited with definite shape and morphology), these have been deposited from other media such as: non-aqueous solutions [41-43], ionic liquids [13, 44-60], surfactant based organized media such as micelles [61-71], reverse micelles [72-74] and microemulsions [75-86].

Reverse microemulsion is thermodynamically stable, optically transparent, microheterogeneous systems that generally defined as nanometer-sized (10-100 nm) water droplets dispersed in apolar solvent with the aid of pure surfactant or mixture of surfactant and co-surfactant [70, 79]. They are widely used to electrodeposit different metals instead of aqueous solution to eliminate the hydrogen evolution reaction and bulk deposition in aqueous solution during electrodeposition. As reverse microemulsions are the aggregated form of different surfactants with water droplets of definite size and shape, they give deposited metals with definite size and shape [72]. The sizes of the reverse microemulsions can be controlled by changing different parameters such as water

to surfactant ratio (w_o), cosurfactants, surfactants etc; consequently, the morphology and structures of the electrodeposited metals can be tuned by controlling different parameters of the reverse microemulsions [72-76].

There are several reports on the electrodeposition of Co, Cu, Zn, Ni, and Sn from reverse microemulsions. Aragon and coworkers [71] reported that in presence of micelles of TX-100 in acid medium, the electrodeposited Sn was smooth and homogeneous because aggregates of TX-100 block the surface and hinders the mass transport of Sn^{2+} through a membrane-like layer that forms on the Sn. Electrodeposition of Ni with tunable microstructure and morphology through systematic variation of the composition of CTAB/1-butanol/water reverse microemulsions was observed by Sultana et al [72]. Saha et al [73] reported that the electrodeposited Co from reverse microemulsion of CTAB has definite shape such as, star-, flower-, and nanorod-like structures depending on the w_o of reverse microemulsions due to the slow kinetics in growth of Co onto CuE and offers the potential to electrochemically tune Co deposit with desirable morphology. Zhou et al [79] reported that the electrodeposited Ni particles on nickel substrate from TX-100/n-hexanol/n-hexane/water has spherical morphology with diameter about 40 nm and the electrochemical reactivity of Ni nanoparticles modified electrode is different from that of the normal watts-Ni modified electrode. They [70] also observed that the size of electrodeposited Ni nanoparticles decreases with the increase of Ni^{2+} concentration and the electrochemical activity of Ni nanoparticles plating electrode is much higher than that of bulk Ni electrode. Cu nanorods have been successfully synthesized using CTAB/tetrabutylammonium bromide/acetone/cyclohexane/water microemulsion with controlled-current electrolysis [71]. Electrodeposition of ZnO from reverse microemulsions containing zinc nitrate and dissolved oxygen have various morphologies: from 2D ultrathin nanosheets to 3D hierarchical flower-like morphologies, which are quite different from those obtained in conventional electrolytes [72].

Inspite of numorous studies there have no reports on the electrodeposition of Co, Cu, Zn, Ni, and Sn from the reverse microemulsions of different type of surfactants. In this work, these metals have been electrodeposited from aqueous solution and reverse microemulsions of CTAB and SDS with different w_o. From aqueous solutions, electrodeposition of different metals was performed at a fixed potential below the reduction potential. The electrodeposition of different metals in reverse microemulsions were carried out with changing w_o at a fixed potential below the reduction potential and with changing the reduction potential at a fixed w_o to understand the change in morphology and structures of electrodeposited metals on CuE with change in reduction potential and w_o. The elctrochemical behavior of these metals has been compared in aqueous solution and reverse microemulsions of CTAB and SDS. The morphology of the electrodeposited metals in reverse mciroemulsions has also been compared with that in aqueous solution.

7.2. Experimental

7.2.1. Materials and Methods

CTAB (E. Merck) and SDS (E. Merck), 1-butanol (Merck), cyclohexane (Merck) were used as received without further purification. Solutions were prepared with double distilled de-ionized water (conductivity: 0.055 μScm^{-1} at 25.0 °C) from HPLC grade water purification systems (BOECO). Cobalt nitrate (Loba Chemie), nickel chloride (Merck), zinc sulfate (Merck), copper sulfate (Merck), stannous chloride (Merck), potassium chloride (Merck) and sodium sulfate (Merck) were of analytical grade and were used as received.

The electrochemical measurements were carried out with a computer-controlled electrochemical analyzer (Model: CHI600D, CH Instruments, Inc., USA) using a conventional single-compartment three-electrode cell. Prior to each measurement, the solution was purged with N_2 gas to maintain an inert atmosphere during the course of the measurement. A homemade copper disc electrode was used as the working electrode. The electrode was mechanically polished using alumina paste (0.05 μm) from Buehler to obtain a uniform surface and then rinsed thoroughly with distilled water and dried. The dried electrode was then introduced into the cell filled with the test solution. Spiral Pt wire and Ag/AgCl electrode were used as the counter and reference electrodes, respectively.

Electrodeposition of these metals was carried out using constant potential bulk electrolysis method with the same analyzer on home-made copper disc electrodes for all the media. The time of electrolysis was 10 min for aqueous and reverse microemulsions using a definite concentration of metals. The copper discs after electrodeposition were washed by water several time to wash out the surfactants and dried. Then the electrodeposited metals with the copper disc were collected by wounding.

Morphology analysis of electrodeposited metals was carried out in JEOL analytical scanning electron microscope, model JSM-6490LA. Round sample stages of aluminum were used throughout the investigation. Elemental analysis or chemical characterization of electrodeposited metals were carried out in energy dispersive x-ray spectroscopy attached with JEOL analytical scanning electron microscope, model JSM-6490LA. Round sample stages of aluminum were used throughout the investigation.

Size distributions of different reverse microemulsions were measured using a Zetasizer Nano ZS90 (ZEN3690, Malvern Instruments Ltd, UK) by dynamic light scattering method (DLS). The particle size detection limit was about 0.3 nm - 5μm (diameter) and accuracy of the Z-average diameter determined has been ± 2%. A He-Ne laser of 632.7 nm wavelength was used and the measurements were made at a fixed scattering angle of 90°. The refractive index of each solution was recorded with an Abbemat 300

refractometer having high resolution optical sensor. Viscosity data, as obtained from viscosity measurements, were also used for interpretation of DLS data. Samples were filtered using VALUPREP 0.45 μm poly(tetra fluoro ethylene), PTFE filter. The temperature of the apparatus was controlled automatically within ± 0.01 K by a built-in Peltier device.

7.3. Results and Discussion

7.3.1. Electrochemical Behavior of Co^{2+}, Cu^{2+}, Zn^{2+}, Ni^{2+} and Sn^{2+} in Aqueous Solution

Electrochemical behaviors of $Co(NO_3)_2$, $CuSO_4$, $ZnSO_4$, $NiCl_2$ and $SnCl_2$ were studied in aqueous solution by cyclic voltammetry using CuE as working electrode, an Ag/AgCl electrode as reference electrode and a spiral platinum wire as counter electrode.

7.3.1.1. Electrochemical Behavior of Cu^{2+} in Aqueous Solution

Figure 7.3.1. represents cyclic voltammograms of 20 mM $CuSO_4$ in aqueous solution of 0.1 M Na_2SO_4 on a CuE at (a) scan rate 0.06 Vs^{-1} and (b) various scan rates within the potential window of 0.2 to -0.6 V.

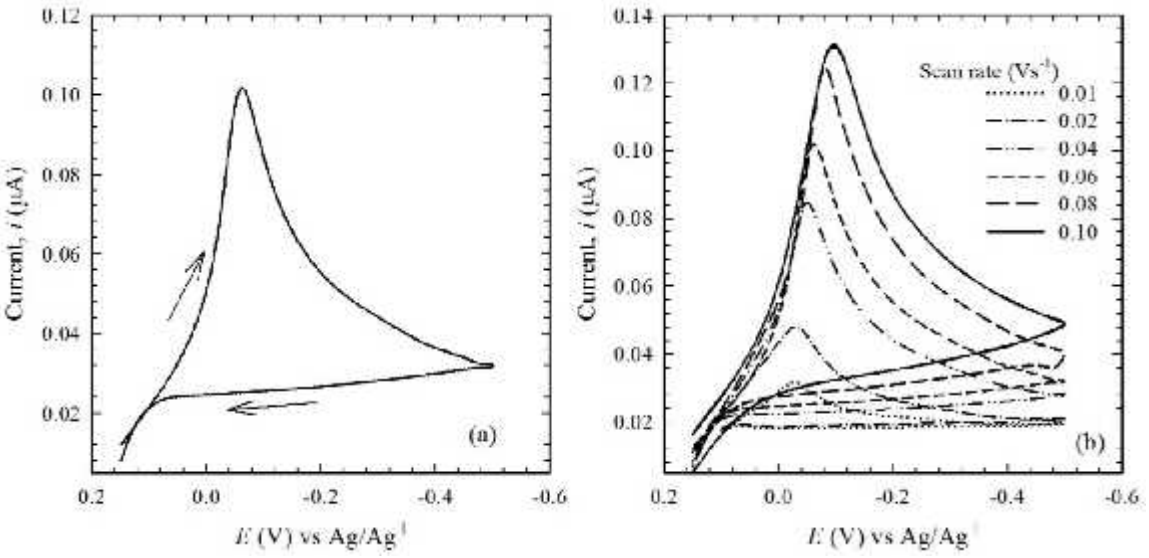

Figure 7.3.1. Cyclic voltammograms of 20 mM Cu^{2+} in N_2-saturated aqueous solution of 0.1 M Na_2SO_4 aqueous solution on CuE at (a) 0.06 Vs^{-1} scan rate and (b) different scan rates.

Cyclic voltammogram recorded for 20 mM Cu^{2+} with scan rate of 0.06 Vs^{-1} showed that the cathodic peak was observed at about -0.064 V which corresponds to the reduction of Cu^{2+} to metallic Cu [22]. With increasing scan rate (Figure 7.3.1(b)), the cathodic peak current, i_{pc} increases and the cathodic peak potential, E_{pc} shifts towards negative values suggest that the electrode process is diffusion controlled and irreversible process.

The cyclic voltammetric studies also ensure that for all cases, the reduction of Cu^{2+} show irreversible characteristic with no reversible peak which can also be concluded from the plot of cathodic peak potential, E_{pc} vs. log v (v is the scan rate). Figure 7.3.2. represents the cathodic peak potential, E_{pc} obtained from the cyclic voltammograms shown in Figure 7.3.1. as a function of log (scan rate) for the reduction of Cu^{2+} on a CuE.

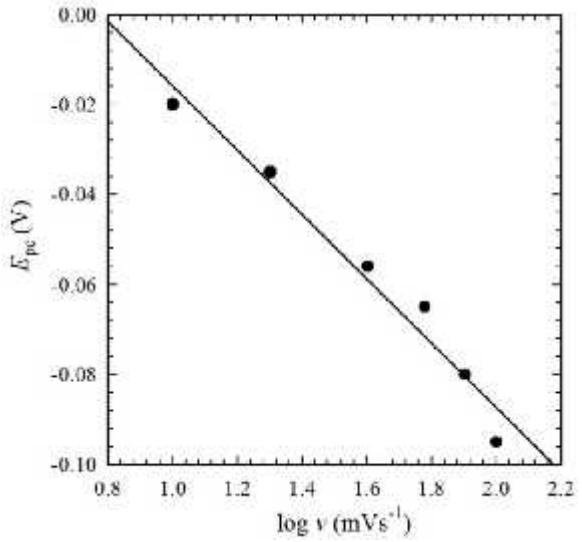

Figure 7.3.2. Cathodic Peak potential, E_{pc} vs log (scan rate, v) for the reduction of Cu^{2+} in 0.1 M Na_2SO_4 solution on CuE.

It can be seen from the Figure 7.3.2. that the E_{pc} decreases linearly with log v (v is the scan rate, mVs^{-1}) indicating that the reduction of Cu^{2+} to Cu on a CuE is an irreversible process [87].

For a diffusion controlled system; *Randles-Sevcick* equation best describes the electrochemical behavior of an irreversible process. According to *Randles-Sevcick* equation for irreversible process cathodic peak current (i_{pc}) is proportional to the square root of scan rates ($v^{1/2}$).

$$i_{pc} = (2.99\times10^5)D^{1/2}\alpha^{1/2}CAn^{3/2}v^{1/2} \qquad (7.1)$$

Cathodic peak current, i_{pc} vs square root of scan rate, $v^{1/2}$ has been plotted to see whether it is a diffusion controlled process or adsorption dominated one. Figure 7.3.3. represents a plot of cathodic peak current, i_{pc}, obtained from the cyclic voltammograms shown in Figure 7.3.1. vs square root of scan rate, $v^{1/2}$ for the reduction of Cu^{2+} in aqueous solution on CuE. Linear increase of cathodic peak current, i_{pc} with $v^{1/2}$ passing through the origin for the reduction of Cu^{2+} in aqueous solution on CuE suggest that the reduction of Cu^{2+} is a diffusion controlled process. Thus it can be stated from the above discussions that the reduction of Cu^{2+} to Cu in aqueous solution of on a CuE is an irreversible and diffusion-controlled process.

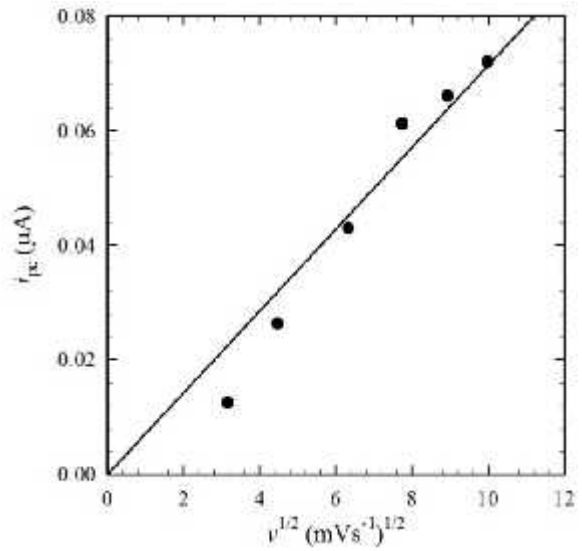

Figure 7.3.3. Cathodic peak current, i_{pc} vs $v^{1/2}$ (v is the scan rate) for the reduction of Cu^{2+} in aqueous solution on CuE.

7.3.1.2. Electrochemical Behavior of Zn^{2+} in Aqueous Solution

Figure 7.3.4. represents cyclic voltammograms of 25 mM $ZnSO_4$ in aqueous solution of 0.1 M KCl on CuE at (a) scan rate 0.01 Vs^{-1} and (b) various scan rates within the potential window of -0.4 to -0.6 V. The cyclic voltammogram 25 mM Zn^{2+} with scan rate of 0.01 Vs^{-1} showed that the cathodic peak was observed at about -0.57 V which corresponds to the reduction of Zn^{2+} to metallic Zn [27].

The cathodic peak current, i_{pc} increases markedly and the cathodic peak potential, E_{pc} shifts towards more negative values with increasing scan rate to indicate that the reduction of Zn^{2+} to Zn is a slow irreversible reaction and the electrode process is diffusion controlled. The cathodic peak potential shifted to more negative value with increasing scan rate may be due to the following reasons:

- For 'slow' reactions (so called quasi-reversible or irreversible electron transfer reactions) the voltage applied will not result in the generation of the concentrations at the electrode surface predicted by the Nernst equation.
- Kinetics of the reduction reaction is 'slow' and thus the equilibria are not established rapidly (in comparison to the voltage scan rate).
- The position of the current maximum shifts depending upon the reduction rate constant (and also the voltage scan rate) which occurs for the reason that the current takes more time to respond to the applied voltage than the reversible case.

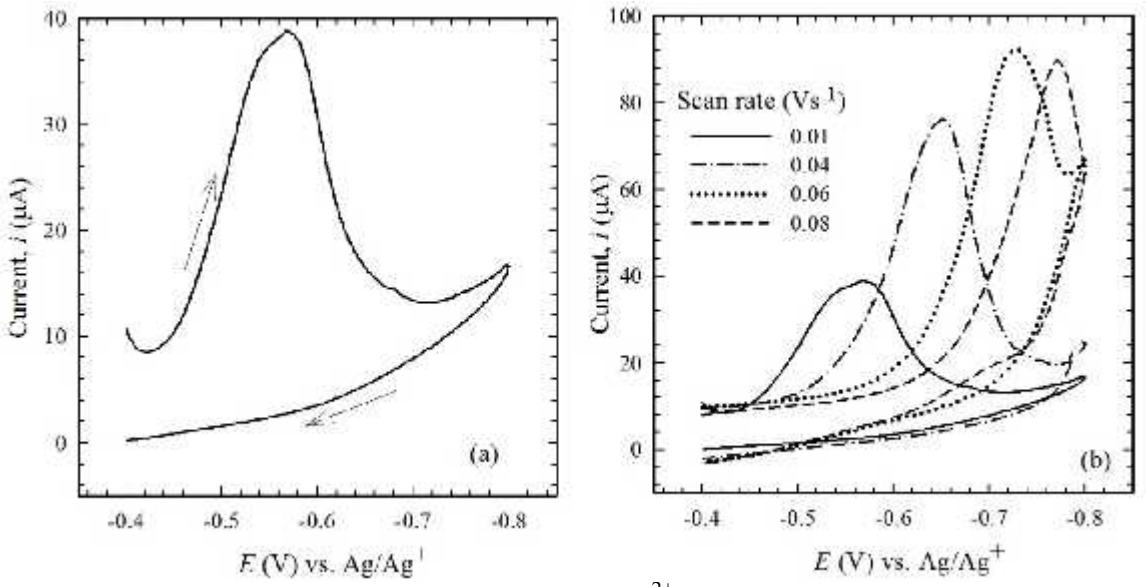

Figure 7.3.4. Cyclic voltammograms of 25 mM Zn^{2+} in N_2-saturated aqueous solution of 0.1 M KCl aqueous solution on CuE at (a) 0.01 Vs^{-1} scan rate and (b) different scan rates.

Linear increase of cathodic peak current, i_{pc} with $v^{1/2}$ passing through the origin for the reduction of Zn^{2+} in aqueous solution on CuE suggests that the reduction of Zn^{2+} is a diffusion controlled process. Thus it can be stated from the above discussions that the reduction of Zn^{2+} to Zn in aqueous solution of on a CuE is an irreversible and diffusion-controlled process.

7.3.1.3. Electrochemical Behavior of Co^{2+} in Aqueous Solution

Cyclic voltammogram of Co^{2+} using 0.4 M KCl shows that the first cathodic peak potential was observed at ca. −0.97 V, which corresponds to the reduction of Co^{2+} [47, 73, 88]. A second cathodic peak was observed at a more negative potential (ca. −1.47 V) due to the reduction of hydrogen ion. Significant contribution by current from hydrogen ion reduction is apparent during electroreduction of Co^{2+}, which agrees well with the literature [16].

7.3.1.4. Electrochemical Behavior of Ni^{2+} in Aqueous Solution

Cyclic voltammogram of 32 mM $NiCl_2$ in aqueous solution containing 0.40 M KCl shows that a well defined cathodic peak was observed at about -0.90 for Ni^{2+} to metallic Ni [72]. Figure 7.3.5. represents cyclic voltammograms of different concentration of Ni^{2+} on CuE and shows the concentration dependence of reduction current. As expected, an increase in the concentration of Ni^{2+}solution resulted in a linear increase in the cathodic peak current, i_{pc} due to Ni^{2+} reduction to Ni [89].

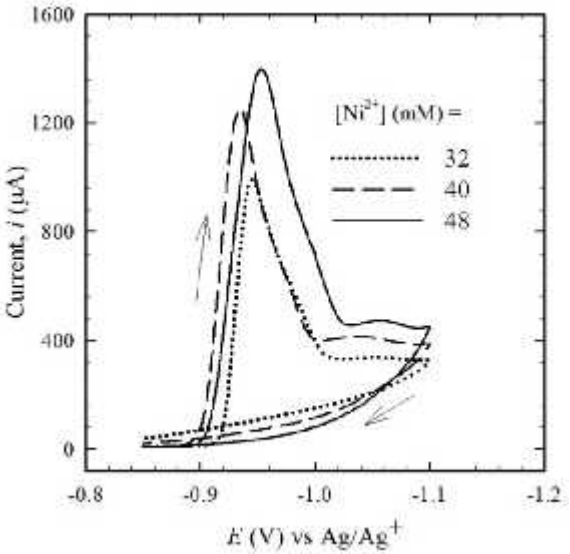

Figure 7.3.5. Cyclic voltammograms of different concentrations of Ni^{2+} in N_2-saturated aqueous solutions containing 0.4 M KCl on CuE at scan rate 0.04 Vs^{-1} [88].

7.3.1.5. Electrochemical Behavior of Sn^{2+} in Aqueous Solution

Figure 7.3.6. represents cyclic voltammograms of 8 mM $SnCl_2$ in aqueous solution with few drops of HCl on CuE at various scan rates within potential window of -0.5 to -0.6 V.

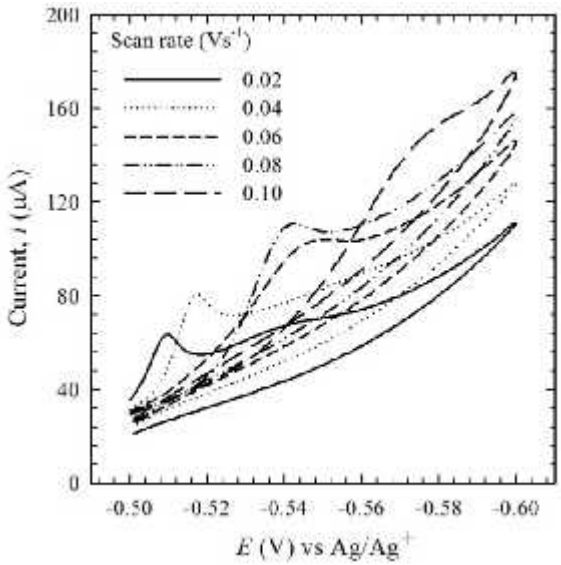

Figure 7.3.6. Cyclic voltammograms of 8 mM $SnCl_2$ in aqueous solution with few drops of HCl on CuE at various scan rates within the potential window of -0.5 to -0.6 V.

The aqueous solution of 8 mM Sn^{2+} was turbid due to the presence of $Sn(OH)_2$ and testing the pH shows the solution to be acidic. Upon addition of a few drops of 10 M HCI, the solution becomes clear. Addition of excess HCl results in the formation of H_2 during the electrolysis. As the $SnCl_2$ is dissolved in water, $SnCl_2$ is hydrolyzed,

$$Sn^{2+} + 2H_2O \Leftrightarrow Sn(OH)_2 + 2H^+ \text{ - - - - - - - - - - - - - - - - (7.2)}$$

Upon subsequent addition of HCI, the turbidity disappeared as the equilibrium shifted to the left in accordance with Le Chatelier's principle [90]. Cyclic voltammogram of 8 mM $SnCl_2$ in aqueous solution containing 2 M HCl shows that a well defined cathodic peak was observed at about -0.51 for reduction of Sn^{2+} to metallic Sn on CuE at scan rate 0.02 Vs^{-1}. The cathodic peak potential shifts to more negative value and the cathodic peak current increases with increasing the scan rate.

7.3.2. Electrochemical Behavior of Co^{2+}, Cu^{2+}, Zn^{2+}, Ni^{2+} and Sn^{2+} in Reverse Microemulsions of CTAB and SDS

7.3.2.1. Electrochemical Behavior of Co^{2+} in Reverse Microemulsions of CTAB

It was reported in literature [73] that the cyclic voltammograms of the reverse microemulsions of CTAB with w_o= 7.0 without Co^{2+} give a broad cathodic peak at about −0.67 V which may be attributed to the adsorption-desorption of CTAB on a CuE since the surface active substances have a tendency to accumulate at the interfaces [91, 92]. As CTAB is a cationic surfactant, its cathodic adsorption can also be expected [91]. In the presence of 20 mM Co^{2+}, a new cathodic peak was observed at a potential more negative than −0.70 V and the cathodic peak current increased as the concentration of Co^{2+} was increased to indicate that the new cathodic peak is due to the reduction of Co^{2+} to metallic Co. It may be worth mentioning that the reduction peak of Co^{2+} is widely separated from the adsorption peak of reverse microemulsions, i.e., the cathodic peak of Co^{2+} occurs at about −0.93 V, whereas observed peak for reverse microemulsions takes place at −0.67 V. Therefore, it is clear that the adsorption of CTAB does not interfere the reduction of cobalt in reverse micellar system [73].

7.3.2.2. Electrochemical Behavior of Co^{2+} in Reverse Microemulsions of SDS

Figure 7.3.7. represents cyclic voltammograms of N_2-saturated reverse microemulsions of SDS (w_o= 20.3) without and with 20 mM Co^{2+} on CuE at a scan rate 0.05 Vs^{-1} with potential window -0.4 to -1.2 V. The cyclic voltammograms of the reverse microemulsions of SDS (w_o= 20.3) without Co^{2+} give a broad cathodic peak at about −0.67 V in analogous to those in reverse microemulsions of CTAB, which may be attributed to the adsorption-desorption of SDS on a CuE [47, 73, 89]. In the presence of 20 mM Co^{2+}, a new cathodic peak was observed at a potential more negative than −0.70 V. The reduction peak of Co^{2+} is widely separated from the adsorption peak of reverse microemulsions, i.e. the cathodic peak of Co^{2+} occurs at about −0.93 V, whereas observed peak for reverse microemulsions takes place at −0.67 V. Therefore, it is clear that the adsorption of SDS does not interfere the reduction of Co^{2+} in reverse microemulsions.

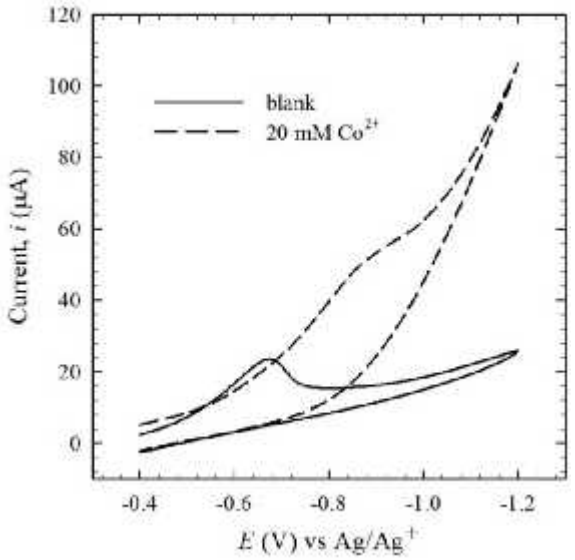

Figure 7.3.7. Cyclic voltammograms of N_2-saturated reverse microemulsions of SDS (w_o= 20.3) without and with 20 mM Co^{2+} on CuE at scan rate 0.05 Vs^{-1}.

The cyclic voltammograms also recorded for N_2-saturated reverse microemulsions of SDS with different w_o containing different concentration of Co^{2+} at a scan rate 0.05 Vs^{-1} on CuE to understand the change in the electrochemical behavior of Co^{2+} depending on the water content of reverse microemulsions of SDS. Figure 7.3.8. represents the cyclic voltammograms of N_2-saturated reverse microemulsions of SDS with different w_o containing different concentrations of Co^{2+} at scan rate 0.05 Vs^{-1} on CuE**.** The cathodic peak current, i_{pc} increases as the concentration of Co^{2+} increases (Figure 7.3.8) to indicate that the new cathodic peak is due to the reduction of Co^{2+} to metallic Co.

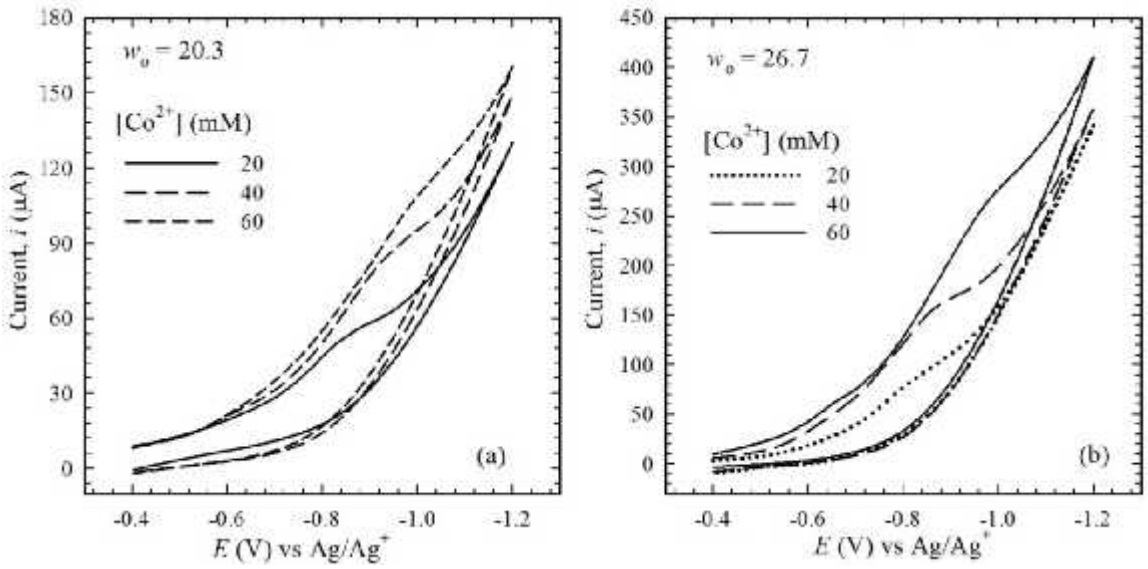

Figure 7.3.8. Cyclic voltammograms of N_2-saturated reverse microemulsions of SDS (a) w_o= 20.3 and (b) w_o= 26.7 with different concentrations of Co^{2+} at scan rate 0.05 Vs^{-1} on CuE.

Figure 7.3.9. represents cyclic voltammograms of N_2-saturated reverse microemulsions of SDS with different w_o containing 40 mM of Co^{2+} at scan rate 0.05 Vs^{-1} on CuE.

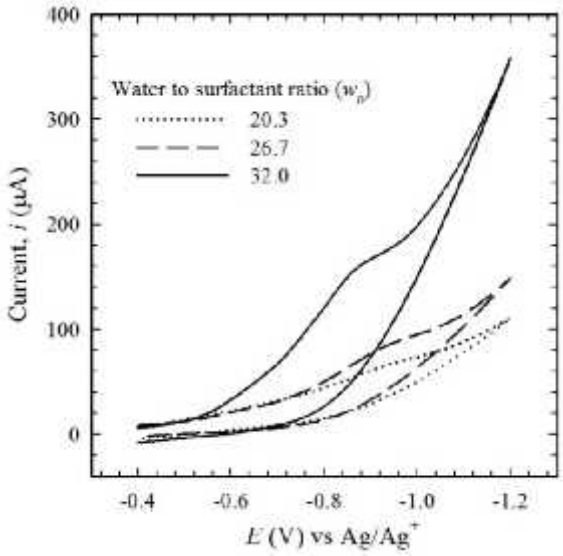

Figure 7.3.9. Cyclic voltammograms of N_2-saturated reverse microemulsions of SDS with different w_o containing 40 mM of Co^{2+} at scan rate 0.05 Vs^{-1} on CuE.

Both the cathodic peak potential, E_{pc} and cathodic peak current, i_{pc} obtained from the cyclic voltammograms of N_2-saturated reverse microemulsions of SDS with different w_o containing 40 mM of Co^{2+} at scan rate 0.05 Vs^{-1} on CuE (figure 7.3.8) changes with increasing w_o of reverse microemulsions of SDS. Table 7.1. represents the values of E_{pc} and i_{pc} for reduction of Co^{2+} with increasing w_o of reverse microemulsions of SDS.

Table 7.1. The values of E_{pc} and i_{pc} for reduction of Co^{2+} with increasing w_o of reverse microemulsions of SDS.

w_o	$-E_{pc}$ (V) vs Ag/Ag$^+$	i_{pc} (μA)
20.3	0.92	17.60
26.7	0.90	47.20
32.0	0.76	132.3

From Table 7.1 it can be seen that, with increase in w_o in the reverse microemulsions of SDS, the reduction peak potential shifts to more positive values and peak current increases. This may be due to the fact that with increasing the value of w_o in the reverse microemulsions, the hydrophilic core size of the reverse microemulsions increases. So, the Co^{2+} ions, trapped into larger hydrophilic core of reverse microemulsions, easily drag out from the core which causes the shifting of the reduction potential to more positive values. For lower value of w_o, release of Co^{2+} from hydrophilic core of reverse microemulsions of SDS is more difficult due to higher electrostatic interaction between

trapped Co^{2+} and anionic hydrophilic part of the SDS. Consequently, the reduction potential for Co^{2+} to Co is more negative than observed in reverse microemulsions containing higher value of w_o.

The peak current increases gradually with increase in w_o in reverse microemulsions. As hydrophilic core size increases with increasing w_o in reverse microemulsions, they can entrapt of more Co^{2+} in the core due to high water content and easily release from the hydrophilic core. As a result, the diffusion rate of Co^{2+} species at a certain potential in reverse microemulsions increases with increasing w_o and consequently increase the cathodic peak current for the reduction of Co^{2+}.

Figure 7.3.10. represents the cyclic voltammograms of 20 mM Co^{2+} in reverse microemulsions of SDS with different w_o on CuE at various scan rates.

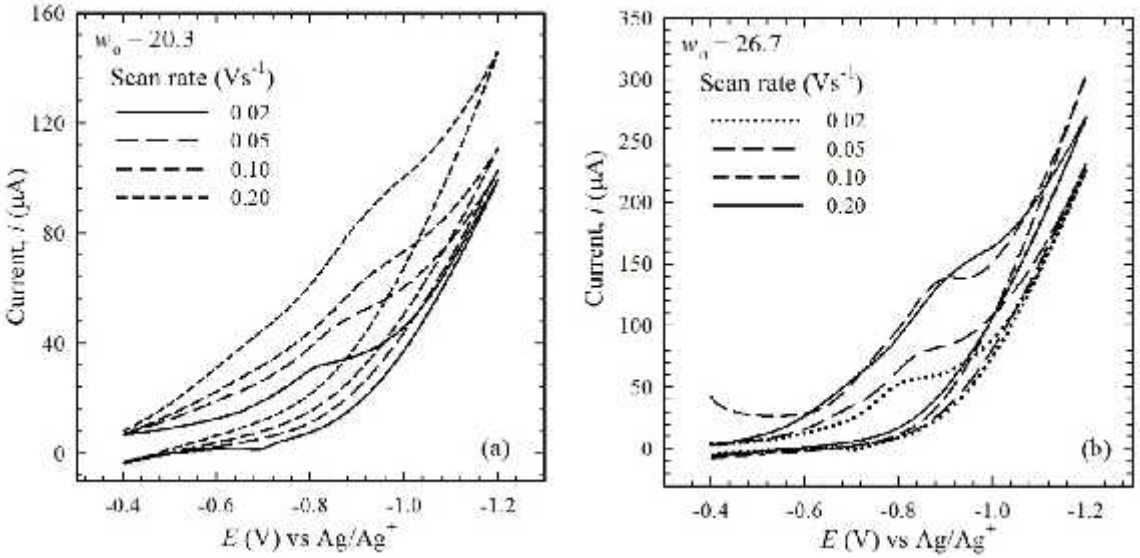

Figure 7.3.10. Cyclic voltammograms of 20 mM Co^{2+} in reverse microemulsions of SDS with (a) w_o= 20.3 and (b) w_o= 26.7 at different scan rates on CuE.

Figure 7.3.11. represents the cathodic peak potential, E_{pc} obtained as a function of log (scan rate) and cathodic peak current, i_{pc} vs square root of scan rate, $v^{1/2}$ profile from the cyclic voltammograms shown in figure 7.3.9 for the reduction of Co^{2+} on a CuE in reverse microemulsions of SDS, respectively. From Figure 7.3.11 (a) and (b), it can be seen that the cathodic peak, E_{pc} decreases linearly with log v (v is the scan rate, mVs^{-1}) and the cathodic peak current, i_{pc} increases linearly and passes through the origin with square root of scan rate ($v^{1/2}$) (*Randles-Sevcick* equation). This indicates that the reduction of Co^{2+} to Co on a CuE in reverse microemulsions of SDS is an irreversible and diffusion controlled process.

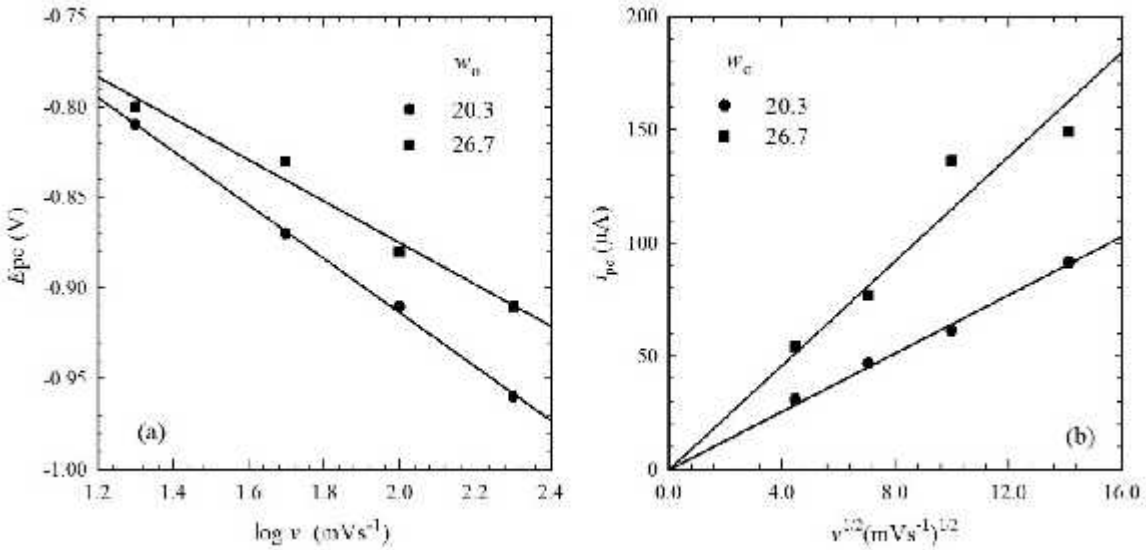

Figure 7.3.11. (a) The cathodic peak potential, E_{pc} vs log (scan rate) and (b) the cathodic peak current, i_{pc} vs square root of scan rate, $v^{1/2}$ profile for the reduction of Co^{2+} on a CuE in reverse microemulsions of SDS.

7.3.2.3. Electrochemical Behavior of Cu^{2+} in Reverse Microemulsions of CTAB

Figure 7.3.12. represents cyclic voltammograms of N_2-saturated reverse microemulsions of CTAB (w_o= 7.0) without and with 5.72 mM Cu^{2+} on CuE at scan rate 0.1 Vs^{-1} with potential window -0.4 to -1.2 V for blank and -0.4 to -1.0 for with Cu^{2+}.

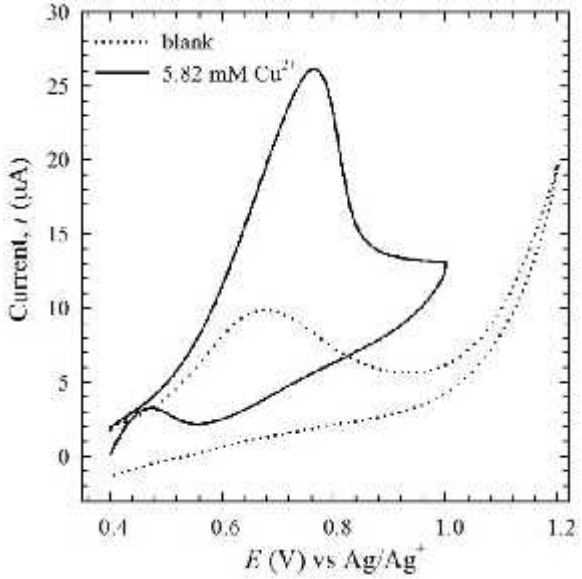

Figure 7.3.12. Cyclic voltammograms of N_2-saturated reverse microemulsions of CTAB (w_o= 7.0) without and with 5.82 mM Cu^{2+} on CuE at scan rate 0.05 Vs^{-1}.

From Figure 7.3.1.2 it has been shown that cyclic voltammograms of the reverse microemulsions of CTAB (w_o= 7.0) with 5.72 mM Cu^{2+} gives the cathodic peak for the reduction of Cu at potential about −0.77 V which is widely separated from the adsorption peak of reverse microemulsions of CTAB at about −0.67 V.

Figure 7.3.13 represents cyclic voltammograms of N_2-saturated reverse microemulsions of CTAB (w_o= 7.0) containing different concentrations of Cu^{2+} at scan rate 0.1 Vs^{-1} and 5.72 mM of Cu^{2+} at different scan rates on CuE**.**

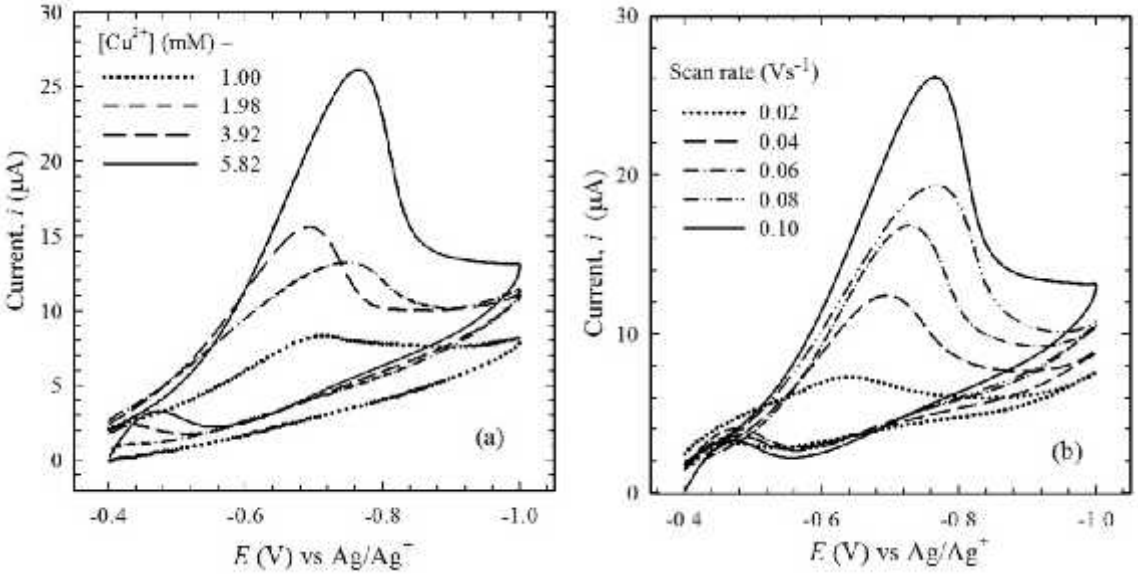

Figure 7.3.13. Cyclic voltammograms of N_2-saturated reverse microemulsions of CTAB (w_o= 7.0) (a) containing different concentrations of Cu^{2+} at scan rate 0.1 Vs^{-1} and (b) 5.82 mM of Cu^{2+} at different scan rates on CuE.

The cathodic peak current increases as the concentration of Cu^{2+} increases. (Figure 7.3.13 (a)) thus indicates that the new cathodic peak is due to the reduction of Cu^{2+} to metallic Cu. With increasing the scan rates (Figure 7.3.13. (b)), the cathodic peak potential, E_{pc} shifted to negative value and the cathodic peak current, i_{pc} increases. The E_{pc} decreases linearly with log v and the i_{pc} increases linearly passing through the origin with square root of scan rate ($v^{1/2}$) (*Randles-Sevcick* equation) (Figures not shown) indicating that the reduction of Cu^{2+} to Cu on a CuE in reverse microemulsions of CTAB is an irreversible and diffusion controlled process.

7.3.2.4. Electrochemical Behavior of Zn^{2+} in Reverse Microemulsions of CTAB

Figure 7.3.14. represents cyclic voltammograms of N_2-saturated reverse microemulsions of CTAB (w_o= 7.0) without and with 25 mM Zn^{2+} on CuE at scan rate 0.02 Vs^{-1} with potential window -0.4 to -1.2 V for blank and -0.4 to -1.0 for with Zn^{2+}. From the cyclic voltammograms of the reverse microemulsions of CTAB (w_o= 7.0) with 25 mM Zn^{2+}, the cathodic peak was observed at about −0.73 and it is separated from the adsorption peak of reverse microemulsio at about −0.67 V.

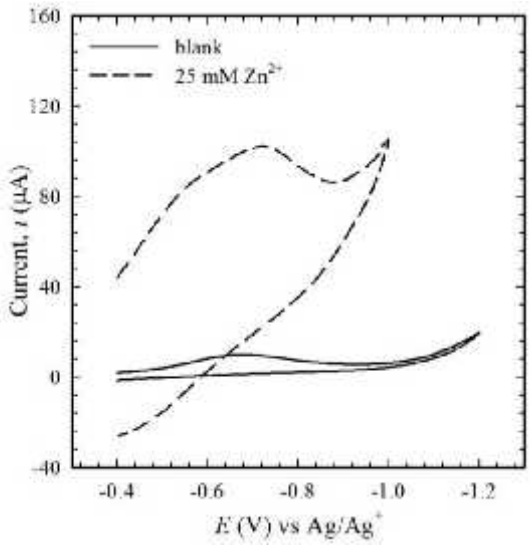

Figure 7.3.14. Cyclic voltammograms of N_2-saturated reverse microemulsions of CTAB (w_o= 7.0) without and with 25 mM Zn^{2+} on CuE at scan rate 0.02 Vs^{-1}.

Figure 7.3.15. represents cyclic voltammograms of N_2-saturated reverse microemulsions of CTAB (w_o= 7.0) containing different concentrations of Zn^{2+} at a scan rate 0.06 Vs^{-1} and 25 mM of Zn^{2+} at different scan rates on CuE**.**

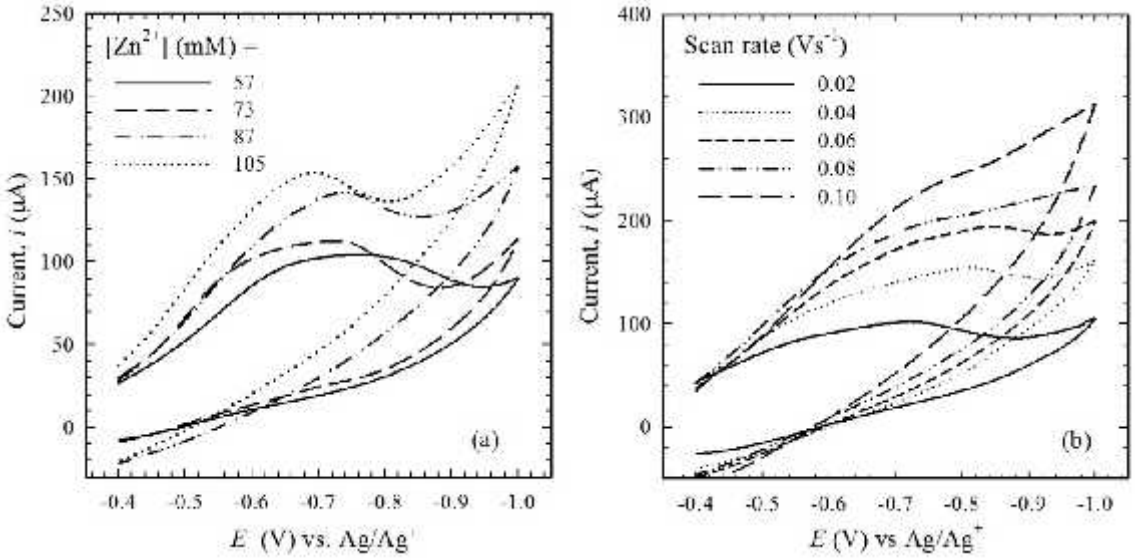

Figure 7.3.15. Cyclic voltammograms of N_2-saturated reverse microemulsions of CTAB with w_o= 7.0 (a) containing different concentrations of Zn^{2+} at scan rate 0.06 Vs^{-1} and (b) 25 mM of Zn^{2+} at different scan rates on CuE.

The cathodic peak current increases as the concentration of Zn^{2+} increases (Figure 7.3.15 (a)) to indicate that the cathodic peak is due to the reduction of Zn^{2+} to metallic Zn. The E_{pc} decreases linearly with log v and the i_{pc} increases linearly passing through the origin with square root of scan rate ($v^{1/2}$) (Figure not shown) indicating that the reduction of

Zn^{2+} to Zn on CuE in reverse microemulsions of CTAB is an irreversible and diffusion controlled process.

7.3.2.5. Electrochemical Behavior of Zn^{2+} in Reverse Microemulsions of SDS

Figure 7.3.16. represents cyclic voltammograms of N_2-saturated reverse microemulsions of SDS (w_o= 20.3) without and with 47 mM Zn^{2+} on CuE at scan rate 0.05 Vs^{-1} with potential window -0.4 to -1.2 V. From the cyclic voltammograms of the reverse microemulsions of SDS (w_o= 20.3) with 47 mM Zn^{2+}, the cathodic peak was observed at a potential −0.73 V that is widely separated from the adsorption peak of reverse microemulsions at about −0.77 V. Therefore, it is clear that the adsorption of SDS does not hinder the reduction of Zn in reverse microemulsion system.

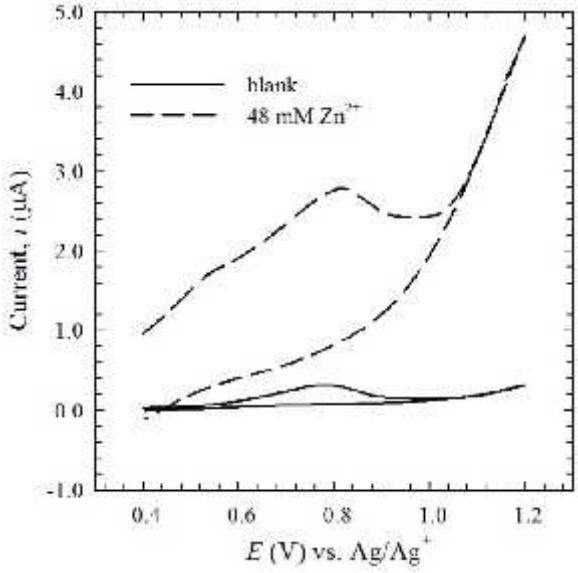

Figure 7.3.16. Cyclic voltammograms of N_2-saturated reverse microemulsions of SDS (w_o= 20.3) without and with 47 mM Zn^{2+} on CuE at scan rate 0.05 Vs^{-1}.

Figure 7.3.17. represents cyclic voltammograms of N_2-saturated reverse microemulsions of SDS (w_o= 20.3) containing different concentrations of Zn^{2+} at scan rate 0.05 Vs^{-1} and 25 mM of Zn^{2+} at different scan rates on CuE**.** The cathodic peak current increases as the concentration of Zn^{2+} increases (Figure 7.3.17 (a)) to indicate that the new cathodic peak is due to the reduction of Zn^{2+} to metallic Zn. The E_{pc} decreases linearly with log v and the i_{pc} increases linearly passing through the origin with square root of scan rate ($v^{1/2}$) (Figure not shown) indicating that the reduction of Zn^{2+} to Zn on CuE in reverse microemulsions of CTAB is an irreversible and diffusion controlled process.

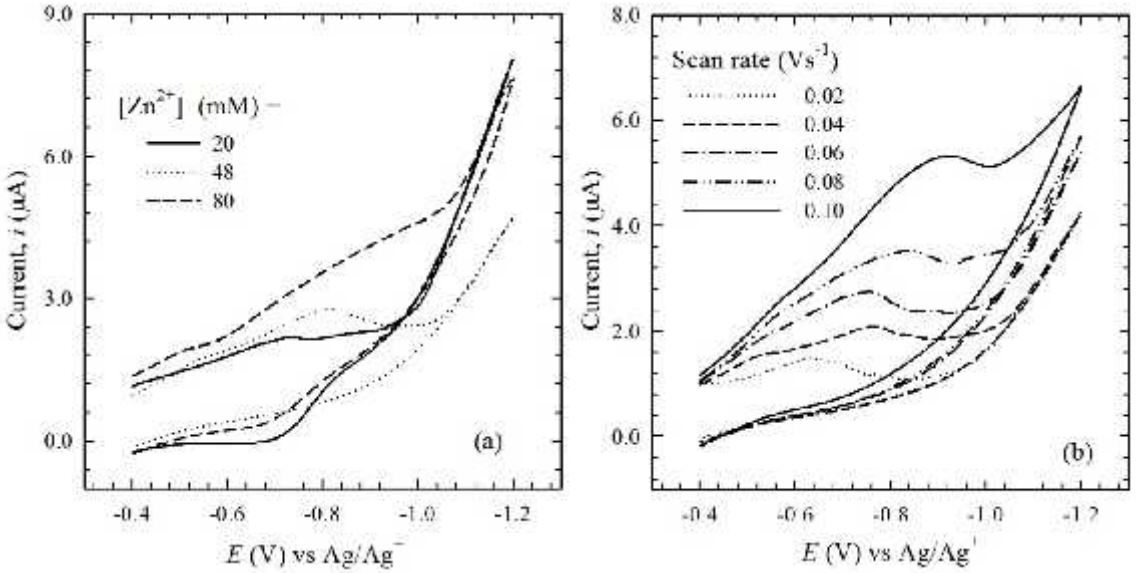

Figure 7.3.17. Cyclic voltammograms of N_2-saturated reverse microemulsions of SDS with w_o= 20.3 (a) containing different concentrations of Zn^{2+} at scan rate 0.05 Vs^{-1} and (b) 25 mM of Zn^{2+} at different scan rates on CuE.

7.3.2.6 Comparative Study of the Electrochemical Behavior of Zn^{2+} in Aqueous Solution, Reverse Microemulsions of CTAB and SDS

Figure 7.3.18. compares cyclic voltammograms of 25 mM Zn^{2+} in N_2-saturated 0.1 M KCl aqueous solution, reverse microemulsions of CTAB (w_o = 7.0) and SDS (w_o = 20.3) at scan rate 0.06 Vs^{-1} on CuE.

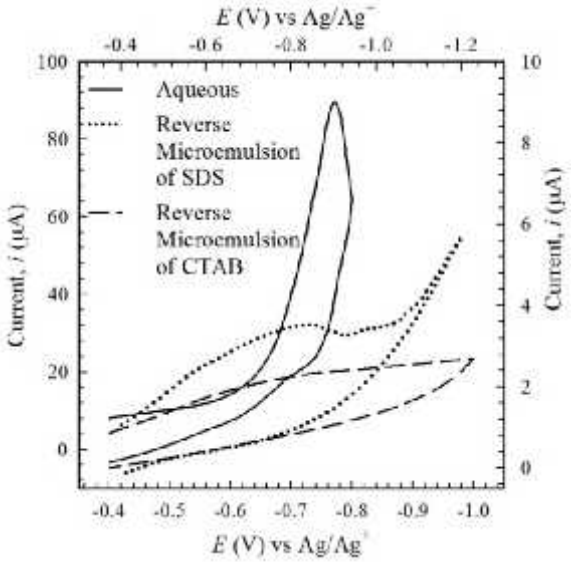

Figure 7.3.18. Cyclic voltammograms of 25 mM Zn^{2+} in 0.1 M KCl aqueous solution in comparison with reverse microemulsions of CTAB (w_o = 7.0) and reverse microemulsions of SDS (w_o = 20.3) at scan rate 0.06 Vs^{-1} on CuE. The values of current in right side and the values of potential in the top are shown for cyclic voltammograms of 25 mM Zn^{2+} in reverse microemulsions of SDS (w_o = 20.3) for clarity.

From Figure 7.3.18 it can be that the potential window as well as the reduction potentials for the reduction of Zn^{2+} to Zn changes noticeably in different media. Table 7.2. represents the cathodic peak potentials, E_{pc} and cathodic peak current, i_{pc} obtained from the cyclic voltammograms of 25 mM Zn^{2+} in N_2-saturated 0.1 M KCl aqueous solution, reverse microemulsions of CTAB (w_o = 7.0) and SDS (w_o = 20.3) at a scan rate 0.07 Vs^{-1} on CuE.

Table 7.2. The cathodic peak potentials, E_{pc} and cathodic peak current, i_{pc} obtained from the cyclic voltammograms of 25 mM Zn^{2+} in N_2-saturated 0.1 M KCl aqueous solution, reverse microemulsions of CTAB (w_o = 7.0) and SDS (w_o = 20.3) at a scan rate 0.07 Vs^{-1} on CuE.

Medium	Cathodic peak current, i_{pc} (μA)	Cathodic peak potential, E_{pc} (V)
Aqueous	72.7	-0.77
Reverse Microemulsion of CTAB	14.2	-0.75
Reverse Microemulsions of SDS	2.60	-0.67

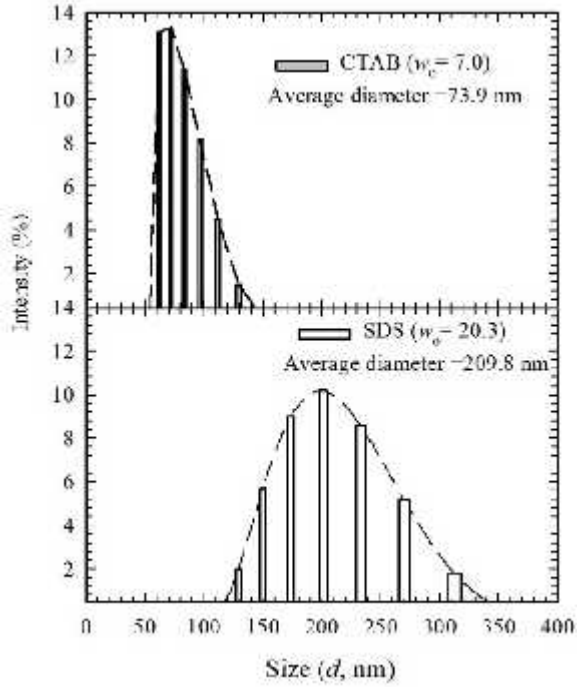

Figure 7.3.19. Size and size distribution of the reverse microemulsions of CTAB (w_o = 7.0) and SDS (w_o = 20.3).

For both reverse microemulsions, the cathodic peak potential, E_{pc} shifts to positive value in compared to aqueous solution. As the SDS is an anionic surfactant, the Zn^{2+} ions trapped into the core of reverse microemulsions of SDS are tightly bound to hydrophillic

groups with electrostatic attraction. So, more energy is required to release the Zn^{2+} from the core of the reverse microemulsions of SDS than reverse microemulsions of CTAB for the reduction of Zn^{2+} and the cathodic peak potential in reverse microemulsions might be shifted to more negative value than in aqueous and reverse microemulsions of CTAB. In contrast, in reverse microemulsions of SDS, the cathodic peak potential, E_{pc} shifts to more positive value than reverse microemulsions of CTAB under identical condition. This may correspond to the fact that the average size of the reverse microemulsions of SDS (= 209.7 nm) is larger than the average size of the reverse microemulsions of CTAB (= 73.9 nm), which makes more available space for incorporation of Zn^{2+} ions in the core of the reverse microemulsions of SDS than in reverse microemulsions of CTAB. Hence, the Zn^{2+} ions easily release from the core of the reverse microemulsions of SDS than in reverse miroemulsions of CTAB. Figure 7.3.19. represents size and size distribution of reverse microemulsions of CTAB and SDS measured by dynamic light scattering method.The cathodic peak current is very low in reverse microemulsions of SDS than in aqueous solution and reverse microemulsions of CTAB due to the slow release of Zn^{2+} from the core of the reverse microemulsions of SDS causing by strong electrostatic interaction between hydrophilic groups of SDS and Zn^{2+}.

7.3.2.7. Electrochemical Behavior of Ni^{2+} in Reverse Microemulsions of SDS

Figure 7.3.20. represents cyclic voltammograms of N_2-saturated reverse microemulsions of SDS (w_o= 20.3) without and with 20 mM Ni^{2+} on CuE at scan rate 0.05 Vs^{-1} with potential window -0.4 to -1.2 V.

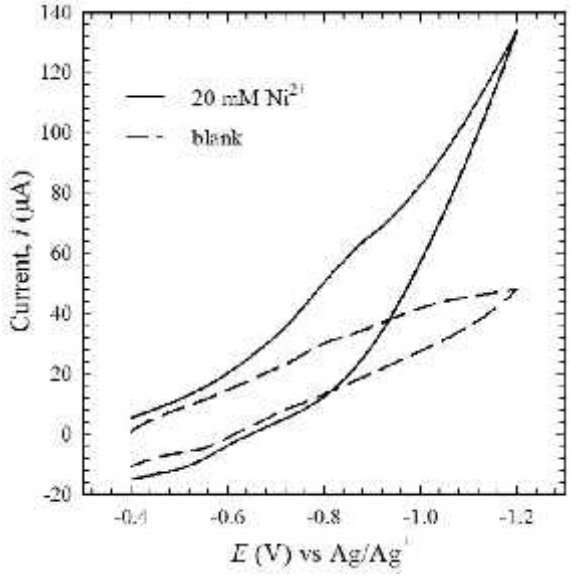

Figure 7.3.20. Cyclic voltammograms of N_2-saturated reverse microemulsions of SDS (w_o= 20.3) without and with 20 mM Ni^{2+} on CuE at scan rate 0.05 Vs^{-1}.

From the cyclic voltammograms of the reverse microemulsions of SDS (w_o= 20.3) with 20 mM Ni^{2+}, the cathodic peak was observed at about −0.77 V which is widely separated from the adsorption peak of reverse microemulsion of SDS (at about −0.70 V).

The cyclic voltammograms were also recorded for N_2-saturated reverse microemulsions of SDS with different w_o containing Ni at scan rate 0.05 Vs^{-1} on CuE to understand the change in the electrochemical behavior of Ni^{2+} depending on the water content of reverse microemulsions of SDS. Figure 7.3.21. represents cyclic voltammograms of N_2-saturated reverse microemulsions of SDS with different w_o containing different concentrations of Ni^{2+} at scan rate 0.05 Vs^{-1} on CuE**.** The cathodic peak current increases as the concentration of Ni^{2+} increases indicate that the new cathodic peak is due to the reduction of Ni^{2+} to metallic Ni.

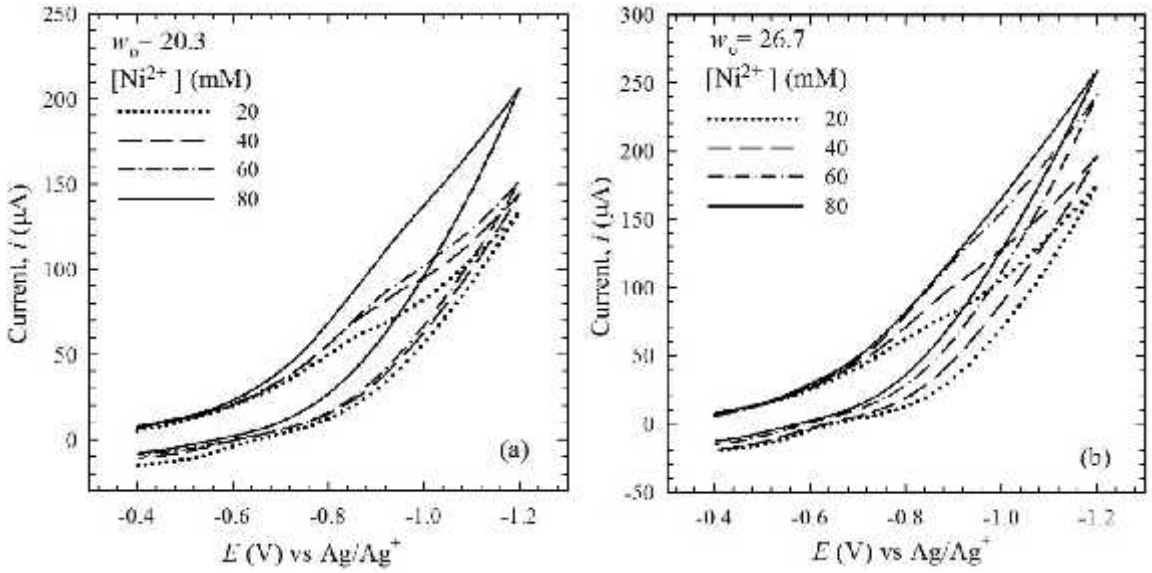

Figure 7.3.21. Cyclic voltammograms of N_2-saturated reverse microemulsions of SDS (a) w_o= 20.3 and (b) w_o= 26.7 with different concentrations of Ni^{2+} at scan rate 0.05 Vs^{-1} on CuE.

Figure 7.3.22. represents cyclic voltammograms of N_2-saturated reverse microemulsions of SDS with different w_o containing 60 mM of Ni^{2+} at a scan rate 0.05 Vs^{-1} on CuE. Both the cathodic peak potential, E_{pc} and cathodic peak current, i_{pc} obtained from the cyclic voltammograms of N_2-saturated reverse microemulsions of SDS with different w_o containing 60 mM of Ni^{2+} at scan rate 0.05 Vs^{-1} on CuE (Figure 7.3.22) changewith increasing the w_o of reverse microemulsions of SDS. Table 7.3. represents the values of E_{pc} and i_{pc} for reduction of Ni^{2+} with increasing w_o of reverse microemulsions of SDS.

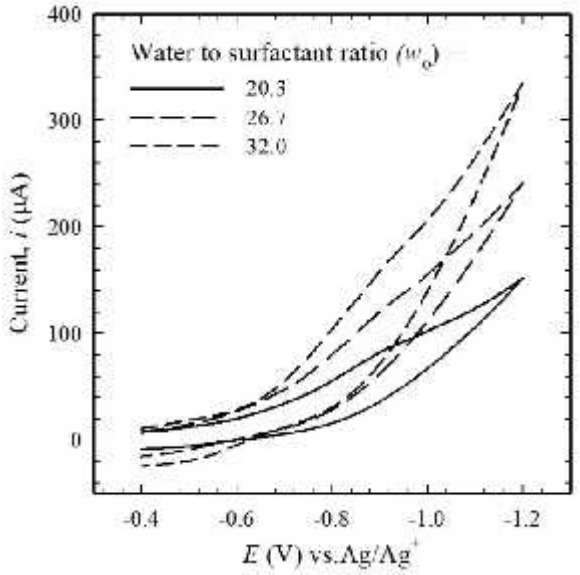

Figure 7.3.22. Cyclic voltammograms of N_2-saturated reverse microemulsions of SDS with different w_o containing 60 mM of Ni^{2+} at scan rate 0.05 Vs^{-1} on CuE.

Table 7.3. The E_{pc} and i_{pc} for reduction of Ni^{2+} with increasing w_o of reverse microemulsions of SDS.

w_o	$-E_{pc}$ (V) vs Ag/Ag^+	i_{pc} (μA)
20.3	0.91	60.1
26.7	0.79	101.7
32.0	0.76	145.3

From Table 7.3 it can be seen that, with increaseing w_o in the reverse microemulsions of SDS, the reduction peak potential shifts to more positive value and peak current increases. This may be due to the fact that with increasing the value of w_o in the reverse microemulsions, the hydrophilic core size of the reverse microemulsions increases. So, the Ni^{2+} ions, trapped into larger hydrophilic core of reverse microemulsions, easily drag out from the core which causes the shifting of the reduction potential to more positive values. For lower value of w_o, release of Ni^{2+} from hydrophilic core of reverse microemulsions of SDS is more difficult due to higher electrostatic interaction between trapped Ni^{2+} and anionic hydrophilic part of the SDS. Consequently, the reduction potential for Ni^{2+} to Ni is more negative than found in reverse microemulsions containing higher value of w_o. The peak current increases gradually with increase in w_o in reverse microemulsions. As hydrophilic core size increases with increasing w_o in reverse microemulsions, they can entrap more Ni^{2+} in the core due to high water content and easily release from the hydrophilic core. As a result, the diffusion rate of Ni^{2+} species at a certain potential in reverse microemulsions increases with increasing w_o and consequently the cathodic peak current for the reduction of Ni^{2+} is increased.

Figure 7.3.23. represents cyclic voltammograms of 20 mM Ni^{2+} in reverse microemulsions of SDS with different w_o on CuE at various scan rates. For both the reverse microemulsions of SDS containing w_o = 20.3 and 26.7, the E_{pc} decreases linearly with log v and the i_{pc} increases linearly passing through the origin with square root of scan rate ($v^{1/2}$) (Figure not shown) to indicate that the reduction of Ni^{2+} to Ni on CuE in reverse microemulsions of SDS is an irreversible and diffusion controlled process.

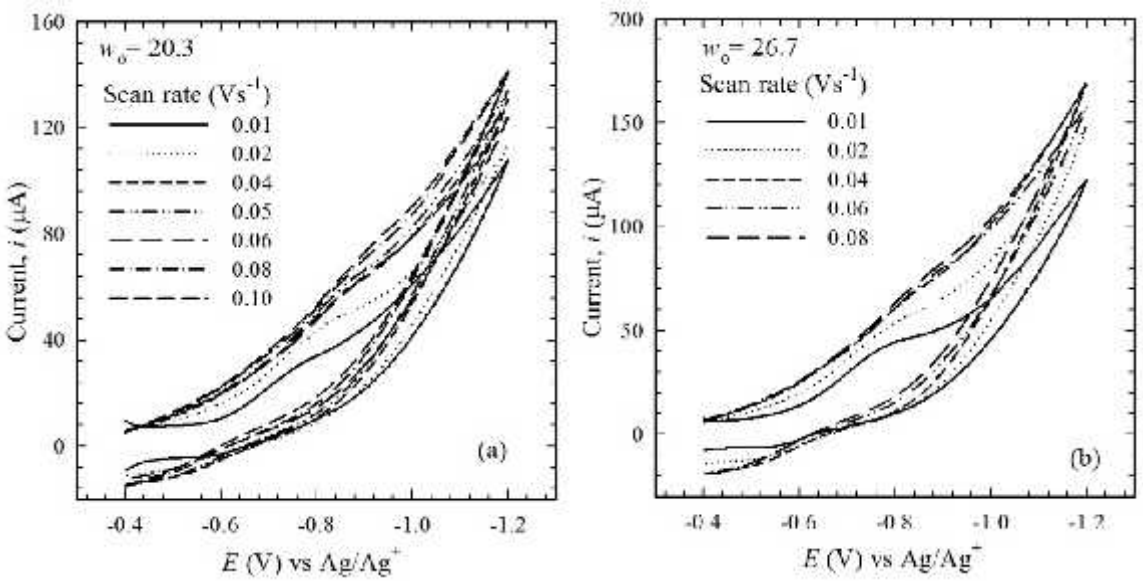

Figure 7.3.23. Cyclic voltammograms of 20 mM Ni^{2+} in reverse microemulsions of SDS with (a) w_o= 20.3 and (b) w_o= 26.7 at different scan rates on CuE.

7.3.2.8. Electrochemical Behavior of Ni^{2+} in Reverse Microemulsions of CTAB

Sultana et al [72] studied the cyclic votammograms of 30 mM Ni^{2+} in reverse microemulsions of CTAB (w_o = 7.0), which showed a reduction peak at about -1.20 V which is widely separated from the absorption peak of reverse microemulsion of CTAB (at about -0.67 V).

7.3.2.9. Comparative Study of the Electrochemical Behavior of Ni^{2+} in Aqueous Solution, Reverse Microemulsions of CTAB and SDS

Figure 7.3.24. compares the cyclic voltammograms of 25 mM Zn^{2+} in 0.1 M KCl aqueous solution, reverse microemulsions of CTAB (w_o = 23.2) and SDS (w_o = 20.3) at scan rate 0.06 Vs^{-1} on CuE. From Figure it has been found that the potential window as well as the reduction potentials for the reduction of Ni^{2+} to Ni changes noticeably in different media. Table 7.4. represents the cathodic peak potentials, E_{pc} and cathodic peak current, i_{pc} obtained from the cyclic voltammogram of 30 mM Ni^{2+} in N_2-saturated 0.1 M KCl aqueous solution, reverse microemulsions of CTAB (w_o = 23.2) and reverse microemulsions of SDS (w_o = 20.3) at scan rate 0.06 Vs^{-1} on CuE.

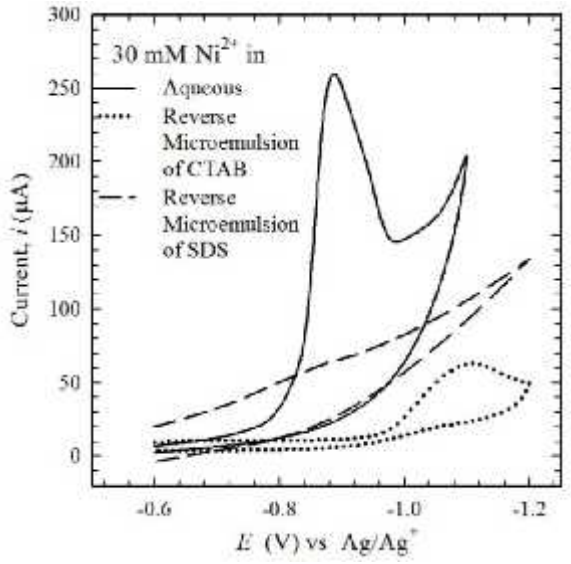

Figure 7.3.24. Cyclic voltammograms of 30 mM Ni^{2+} in 0.1 M KCl aqueous solution in comparison with reverse microemulsions of CTAB (w_o = 23.2) and SDS (w_o = 20.3) at scan rate 0.06 Vs^{-1} on CuE.

Table 7.4. The cathodic peak potentials, E_{pc} and cathodic peak current, i_{pc} obtained from the cyclic voltammogram of 30 mM Ni^{2+} in N_2-saturated 0.1 M KCl aqueous solution, reverse microemulsions of CTAB (w_o = 23.2) and SDS (w_o = 20.3) at scan rate 0.06 Vs^{-1} on CuE.

Medium	Cathodic peak current, i_{pc} (μA)	Cathodic peak potential, E_{pc} (V)
Aqueous	232.7	-0.77
Reverse Microemulsion of CTAB	37.0	-1.10
Reverse Microemulsions of SDS	14.3	-0.77

For the reverse microemulsions of CTAB, the cathodic peak potential shifts to negative value but in reverse microemulsions of SDS, the cathodic peak potential shifted to slightly positive value as compared to aqueous solution. As the SDS is an anionic surfactant, the Ni^{2+} ions trapped into the core of reverse microemulsions of SDS are tightly bound to hydrophillic groups of SDS with electrostatic attraction. So, more energy is needed to release the Ni^{2+} from the core of the reverse microemulsions of SDS than reverse microemulsions CTAB for the reduction of Ni^{2+} and the cathodic peak potential in reverse microemulsions shifted to more negative value than in aqueous and reverse microemulsions of CTAB under identical condition. In addition, the average sizes of reverse microemulsions of SDS (= 209.7 nm) with w_o= 20.3 is slightly larger than the average size of the reverse microemulsions of CTAB (= 196.0 nm) [72] with w_o = 23.2, give more space for Ni^{2+} ions in the core of the reverse microemulsions of SDS than in reverse microemulsions of CTAB. Figure 7.3.25. represents size and size distribution of

reverse microemulsions of CTAB and SDS measured by dynamic light scattering method.

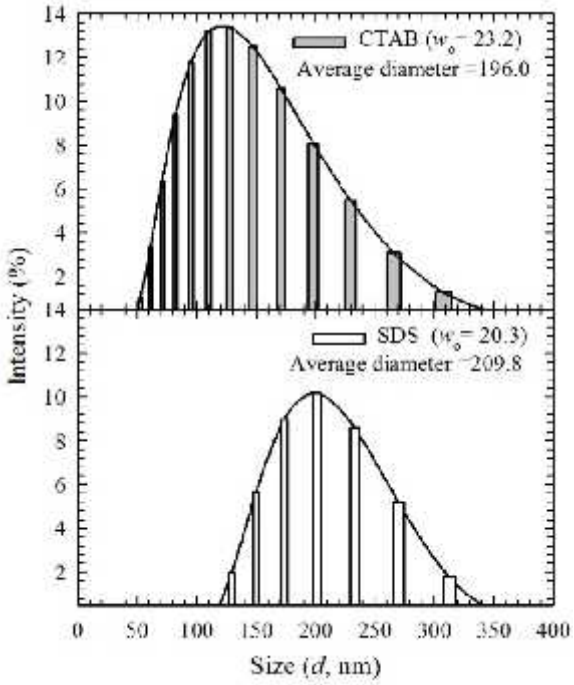

Figure 7.3.25. Sizeand size distribution of the reverse microemulsions of CTAB (w_o = 23.2) and SDS (w_o = 20.3).

The observed small cathodic peak current in reverse microemulsions of SDS is ascribed to slow diffusion of Ni^{2+} trapped into the core of reverse microemulsions of SDS which are tightly bound to hydrophillic groups of SDS with electrostatic attraction to the electrode/solution interface.

7.3.2.10. Electrochemical Behavior of Sn^{2+} in Reverse Microemulsions

Addition of 0.001 g of $SnCl_2$ in 2.5 ml of reverse microemulsions of CTAB (w_o =7.0) and SDS (w_o=20.3) ([Sn^{2+}] = 10 mM) makes the turbid like aqueous solution due to the presence of water in reverse microemulsions where $Sn(Cl)_2$ is hydrolyzed to give $Sn(OH)_2$ as. Upon addition of HCl, the solution became more turbid due to the reverse microemulsions of CTAB and SDS, which were not stable in acidic condition. So, it has not been possible to study the electrochemical behavior of Sn^{2+} in reverse microemulsions of CTAB and SDS.

7.3.3. Electrodeposition of Co, Cu, Zn, Ni and Sn from Aqueous Solution

From cyclic voltammograms of Co^{2+}, Cu^{2+}, Zn^{2+}, Ni^{2+} and Sn^{2+} in aqueous solution, the cathodic peak for reduction of those metals was found at about -0.96 [73], -0.064, -0.57, -0.90 and -0.50 V for CuE, respectively. To ensure a slower deposition and avoid hydrogen embrittlement, electrodeposition of these metals was carried out at a potential below the reduction potential for each metal with a time period of 10-15 min on CuE.

Morphology of electrodeposits was studied using SEM. Figure 7.3.26. shows SEM images of electrodeposited Co from 20 mM of Co^{2+} on CuE with a time period of 10 min at -0.90 V (below reduction potential) [73].

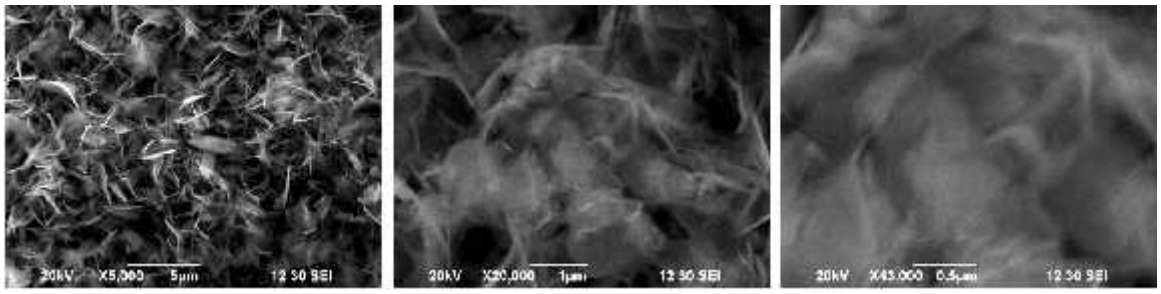

Figure 7.3.26. SEM images of electrodeposited Co from aqueous solution using 20 mM Co^{2+} on CuE at -0.90 V (below the reduction potential) for the deposition time of 10 min.

Figure 7.3.27. shows the SEM images of the electrodeposited Cu from 20 mM of Cu^{2+} on CuE with a time period of 10 min at -0.060 V(below the reduction potential).

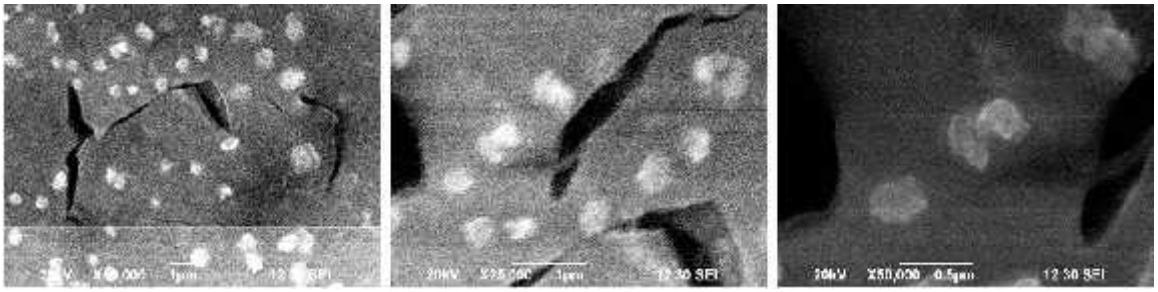

Figure 7.3.27. SEM images of electrodeposited Cu from aqueous solution using 20 mM Cu^{2+} on CuE at -0.060 V (below the reduction potential) for the deposition time of 10 min.

Figure 7.3.28. shows the SEM images of the electrodeposited Zn from 20 mM of Zn^{2+} on CuE with a time period of 10 min at -0.50 V(below the reduction potential).

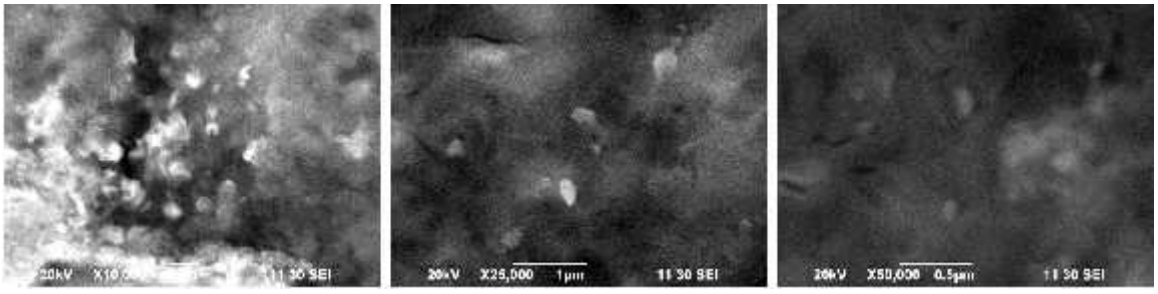

Figure 7.3.28. SEM images of electrodeposited Zn from aqueous solution using 20 mM Cu^{2+} on CuE at -0.50 V (below the reduction potential) for the deposition time of 10 min.

Figure 7.3.29. shows the SEM images of the electrodeposited Ni from 20 mM of Ni^{2+} on CuE with a time period of 15 min at -0.75 V [72].

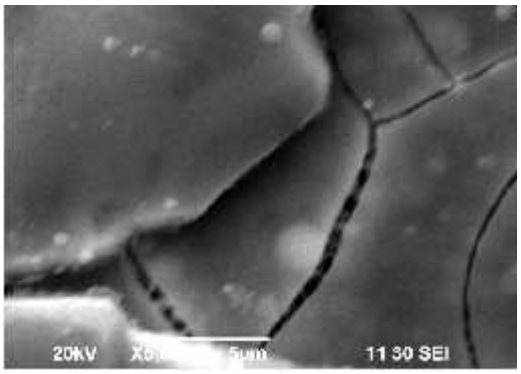

Figure 7.3.29. SEM images of electrodeposited Ni from aqueous solution using 20 mM Ni^{2+} on CuE at -0.75 V (below the reduction potential) for the deposition time of 15 min [72].

Figure 7.3.30. shows the SEM images of the electrodeposited Sn from 8 mM of Sn^{2+} on CuE with a time period of 10 min at -0.50 V.

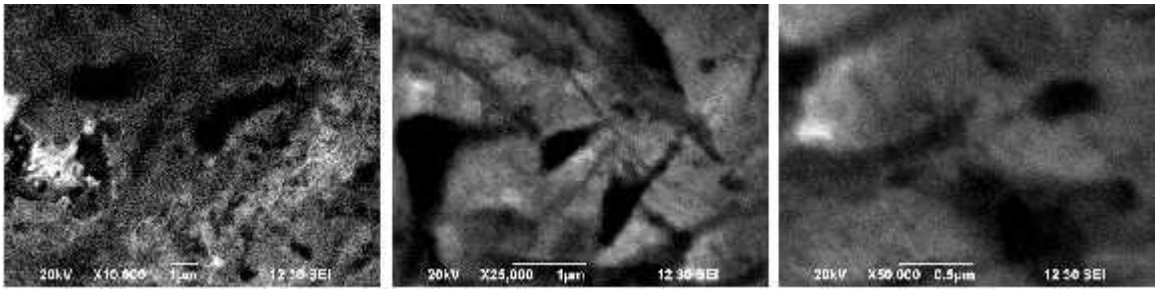

Figure 7.3.30. SEM images of electrodeposited Sn from aqueous solution using 8 mM Sn^{2+} on CuE at -0.75 V (below the reduction potential) for the deposition time of 10 min.

From SEM images (Figure 7.3.26.- 7.3.30.) for all metals, it is apparent that the elctrodeposited metals have no definite structure indicating gross deposition of metals from aqueous solution due to faterdiffusion of metal ions to the surface under the influence of potential. The kinetics of electrode reaction should also be fast as the electrode surface is free from hindrance by the formation of thick double layer. Thus, electrodeposition of the metals from aqueous solution occurs very rapidly and random morphology is observed. A gross deposition of bulk metals results without any definite morphology. Additionally, hydrogen embrittlement also occurs in aqueous solution which makes it impossible to deposit smooth layer of metal.

7.3.4. Electrodeposition of Co, Cu, Zn and Ni from Reverse Microemulsions of CTAB and SDS

7.3.4.1. Electrodeposition of Co from Reverse Microemulsions of CTAB and SDS

In reverse microemulsions of CTAB, the cathodic peak potential of reduction of Co^{2+} to Co is -1.11, -0.97 and -0.94 V for w_o= 7.0, w_o = 13.1 and w_o = 23.2, respectively [92]. The electrodepostion was carried out with different w_o at a fixed reduction potential (below the reduction potential). Figure 7.3.31. represents the SEM images of the elctrodeposited Co from 20 mM Co^{2+} in reverse microemulsions of CTAB with different w_o at below the reduction potential [93].

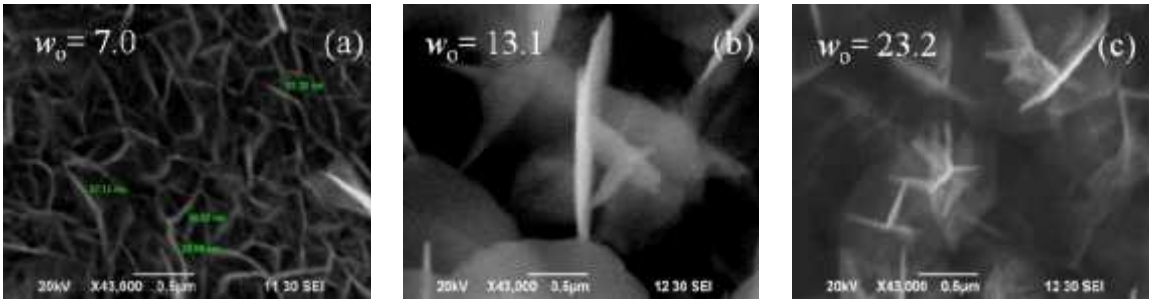

Figure 7.3.31. SEM images of the elctrodeposited Co from 20 mM Co^{2+} in reverse microemulsions of CTAB with (a) w_o = 7.0, (b) w_o = 13.1 and (c) w_o= 23.2 at -0.90 V (below the reduction potential) [93].

In reverse microemulsions of SDS, the cathodic peak potential of reduction of Co^{2+} to Co is -0.92 and -0.90 V for w_o= 20.3 and w_o = 26.7, respectively. Figure 7.3.32. represents the SEM images of the elctrodeposited Co from 20 mM Co^{2+} in reverse microemulsions of SDS with w_o= 20.3 at -0.75 V and w_o = 26.7 at -0.75 V (below the reduction potential).

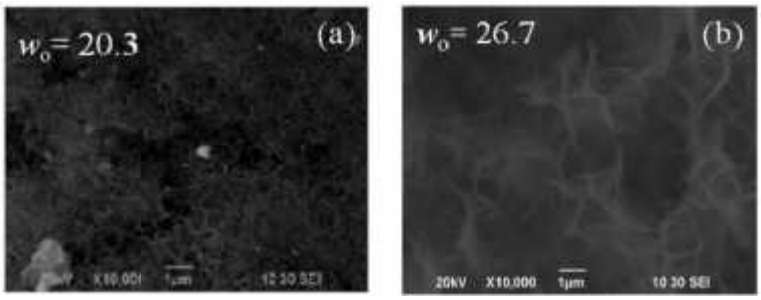

Figure 7.3.32. SEM images of the elctrodeposited Co from 20 mM Co^{2+} in reverse microemulsions of SDS with different w_o at below the reduction potential.

SEM images displayed in figure 7.3.31 and 7.3.32 shows that morphology of the deposited cobalt has been changed with change of w_o of reverse microemulsions of CTAB and SDS. Such structural variation of the deposited Co with w_o of reverse microemulsions occurs due to change in diffusion rate as well as deposition rate. For reverse microemulsions, size of the hydrophilic cores depends on the w_o. Reverse

microemulsions with high w_o is a micelle dominated system over reverse micelles. This is due to the fact thatfor high w_o, the head groups of the surfactants are not sufficiently ordered. As a result number of the Co^{2+} ions existing in the bulk solution is higher than in the core of the reverse microemulsions. Therefore, the rate of diffusion as well as deposition will be faster. On the other hand, the diffusion rate decreased gradually for reverse microemulsions of low w_o due to the fact that at low w_o, reverse micelles are dominated and effective trapping of Co^{2+} species within such hydrophilic cores can take place. With further decrease of w_o, the hydrophilic core size also decreases which causes higher interaction between the trapped Co^{2+} species and the hydrophilic cores. Thus, release of Co^{2+} from the core becomes difficult which results in a significantly slower deposition rate in a more controlled way.

The electrodeposition of Co was also performed in reverse microemulsions of SDS with w_o= 20.3 at different reduction potentials to understand the change in morphology and structure of electrodeposited Co by changing the reduction potential at fixed w_o. Figure 7.3.33. represents the SEM images and EDX spectra of elctrodeposited Co from 20 mM Co^{2+} in reverse microemulsions of SDS (w_o= 20.3) with different reduction potentials below the reduction potential, at the reduction potential and above the reduction potential.

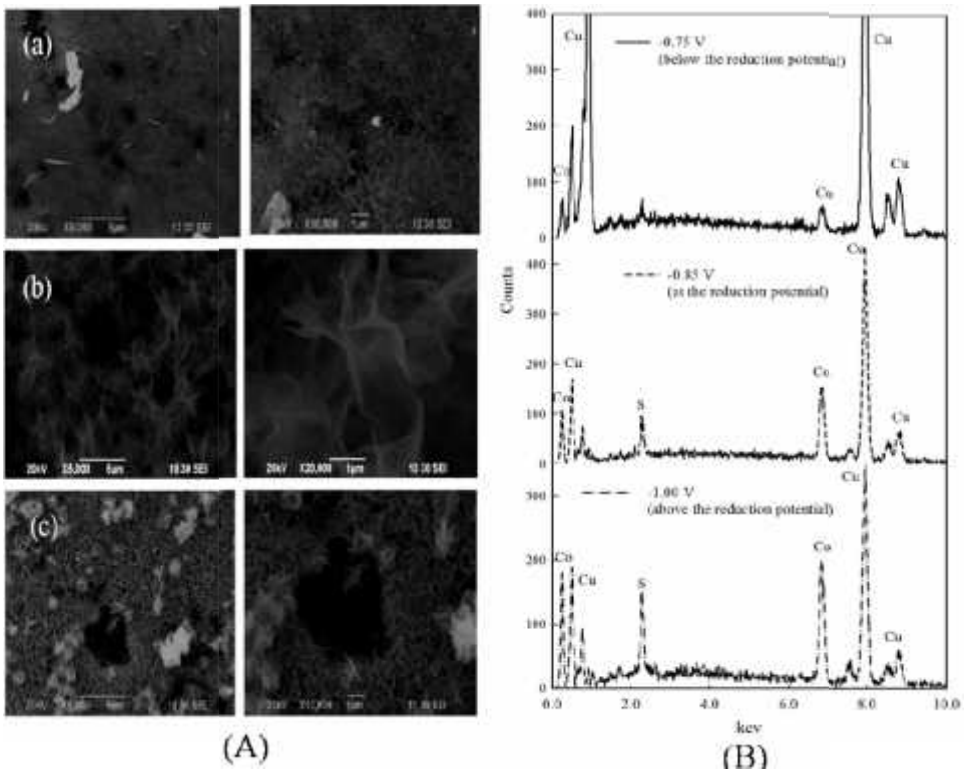

Figure 7.3.33. (A) SEM images and (B) EDX spectra of the elctrodeposited Co from 20 mM Co^{2+} in reverse microemulsions of SDS (w_o=20.3) at (a) -0.75 V (below the reduction potential) (b) -0.75 V (at the reduction potential) and (c) -1.0 V (above the reduction potential) on CuE with deposition time 10 min.

From SEM images at fixed w_o with different reduction potential, it has been found that only the deposition rate varies with change in applied potentials and the thickness of the deposited Co changed due to a faster growth being apparent at a potential more negative than the reduction potential. Thus, at a potential below the reduction potential, as the concentration of Co^{2+} is fixed, the deposition occurs slowly and the thickness of the deposited Co on CuE is small as compared to above the reduction potential.

The EDX spectra confirmed the presence of metallic Co in the deposits. With changing the reduction potential to more negative value, the thickness as well as the content of electrodeposited Co increases due to faster growth is noticeable for a potential more negative than the reduction potential. The schematic diagram of the possible mechanism is as follows:

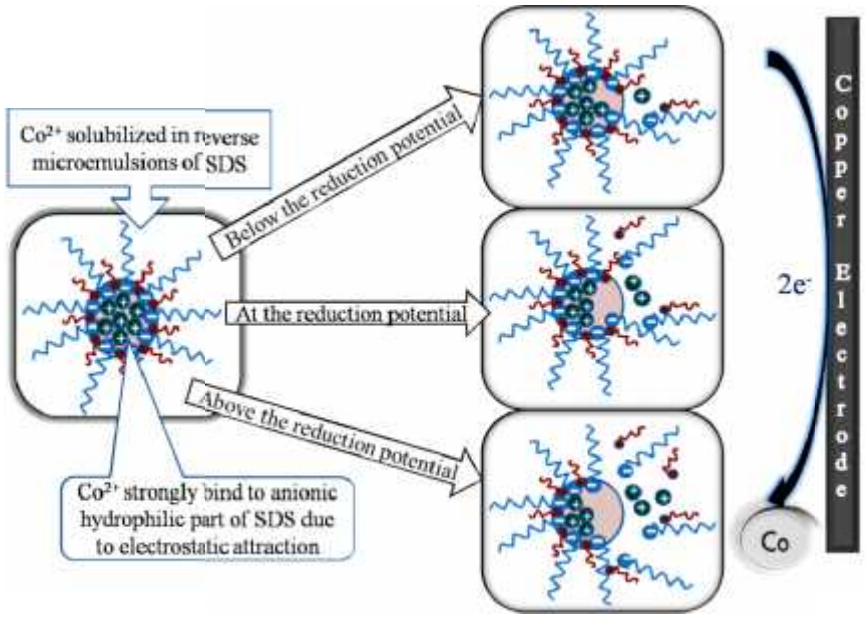

Scheme 7.1. The probable mechanism of elctrodeposition of Co from reverse microemulsions of SDS at a fixed w_o (=20.3) with different reduction potentials.

7.3.4.2. Electrodeposition of Cu from Reverse Microemulsions of CTAB

In reverse microemulsions of CTAB with w_o = 7.0, the cathodic peak potential of reduction of Cu^{2+} to Cu is about –0.77 V. The electrodepostion was carried out with –0.75 V (below the reduction potential). Figure 7.3.34. represents the SEM images of the elctrodeposited Cu from 2 mM Co^{2+} in reverse microemulsions of CTAB with w_o = 7.0 at below the reduction potential on CuE. The SEM images of the electrodeposited Cu from reverse microemulsions of CTAB (w_o= 7.0) shows that the Cu has uniform cubic like structure and the size of the Cu is within nanometer sized may be due to the control release of Cu from the hydrophobic core of the reverse microemulsions which lowers the diffusion rate.

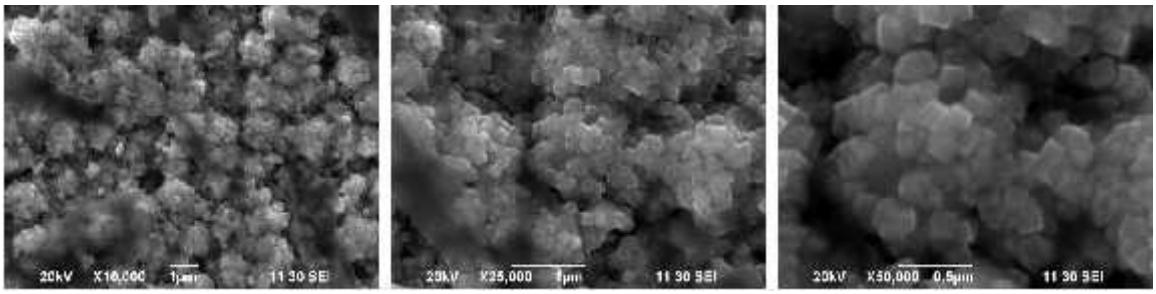

Figure 7.3.34. SEM images of the elctrodeposited Cu from 2 mM Co^{2+} in reverse microemulsions of CTAB with w_o = 7.0 at below the reduction potential on CuE.

7.3.4.3. Electrodeposition of Zn from Reverse microemulsions of CTAB

In reverse microemulsions of CTAB with w_o = 7.0, the cathodic peak potential of reduction of Zn^{2+} to Zn is about –0.73 V. The electrodepostion was carried out with –0.70 V (below the reduction potential). Figure 7.3.35. represents the SEM images of the elctrodeposited Zn from 20 mM Zn^{2+} in reverse microemulsions of CTAB with w_o = 7.0 at below the reduction potential on CuE. The SEM images of the electrodeposited Zn from reverse microemulsions of CTAB (w_o= 7.0) shows that the Zn has rod like structure due to the controlled release of Zn which is trapped into the hydrophobic core of the reverse microemulsions and lowers the diffusion rate.

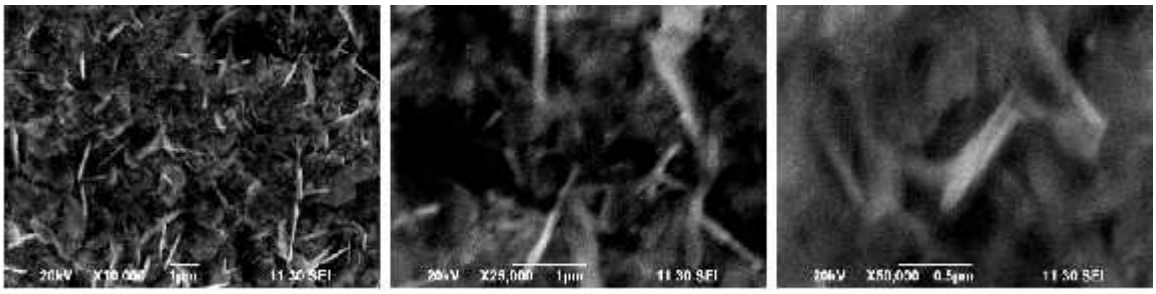

Figure 7.3.35. SEM images of the elctrodeposited Zn from 20 mM Zn^{2+} in reverse microemulsions of CTAB with w_o = 7.0 at below the reduction potential on CuE.

7.3.4.4. Electrodeposition of Ni from Reverse Microemulsions of CTAB and SDS

In reverse microemulsions of CTAB, the cathodic peak potential of reduction of Ni^{2+} to Ni is -1.20, -1.10 and -1.11 V for w_o= 7.0, w_o = 13.1 and w_o = 23.2, respectively [91]. The electrodepostion was carried out with different w_o at a fixed reduction potential (below the reduction potential). Figure 7.3.36. represents the SEM images of the elctrodeposited Co from 20 mM Co^{2+} in reverse microemulsions of CTAB with different w_o at a potential below the reduction potential [91].

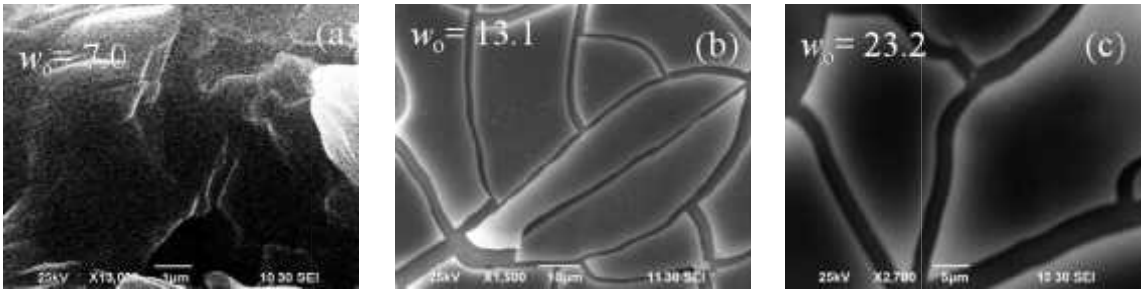

Figure 7.3.36. SEM images of the elctrodeposited Ni from 20 mM Ni^{2+} in reverse microemulsions of CTAB with (a) w_o = 7.0, (b) w_o = 13.1 and (c) w_o= 23.2 at -0.90 V (below the reduction potential) [91].

The electrodeposition of Ni performed in reverse microemulsions of SDS with w_o= 20.3 at different reduction potentials to understand the change in morphology and structure of electrodeposited Ni by changing the reduction potential at fixed w_o. Figure 7.3.37. represents the SEM images of the elctrodeposited Ni from 20 mM Ni^{2+} in reverse microemulsions of SDS (w_o=20.3) with different reduction potential; below the reduction potential, at the reduction potential and above the reduction potential.

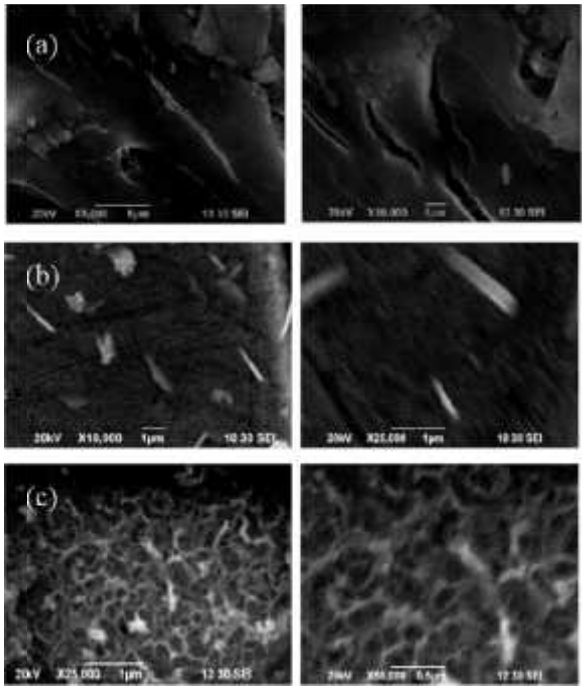

Figure 7.3.37. SEM images of the elctrodeposited Ni from 20 mM Ni^{2+} in reverse microemulsions of SDS (w_o= 20.3) with (a) -0.75 V (below the reduction potential), (b) -0.92 V (at the reduction potential) and -1.0 V (above the reduction potential).

The SEM images at fixed w_o with different reduction potentials show that only the thickness of the deposited Ni changes depending on the deposition rate due to a faster growth at a potential more negative than the reduction potential.

7.4. Conclusions

Electrodeposition of Co, Cu, Zn, Ni and Sn on CuE in aqueous solution occurs grossly without giving any definite shape and size of the electrodeposits due possibly to faster deposition rate and hydrogen embrittlement. In contrast, electrodeposition of different metals from reverse microemulsions of CTAB and SDS carried out on CuE results in electrodeposited metals with definite shape and structure. In reverse microemulsions of CTAB and SDS, hydrophilic cores formed by the aggregation of the hydrophilic polar head groups of the surfactants which incorporates the metal ions and diffusion of the metals ions occur with a controlled rate which in turn contributes towards deposition with definite morphology and also the structure changes with increasing w_o in reverse microemulsions. With decreasing the w_o in reverse micellar solution of CTAB and SDS, the size of the hydrophilic core formed by the hydrophilic polar head groups also decreases so the hydrophilic interaction between the hydrophilic core and the entrapped metals ions within the hydrophilic core increases gradually. As a result diffusion rate of the metal ions decreases and deposition occurs with a more controlled way which causes the morphological variation of the deposited metals in reverse microemulsions of CTAB and SDS at different composition. With changing the reduction potential at a fixed w_o, only the thickness of the deposited metal changed due to a faster growth being apparent at a potential more negative than the reduction potential.

References

[1] A. Brenner, *Electrodeposition of alloys I-II*, Academic Press, NewYork, USA, 1963.

[2] M. Schlesinger, M. Paunovic, *Modern electroplating*, John Wiley & Sons, New Jersey, USA, 2010.

[3] Y. D. Gamburg, G. Zangari, *Theory and practice of metal electrodeposition-1*, NewYork, USA, 2011.

[4] M. Ando, T. Kobayashi, S. Iijima, M. Harita, *A voltammetric study of the underpotential deposition of cobalt onto a glassy carbon electrode*, *Journal of Material Chemistry*, 1997, **7**, 1779-1773.

[5] H. Yamaura, J. Tamaki, K. Moriya, N. Miura, N. Yamazoe, *Highly selective co sensor using indium oxide doubly promoted by cobalt oxide and gold*, Journal of Electrochemical Society, 1997, 144, 157-160.

[6] P. Nkeng, J. Koening, J. Gautier, P. Chartier, G. Poillerat, *Enhancement of surface areas of Co_3O_4 and $NiCo_2O_4$ electrocatalysts prepared by spray pyrolysis*, Journal of Electroanalytical Chemistry, 1996, 402, 71-79.

[7] S. Weichel, P. J. Møller, , *Annealing-induced microfaceting of the CoO(100) surface investigated by LEED and STM*, Surfactant Science, 1997, 399, 219-224.

[8] Y. Okamoto, T. Imanaka, S. Teranishi, *Surface structure of full-size image CoO-MoO_3/Al_2O_3 catalysts studied by X-ray photoelectron spectroscopy*, Journal of Catalysis, 1970, 65, 447-460.

[9] Y. Sun, C. Liu, D. C. Grauer, J. Yano, J. R. Long, P. Yang, C. J. Chang, *Electrodeposited cobalt-sulfide catalyst for electrochemical and photoelectrochemical hydrogen generation from water*, Journal of American Chemical Society, 2013, 135, 17699-17702.

[10] K. Ramachandram, C. O. Oriakhi, M. M. Lerner, V. R. Koch, *Intercalation chemistry of cobalt and nickel dioxides - a facile route to new compounds containing organocations*, Material Research Bulletin, 1996, 31, 767-772.

[11] M. G. Hutchins, P. J. Wright, P. D. Grebenik, *Comparison of different forms of black cobalt selective solar absorber surfaces*, Solar Energy Materials, 1977, 16, 113-131.

[12] E. Barrera, I. Gonzales, T. Viveros, *A new cobalt oxide electrodeposit bath for solar absorbers*, Solar Energy Materials and Solar Cells, 1997, 51, 69-72.

[13] F. Endres, D. MacFarlane, A. Abbott, *Electrodeposition from ionic liquids*, Wiley-VCH, New Delhi, 2007.

[14] S. Blunden, T. Wallace, *Tin in canned food: a review and understanding of occurrence and effect*, Food and Chemical Toxicology, 2003, 41, 1651-1662.

[15] C. H. Rios-Reyes, *Kinetic study of the cobalt electrodeposition onto glassy carbon electrode from ammonium sulfate solutions*, Química Nova, 2009, 32, 2372-2376.

[16] C. Q. Cui, S. P. Jiang, A. C. C. Tseung, *Electrodeposition of cobalt from Aqueous chloride solutions*, Journal of Electrochemical Society, 1990, 137, 3417-3423.

[17] D. Grujicic, B. Pesic, *Electrochemical and AFM study of cobalt nucleation mechanisms on glassy carbon from ammonium sulfate solutions*, Electrochimica Acta, 2004, 49, 4719-4732.

[18] A. Bodaghi, J. Hosseini, *Corrosion behavior of electrodeposited cobalt-tungsten alloy coatings in NaCl Aqueous Solution*, International Journal of Electrochemical Science, 2012, 7, 2574-2595.

[19] M. G. Neri, L. H. M. Huizar, *Cobalt electrodeposition process from electrolytic baths based on $CoSO_4$ and $(NH_4)_2(SO_4)$. Influence of [Co(II)]*, Journal of The Electrochemical Society, 2009, 20, 375-373.

[20] H-C. Taoa, M. Lianga, W. Lia, L-J Zhanga, J-R. Nia, W-M. Wuc, *Removal of copper from aqueous solution by electrodeposition in cathode chamber of microbial fuel cell*, Journal of Hazardous Materials, 2011, 179, 176-192.

[21] J. C. Ballesteros, E. Chainet, P. Ozil, Y. Meas, G. Trejo, *Electrodeposition of copper from non-cyanide alkaline solution containing tartrate*, International Jounal of Electrochemical Science, 2011, 6, 2632 - 2651.

[22] N. D. Nikolic, K. I. Popov, *Hydrogen codeposition effects on the structure of electrodeposited copper*, Electrodeposition: Theory and Practice, S. S. Djokic, New York, USA, 2010.

[23] M. Yokoi, Copper Electrodeposition, *Copper electrodeposition for nanofabrication of electronics devices*, K. Kondo, Rohan N. Akolkar, D. P. Barkey, M. Yokoi, New York, USA, 2014.

[24] A. T. Kuhn, P. Neufeld, K. Young, *The electrodeposition of copper-silver and copper-nickel alloy powders from aqueous ammoniacal solutions*, Journal of Applied Electrochemistry, 1974, 14, 605-613.
[25] I. G. Casella, M. Gatta, *Anodic electrodeposition of copper oxide/hydroxide film by alkaline solutions containing cuprous cyanide solutions*, Journal of electrochemistry, 2000, 494, 12-20.
[26] G. Heidari, S. M. M. Khoie, M. E. Abrishami, M. Javanbakh, *Electrodeposition of Cu–Sn alloys: theoretical and experimental approaches*, Journal of Materials Science: Materials in Electronics, 2015, 26, 1969-1976.
[27] S. Peulon, D. Lincot, *Mechanistic study of cathodic electrodeposition of zinc oxide and zinc hydroxychloride films from oxygenated aqueous zinc chloride solutions*, Journal of the Electrochemical Society, 1997, 145, 764-774.
[28] L. H. Mendoza-Huízar, C. H. Rios-Reyes, M. G. Gómez-Villegas, *Zinc electrodeposition from chloride solutions onto glassy carbon electrode*, Journal of the Mexican Chemical Society, 2009, 53, 243-247.
[29] G. Riveros, D. Ramírez, A. Tello, R. Schrebler, R. Henríquez, H. Gómez, *Electrodeposition of ZnO from DMSO solution: influence of anion nature and its concentration in the nucleation and growth mechanisms*, Journal of Brazilian Chemical Society, 2012, 23, 505-512.
[30] T. Edamura, J. Muto, *Electrodeposition of zinc cadmium sulphide thin films from acidic aqueous electrolyte solution at room temperature*, Journal of Materials Science Letters, 1995, 14, 779-791.
[31] Y. A. Naik, T. V. Venkatesha, P. V. Nayak, *Electrodeposition of zinc from chloride solution*, Turkish Journal of Chemistry, 2002, 26, 725-733.
[32] A. Naora, N. Eliaza, E. Gileadib, *Electrodeposition of rhenium–nickel alloys from aqueous solutions*, Electrochimica Acta, 2009, 54, 6027-6035.
[33] G. Z. Cheng, G. Y. Peng, L. W. Chang, *Electrochemical studies of nickel deposition from aqueous solution in super-gravity field*, Science in China Series E: Technological Sciences, 2007, 50, 39-50.
[34] G. Fu, Z. Hu, L. Xie, X. Jin, Y. Xie, Y. Wang, Z. Zhang, Y. Yang, H. Wu, *Electrodeposition of nickel hydroxide films on nickel foil and its electrochemical performances for supercapacitor*, International Journal of Electrochemical Science, 2009, 4, 1052-1062.
[35] H. Kazimierczak, P. Ozga, M. Słupska, Z. Swiatek, K. Berent, *Electrodeposition of Sn-Mn layers from aqueous citrate electrolytes*, Journal of The Electrochemical Society, 2014, 161, 309-320.
[36] A. Survila, Z. Mockus, R. Juskenas, V. Jasulaitiene, *Electrodeposition of Sn and Co coatings in citrate solutions*, Journal of Applied Electrochemistry, 2001, 31, 1109-1116.
[37] M. R. Buchner, F. Kraus, H. Schmidbaur, *Pyrophosphate complexation of tin(II) in aqueous solutions as applied in electrolytes for the deposition of tin and tin alloys such as white bronze*, Inorganic Chemistry, 2012, 51, 7760-7767.
[38] E. Rudnik, *Effect of anions on the electrodeposition of tin from acidic gluconate baths*, Ionics, 2013, 19, 1047-1059.

[39] R. M. El-Sherif, W. A. Badawy, *Mechanism of corrosion and corrosion inhibition of tin in aqueous solutions containing tartaric acid*, International Journal of Electrochemical Science, 2011, 6, 6469-6472.

[40] F. Xiao, X. Shen, F. Ren, A. A. Volinsky, *Additive effects on tin electrodepositing in acid sulfate electrolytes*, International Journal of Minerals, Metallurgy and Materials, 2013, 20, 472-477.

[41] K. Neuróhra, L. Pogánya, B. G. Tótha, Á. Révészb, I. Bakonyia, L. Pétera, *Electrodeposition of Ni from various non-aqueous media: the case of alcoholic solutions*, Journal of Electrochemical Society, 2015, 162, 256-264.

[42] H. Gu, T. J. O'Keefe, M. J. O'Keefe, *Spontaneous electrochemical deposition of metals from organic solutions*, Fundamental Aspects of Electrochemical Deposition and Dissolution, M. Matlosz, The Electrochemical Society, New Jersey, USA, 2000, 242-250.

[43] R. G. Billinghurst, J. Rajki, K. G. Rutherford, *Electrodeposition of some metals from tetramethylurea*, Journal of Applied Chemistry, 1966, 16, 339-340.

[44] S. Schaltin, A. Shkurankov, K. Binnemans, J. Fransaer, *Direct Co-on-Ta electroplating from ionic liquid in high vacuum*, Journal of The Electrochemical Society, 2010, 25, 119-127.

[45] C-H. Hsu, C-H. Yang, Y-C. Wanga, J-K. Chang, *Nanostructured tin electrodeposited in ionic liquid for use as an anode for Li-ion batteries*, Journal of Material Chemistry A, 2014, 2, 16547-16553.

[46] P. Giridhar, A. M. Elbasiony, S. Z. El Abedin, F. Endres, *A comparative study on the electrodeposition of tin from two different ionic liquids: influence of the anion on the morphology of the tin deposits*, ChemElectroChem, 2014, 1, 1549-1556.

[47] M. A. B. H. Susan, S. Saha, S. Ahmed, F. Begum, M. M. Rahman, M. Y. A. Mollah, *Electrodeposition of cobalt from a hydrophilic ionic liquid at ambient condition*, Materials Research Innovations, 2012, 16, 345-349.

[48] A. P. Abbott, K. J. McKenzie, *Application of ionic liquids to the electrodeposition of metals*, Physical Chemistry Chemical Physics, 2006, 7, 4265-4279.

[49] W. Freyland, C. A. Zell, S. Zein El Abedin, F. Endres, *Nanoscale electrodeposition of metals and semiconductors from ionic liquids*, Electrochimica Acta, 2003, 47, 3053-3061.

[50] F. Liua, Y. Dengc, X. Hanb, W. Hua, C. Zhong, *Electrodeposition of metals and alloys from ionic liquids,* Journal of Alloys and Compounds, 2015, 654, 163-170.

[51] A. P. Abbott, K. S. Ryder, U. Ko¨nig, *Electrofinishing of metals using eutectic based ionic liquids*, Transactions of the Institute of Metal Finishing, 2007, 7,196-204.

[52] F. Endres, *Ionic liquids: Solvents for the electrodeposition of metals and semiconductors*, ChemPhysChem, 2002, 3, 145-154.

[53] H. Ohno, *Electrochemical aspects of ionic liquids*, Wiley and Jones, New Jersey, Canada, 2011.

[54] Z. Lui, S. Z. El Abedin, F. Endres, *Electrodeposition of zinc films from ionic liquids and ionic liquid/water mixtures*, Electrochemica Acta, 2013, 79, 635-643.

[55] W. Caia, C. A. Schuha, *Microstructure and mechanical properties of electrodeposited* Al_{1-x} Mn_x /Al_{1-y} Mn_y *nanostructured multilayers*, Journal of Materials Research, 2014, 29, 2229-2239.

[56] F. Endres, S. Z. E. Abedin, *Air and water stable ionic liquids in physical chemistry*, Physical Chemistry Chemical Physics, 2006, 7, 2101-2116.

[57] Y. K. Kee, W. J. Basirun, K. H. Lee, *Electrodeposition of tin using tin(II) methanesulfonate from a mixture of ionic liquid and methane sulfonic acid*, Advanced Materials Research, 2011, 264, 1462-1467.

[58] C-H. Hsu, C-H. Yang, Y-C. Wanga, J-K. Chang, *Nanostructured tin electrodeposited in ionic liquid for use as an anode for Li-ion batteries*, Journal of Materials Chemistry A, 2014, 2, 16547-16553.

[59] S. Srinivasan, M. Selvam, *Electrodeposition of zinc from low temperature molten salt electrolyte: Part I-imidazole and zinc-chloride electrolyte*, International Journal of Scientific Engineering and Technology, 2013, 2, 711-716.

[60] J-F. Huang, I-Wen, *Electrochemical studies of tin in zinc chloride-1-ethyl-3-methylimidazolium chloride ionic liquids*, Journal of The Electrochemical Society, 2003,150, 299-306.

[61] Y. Tan, S. Srinivasan, K-S. Choi, *Electrochemical deposition of mesoporous nickel hydroxide films from dilute surfactant solutions*, Journal of American Chemical Society, 2005, 127, 3596-3604.

[62] N. Sakmeche, J-J Aaron, S. Aeiyach, P-C Lacaze, *Usefulness of aqueous anionic micellar media for electrodeposition of poly-(3,4-ethylenedioxythiophene) films on iron, mild steel and aluminum*, Electrochimica Acta, 2000, 45, 1921-1931.

[63] J. D. Wadhawan, R. G. Compton, M. Etienne, P. D. Richemont, *Electrochemistry: Nanosystems Electrochemistry*, The Royal Society of Chemistry, 2013.

[64] T. Ye, K. Seo, E. Borguet, *Electrodeposition of metal nanowires onto a molecular scale template: An insitu investigation*, Langmuir, 2009, 25, 5491-5495.

[65] C. Boeckler , T. Oekermann , A. Feldhoff, M. Wark, L. U. Hannover, *Role of the critical micelle concentration in the electrochemical deposition of nanostructured ZnO films under utilization of amphiphilic molecules*, Langmuir, 2006, 22, 9427-9430.

[66] N. Tabakova, I. Pojarliejf, V. Mircheva, J. Stejska, The *role of micelles of multiblock copolymers of ethylene oxide and propylene oxide in ion transport during acid bright copper electrodeposition*, Macromolecular Symposia, 2004, 212**,** 467-472.

[67] P. N. Bartlett, *Electrodeposition of nanostructured films using self-organizing templates*, The Electrochemical Society Interface, 2004, 13, 27-33.

[68] M. A. Malik, M. A. Hashim, F. Nabi, S. A. AL-Thabaiti, Z. Khan, *Anti-corrosion ability of surfactants: A review*, International Journal of Electrochemistry of Science, 2011, 6, 1927-1947.

[69] V. P. Grigor'ev, S. P. Shpan'ko, O. V. Dymnikova*, Electrodeposition of metals in the presence of surfactant mixtures of several reaction series with variable number and concentration of components*, Protection of Metals, 2004, 40, 320-325.

[70] C. Li, H. Wang, Y. Yamauchi, *Electrochemical deposition of mesoporous Pt-Au alloy films in aqueous surfactant solutions: towards a highly sensitive amperometric glucose sensor*, Chemistry - A European Journal, 2013, 19, 2242-2246.

[71] A. Aragon, M. G. Figueroa, R. E. Gana, J. H. Zagal, *Effect of a polyethoxylate surfactant on the electrodeposition of tin*, Journal of Applied Electrochemistry, 1992, 22, 557 - 562.

[72] S. Sultana, S. Saha, M. M. Islam, M. M. Rahman, M. Y. A. Mollah, M. A. B. H. Susan, *Electrodeposition of nickel from reverse micellar solutions of cetyltrimethylammonium bromide*, Journal of The Electrochemical Society, 2013, 160, 524-529.

[73] S. Saha, S. Sultana, M. M. Islam, M. M. Rahman, M. Y. A. Mollah, M. A. B. H. Susan, *Electrodeposition of cobalt with tunable morphology from reverse micellar solution*, Ionics, 2014, 20, 1175-1171.

[74] S. Park , S. Y. Lee, H. Boo, H-M Kim, K-B Kim, H. C. Kim ,Y. J. Song, T. D. Chung, *Three-dimensional interstitial nanovoid of nanoparticulate Pt film electroplated from reverse micelle solution*, *Chemistry of Materials*, 2007, 19, 3373-3375.

[75] D. A. Kaplin, S. Qutubuddin, *Electrodeposition of pyrrole into a porous film prepared by microemulsion polymerisation*, Synthetic metals, 1994, 63,177-194.

[76] C. Fu, H. Zhou, D. Xie, L. Sun, Y. Yin, J. Chen, Y. Kuang, *Electrodeposition of gold nanoparticles from ionic liquid microemulsion*, Colloid and Polymer Science, 2010, 277, 1097-1103.

[77] A. Serrà, E. Gómez, G. Calderó, J. Esquena, C. Solans, E. Vallés, *Microemulsions for obtaining nanostructures by means of electrodeposition method*, Electrochemistry Communications, 2013, 27, 14-17.

[78] A. Serrà, E. Gómez, G. Calderó, J. Esquena, C. Solans, E. Vallés, *Conditions that bicontinuous microemulsions must fulfill to be used as template for electrodeposition of nanostructures*, Journal of Electroanalytical Chemistry, 2014, 720, 101-106.

[79] H. Zhou, C. Peng, S. Jiao, W. Zeng, *Electrodeposition of nanoscaled nickel in a reverse microemulsion*, Electrochemistry Communications, 2006, 7, 1142-1146.

[80] H. Zhou, C. Peng, F. C. Peng, A. N. Jing, H. Zou, W. Y. Dong, X. Yan, K. Y. Fei, *Preparation of Ni nanoparticles plating by electrodeposition using reverse microemulsion as template*, Journal of Central South University of Technology, 2010, 17, 40-44.

[81] X. Yang, S. Chen, S. Zhao, D. Li and Houyima, *Synthesis of copper nanorods using electrochemical methods*, Journal of the Serbian Chemical Society, 2003, 67, 743-747.

[82] H. Liwen , H. Zongqian, L. Chang, Y. Zhijing, C. Xiangyu, Y. Hana, J. Shuqiang, *Electrochemical assembly of ZnO architectures via deformation and coalescence of soft colloidal templates in reverse microemulsion*, Royal Society of Chemistry, 2014, 4, 24103-24109.

[83] M. A. López-Quintela, *Synthesis of nanomaterials in microemulsions: formation mechanisms and growth control*, Current Opinion in Colloid and Interface Science, 2003, 7, 137-144.

[84] S. U. Nandanwar, J. Barad, S. Nandwani, M. Chakraborty, *Optimization of process parameters for ruthenium nanoparticles synthesis by (w/o) reverse microemulsion*, Applied Nanoscience, 2015, 5, 321-329.

[85] L. Xiong, A. Manthiram, *Catalytic activity of Pt-Ru alloys synthesized by a microemulsion method in direct methanol fuel cells*, Journal of Solid State Ionics, 2005, 176, 375-392.

[86] X. Zhang, K. Y. Chan, *Water-in-oil microemulsion synthesis of platinum ruthenium nanoparticles, their characterization and electrocatalytic properties*, Journal of Chemistry Material, 2003, 15, 451-459.

[87] M. Jayakumar, K. A. Venkatesan, T. G. Srinivasan, *Electrochemical behavior of fission palladium in 1-butyl-3-methylimidazolium chloride*, Electrochimica Acta, 2007, 52**,** 7121-7127.

[88] K. Soropogui, M. Sigaud, O. Vittori, *A cobalt film electrode for nitride determination in natural water*, Electroanalysis, 2007, 19, 2559-2564.

[89] S. Sultana, *Electrodeposition of nickel from aqueous, reverse micellar and hydrophilic ionic liquid media for electrochemical capacitors*, MS thesis submitted to the Department of Chemistry, University of Dhaka, Bangladesh, 2014.

[90] M. Pettine, F. J. Millero, G. Macci, *Hydrolysis of tin(II) in aqueous solutions,* Analytical Chemistry, 1981,53, 1039-1043.

[91] K. C. Narasimham, S. Vasundara, H. V. Udupa, *Consumption of cetyltrimethylammonium bromide (CTAB) during electrodeposition of lead dioxide*, Canadian Journal of Chemistry, 1975, 53, 3327-3329.

[92] J. J. Keya, M. M. Islam, M. M. Rahman, M. Y. A. Mollah, M. A. B. H. Susan *Effect of a water structure modifier on the aqueous electrochemistry of supramolecular systems: redox-active versus conventional surfactants*, Journal of Electroanalytical Chemistry, 2014, 712, 161-166.

[93] S. Saha, *Electrodeposition of cobalt with tunable morphology from aqueous solution, reverse micelles and hydrophilic ionic liquids*, MS thesis submitted to the Department of Chemistry, University of Dhaka, Bangladesh, 2012.

Abstract

Physicochemical properties: turbidity, conductivity, density, viscosity, refractive index and interfacial tension of micelles, reverse micelles and microemulsions of CTAB and SDS have been correlated with each other and with kinetic results of hydrolysis of CV and Bz and morphology of electrodeposited metals. With increasing ϕ_W, conductivity and density increase while refractive index decreases. Viscosity, turbidity and interfacial tension-ϕ_W profiles show specific patterns due to existence of three different microstructure regions in *w*/*o*, *BC* and *o*/*w* microemulsions with increasing ϕ_W. The structural change from *w*/*o* to *BC* and *BC* to *o*/*w* microemulsions was also confirmed by percolation thresholds obtained by applying percolation theory and percolation scaling law on conductivity results. The CTAB/1-butanol/cyclohexane/water and SDS/1-butanol/cyclohexane/water microemulsions have been used as media for kinetic studies of hydrolysis of CV and Bz. The k' - ϕ_W profiles for hydrolysis of CV and Bz show that the hydrolysis rates are greatly affected by structures and structural transitions of CTAB/1-butanol/cyclohexane/water and SDS/1-butanol/cyclohexane/water microemulsions. The rates are higher in *w*/*o* microemulsions having lower conductivity and viscosity and decrease with ϕ_W. The rates are almost constant in *BC* microemulsions and decrease in *o*/*w* microemulsions having higher conductivity and viscosity. The transition of the hydrolysis rates could be observed at the structural transitions from *w*/*o* to *BC* and from *BC* to *o*/*w* obtained. Electrochemical behaviors of Co and morphology of the electrodeposited Co were also correlated with conductivity of reverse microemulsions. Cathodic peak potential and peak current as well as morphology of electrodeposits change with increasing conductivity of reverse microemulsions.

8.1. Introduction

Microemulsions, as stated in Chapter 1, are systems composed of water, oil, and surfactants, which are single-phase, thermodynamically stable and isotropic. They have been described as consisting of spherical droplets of a disperse phase separated from a continuous phase by a film of surfactant [1, 2]. Because they provide both organic and aqueous environments, microemulsions can simultaneously dissolve both hydrophobic and hydrophilic compounds, each compound being distributed among water, organic solvent, and surfactant film in accordance with its physicochemical properties. Some advantages of microemulsions such as thermodynamic stability, spontaneous formation, easy scale up, large interfacial area, nano-size droplets, isotropy, and low viscosity have made them applicable for many fields of scientific and technological applications: they afford control over the size of synthesized nanoparticles [3-6], they have numerous applications in the fields of solubilization and extraction [7-12], they serve as a suitable media for chemical reactions [13-21] and elctrodeposition of metals [22-33] with definite shape and structure.

In microemulsion systems, a variety of phases can exist in equilibrium with another phase, with each phase having different structures. The phases of microemulsions are changed from Winsor-I (*w*/*o*) to Winsor-II (*o*/*w*) through Winsor-III (*BC*) by systematic variation of salinity at a particular temperature and pressure [34, 35]. The different structures in three phases of microemulsions can be observed by measuring physicochemical properties of microemulsions. The factors that affect the phase transition between different types of microemulsions and physicochemical properties include salinity, temperature, molecular structure and nature of the surfactant and cosurfactant, nature of the oil and the water/oil to surfactant ratio [36-41].

The studies of physicochemical properties: turbidity, conductivity, viscosity, interfacial tension, density and refractive index etc of microemulsions provide information about the possible structures such as *w*/*o*, *BC* and *o*/*w* in different phases of microemulsions [42-50]. The change in different physicochemical properties of microemulsions with different parameter can be correlated with each other. Few studies have been made to correlate the physicochemical properties of microemulsions. Chen et al [51] correlated the properties of microemulsions: viscosity, electrical conductivity, electrochemical diffusion coefficient and polarity measured by fluorescent probe method and reported that all the results evidence the well-known structural transitions: water continuous, bicontinuous and oil continuous in the single monophasic area of the brine/SDS/n-pentanol/dodecane system; premicellar aggregates and water swollen micelles in *w*/*o* area of the brine/SDS/n-heptanol/dodecane system. Paul et al [52] correlated the viscosity and conductivity of biological microemulsion prepared from saffola/sodium di-2-ethyl hexyl sulphosuccinate/hexylamine/water by Walden rule and the Walden product has evidenced noncompansation of ion transport by conduction with viscosity of the medium. Xiaopeng et al [53] shown that optical activity can occur in water/Span80/transformer oil microemulsion under external electric field and correlated the optical activity with the conductivity of microemulsions and reported that a moderate conductivity is essential for the polarization, deformation and alignment of the water droplets of microemulsions, however too large conductivity will make water droplets broken, which weakens the optical anisotropy and optical activity of microemulsion. Begum et al [20] correlated the viscosity, conductivity and droplet sizes of CTAB/1-butanol/cyclohexane/water microemulsions with the kinetic results of the acid hydrolysis of Bz occur in microemulsions.

Despite few studies, there have no reports on the correlation of different physichochemical properties with each other. In this work, the different physicochemical properties of reverse micelles and microemulsions of CTAB/1-butanol/cyclohexane/water and SDS/1-butanol/cyclohexane/water were correlated with each other. The different physicochemical properties of those reverse micelles and microemulsions were also correlated with the kinetic results of the hydrolysis of CV and

Bz and the morphology and structure of the electrodeposited Co studied in those microemulsions.

8.2. Experimental

8.2.1. Materials and Methods

Materials used and methods followed have been described in detail in Sections 2.2.1, 4.2.1, 5.2.1 and 7.2.1.

8.3. Results and Discussion

8.3.1. Correlation of Different Physicochemical Properties of Reverse Micelles and Microemulsions of CTAB and SDS

8.3.1.1. Conductivity and Viscosity

In reverse micelles and microemulsion, macroscopic transport properties: conductivity (σ) and viscosity (η) are controlled by the microstructures. This is due to the fact that the η reflects the magnitude of inter-droplet interactions [54] and σ depends on the local viscosity experienced by the charge carries [55]. The σ and η increases with increasing ϕ_W. The η-ϕ_W profile shows special patterns in different structure of reverse micelles and microemulsions, while the σ increases monotonically with ϕ_W, as shown in Figure 2.3.5-2.3.6 and 2.3.15-2.3.16 for reverse micelles and microemulsion CTAB and SDS, respectively [20]. The sharp increase in the σ with ϕ_W indicates the first appearance of a macroscopic chain of droplets. Additionally, the special patterns in η results corresponds to the different inter-droplets interaction between the water droplets in oil phase and oil droplets in oil phase with increasing ϕ_W [20]. Thus, from η results, three different microstructures can be envisaged in reverse micelles and microemulsions.

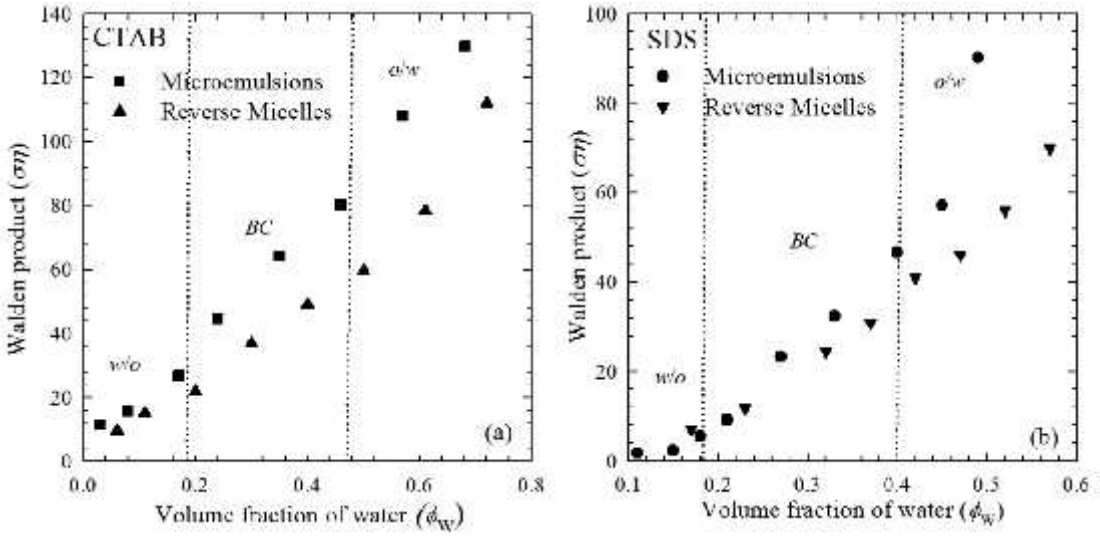

Figure 8.3.1. The $\eta\sigma$ vs. ϕ_W profiles for (a) CTAB/1-butanol/cyclohexane/water microemulsions and CTAB/1-butanol/water reverse micelles and (b) SDS/1-butanol/cyclohexane/water microemulsions and SDS/1-butanol/water reverse micelles.

According to electrolyte theory, the two transport phenomena, η and σ should have an inverse correlation with the product $\eta\sigma$ = constant (Walden rule) [56]. Figure 8.3.1 represents the Walden product ($\eta\sigma$) - ϕ_W profile for (a) CTAB/1-butanol/cyclohexane/water microemulsions and CTAB/1-butanol/water reverse micelles and (b) SDS/1-butanol/cyclohexane/water microemulsions and SDS/1-butanol/water reverse micelles. From Figure 8.3.1, it is apparent that, the Walden product is never constant; the regular increasing trend is a consequence of sharp change in conductivity and viscosity increase can also compensate for it. The variation of $\eta\sigma$ with ϕ_W for both systems shows structural transitions. These transitions are due to special internal structural organization; from *w/o* to *BC* and from *BC* to *o/w* phases, which is reflected on viscosity and not much on conductance [57].

8.3.1.2. Conductivity and Turbidity

The presence of the non-conducting species led to the turbidity (τ) of microemulsions and reverse micelles, so the higher the levels of these species, the lower the σ of the microemulsions and reverse micelles. The inverse relationship between σ and τ was demonstrated by Koning and Ross [58]. Figure 8.3.2 represents the σ and τ of CTAB/1-butanol/water reverse micelles and CTAB/1-butanol/cyclohexane/water microemulsions.

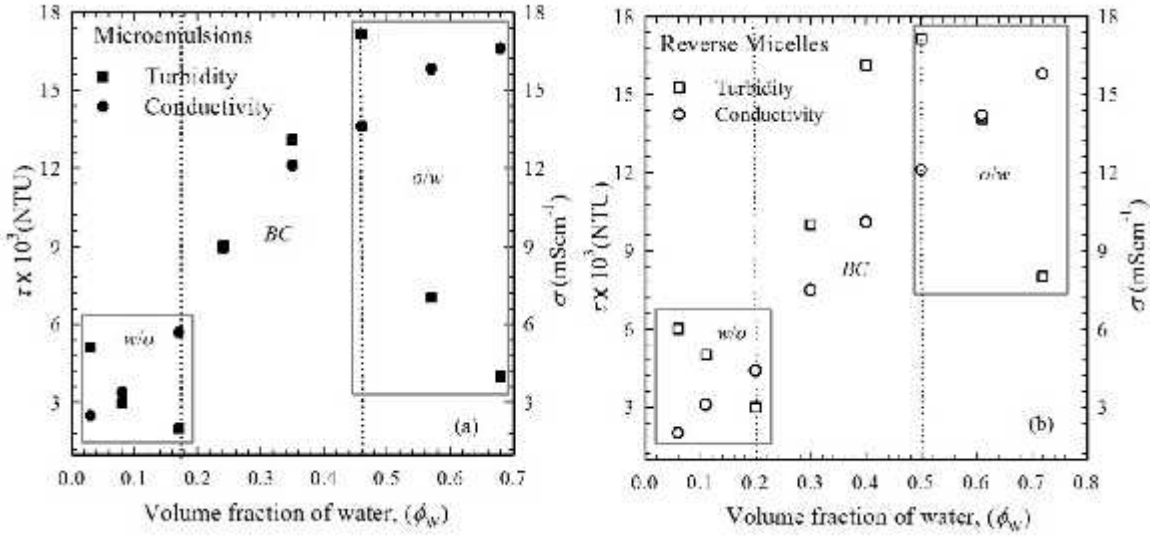

Figure 8.3.2. Relationship between σ and τ for (a) CTAB/1-butanol/cyclohexane/water microemulsions and (b) CTAB/1-butanol/water reverse micelles. The results shown in rectangular box illustrate inverse relationship between σ and τ in *w/o* and *o/w* microemulsions.

At lower value of ϕ_W, the turbidity is high and the conductivity is low due to the presence of higher number of non-conducting species in *w/o* microemulsions. With increasing ϕ_W, the number of conducting species increase as well as the number of non-conducting species decrease causes increase in conductivity and decrease in turbidity. At higher value of ϕ_W, the conducting species are higher in *o/w* microemulsions that give higher

value in conductivity and hence lower value of turbidity. Thus, in droplet phase (such as *w*/*o* and *w*/*o*) microemulsions, the conductivity and turbidity are inversely related but in *BC* microemulsions, the conductivity increases due to the formation of network channel through which the counterions of CTAB easily move and the turbidity increases due to either droplet growth by coalescence, increased attractive interactions, or a combination of these two effects.

Figure 8.3.3. represents the σ and τ of SDS/1-butanol/water reverse micelles and SDS/1-butanol/cyclohexane/water microemulsions. Both the conductivity and turbidity increase in microemulsions for all types of microemulsions but in reverse micelles, the conductivity increases and turbidity decreases in *w*/*o* and *o*/*w* microemulsions due to increase in the number of conducting species and decrease in the number of non-conducting species with increasing ϕ_W.

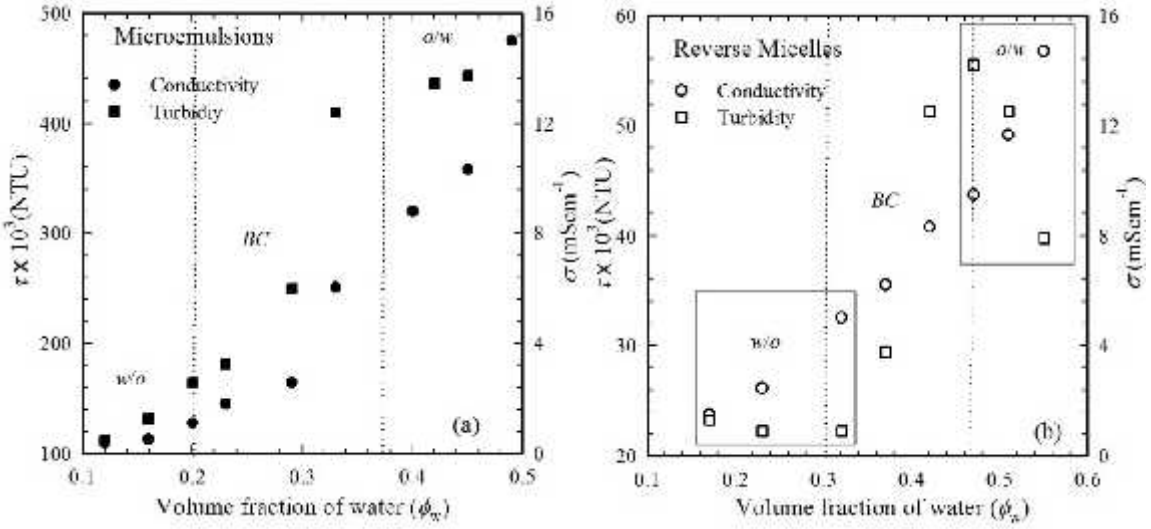

Figure 8.3.3. Relationship between σ and τ for (a) SDS/1-butanol/cyclohexane/water microemulsions and (b) SDS/1-butanol/water reverse micelles. The results shown in rectangular box illustrate inverse relationship between σ and τ in *w*/*o* and *o*/*w* microemulsions.

In contrast, in *BC* phases of reverse micelles, both the conductivity and turbidity increase due to easy movement of the counterions of SDS through network channel formed by aggregation of droplets and droplet growth by coalescence that increased attractive interactions, respectively. Thus, the inverse relationship between the conductivity and turbidity was only observed in droplet phases (such as *w*/*o* and *w*/*o*) of reverse micelles.

8.3.1.3. Viscosity and Turbidity

Both the turbidity and viscosity of reverse micelles and microemulsions depend on the coagulation (or aggregation) of the dispersed droplets and also on the interdroplet interactions. The appearance of the large aggregates leads to an increase in viscosity [59]

and turbidity. Figure 8.3.4. represents the η and τ of CTAB/1-butanol/water reverse micelles and CTAB/1-butanol/cyclohexane/water microemulsions with increasing ϕ_W.

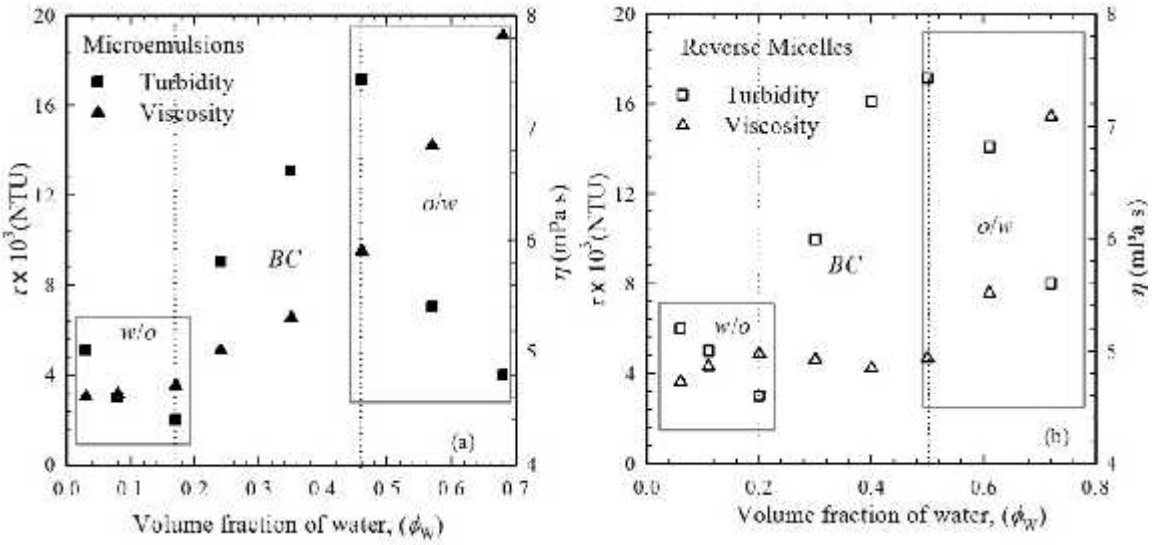

Figure 8.3.4. Relationship between η and τ for (a) CTAB/1-butanol/cyclohexane/water microemulsions and (b) CTAB/1-butanol/water reverse micelles. The results shown in rectangular box illustrate inverse relationship between η and τ in *w*/*o* and *o*/*w* microemulsions.

In *BC* microemulsions, the viscosity and turbidity increase due to the formation of clusters by aggregation of water and 1-butanol droplets in *w*/*o* and *o*/*w* microemulsions with increasing ϕ_W; aggregates immobilize part of water inside them and therefore increase the viscosity. However, in *w*/*o* and *o*/*w* microemulsions, the turbidity and viscosity are inversely related which is reminiscent to the relationship of conductivity and turbidity. The increase in viscosity with increasing ϕ_W is due to the attractive interaction of water droplets in CTAB/1-butanol reverse micelles (*w*/*o* microemulsions) and 1-butanol droplets in CTAB/water micelles (*o*/*w* microemulsions). On the other hand, the turbidity decreases due to the incorporation of water having lower value of turbidity into those microemulsions.

Figure 8.3.5. represents the η and τ of SDS/1-butanol/water reverse micelles and SDS/1-butanol/cyclohexane/water microemulsions with increasing ϕ_W. For microemulsions, both the viscosity and turbidity increase for all types of microemulsions and for reverse micelles, the viscosity and turbidity increase for *BC* microemulsions due to attractive interaction and droplet growth and decrease for *o*/*w* microemulsions due to electrostatic repulsions between the oil droplets in water.

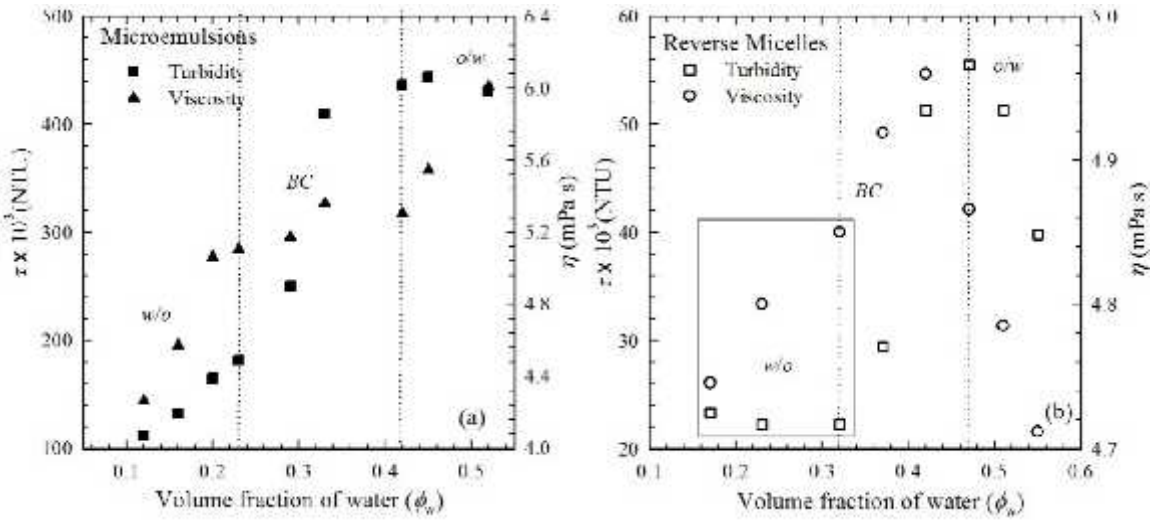

Figure 8.3.5. Relationship between η and τ for (a) SDS/1-butanol/cyclohexane/water microemulsions and (b) SDS/1-butanol/water reverse micelles. The results shown in rectangular box illustrate inverse relationship between η and τ in *w*/*o* and *o*/*w* microemulsions.

8.3.1.4. Turbidity and Droplet Sizes

Turbidity (the interaction between light and droplets) measures the amount of scattered light by droplets [60] in reverse micelles and microemulsions. Moreover, light transmittance is related to the size, shape and composition of the droplets and the wavelength of the incident light. A smaller size droplet interacts with incident light by absorbing the light energy and then radiating the light energy in all directions. This omni directional radiation constitutes the scattering of the incident light. The spatial distribution of scattered light depends on the ratio of droplet size to wavelength of incident light.

Figure 8.3.6 represents the Z-average diameters, d and τ of CTAB/1-butanol/water reverse micelles and CTAB/1-butanol/cyclohexane/water microemulsions with increasing ϕ_W. For both reverse micelles and microemulsions, the *w*/*o* microemulsions having larger droplet sizes give the higher value of turbidity; larger droplets scatter long wavelengths more readily than they scatter short wavelengths of light and light scattering intensifies as the size and number of droplet increases [61]. But as scattered light strikes larger and more droplets, multiple scattering occurs and absorption of light increases gives high value in turbidity.

In other words, droplets much smaller than the wavelength of incident light exhibit a fairly symmetrical scattering distribution with approximately equal amounts of light scattered both forward and backward. In addition, smaller droplets in *o*/*w* microemulsions scatter shorter wavelengths more intensely while having little effect on longer wavelengths as well as absorption of light is lower than in larger droplet results lower

value in turbidity. Furthermore, the decrease in turbidity due to the decrease in the droplet sizes of *w*/*o* and *o*/*w* microemulsions with increasing the ϕ_W for reverse micelles and microemulsions. In *BC* microemulsions, the turbidity increases owing to the presence of clusters having larger size.

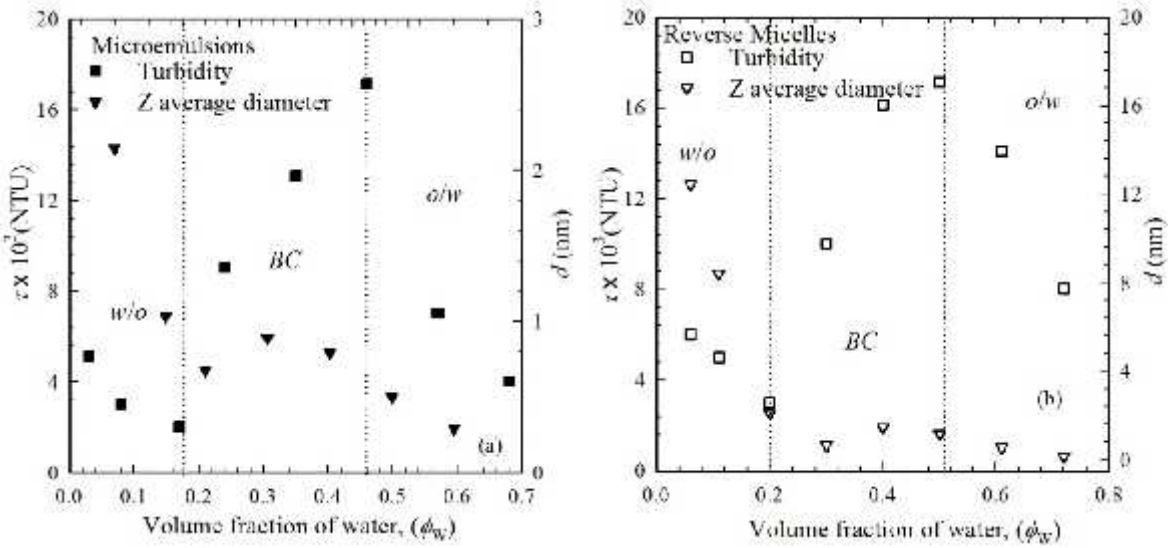

Figure 8.3.6. Relationship between d and τ for (a) CTAB/1-butanol/cyclohexane/water microemulsions and (b) CTAB/1-butanol/water reverse micelles.

8.3.1.5. Turbidity and Interfacial Tension

When the other conditions (temperature, pressure etc) are the same; the turbidity is directly proportional to the concentration of colloidal species (droplets) and attraction between the droplets presence in reverse micelles and microemulsions [62]. The interfacial tension at the interface between oil phase (cyclohexane with 1-butanol) and water, in turn, is also directly proportional to the concentration of colloidal surface-active substances in addition with the content/volume fraction of water or oil phase presence in reverse micelles and microemulsions [63]. Thus, the changes in interfacial tension are linearly correlated with the change in turbidity of reverse micelles and microemulsions.

Figure 8.3.7. represents the change in γ and τ of CTAB/1-butanol/water reverse micelles and CTAB/1-butanol/cyclohexane/water microemulsions with increasing ϕ_W. In *w*/*o* microemulsions, the turbidity decrease due to the reduction of attraction between water droplets [64] and the interfacial tension also decreases (although the concentration of CTAB is constant) due to the decrease in the hydrophobic interaction between the droplet upon addition of water. The turbidity increase in *BC* microemulsions corresponds to the fact that with increasing the ϕ_W, after a certain point ($\phi_W = 0.18$), the interaction between the droplets increases by droplet growth forming larger droplets or clusters and the hydrophobic-hydrophillic interactions in those clusters also increases to cause a slight increase in interfacial tensions. In contrast, the turbidity and interfacial tension show inverse relationship in *o*/*w* microemulsions. This may be due to the repulsion between the

charge surface of CTAB/water micelles among themselves which lowers the turbidity and the hydrophillic-hydrophillic interaction between 1-butanol droplets in water increase brings about an increase in interfacial tension [65].

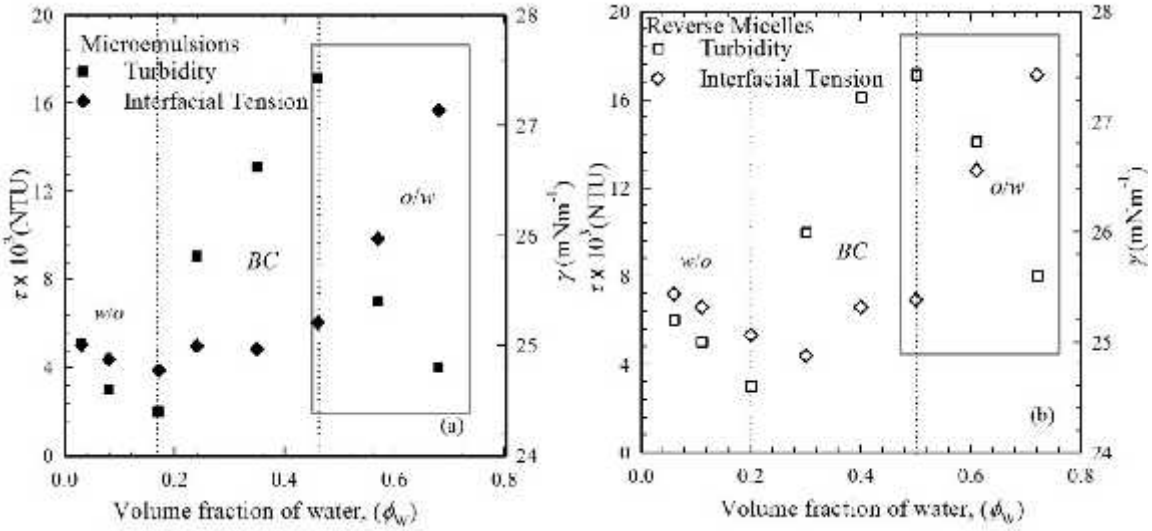

Figure 8.3.7. Relationship between γ and τ for (a) CTAB/1-butanol/cyclohexane/water microemulsions and (b) CTAB/1-butanol/water reverse micelles. The results shown in rectangular box provide inverse relationship between γ and τ in *w*/*o* microemulsions.

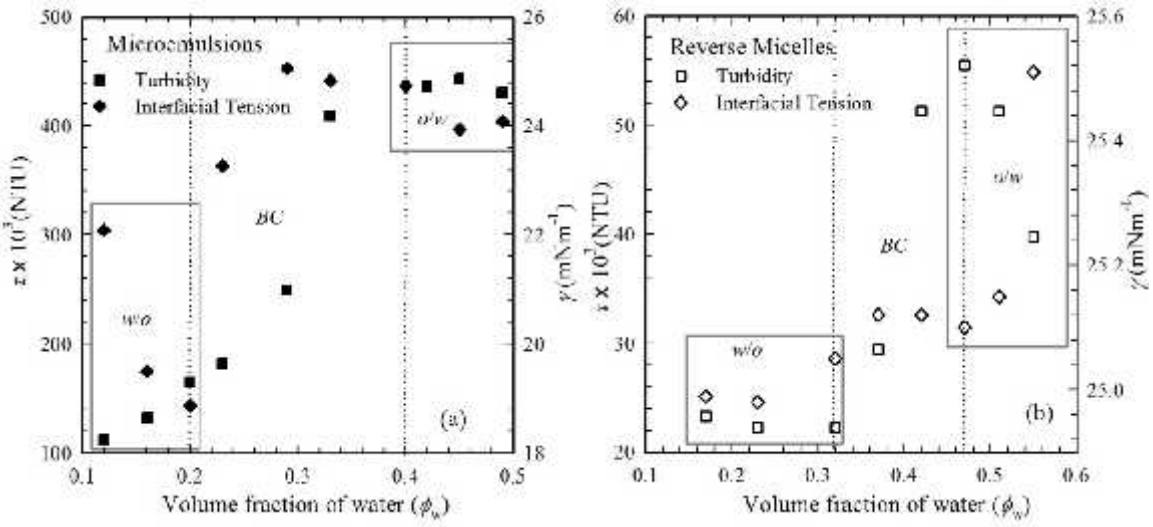

Figure 8.3.8. Relationship between γ and τ for (a) SDS/1-butanol/cyclohexane/water microemulsions and (b) SDS/1-butanol/water reverse micelles. The results shown in rectangular box provide inverse relationship between γ and τ in *w*/*o* microemulsions.

Figure 8.3.8. represents the change in γ and τ of SDS/1-butanol/water reverse micelles and SDS/1-butanol/cyclohexane/water microemulsions with increasing ϕ_W. Only the bicontinuous microemulsions show the linear relationship between the turbidity and interfacial tension otherwise the turbidity is inversely related to the interfacial tension for

w/*o* and *o*/*w* microemulsions due to variation in electrostatic as well as hydrophobic-hydrophillic interaction between the water droplets in CTAB/1-butanol reverse micelles and 1-butanol droplets in CTAB/water micelles, respectively.

8.3.1.6. Viscosity and Interfacial Tension

The viscosity and interfacial tension both depend on the interdroplet interaction in reverse micelles and microemulsions. But, the viscosity is determined by the interaction between the droplets, while the interfacial tension is determined by the difference of the interactions between the droplets themselves and interaction of these droplets with the interface of oil/water [66]. So, there might be a tendency for both viscosity and interfacial tension to increase with increasing strength of interdroplet interactions by increasing the volume fraction of water or oil. Figure 8.3.9. represents the change in γ and η of CTAB/1-butanol/water reverse micelles and CTAB/1-butanol/cyclohexane/water microemulsions with increasing ϕ_W. In bicontinuous and *o*/*w* microemulsions, the viscosity shows linear relationship with the interfacial tension while in *w*/*o* microemulsions, they are inversely related due to the decrease in hydrophobic-hydrophobic interaction and attractive interaction between the water droplets.

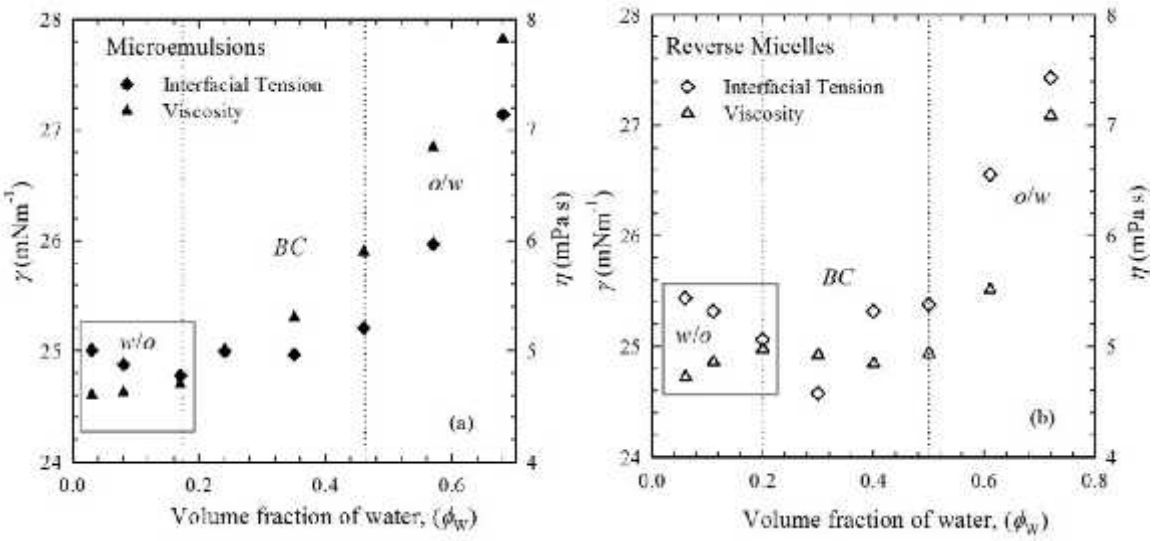

Figure 8.3.9. Relationship between γ and η for (a) CTAB/1-butanol/cyclohexane/water microemulsions and (b) CTAB/1-butanol/water reverse micelles. The results shown in rectangular box provide inverse relationship between γ and η in *w*/*o* microemulsions.

Figure 8.3.10. represents the change in γ and η of SDS/1-butanol/water reverse micelles and SDS/1-butanol/cyclohexane/water microemulsions with increasing ϕ_W. In microemulsions, only bicontinuous region show linear relationship with the interfacial tension and in *w*/*o* and *o*/*w* region, they are inversely related. The viscosity and interfacial tension increase with increasing ϕ_W for both the bicontinuous and *w*/*o* regions of reverse micelles.

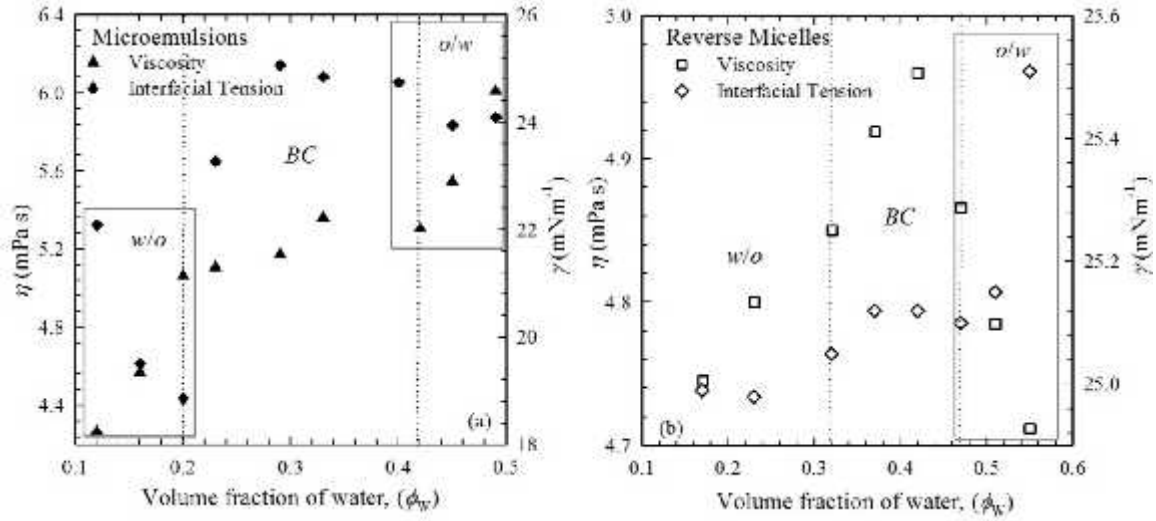

Figure 8.3.10. Relationship between γ and η for (a) SDS/1-butanol/cyclohexane/water microemulsions and (b) SDS/1-butanol/water reverse micelles. The results shown in rectangular box provide inverse relationship between γ and η in *o/w* microemulsions.

8.3.2. Correlation of Physicochemical Properties of Reverse Micelles and Microemulsions of CTAB with Kinetic Results of Hydrolysis of CV and Bz

Hydrolysis of CV and Bz was studied by using CTAB/1-butanol/cyclohexane/water microemulsions and CTAB/1-butanol/water reverse micelles as reaction media. The k'-ϕ_W profiles for both reactions show different patterns in diverse structures of reverse micelles and microemulsions. The physicochemical properties also changes with different pattern with increasing ϕ_W. Thus, kinetic results can be correlated with the physicochemical properties of reverse nicelles and microemulsions. As the rate of reaction depends on the conductivity and viscosity of the media, the reaction rates of the hydrolysis of CV and Bz are well correlated with the conductivity and viscosity of microemulsions:

8.3.2.1. Conductivity with Kinetic Results of Hydrolysis of CV and Bz

Figure 8.3.11. represents the change in σ of CTAB/1-butanol/water reverse micelles and CTAB/1-butanol/cyclohexane/water microemulsions and k' of the hydrolysis of CV and Bz occurred in those media with increasing ϕ_W. The reaction rates for both reaction decrease and conductivity increases with increasing ϕ_W.

The conductivity increases due to increase in number of free counterions of CTAB as well as the mobility of those counterions of reverse micelles and microemulsions. At lower value of ϕ_W, the conductivity is low due to the presence of *w/o* microemulsions where the counterions of CTAB are trapped inside the core and cannot move easily and thereby results in higher value of k'. The reactants come to closer approach to each other easily. The conductivity increases with increasing the ϕ_W as a result of the formation of network channel by aggregation of water droplets and the k' gradually decreases: complex structure of the media inhibits the reaction. The rate of the reaction is low at the higher

value of ϕ_W due to the presence of easily movable free counterions of CTAB, which creates difficulty to occur the reaction. Thus, with increasing the conductivity of the reverse micelles and microemulsions, the k' of the hydrolysis of CV and Bz in those reverse micelles and microemulsions decreases.

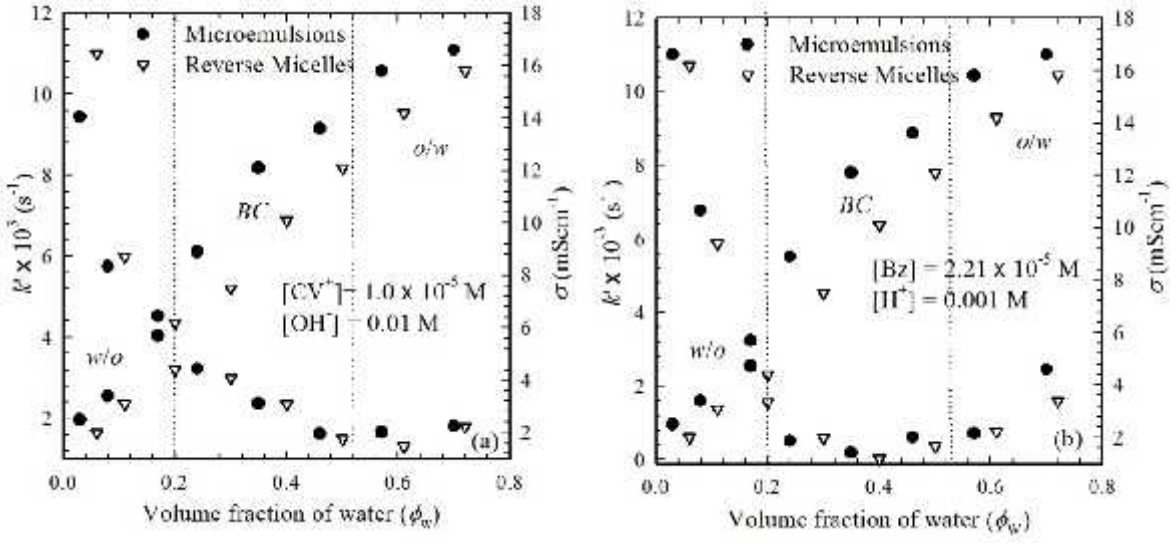

Figure 8.3.11. The change in σ of CTAB/1-butanol/water reverse micelles and CTAB/1-butanol/cyclohexane/water microemulsions and k' of the hydrolysis of (a) CV and (b) Bz occurred in those media with increasing ϕ_W.

8.3.2.2. Viscosity with Kinetic Results of Hydrolysis of CV and Bz

Figure 8.3.12. represents the change in η of CTAB/1-butanol/water reverse micelles and CTAB/1-butanol/cyclohexane/water microemulsions and k' of the hydrolysis of CV and Bz occurred in these media with increasing ϕ_W.The viscosity of the reverse micelles and microemulsions largely depends on aggregation of the droplets and interdroplet interaction which largely influences the flow behavior. At lower value of ϕ_W, the viscosity low due to the presence of water droplets in 1-butanol which have low viscosity and increases with increasing ϕ_W corresponds to the attractive interaction and aggregation of water droplets. Consequently, the k' of both reactions have higher values at low ϕ_W where the reactants easily collide each other to and then decreases with ϕ_W. In contrast, at higher value of ϕ_W, the viscosity is higher and collision of the reactants is difficult and consequently results in lower value of the reaction rate. Thus, with increasing viscosity of the reverse micelles and microemulsions, the k' of the hydrolysis of CV and Bz in those reverse micelles and microemulsions decrease.

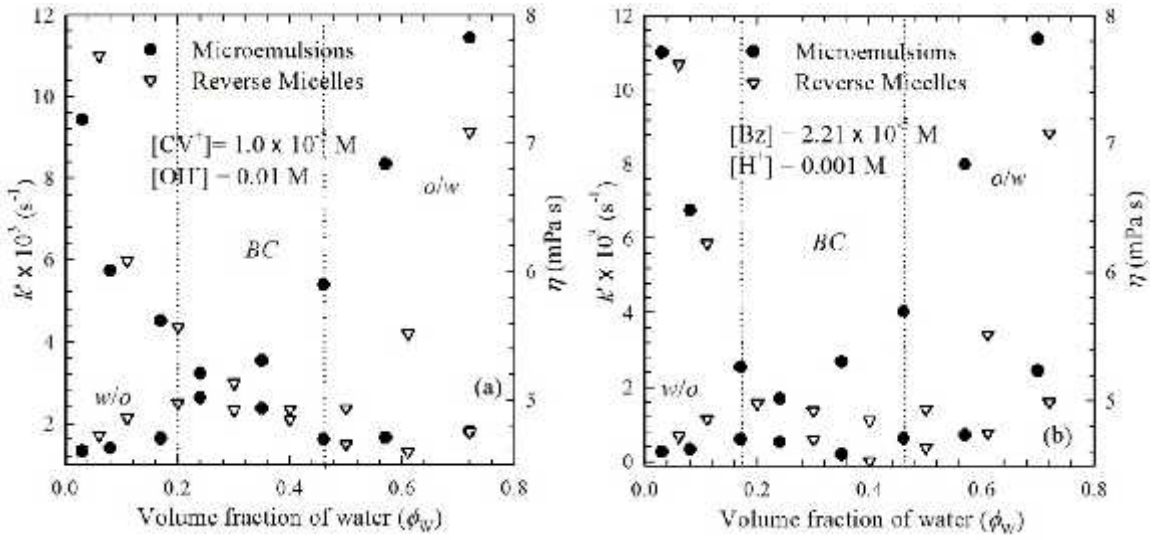

Figure 8.3.12. The change in η of CTAB/1-butanol/water reverse micelles and CTAB/1-butanol/cyclohexane/water microemulsions and k' of the hydrolysis of (a) CV and (b) Bz occurred in those media with increasing ϕ_W.

8.3.3. Correlation of Physicochemical Properties of Reverse Micelles and Microemulsions of SDS with Kinetic Results of Hydrolysis of CV

Hydrolysis of CV was also studied by using SDS/1-butanol/cyclohexane/water microemulsions and SDS/1-butanol/water reverse micelles as reaction media. The k'- ϕ_W profiles shows different patterns in diverse structures of reverse micelles and microemulsions. The physicochemical properties also changes with different patterns with increasing the ϕ_W. Thus, kinetic results can be correlated with the physicochemical properties of reverse micelles and microemulsions.

8.3.3.1. Conductivity with Kinetic Results of Hydrolysis of CV

Figure 8.3.13. represents the change in σ of SDS/1-butanol/water reverse micelles and SDS/1-butanol/cyclohexane/water microemulsions and k' of the hydrolysis of CV in those media with increasing ϕ_W. The reaction rates decrease and conductivity increases with increasing ϕ_W. At lower value of ϕ_W, the k' is high due to the lower conductivity of reverse micelles and microemulsions where the counterions of SDS are trapped into the water droplets and cannot move easily and the reactants come to close each other easily. With increasing ϕ_W, the network channel is formed by aggregation of water droplets and the k' gradually decreases. The presence of easily movable free counterions of SDS in *o*/*w* microemulsions (at high value of ϕ_W) give higher value of conductivity and lower value of k'. Thus, with increasing conductivity of the reverse micelles and microemulsions, the k' of the hydrolysis of CV and Bz in those reverse micelles and microemulsions decreases.

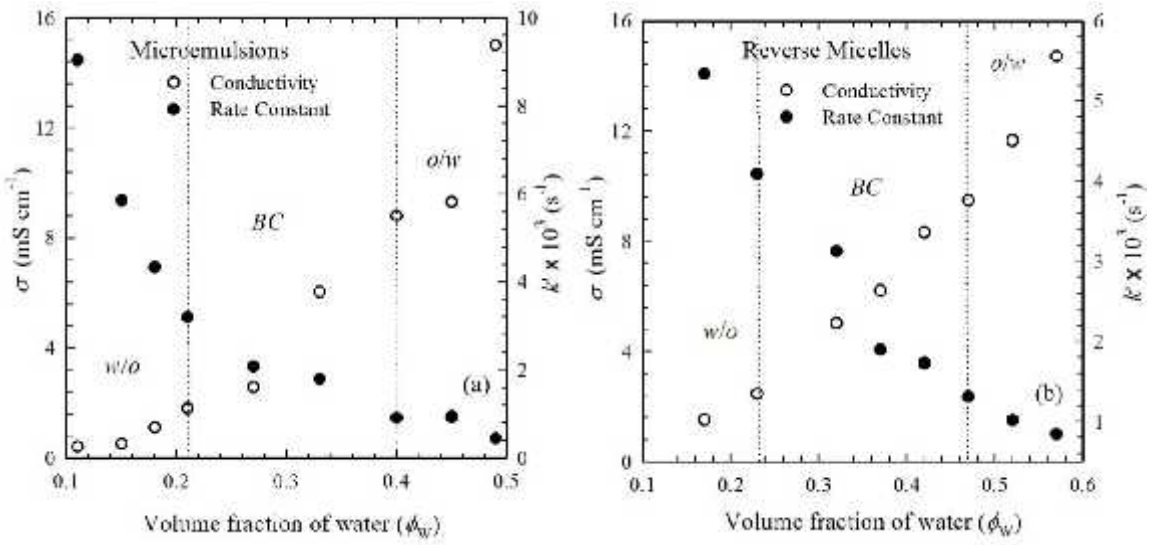

Figure 8.3.13. The change in σ of (a) SDS/1-butanol/cyclohexane/water microemulsions and (b) SDS/1-butanol/water reverse micelles and k' of the hydrolysis of CV in those media with increasing ϕ_W.

8.3.3.2. Viscosity with Kinetic Results of Hydrolysis of CV

Figure 8.3.14. represents the change in η of SDS/1-butanol/water reverse micelles and SDS/1-butanol/cyclohexane/water microemulsions and k' of the hydrolysis of CV occurred in those media with increasing ϕ_W.

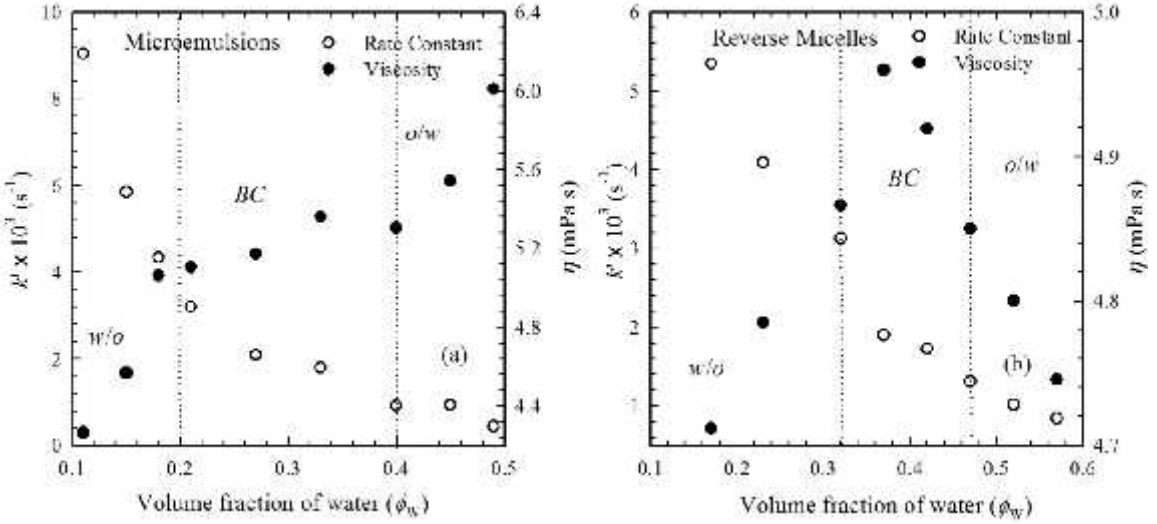

Figure 8.3.14. The change in η of (a) SDS/1-butanol/cyclohexane/water microemulsions and (b) SDS/1-butanol/water reverse micelles and k' of the hydrolysis of CV in those media with increasing ϕ_W.

In SDS/1-butanol/cyclohexane/water microemulsions, the k' decreases and viscosity increases with increasing ϕ_W which is similar to that observed for CTAB/1-

butanol/cyclohexane/water microemulsions. In contrast, both the viscosity of SDS/1-butanol/water reverse micelles and the *k*' decreases to correspond to electrostatic repulsions between the charged surface of 1-butanol droplets in SDS/water micelles and the reactants OH^- in the reaction.

8.3.4. Correlation of Physicochemical Properties of Reverse Microemulsions of CTAB and SDS with Electrochemical Behavior of Co

The electrochemical behavior of Co was studied in reverse microemulsions of CTAB and SDS with increasing w_o by cyclic voltammetry using CuE as working electrode, an Ag/AgCl electrode as reference electrode whereas a spiral platinum wire as counter electrode. The cathodic peak potential, E_{pc} and cathodic peak current, i_{pc} of the reduction of metal ions to metal can be correlated with the conductivity of the reverse microemulsions.

8.3.4.1. Conductivity with Electrochemical Behavior of Co^{2+}

Figure 8.3.15. represents the change in the E_{pc} for the reduction of Co^{2+} and conductivity of CTAB/1-butanol/water and SDS/1-butanol/water reverse microemulsions with increasing w_o. It appears from Figure 8.3.13 that the conductivity of reverse micelles and microemulsions of CTAB and SDS increases and the E_{pc} for the reduction of Co^{2+} decreases with increasing w_o. This corresponds to the fact that more conductive media permit to decrease potential [67].

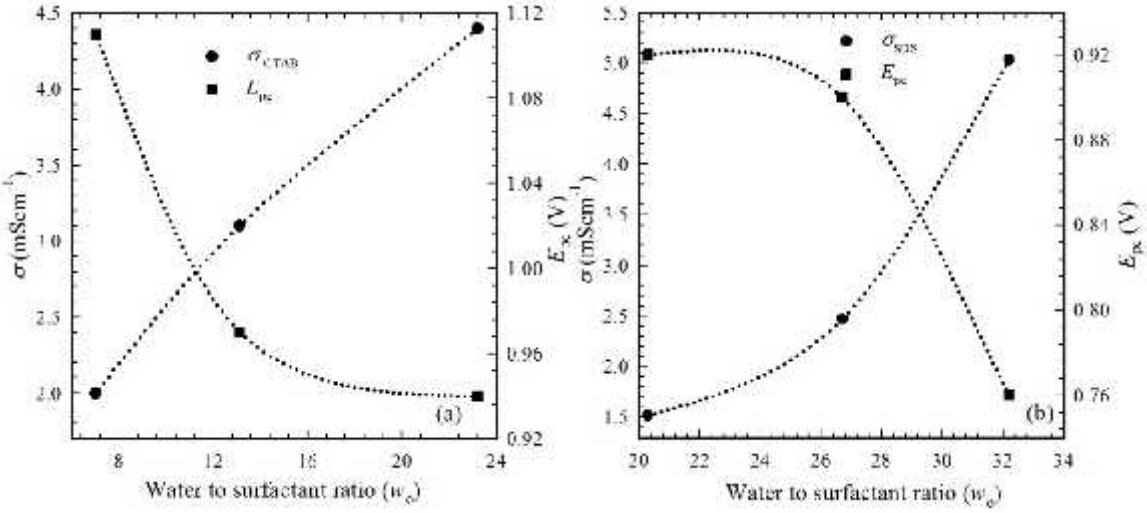

Figure 8.3.15. The change in E_{pc} for reduction of Co^{2+} and conductivity of (a) CTAB/ 1-butanol/water and (b) SDS/1-butanol/water reverse microemulsions with increasing w_o.

Figure 8.3.16. represents the change in i_{pc} for reduction of Co^{2+} and conductivity of CTAB/1-butanol/water and SDS/1-butanol/water reverse microemulsions with increasing w_o.

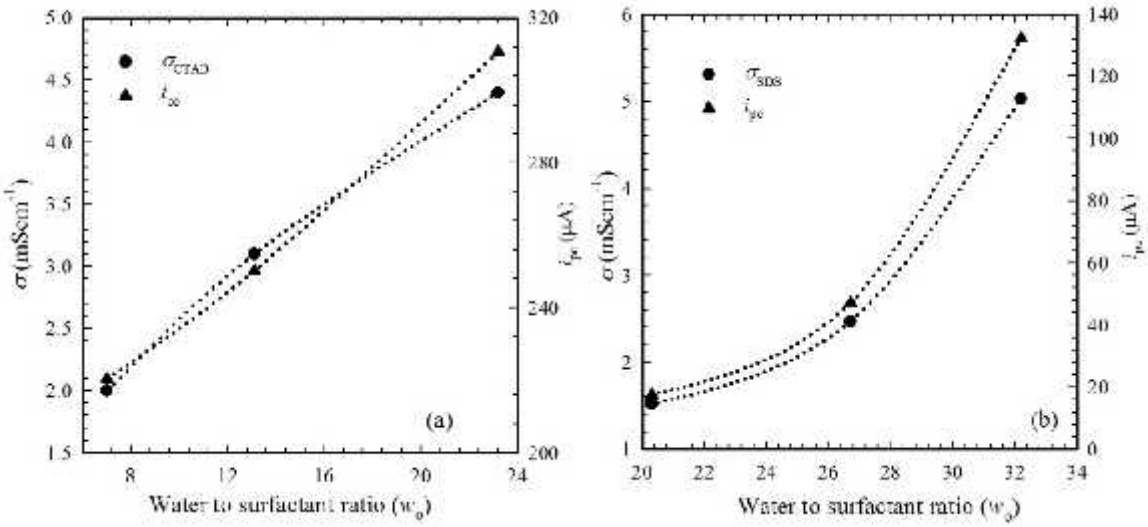

Figure 8.3.16. The change in i_{pc} for reduction of Co^{2+} and conductivity of (a) CTAB/ 1-butanol/water and (b) SDS/1-butanol/water reverse microemulsions with increasing w_o.

With increasing w_o, the hydrophillic core sizes as well as the conductivity of reverse microemulsions increases due to droplet fusion-fission mechanism. As a result, the concentration of Co^{2+} is diluted with increasing w_o and the rate of diffusion of Co^{2+} as well as deposition will be faster resulting in high value of cathodic peak current. At lower value of w_o, the Co^{2+} ions are effectively trapped into the core of the reverse microemulsions and the rate of diffusion as well as the deposition will be slower to give lower value of peak current.

8.3.4.2. Conductivity with Morphology of Electrodeposited Co

Figure 8.3.17. represents the change in structures of the electrodeposited Co and conductivity of CTAB/1-butanol/water reverse microemulsions with increasing w_o.

SEM images displayed in Figure 8.3.17 shows that morphology of the deposited Co has been changed from matrix like structure with nanorods to flower like structure to star like structure with increasing w_o. Such structural variation of the deposited Co with w_o of reverse microemulsions is marked due to change in diffusion rate as well as deposition rate which depends on the conductivity of the media. Reverse microemulsions with high w_o having higher value of conductivity can accommodate more Co^{2+} ions causing dilution of the concentration of Co^{2+}. Therefore, the rate of diffusion as well as deposition will be faster. But the diffusion rate decreased gradually for reverse microemulsions of low w_o having lower conductivity. This is due to the fact that at lower value of w_o, thehydrophilic cores do not have sufficient volume and effective trapping of Co^{2+} species within such hydrophilic cores can take place. Due to such effective trapping with increased hydrophilic interaction, dragging out of Co^{2+} species becomes difficult which results in the deposition at a significantly slower rate in a more controlled way.

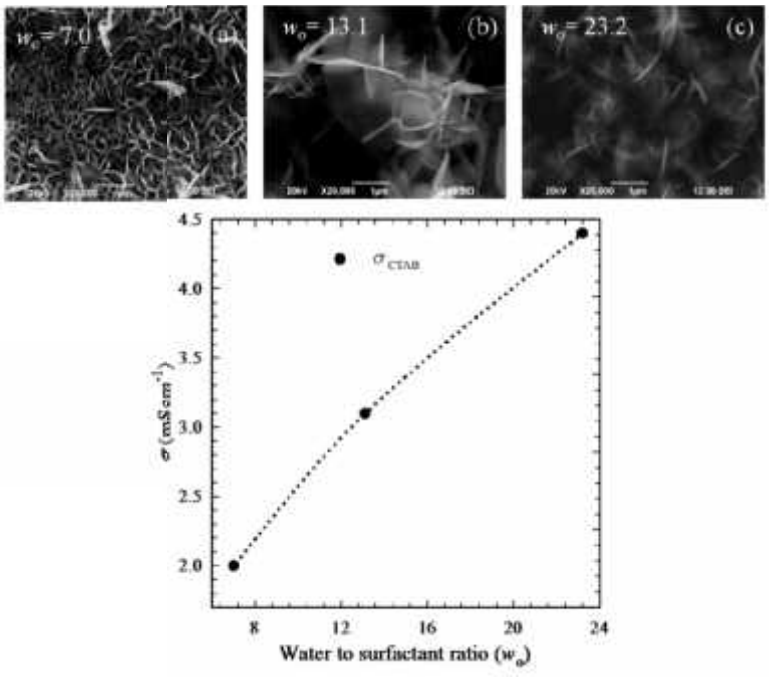

Figure 8.3.17. The change in structures of the electrodeposited Co and conductivity of CTAB/1-butanol/water reverse microemulsions with increasing w_o.

8.4. Conclusions

Different physicochemical properties such as turbidity, conductivity, viscosity and interfacial tension and sizes of the reverse micelles and microemulsions of CTAB and SDS are interrelated with each other. Conductivity increases and viscosity, turbidity, interfacial tension and droplet sizes show different patterns in three regions: water in oil, bicontinuous and oil in water of those reverse micelles and microemulsions. Viscosity and conductivity resulted correlated by Walden rule indicates that Walden products are not constant for reverse micelles and microemulsions. Turbidity, viscosity, interfacial tension and droplet sizes shows special correlation with each other for different phases of reverse micelles and microemulsions. The reaction rates of hydrolysis of CV and Bz markedly changes in three regions of reverse micelles and microemulsions which can be correlated with conductivity and viscosity and the k' decreases with increasing conductivity and viscosity of reverse micelles and microemulsions. Electrochemical behavior of Co is also correlated with conductivity of reverse microemulsions of CTAB and SDS and cathodic peak potential decreases and cathodic peak current for reduction of Co increases with increasing conductivity of reverse microemulsions. Morphology and structure of electrodeposited Co also correlated well with conductivity of reverse micremulsions. Thus, physicochemical properties of reverse micelles and microemulsions have excellent correlation with each other and with kinetic results of hydrolysis reactions and morphology of electrodeposited metals.

References

[1] G. M. Eccleston, *Microemulsions, Encyclopedia of pharmaceutical technology.* Marcel Dekker, NewYork, 1992, 9, 375.

[2] M. Fanun, Microemulsions: *Properties and application,* Surfactant science series, vol. 144, CRC press.

[3] A. K. Ganguli, T. Ahmad, S. Vaidya, J. Ahmed, *Microemulsion route to the synthesis of nanoparticles*, Pure and Applied Chemistry, 2008, 80, 2451-2477.

[4] M. A. Malika, M. Y. Wanib, M. A. Hashima, *Microemulsion method: A novel route to synthesize organic and inorganic nanomaterials: 1st nano update*, Arabian Journal of Chemistry, 2012, 5, 397-417.

[5] M. A. Lo´pez-Quintela, *Synthesis of nanomaterials in microemulsions: formation mechanisms and growth control*, Current Opinion in Colloid and Interface Science 2003, 8, 137-144.

[6] S. F. Chin, A. Azman, S. C. Pang, *Size controlled synthesis of starch nanoparticles by a microemulsion method*, Journal of Nanomaterials, 2014, 2014, 1-7.

[7] V. Tchakalova, F. Testard, K. Wong, A. Parker, D. Benczédi, T. Zemb, *Solubilization and interfacial curvature in microemulsions: I. Interfacial expansion and co-extraction of oil*, Colloids and Surfaces A Physicochemical and Engineering Aspects, 2008, 331, 31-39.

[8] M. Radi, S. Abbasi, Z. Hamidi, M. H. Aziz, *Development of a new method for extraction of canola oil using lecithin based microemulsion systems*, Food Technologies, 2013, 24, 70-72.

[9] P. Kumar, K. L. Mittal, *Handbook of microemulsion science and technology*, Mercel Dekker, CRC press, New York, 1999.

[10] B. K. Paul, S. P. Moulik, *Uses and application of microemulsions*, Current Science, 2001, 80, 990-1001.

[11] M. C. K. Oliveira, E. F. Lucas, G. Gonzalez, J. F. Oliveira, *Heavy oil fraction removal from sand using hydrotropes containing oil-in-water microemulsions*, Progress Colloid Polymer Science, 2004, 128, 288-292.

[12] A. Naksuk, D. A. Sabatinib, C. Tongcumpoua, *Microemulsion-based palm kernel oil extraction using mixed surfactant solutions*, Industrial Crops and Products, 2009, 30, 194-198.

[13] J. Hao, *Effect of the structures of microemulsions on chemical reactions*, Colloid and Polymer Science, 2000, 278,150-154.

[14] F. Tafesse, K. Eguzozie, *Efficient hydrolysis of 4-nitrophenylphosphate catalyzed by copper bipyridyl in microemulsions*, Ecotoxicology and environmental safety, 2009, 72, 954-959.

[15] Z. Y. Chen, J. H. Zhao, W. He, X. Qinan, W. G. Shen, *Study of association thermodynamics between crystal violet and sodium bis(2-ethylhexyl)sulfosuccinate and kinetics of basic fading of crystal violet in microemulsions*, International Journal of Chemical Kinetics, 2008, 40, 294-300.

[16] M. Valientie, E. Rodenas, *Influence of CTAB/alkanol/cyclohexane w/o microemulsions on the basic hydrolysis of crystal violet*, Colloid and Polymer Science, 1993, 271, 494-498.

[17] A. B. Mirgorodskaya, F. G. Valeeva, L. A. Kudryavtseva, N. N. Vylegzhanina, Yu. F. Zuev, *Reaction of carboxylic acid esters with phenolates in oil-in-water microemulsions based on cetyltrimethylammonium bromide*, *Russian Journal of General Chemistry,* 2006, 76, 590-595.

[18] K. K. Ghosh, M. L. Satnami, *Nucleophilic substitution reaction of carboxylate and phosphate esters with hydroxamate ions in microemulsions*, Colloids and Surfaces A: Physicochemical and Engineering Aspects*,* 2006, 274, 125-129.

[19] M. Häger, F. Currie, K. Holmberg, *A nucleophilic substitution reaction in microemulsions based on either an alcohol ethoxylate or a sugar surfactant*, Colloids and Surfaces A: Physicochemical and Engineering Aspects, 2004, 250,163-170.

[20] F. Begum, M. Y. A. Mollah, M. M. Rahman, M. A. B. H. Susan, *Acid hydrolysis of bromazepam catalyzed by micelles, reverse micelles, and microemulsions*, Journal of Chemistry, 2015, 2015, 1-10.

[21] F. Begum, M. Y. A. Mollah, M. M. Rahman, M. A. B. H. Susan, *Kinetics of the alkaline hydrolysis of crystal violet in micelles, reverse micelles and microemulsions of cetyltrimethylammonium bromide*, Journal of Bangladesh Chemical Society, 2011, 24, 173-184.

[22] D. A. Kaplin, S. Qutubuddin, *Electrodeposition of pyrrole into a porous film prepared by microemulsion polymerisation*, Synthetic metals, 1994, 63,187-194.

[23] C. Fu, H. Zhou, D. Xie, L. Sun, Y. Yin, J. Chen, Y. Kuang, *Electrodeposition of gold nanoparticles from ionic liquid microemulsion*, Colloid and Polymer Science, 2010, 288, 1097-1103.

[24] A. Serrà, E. Gómez, G. Calderó, J. Esquena, C. Solans, E. Vallés, *Microemulsions for obtaining nanostructures by means of electrodeposition method*, Electrochemistry Communications, 2013, 27, 14-18.

[25] A. Serrà, E. Gómez, G. Calderó, J. Esquena, C. Solans, E. Vallés, *Conditions that bicontinuous microemulsions must fulfill to be used as template for electrodeposition of nanostructures*, Journal of Electroanalytical Chemistry, 2014, 720, 101-106.

[26] H. Zhou, C. Peng, S. Jiao, W. Zeng, *Electrodeposition of nanoscaled nickel in a reverse microemulsion*, Electrochemistry Communications, 2006, 8, 1142-1146.

[27] H. Zhou, C. Peng, F. C. Peng, A. N. Jing, H. Zou, W. Y. Dong, X. Yan, K. Y. Fei, *Preparation of Ni nanoparticles plating by electrodeposition using reverse microemulsion as template*, Journal of Central South University of Technology, 2010, 17, 40-44.

[28] X. Yang, S. Chen, S. Zhao, D. Li and Houyima, *Synthesis of copper nanorods using electrochemical methods*, Journal of the Serbian Chemical Society, 2003, 68, 843-847.

[29] H. Liwen , H. Zongqian, L. Chang, Y. Zhijing, C. Xiangyu, Y. Hana, J. Shuqiang, *Electrochemical assembly of ZnO architectures via deformation and coalescence of soft colloidal templates in reverse microemulsion*, Royal Society of Chemistry, 2014, 4, 24103-24109.

[30] M. A. López-Quintela, *Synthesis of nanomaterials in microemulsions: formation mechanisms and growth control*, Current Opinion in Colloid and Interface Science, 2003, 8, 137-144.

[31] S. U. Nandanwar, J. Barad, S. Nandwani, M. Chakraborty, *Optimization of process parameters for ruthenium nanoparticles synthesis by (w/o) reverse microemulsion*, Applied Nanoscience, 2015, 5, 321-329.

[32] L. Xiong, A. Manthiram, *Catalytic activity of Pt-Ru alloys synthesized by a microemulsion method in direct methanol fuel cells*, Journal of Solid State Ionics, 2005, 176, 385-392.

[33] X. Zhang, K. Y. Chan, *Water-in-oil microemulsion synthesis of platinum ruthenium nanoparticles, their characterization and electrocatalytic properties*, Journal of Chemistry Material, 2003, 15, 451-459.

[34] A. Bera, K. Ojha, T. Kumar, A. Mandal, *Phase behavior and physicochemical properties of (sodium dodecyl sulfate + brine + propan-1-ol + heptane) microemulsions*, Journal of Chemical and Engineering Data, 2012, 57, 1000-1006.

[35] A. Bera, A. Mandal, T. Kumar, *Physicochemical characterization of anionic and cationic microemulsions: water solubilization, particle size distribution, surface tension, and structural parameters*, Journal of Chemical and Engineering Data, 2014, 59, 2490-2498.

[36] J. L. Chai, J. R. Zhao, Y. H. Gao, X. D. Yang, C. J. Wu, *Studies on the phase behavior of the microemulsions formed by sodium dodecyl sulfonate, sodium dodecyl sulfate and sodium dodecyl benzene sulfonate with a novel fishlike phase diagram*, Colloids Surfaces A, 2007, 302, 31-35.

[37] L. Chen, Y. Shang, H. Liu, Y. Hu, *Middle-phase microemulsion induced by brine in region of low cationic gemini surfactant content*, Colloids Surfaces A , 2007, 305, 29-35.

[38] P. A. Winsor, *Solvent properties of amphiphilic compounds*, Butterworths Scientific Publication Limited, London, 1954.

[39] M. G. Aarra, H. Hoiland, A. Skauge, *Phase behavior and salt partitioning in two-and three-phase anionic surfactant microemulsion systems: part I, phase behavior as a function of temperature*, Journal of Colloid Interface Science, 1999, 215, 201-215.

[40] M. Nakamae, M. Abe, K. Ogino, *The effects of alkyl chain lengths of sodium alkyl sulfates and n-alkanes on microemulsion formation*, Journal of Colloid Interface Science, 1988, 31, 466-472.

[41] R. Sripriya, K. Muthu Raja, G. Santhosh, M. Chandrasekaran, M. Noel, *The effect of structure of oil phase, surfactant and co-surfactant on the physicochemical and electrochemical properties of bicontinuous microemulsion*, Journal of Colloid Interface Science, 2007, 314, 712-717.

[42] K. Zielinska, K. A. Wilk, A. Jezierski, T. Jesionowski, *Microstructure and structural transition in microemulsions stabilized by aldonamide-type surfactants*, Journal of Colloid and Interface Science, 2008, 321, 408-417.

[43] V. Patidar, A. Chandra, M. Singh, R. K. Kale, *Physiochemical and phase behaviour study of jatropha curcus oil - ethanol microemulsion fuels using sorbitane fatty esters*, International Journal of Renewable and Sustainable Energy, 2014, 3, 13-19.

[44] J. Kestin, M. Sokolov, W. A. Wakeham, *Viscosity of liquid water in the range - 8 ^{o}C to 150 ^{o}C*, Journal of Physical Chemistry Reference Data, 1978, 7, 941-948.

[45] B. K. Paul, S. P. Moulik, *The viscosity behaviours of microemulsions: an overview*, Proceedings of the Indian National Science Academy, 2000, 66, 499 - 519.

[46] A. Zvonar, B. Rozman, M. B. Rogac, M. Gasperlin, *The influence of microstructure on celecoxib release from a pharmaceutically applicable system*, Acta Chimica Slovenica, 2009, 56, 131-138.

[47] L. M. Kushner, W. D. Hubbard, R. A. Parker, *Turbidity and viscosity measurements on Some cationic detergents in water and in sodium chloride solutions*, Journal of Research of the National Bureau of Standards,1957, 59, 113-119.

[48] A.V. Sineva, D. S. Ermolatev, A. V. Pertsov, *Structural transformations in a water-n-octane + chloroform-sodium dodecyl sulfate-n-pentanol microemulsion*, Colloid Journal, 2007, 69, 89-94.

[49] M. Fanun, Z. Ayad , S. Mudalal , S. Dahoah, D. Meltzer, M. Schwarze, R. Schomacker, J. Blum, *Characterization of water/sucrose laurate/n-propanol/allylbenzene microemulsions*, Journal of Surfactants and Detergents, 2012, 15, 505-512.

[50] S. K. Mehta, Kawaljit, *Isentropic compressibility and transport properties of CTAB-alkanol-hydrocarbon-water microemulsion systems*, Colloids and Surfaces A: Physicochemical and Engineering Aspects, 1998, 136, 35 - 41.

[51] J. Georges, J. W. Chen, *Microemulsions studies: Correlation between viscosity, electrical conductivity and electrochemical and fluorescent probe measurements*, Colloid and Polymer Science, 1986, 264, 896-902.

[52] B. K. Paul, S. P. Moulik, *Biological microemulsions: Part III—The formation characteristics and transport properties of saffola-aerosol OT-hexylamine-water system*, Indian Journal of Biochemistry and Biophysics, 1991, 28, 174-183.

[53] Z. Xiaopeng, Z. Qian, X. Liqin, *Optical activity of microemulsion induced by electric field and its tunable behaviors*, Science in China, 2003, 46, 164-172.

[54] C. Gamba, L. Sepulvada, *High viscosities of cationic and anionic micellar solutions in the presence of added*, Journal of Colloid and Interface Science, 1986, 113, 566-576.

[55] K. L. Mittal, B. Lindman, *Surfactants in solutions*, Plenum, New York, 1984.

[56] R. A. Robinson, R. H. Stokes, *Electrolyte solution*, Butterworths, London, 1965.

[57] L. Mukhopadhyay, P. K. Bhattacharya, S. P. Moulik, *Water-induced precipitation of cholesterol dissolved in organic solvents in the absence and presence of surfactants and salts*, Indian Journal of Biochemistry and Biophysics, 1989, 26,178-185.

[58] N. Koning, J. C. Ross, *The continued influence of organic pollution on the water quality of the turbid modder River*, Water S.A. 1999, 25, 285-292.

[59] G. Barthelmesa, S. E. Pratsinisa, H. Buggischb, *Particle size distributions and viscosity of suspensions undergoing shear-induced coagulation and fragmentation*, Chemical Engineering Science, 2003, 58, 2893-2902.

[60] L. H. X. Daphne, H. D. Utomo, L. Z. H. Kenneth, *Correlation between turbidity and total suspended solids in singapore rivers*, Journal of Water Sustainability, 2011, 1, 313-322.

[61] J. Zhang, *Novel emulsion-based delivery systems*, Ph. D. thesis, 2011.

[62] Y. S. Lyalikov, *Physical-chemical analysis techniques* [in Russian], Khimiya, Moscow, 1974.

[63] S. S. Voyutskii, *A course in colloidal chemistry* [in Russian], Khimiya, Moscow, 1975.

[64] P. D. I. Fletcher, K. Suhling, *Interactions between weakly charged oil-in-water microemulsion droplets*, Langmuir, 1998, 14, 4065-4069.

[65] V. Patidar, A. Chandra, M. Singh, R. K. Kale, *Physiochemical and phase behaviour study of jatropha curcus oil - ethanol microemulsion fuels using sorbitane fatty esters*, International Journal of Renewable and Sustainable Energy, 2014, 3, 13-19.

[66] A. J. Queimada, I. M. Marrucho, E. H. Stenby, J. A. P. Coutinho, *Generalized relation between surface tension and viscosity: a study on pure and mixed n-alkanes*, Fluid Phase Equilibria, 2004, 222, 161-168.

[67] Y. D. Gamburg, G. Zangari, *Theory and practice of metal electrodeposition*, New York, USA, 2011.

9.1. General Conclusions

The hydrolysis of CV and Bz is catalyzed by micelles, reverse micelles and microemulsions of CTAB, SDS/SDBS and TX-100. The micellar solutions CTAB and TX-100 accelerate while the micellar solution of SDBS inhibits the alkaline hydrolysis of CV. The addition of CTAB has been found to enhance the rate of the hydrolysis of Bz while presence of SDBS/SDS and TX-100 produces an inhibitory effect at concentrations below the CMC. Above the CMC, the rate constant increases slightly for some concentration of SDBS/SDS whereas for TX-100, the *k*' remains almost constant. As the [CTAB] increases at low [H^+], the rate constant attains a limiting value; while at a high [H^+], the rate constant passes through a maximum and then decreases. The acceleration and inhibition effect of the CTAB, SDBS/SDS and TX-100 on the reactions at below the CMC has been satisfactorily explained with the help of Piszkiewicz model via formation of premicellar aggregates. The kinetic results in presence of CTAB and SDS/SDBS also showed good fit to the PPIE model for the reactions with reasonable values of the parameters. The rate of the reactions changes markedly in different regions such as *w*/*o*, *BC* and *o*/*w* of reverse micelles and microemulsions of CTAB, SDS and TX-100. The physicochemical properties of reverse micelles and micromeulsions also change with compositions of the media. The viscosity, turbidity, conductivity, density and interfacial tension increase while refractive index decreases with increasing ϕ_W. The viscosity, conductivity, turbidity and interfacial tension - ϕ_W profiles show nonlinear behavior with different patterns indicating different microregions in reverse micelles and microemulsions; also supported by applying percolation theory and percolation scaling law on conductivity results. The percolation thresholds obtained is due to the structural transition from *w*/*o* to *BC* and *BC* to *o*/*w* microemulsions.

Electrodeposition of Co, Cu, Zn, Ni and Sn on CuE from aqueous solution occurs grossly without any definite shape and size due possibly to faster deposition rate and hydrogen embrittlement. In contrast, the electrodeposition of different metals from reverse microemulsions of CTAB and SDS carried out on CuE gives electrodeposited metals with definite shape and structure. In reverse microemulsions of CTAB and SDS, hydrophilic cores formed by the aggregation of the hydrophilic polar head groups of the surfactants which incorporates the metal and diffusion of the metals ions occur with a controlled rate which in turn contributes towards deposition with definite morphology and also the structure changes with increasing w_o in reverse microemulsions. With decreasing w_o in reverse microemulsions of CTAB and SDS, the size of the hydrophilic core formed by the hydrophilic polar head groups also decreases, so the hydrophilic interaction between the hydrophilic core and the entrapped metals ions within the hydrophilic core increases gradually. As a result diffusion rate of the metal ions decreases and deposition occurs with a more controlled way which results in the morphological variation of the deposited metals in reverse microemulsions of CTAB and SDS at different composition. With changing the reduction potential at a fixed w_o, only the

thickness of the deposited metal changed due to a faster growth being apparent at a potential more negative than the reduction potential.

9.2. Outlook

Supramolecular self-assembly: surfactant-based organized media such as micelles, reverse micelles and microemulsions can influence the hydrolysis reactions and electrodeposition of metals depending on the different organization of the media. As they can solubilize both the polar and nonpolar substrate, they have therefore a bright prospect in the field of supramolecular chemistry and can be a suitable a candidate for versatile applications in controlled release of drugs, formation of organic thin films and constructing bio-sensor devices. Moreover, ionic liquid (IL) based microemulsions where water and oil phase can be replaced by hydrophilic or hydrphobic IL, respectively for exploiting the selectivity of the novel microemulsions for diverse applications such as fabricating nanoparticles, material science, pollution control, food and pharmaceutical industry, cosmetics and new kind of reaction media.

List of Publications

1. **Ferdousi Begum**, Md. Yousuf A. Mollah, M. Muhibur Rahman and Md. Abu Bin Hasan Susan*, Kinetics of the Alkaline Hydrolysis of Crystal Violet in Micelles, Reverse Micelles and Microemulsions of Cetyltrimethylammonium Bromide,* Journal of Bangladesh Chemical Society, Vol. 24(2), 173-184, 2011.

2. Md. Abu Bin Hasan Susan, Shimul Saha, Saika Ahmed, **Ferdousi Begum**, M. Muhibur Rahman and Md. Yousuf A. Mollah, *Electrodeposition of Cobalt from a Hydrophilic Ionic Liquid at Ambient Condition*, Materials Research Innovations, Vol. 16 (5), 345-349, 2012.

3. **Ferdousi Begum**, M. Yousuf A. Mollah, M. Muhibur Rahman and Md. Abu Bin Hasan Susan, *Acid Hydrolysis of Bromazepam Catalyzed by Micelles, Reverse Micelles, and Microemulsions*, Journal of Chemistry, 2015, 1-10, 2015.

4. **Ferdousi Begum**, M. Yousuf A. Mollah, M. Muhibur Rahman and Md. Abu Bin Hasan Susan, *Microstructures of Cetyltrimethylammoniun Bromide/1-Butanol/Cyclohexane/Water Microemulsions: Analyzed by Percolation Theory,* In progress.

5. **Ferdousi Begum**, M. Yousuf A. Mollah, M. Muhibur Rahman and Md. Abu Bin Hasan Susan, *Effect of Microstructures of Sodium Dodecyl Sulfate/1-Butanol/Cyclohexane/Water Microemulsions on Alkaline Hydrolysis of Crystal Violet,* In progress.

6. **Ferdousi Begum**, M. Yousuf A. Mollah, M. Muhibur Rahman and Md. Abu Bin Hasan Susan, *Reverse Microemulsions used as Media for Electrodeposition of Cobalt*, in progress.

7. **Ferdousi Begum**, M. Yousuf A. Mollah, M. Muhibur Rahman and Md. Abu Bin Hasan Susan, *Electrodeposition of Copper from Water in Oil Microemulsions of Cetytrimethylammonium Bromide*, in progress.

8. **Ferdousi Begum**, M. Yousuf A. Mollah, M. Muhibur Rahman and Md. Abu Bin Hasan Susan, *Comparative Study of the Electrodeposition of Zinc from Aqueous Solution and Reverse Microemulsions of Cetyltrimethylammonium Bromide and Sodium Dodecyl Sulfate*, in progress.

9. **Ferdousi Begum**, M. Yousuf A. Mollah, M. Muhibur Rahman and Md. Abu Bin Hasan Susan*, Morphology and Structural Studies of Electrodeposited Nickel from Reverse Microemulsions*, in progress.

10. **Ferdousi Begum**, M. Yousuf A. Mollah, M. Muhibur Rahman and Md. Abu Bin Hasan Susan, *Correlation of the Physicochemical Properties of Reverse Micelles and Miroemulsions of Sodium Dodecyl Sulfate with the Kinetic Results of the Hydrolysis of Crystal Violet*, in progress.

List of Attended Seminars

1. Seminar on Novel Functional Materials, organized by the Higher Education Quality Enhancement Project (HEQEP) of the University Grants Commission of Bangladesh, May 12 (2011).

2. Seminar on Synthesis and Characterization of Binary and Ternary Solid Materials, organized by the Higher Education Quality Enhancement Project (HEQEP) of the University Grants Commission of Bangladesh, July 30 (2011).

3. Seminar on Supramolecular Systems, organized by the Higher Education Quality Enhancement Project (HEQEP) of the University Grants Commission of Bangladesh, November 15 (2012).

4. Bangladesh Chemical Congress, December 07-09, 2012, Dhaka, Bangladesh.

5. Seminar on Electrochemistry for Material Science, organized by the Higher Education Quality Enhancement Project (HEQEP) of the University Grants Commission of Bangladesh, December 10 (2012).

6. International Bose Conference, February 04, 2013, Dhaka, Bangladesh.

7. 19th Conference of Islamic World Academy of Sciences, May 06-10, 2013 in Dhaka, Bangladesh.

8. 1st National Conference of Bangladesh Crystallographic Association (BCA), 05 December, 2013, Dhaka, Bangladesh.

9. Seminar on Tendam Mass Spectrometry and its Application for Analysis of Chemical Contaminats in Food Stuff, 02 June 2015, Dhaka, Bangladesh.

10. Seminar on 3D Gel Printer and Future Life Innovation, organized by the Material Chemistry Research Laboratory, Department of Chemistry, University of Dhaka, August 30, 2015.

Abstracts Published as Contribution in the Scientific Meetings

1. **Ferdousi Begum**, Md. Yousuf A. Mollah, M. Muhibur Rahman and Md. Abu Bin Hasan Susan*, Kinetics of the Alkaline Hydrolysis of Crystal Violet in Micelles, Reverse Micelles and Microemulsions of Cetyltrimethylammonium Bromide,* 34th Annual Conference of Bangladesh Chemical Society, Dhaka, Bangladesh, 19-20 December, 2011. (Poster presentation)

2. **Ferdousi Begum**, Md. Yousuf A. Mollah, M. Muhibur Rahman and Md. Abu Bin Hasan Susan*, Kinetic Investigation of the Acid Hydrolysis of Bromazepam Catalyzed by Supramolecular Self-Assembled Systems of Cetyltrimethylammonium Bromide,* 35th Annual Conference of Bangladesh Chemical Society, Dhaka, Bangladesh, 07- 09 December, 2012. (Oral presentation)

3. **Ferdousi Begum**, Md. Yousuf A. Mollah, M. Muhibur Rahman and Md. Abu Bin Hasan Susan, *Supramolecular Self-assembled Systems of Sodium Dodecyl Sulfate as Reaction Media for Basic Hydrolysis of Crystal Violet,* 36th Annual Conference of

Bangladesh Chemical Society, Haji Mohammad Danesh Science and Technology University, Dinajpur, Bangladesh, 01-03 March, 2014. (Oral presentation)

4. **Ferdousi Begum**, Md. Yousuf A. Mollah, M. Muhibur Rahman and Md. Abu Bin Hasan Susan, *Hydrolysis of Crystal Violet Catalyzed by Supramolecular Self-Assembled System of Sodium Dodecyl Sulfate,* Sixth HOPE Meeting with Nobel Laureates, Tokyo, Japan, 11-16 March, 2014. (Poster presentation)

5. **Ferdousi Begum**, Md. Yousuf A. Mollah, M. Muhibur Rahman and Md. Abu Bin Hasan Susan, *Cetyltrimethylammonium bromide/1-Butanol/Cyclohexane/Water Microemulsions as Media for the Hydrolysis of Crystal Violet and Bromazepam,* International Conference on Materials Chemistry (ICMC-2014), Shahjalal University of Science and Technology, Sylhet, Bangladesh, December 06, 2014. (Poster presentation)

6. **Ferdousi Begum**, Md. Yousuf A. Mollah, M. Muhibur Rahman and Md. Abu Bin Hasan Susan, *Electrodeposition of Cobalt from Reverse Microemulsion of Sodium Dodecyl Sulfate,* 2nd Conference of Bangladesh Crystallographic Association (BCA), 10 January, 2015, Dhaka, Bangladesh. (Poster presentation)

7. **Ferdousi Begum**, Md. Yousuf A. Mollah, M. Muhibur Rahman and Md. Abu Bin Hasan Susan, *Sodium Dodecyl Sulfate/1-Butanol/Cyclohexane/Water Microemulsions as Media for Basic Hydrolysis of Crystal Violet,* 37th Annual Conference of Bangladesh Chemical Society (ACBCS), 37th Annual Conference of Bangladesh Chemical Society (ACBCS), 11 April, 2015, Comilla University, Comilla, Bangladesh. (Oral presentation)

8. **Ferdousi Begum**, Md. Yousuf A. Mollah, M. Muhibur Rahman and Md. Abu Bin Hasan Susan, *Effect of Microstuctures of Sodium Dodecyl Sulfate/1-Butanol/Cyclohexane/Water Microemulsions on Hydrolysis of Crystal Violet,* 16th Assian Chemical Congress (16 ACC), will be held on 18-21 November, 2015. (Oral presentation)

List of Workshops Attended

1. International Workshop on Nanotechnology, December 21-23, 2012, Dhaka, Bangladesh.
2. Characterization and Application of Novel Functional Materials, 31 August and 01 September, 2013, Department of Chemistry, University of Dhaka, Bangladesh.
3. Black Carbon Emission from Brick Kilns in Bangladesh, November 16, 2014.